Investigation of Pathomechanisms in Parkinson's Disease Mouse Models

Untersuchung der Pathomechanismen in Parkinson Maus Modellen

Dissertation to obtain the degree

Doctor Rerum Naturalium (Dr. rer. nat.)

at the Faculty Biology und Biotechnology

Ruhr University Bochum

International Graduate School of Biosciences

Ruhr University Bochum

Department of Animal Physiology

submitted by

Max Oliver Rybarski

From

Gelsenkirchen, Germany

Bochum,

October 2021

First supervisor: Prof. Dr. Hermann Lübbert

Second supervisor: Prof. Dr. Melanie Mark

Abstract

Parkinson's disease (PD) is a currently incurable neurodegenerative disorder, where patients suffer from motor symptoms like *tremor*, *rigor*, and *bradykinesia*. PD is primarily caused by a loss of dopaminergic neurons in the *substantia nigra* (SN), a brain region responsible for motor planning, ultimately leading to a reduced dopaminergic innervation of the *striatum* (ST). The reason for neuronal degradation is still barely understood, but different gene mutations, like Parkin or α-Synuclein have been identified leading to disease formation. To explore PD onset and pathomechanisms, the department of animal physiology created two distinct Parkinson's disease mouse models, the Padel and Basyn mouse, by introducing Parkin and α-Synuclein mutations into the murine genome. Although these mice do not display signs of neurodegeneration, both mouse models exhibit damaged mitochondria in neurons and glial cells in the SN *in vivo.* The discovery *of* mitochondrial damage in both PD mouse models has promoted the prevalent theory of impaired mitophagy in PD, which consequently leads to mitochondrial accumulation. Mitophagy is tightly linked to mitochondrial-endoplasmic reticulum (ER) tethering, which has been proposed to be altered in PD. However, this theory is controversially discussed in the literature and needs further examination. In addition to the observed mitochondrial damage, impaired neuronal differentiation was observed in both PD mouse models, as well as indications for the exchange of deficient mitochondria between neurons and astrocytes, suggesting their contribution to disease formation.

To shed light on this complex and multifactorial disease, both PD mouse models were analyzed by RNA-Seq to identify disease-associated alterations. To do so, a previously obtained transcriptome data set of SN and ST tissue from adult Padel and Basyn mice was re-analyzed with the latest software. This analysis revealed 150 differentially expressed genes, which were subsequently evaluated in qPCR experiments in the Padel mouse line. Stringent quality control measures and different validation methods led to the identification of the ER calcium-binding protein Reticulocalbin1 (Rcn1) and the lysosomal cysteine protease Cathepsin C (Ctsc), which were both upregulated in the Padel mouse model.

Rcn1 characterization via immunocytochemistry in astrocytes and fibroblasts, as wee as cell fractionation experiments with brain tissue, has shown that Rcn1 is located in the ER and mitochondrial-associated membranes.

During calcium experiments, a reduced ER-mediated calcium release was found in primary Padel astrocytes, which could be rescued and restored to wild type levels with Rcn1 siRNA treatment, indicating that Rcn1 may at least be partially responsible for the reduced ER calcium

response in Padel astrocytes, thereby being the first discovered ER protein mediating Parkin-dependent calcium release.

To investigate a potentially impaired mitophagy, the autophagosome membrane protein LC3b was used for colocalization analysis with mitochondria in primary culture and parallelly for quantitative autophagy measurement on a western blot. No significant Parkin-dependent changes in basal mitophagy could be observed in the experiments.

Investigation of a potential intercellular mitochondrial exchange between mesencephalic astrocytes and catecholaminergic neurons found, for the first time that primary murine mesencephalic astrocytes can release and take up mitochondria and incorporate them into their own mitochondrial network *in vitro*. Vesicles containing mitochondria have been identified in these cultures, indicating vesicular transport is one mechanism of mesencephalic mitochondrial exchange. It was demonstrated, that primary catecholaminergic neurons can take up mitochondria from mesencephalic astrocytes into their soma, their dendrites, or their axon.

Lastly, the impact of Parkin-deficiency on the differentiation of mesencephalic neurons in an astrocyte-neuron co-culture was examined. Parkin-deficient co-cultures showed a significant reduction of neuronal processes but only if both cell types exhibited the Parkin mutation indicating impaired differentiation requires neuron-glia interaction.

Taken together, this work was able to identify two overexpressed genes (Rcn1, Ctsc) in the *substantia nigra* of a Parkin-deficient mouse model, which were previously not associated with Parkinson's disease. Rcn1 was successfully linked to the decreased ER-mediated calcium response of Padel astrocytes, thereby being the first endoplasmic reticulum protein facilitating Parkin-dependent calcium release. Additionally, for the first time, intercellular mitochondrial exchange from murine mesencephalic astrocytes into catecholaminergic midbrain neurons has been demonstrated *in vitro*. This mechanism, combined with impaired mitophagy or damaged mitochondria in a Parkinson's disease context could potentiate its pathogenesis via donation of defective mitochondria into SN dopaminergic neurons.

Zusammenfassung

Morbus Parkinson (PD) ist eine unheilbare, neurodegenerative Erkrankung, bei der Patienten unter Motorsymptomen wie Tremor, Rigor und Bradykinesie leiden. Die Ursachen dieser Erkrankung sind nicht eindeutig geklärt, pathopysiologisch fällt jedoch ein Verlust dopaminerger Neurone in der *Substantia nigra (SN)* auf, das Gehirnareal, dass für das Planen von Bewegungen verantwortlich ist. Das Absterben dieser Neurone resultiert in einer unzureichenden des *Striatums (ST),* welches für die Hemmung von Bewegungen verantwortlich ist. Die Ursachen dieser Erkrankungen sind nicht eindeutig geklärt, aber es konnten Genmutationen im Parkin oder α-Synuclein Gen identifiziert werden, die zu familiärem Parkinson führen. Durch die jeweilig gezielte Mutation dieser Gene wurden vom Lehrstuhl für Tierphysiologie zwei Mausmodelle erzeugt, die Padel und Basyn Maus, um die Pathomechanismen dieser Erkrankung zu untersuchen. Diese Modelle weisen keine Anzeichen von Neurodegeneration auf, allerdings konnten beschädigte Mitochondrien in Neuronen und Gliazellen der SN *in vivo* nachgewiesen werden. Diese Befunde verstärkten die gängige Theorie einer gestörten Mitophagie in Parkinson, wodurch es zu einer Akkumulation von Mitochondrien in den Zellen kommt. Als Ursprungsort der Mitophagie werden Verbindungsstellen zwischen dem endoplasmatischen Retikulum (ER) und den Mitochondrien diskutiert, deren Anzahl bei Parkinson verändert sein soll. Diese These aufgrund einer widersprüchlichen Datenlage kontrovers diskutiert. Des Weiteren gibt es Hinweise auf eine verminderte neuronale Differenzierung und einen möglichen Austausch von beschädigten Mitochondrien bei Morbus Parkinson.

Für die Untersuchung von PD-assoziierten Pathomechanismen wurde eine zuvor durchgeführte Transkriptionsanalyse der SN in den generierten Mausmodellen mit modernen Analyseprogrammen neu ausgewertet, um unbekannte Variablen der Pathogenese zu identifizieren. Die resultierenden 150 Gene wurden daraufhin in der Padel Mauslinie in qPCR Experimenten unter strengen methodischen Kontrollen überprüft, was zu der Identifizierung des Calcium-bindenden ER Protein Reticulocalbin (Rcn1) und der lysosomalen Cystein Protease Cathepsin C (Ctsc) führte.

Der zelluläre Standort von Rcn1 wurde durch immunzytochemische Untersuchungen (Astrozyten, Fibroblasten) und Zellfraktionierungen (Gehirngewebe) im ER und den Kontaktstellen zwischen ER und Mitochondrien lokalisiert.

Daraufhin wurde in Padel Astrozyten ein signifikant reduzierter ER-vermittelter Calcium Ausstrom gemessen, welcher durch die Behandlung mit Rcn1 siRNA wieder auf Wildtyp-

Niveau zurückgesetzt werden konnte. Daraus folgt, dass Rcn1 verantwortlich für die reduzierte Calcium Antwort in Padel Astrozyten ist und damit das erste bekannte Protein darstellt, welches Parkin-abhängig die Calcium Dynamik im endoplasmatischen Retikulum reguliert.

Für die Untersuchung einer potenziell gestörten Autophagie/Mitophagie wurden die Autophagosomen in Padel Fibroblasten via Western Blot quantifiziert und immunzytochemisch mit Mitochondrien kolokalisiert. Dabei konnten keine signifikanten Parkin-abhängigen Veränderungen beobachtet werden.

Dahingegen konnte bei der Untersuchung eines möglichen interzellulären Mitochondrien Austausches *in vitro* bei Mittelhirnzellen der Maus zwischen Astrozyten und catecholaminergen Neuronen zum ersten Mal gezeigt werden, dass die Astrozyten in der Lage sind Mitochondrien auszuschütten, aufzunehmen und in ihr mitochondriales Netzwerk zu integrieren. Dabei konnten mit Mitochondrien gefüllte Vesikel in diesen Kulturen beobachtet werden, die einen wahrscheinlichen Transportmechanismus für diesen Austausch darstellen. Es wurde ebenfalls eine Aufnahme von Astrozyten-Mitochondrien in das Soma, die Dendriten und das Axon von catecholaminergen Neuronen nachgewiesen.

Zuletzt wurde der Einfluss von Parkin auf die Differenzierung von mesencephalen Neuronen in einem Astrozyten-Neuronen Ko-Kultur System untersucht. Parkin-defiziente Kulturen zeigten eine signifikante Reduktion neuronaler Fortsätze, allerdings nur, wenn beide Zelltypen die Mutation besaßen. Parkin-abhängige gestörte neuronale Differenzierung setzt also Neuron-Astrozyten Interaktion voraus.

In dieser Arbeit konnten zwei überexprimierte Gene (Rcn1, Ctsc) in der SN eines Parkin knock-out Models identifiziert werden, die vorher noch nicht mit Parkinson assoziiert waren. Rcn1 konnte erfolgreich mit funktionell mit einer reduzierten Calcium Ausschüttung des endoplasmatischen Retikulums verknüpft werden und stell somit das erste ER Protein dar, welches Parkin-abhängig die Calcium Ausschüttung reguliert. Zusätzlich konnte ein mitochondrialer Austausch zwischen murinen Mittelhirn Astrozyten und catecholaminergen Neuronen in vitro nachgewiesen werden. Dieser Mechanismus könnte in Kombination mit einer gestörten Mitophagie oder beschädigten Mitochondrien im Zusammenhang mit PD den Krankheitsverlauf beschleunigen, falls dort Astrozyten beschädigte Mitochondrien an dopaminerge Neurone weitergeben.

Table of contents

List of figures

Attachment:

List of tables

Attachment:

List of abbreviations

Abbreviation	Meaning
5-FDU	2'-Deoxy-5-fluorouridine
A. dest	Distilled water
APS	Ammonium persulfate
ATP	Adenosine triphosphate
BBB	Blood brain barrier
BFB	Brain fractionation buffer
BSA	Bovine serum albumin
CaMK	Ca^{2+}/calmodulin-dependent protein kinase
CCG	Cologne Center of Genomics
CMV	Cytomegalovirus
cDNA	Complementary DNA
Cre	Cre-recombinase
CT	Cycle threshold
Ctsc	Cathepsin C
DA	Dopaminergic
DEG	Differentially expressed genes
DMEM	Dulbeccos's modified Eagle's medium
DMSO	Dimethyl sulfoxide
DNA	Deoxyribonucleic acid
DNase	Deoxyribonuclease
ECL	Enhanced chemo luminescence
EDTA	Ethylenediaminetetraacetic acid
EGTA	Ethylene glycol-bis(β-aminoethyl ether)-N,N,N',N'-tetraacetic acid
ER	Endoplasmic reticulum
Ermard	ER membrane-associated RNA degradation protein
FA	Formaldehyde
FCS	Fetal calf serum
FGF	Fibroblast growth factor
GDNF	Glial cell-derived neurotrophic factor
Gfap	Glial fibrillary acidic protein
GOI	Gene of interest
HBSS	Hank's balanced salt solution
HEPES	4-(2-hydroxyethyl)-1-piperazineethanesulfonic acid
HKG	Housekeeping gene
Homo	Genetically homozygote
Hprt	Hypoxanthine-guanine phosphoribosyltransferase
Hsp60	Heat shock protein 60
Hsp90b1	Endoplasmin
IP_3R1	Inositol triphosphate receptor 1
iPSC	Induced pluripotent stem cell

…List of abbreviations continued.

Abbreviation	Meaning
kDa	Kilodalton
LC3	Microtubule-associated proteins1A/1B light chain 3
MAM	Mitochondrial associated membrane
MAO	Monoamine oxidase
Mes	*Mesencephalon*
MPTP	1-Methyl-4-phenyl-1,2,3,6-tetrahydropyridin
NGS	Next generation sequencing
NTC	Non template control
P	Passage
PBS	Phosphate buffered saline
PCR	Polymerase chain reaction
PD	Parkinson's disease
PDL	Poly-D-Lysine
PLA	Proximity ligation assay
PN	Postnatal
PVDF	Polyvinylidene fluoride
qPCR	Semi-quantitative real-time PCR
Rcn1	Reticulocalbin
RNA	Ribonucleic acid
RNase	Ribonuclease
ROS	Reactive oxygen species
RT	Room temperature
RT^-	Without reverse transcriptase
RT-qPCR	Semiquantitative real-time PCR
sec	Seconds
SDS	Sodium dodecyl sulfate
siRNA	Small interfering RNA
SN	*Substantia nigra*
SNP	*Single-nucleotide polymorphism*
ST	*Striatum*
TBS	Tris buffered saline
TBST	Tris buffered saline + Tween20
TEMED	Tetrametylethylenediamine
TH	*Tyrosine-hydroxylase*
WT	Wild type

Introduction

Parkinson's Disease is an inheritable, age-dependent neurodegenerative disorder which's prevalence is on the rise in developed countries worldwide, however its pathogenesis is still unknown. Symptoms occur late when the disease has progressed and dopaminergic neurons in the *substantia nigra*, a brain region responsible for motor planning, already started to die, resulting in tremors, bradykinesia, and gait imbalances. Although symptoms can be treated, a deeper understanding of Parkinson's Disease formation is required to develop early diagnosis tools. Therefore, this thesis investigates different pathomechanisms in Parkinson's Disease mouse models to gain a deeper understanding of the disease as a basis for the development of treatment options in the future.

1.1 Parkinson's Disease – a short overview, relevance of research

Parkinson's disease (PD) is the second most common neurodegenerative disease in the western world (Nussbaum and Ellis, 2003) and its incidence is on the rise due to its age dependency. The number of patients doubled from 1990 to 2015 to 6 million globally and due to an increased life expectancy, the predicted cases are expected to double again by 2040 (Dorsey et al., 2015). This fact makes basic research and investigation of pathomechanisms a relevant objective for research projects all over the world.

The cardinal symptoms of Parkinson's Disease are rigor, tremor, slowness of movement, and postural instability. One key feature of the disease is the degeneration of the dopaminergic neurons in the *substantia nigra pars compacta*, a brain region of the basal ganglia that is important for motor planning, resulting in a reduced innervation of the *striatum*, thereby disrupting normal motor function (Damier et al., 1999; Olanov and Tatton, 1999).

The pathomechanisms and disease onset are still not fully understood. However, in some cases of PD, cytoplasmatic aggregations were found *postmortem* in different organs including the basal ganglia of PD patients (Spillatini et al., 1997; Zarranz et al., 2003; Lesage et al., 2013). These aggregations could be a cellular hallmark of certain PD subtypes, besides neurodegeneration (Braak et al., 2003; Rodriguez-Leyva et al., 2014). These aggregations are called Lewi bodies and consist of α-Synuclein, neurofilaments, and ubiquitin (Goldmann et al., 1983). Different theories were discussed how α-Synuclein, a presynaptic neuroprotein involved in synaptic vesicle trafficking, catalyzes PD onset, but basically, it is believed that abnormal protein folding leads to oligomers (protofibrils), that promote the disruption of cellular homeostasis and synaptic functionality via multiple intracellular targets, ultimately leading to neuronal degeneration (Review: Stefanis et al., 2012). In the late stages of the disease, brain lesions can be observed outside the *substantia nigra* as well, resulting in dementia in roughly 30% of all PD patients (Aarsland et al., 1996).

The major problem in a clinical context is, that these cardinal symptoms only start to manifest, when approximately 50% of dopaminergic neurons degenerated, leading to a diagnosis when irreversible neuronal damage has already occurred (Fahn et al., 2006; Kordower et al., 2013).

Studies have revealed that all analyzed PD patients who exhibit motoric symptoms, also suffer from non-motor symptoms (Aarsland et al., 1996; Krishan et al., 2011; Kim et al., 2013). Before motor symptoms arise, cognitive deficits can be observed in many patients. Depression and anxiety have been shown to be very prevalent in patients before PD diagnosis, making psychological disorders a potential early warning sign for this neurodegenerative disease (Bodis-Wollner, 2003; Lian et al., 2019).

The main treatment for PD is the blood-brain-barrier (BBB) permeable dopamine precursor L-Dopa, which increases dopamine release from remaining dopaminergic neurons, thereby temporarily reinstating sufficient dopamine innervation in the *striatum*, consequently alleviating motoric deficits (Cotzias et al., 1969). However, this treatment option solely ameliorates PD symptoms but does not hinder disease progression. Unfortunately, most patients die within approximately 7-15 years after they have been diagnosed with PD (Sveinbjornsdottir, 2016).

The molecular basis for PD neurodegeneration is poorly understood and underlying pathomechanisms are still up to debate. Because of its rising incidence, late diagnosis, and insufficient treatment options, the necessity for a basic understanding of PD pathomechanisms becomes evident. By use of genetically engineered mouse models, the pathology of Parkinson's Disease can be explored, leading to a better understanding of this poorly understood illness.

1.2 Genetic background of Parkinson's disease and mouse models

Most PD cases occur sporadically; however, some familial forms have been identified, where the disease is inherited in an autosomal dominant or recessive fashion (De lau and Breteler, 2006). The genetic form of PD usually has an early onset and is defined as juvenile PD, if patients are under 21 years old (Lücking et al., 1998; Kitada et al., 1998; Abbas et al., 1999; Anwar et al., 2019). Currently, 26 genes have been identified, which are strongly linked to an increased PD risk (Lill, 2016). Prominent genes in this category are α-Synuclein (SNCA), Pink1 (PINK1), and Parkin (PARK2), which are described in the following sections. (Ishikawa et al., 1996; Polymeropoulus et al., 1996; Valente et al., 2001).

α-Synuclein

α-Synuclein is a presynaptic neuronal protein, whose physiological function is still not fully understood. It is thought to play a role in synaptic membrane remodeling and vesicle trafficking, thereby modulating dopaminergic transmitter release (Bendor et al., 2013).

Two genetic α-Synuclein variants were identified, both causing Parkinson's Disease via mutations at either A53T or A30P (Polymeropoulus et al., 1997, Krüger et al., 1998).

To facilitate examination of molecular pathomechanisms of this α-Synuclein associated PD subtype, the department of animal physiology generated a transgenic

mouse strain through a construct injection of the human double mutated α-Synuclein with an β-Actin promotor and cytomegalovirus (CMV) enhancer in oocytes of C57BL/6N mice (Maskri et al., 2004). The construct integrated between the exon 15 and 16 of the neurexin1 gene on chromosome 17 and causes overexpression of the human double mutated α-Synuclein in these so-called Basyn mice. Homozygous animals die prenatally, only heterozygous animals are viable and can be utilized to study disease mechanisms.

Behavioral characterization of Basyn mice did not reveal signs of motoric impairment or neurodegeneration in one-year-old animals (Stichel et al., 2007; Malkemper, 2011). However, compared to WT littermates, Basyn mutant mice exhibit an accumulation of defective mitochondria in neurons and glial cells of the *substantia nigra in vivo* (Stichel et al., 2007; Schmidt et al., 2011). This finding is in alignment with other published results of similar Basyn mouse lines with mitochondrial defects (Chen et al., 2013; Subramaniam et al., 2015). Nevertheless, the functional link between α-Synuclein overexpression and damaged mitochondria remains unknown.

Parkin

Under physiological conditions, Parkin acts as an E3-ubiquitin-ligase (Imai et al., 2000; Shímura et al., 2000). This enzymatic pathway marks proteins for degradation, which can have regulatory purposes or cleans the cell from damaged or misfolded proteins/organelles. However, evidence emerged that Parkin may also mediate neuroprotective function (Doss-Pepe et al., 2005; Mckeon et al., 2015).

Mutations within the Parkin gene are responsible for most inherited cases of autosomal recessive PD with early-onset, accounting for 77% of familial cases (Lücking et al., 2000). One prominent Parkin variant is known to cause PD contains an exon 3 deletion, which leads to a loss of function of the protein (Kitada et al., 1998). One hypothesis for Parkin-mediated PD onset is the accumulation and/or aggregation of Parkin substrates leading to the degeneration of dopaminergic neurons (Imai et al., 2000; Shímura et al., 2000).

To investigate Parkin-dependent pathomechanisms, the department of animal physiology has created a Parkin knock-out line through homologous recombination in

129Sv/J embryonic stem cells replacing the third exon of Parkin with a LoxP flanked neomycin cassette (Zhu et al., 2007). This so-called PaKO mouse was crossed with a Deleter mouse, which overexpresses Cre-recombinase, to remove the neomycin cassette via Cre-LoxP mediated recombination to create a new PaKO line: the Padel mouse (Schwenk et al., 1995). This strain was backcrossed with wild type C57BL/6N for more than 20 generations to establish a Padel mouse strain, that carries a relatively pure C57BL/6N background and no neomycin cassette.

Padel mice do not display signs of neurodegeneration or motoric deficits, exactly like their precursor, the PaKO mouse (Stichel et al., 2007; Zhu et al., 2007; Hemmersbach, 2016; Mrohs, 2017). These findings are in accordance with similar published Parkin knock-out lines (Goldberg et al., 2003; Itier et al., 2003). However, examination of Padel animals revealed, that the nucleolus integrity of *substantia nigra* dopaminergic neurons is reduced in comparison to their littermates (Swatschek, 2016). A similar finding was observed *postmortem* in brain tissue of PD patients and is generally associated with neurodegeneration (Rieker et al., 2011). Like Basyn mice, Padel mice exhibit an accumulation of defect mitochondria as was observed in electron microscopy (Schmidt et al., 2011). This deficiency was also observed in its precursor line PaKO, indicating the effect is based on the Parkin knock-out and not caused by genetic heterogeneity (Stichel et al., 2007). Interestingly, the number of undamaged mitochondria was not statistically different between knock-out mice and littermates, indicating Parkin knock-out does not actively damage mitochondria, it rather prevents their prompt degradation.

Mitochondrial abnormalities in Parkin knock-out mouse lines were characterized by other research groups, too, including an altered mitochondrial morphology in dopaminergic axons or a reduction of proteins associated with mitochondrial function (Palacino et al., 2004; Pinto et al., 2018). Those findings are in accordance with observations in PD patients, who also show accumulation of defective mitochondria (1.3). It is possible, that Basyn and Padel mouse models represent an early stage of PD pathology, rather than the late stage where neurodegeneration occurs.

1.3 Mitochondrial involvement in PD and Pink1/Parkin-dependent mitophagy

In 1979, four persons developed Parkinson's disease-like symptoms after consumption of the mitochondrial toxin MPTP, which passes the blood-brain-barrier and gets converted to its metabolite MMP^+ by Monoamine oxidase B. MPP^+ acts as a substrate for the synaptic dopamine transporter, thereby causing selective dopaminergic cell toxicity by irreversible inhibition of the respiratory electron transport chain complex I (Davis et al., 1979; Langston et al., 1983; Javitch et al., 1985; Vyas et al., 1986). Later, *postmortem* studies of the *striatum* and *substantia nigra* of PD patients revealed a deficiency of the respiratory chain complex I (Mizuno et al., 1989; Schapira et al., 1990; Haas et al., 1995). Since then, both the genetic as well as sporadic form of PD have been linked to mitochondrial dysfunction in a variety of publications. (Betarbet et al., 2000; Bonifati et al., 2003; Valente et al., 2004).

Damaged organelles can also occur under physiological conditions, and their targeted removal is called macroautophagy (Yoshimori et al., 2004). For mitochondria, their regulated macro autophagic elimination is called mitophagy (Lemasters et al., 2005; Youle and Narendra, 2011). The recycling of mitochondria is crucial for maintaining vital cell function because heavily mutated mitochondria can alter oxidative stress levels, calcium homeostasis, and oxidative phosphorylation, thereby disrupting cell homeostasis (James and Murphy, 2002).

One mechanism, which can potentially explain mitochondrial deficiencies in some forms of PD, is a defect in the Pink1/Parkin mediated mitophagy. As already mentioned, both genes have variants that lead to the familial form of PD and their corresponding mouse models also exhibit signs of mitochondrial deficiency (Stichel et al., 2007; Schmidt et al., 2011; Gautier et al., 2008; Heeman et al., 2011; Moisoi et al., 2014).

Under physiological conditions, the serine/threonine-protein kinase Pink1 is imported into the mitochondrial lumen and proteolytically degraded. Defective mitochondria, which have lost their physiological membrane potential, can't import Pink1 anymore, resulting in an accumulation of the kinase on the outer mitochondrial membrane, acting

as a mitochondrial damage sensor. The ubiquitin ligase Parkin gets subsequently recruited by Pink1 and facilitates the formation and extension of the autophagosome membrane (Narendra et al., 2008; Kawajiri et al., 2010). This membrane consists mainly of processed MAP1LC3A-C (LC3) proteins. Before autophagosome biogenesis, LC3 is an 18 kDa heavy cytoplasmatic protein (LC3-I), which can be proteolytically cleaved at the N-terminus generating the mature 16 kDa heavy protein, which is embedded in the autophagosomal membrane (LC3-II) (Ishimura et al., 2000). The LC3-II/LC3-I ratio can be utilized as a parameter for autophagy measurements (Kabeya et al., 2000).

However, the mechanism of Pink1/Parkin-dependent mitophagy was only described *in vitro,* using autophagy-inducing substances, or manipulated expression levels of the participating proteins (Cai et al., 2012; Ashrafi et al., 2014; Bingol et al., 2014). *In vivo* information or proof of basal mitophagy via this pathway is still missing.

1.4 PD and its impact on mitochondrial associated membranes (MAMs)

It is commonly assumed, that the disease formation of at least some types of PD is linked to mitochondrial deficiency. It is known that the mitochondrial network regularly forms reversible connections with the endoplasmic reticulum (ER). These connection sites are called mitochondrial associated membranes (MAM). They act as tethers, thereby enabling communication and modulation between mitochondria and the ER. MAMs have been shown to regulate different cellular processes, like calcium homeostasis, lipid metabolism, and autophagy (Vance et al., 2014; Naon et al., 2014; Yang et al., 2020). Additionally, MAMs have been shown to be essential for maintaining physiological mitochondrial morphology, which is often impaired in PD context (Friedmann et al., 2011; Hoppins and Nunnari, 2012; Youle and van der Bliek, 2016).

Recently, a link between PD and MAM dysfunction has been identified, making this organelle a promising target for PD research (Guardia-Laguarta et al., 2014;

Ottolini et al., 2013). Interestingly, MAMs are currently discussed as the location for Parkin-mediated autophagy of damaged mitochondria (Yang and Yang, 2013). Different publications postulated an influence of Parkin on mitochondrial-associated membrane tethering, but the results contradict each other (Cali et al., 2012; Gautier et al., 2016). Taken together, altered mitochondria–ER crosstalk has been implicated with PD pathology, but there is contradicting evidence regarding the impact of Parkin expression on MAM tethering (Gomez-Suaga et al., 2018).

1.5 Astrocytic involvement in PD and mitochondrial exchange

For a long time, the focus of PD research was directed at the degenerating dopaminergic neurons. Recently, more and more studies investigated a potential connection between astrocytes and PD pathology. Astrocytes nourish and protect neurons, e.g., by releasing glutathione and GDNF, which is directly correlated with the survival of dopaminergic neurons (Raps et al., 1989; Lin et al., 1993; Schar et al., 1993). Indirect co-culture experiments with cortical neurons have shown, that Parkin-deficient astrocytes are incapable to support neuronal differentiation compared to wild type astrocytes (Schmidt et al., 2011). This hints at a deficiency in their supportive capabilities in PD. There are also reports of harmful astrocytic actions in PD context. Isolated and cultivated astrocytes from PD patients exhibited increased release of cytokines on stimulation, indicating an increased inflammatory response (Sonninen et al., 2020).

Another important ability of astrocytes is the disposal of neuronal waste products. Astrocytes can take up neuronal α-Synuclein followed by lysosomal degradation (Tsunemi et al., 2020). This ability could also explain the findings in our previous work, where damaged mitochondria were seen to a greater extent in astrocytes than in neurons in the *substantia nigra* of Padel and Basyn animals *in vivo* (Schmidt et al., 2011). We found the same effect also in a third PD mouse model, the THsyn mouse, which overexpresses the mutated α-Synuclein in catecholaminergic

neurons. This was unexpected because the damaged mitochondria in glial cells did not even express the transgene protein.

This phenomenon was hard to explain at first, but evidence of mitochondrial exchange mechanics in different cell types emerged in recent years, giving the observed effect a new context (Ahmad et al., 2014; Dong et al., 2017; Diaz-Carballo et al., 2015). Two studies even found a bidirectional mitochondrial exchange between neuronal cell types and astrocytes (Davis et al., 2014; Hayakawa et al., 2018).

Based on the previous finding that the accumulation of defect mitochondria was found in non-transgenic cells next to cells overexpressing the α-Synuclein transgene in the SN *in vivo* combined with the published studies of mitochondrial transfer between neurons and glial cells, it could be assumed that such an intracellular transfer may also take place between dopaminergic neurons and surrounding glial cells in the *substantia nigra*.

Taken together, it is clear, that astrocytes play an important role under both physiological and pathological conditions. This raises the question, whether PD neurodegeneration is solely caused by pathological processes in neuronal cells, or might astrocytes contribute or even cause PD pathology via the loss of supporting function or even actively harmful actions. Either way, it is mandatory to further examine the role of astrocytes in PD context to obtain insight into astrocyte-related PD pathomechanisms.

1.6 NGS analysis to identify new key players in PD pathogenesis

As previously described, multiple pathomechanisms for PD have been postulated. However, none of the postulated mechanisms can explain how the identified PD-causing mutations found in patients ultimately lead to disease outbreak, yet can they explain the role of defective mitochondria accumulation in PD pathogenesis. It is necessary to identify unknown molecular key players with an unbiased approach to

close the gaps in knowledge and thereby establish a broader understanding of this disease as a basis for the development of diagnosis and treatment options.

Many biological processes are regulated on the transcriptional level and can change during a diseased state, such as PD (Lee and Young, 2014; Nido et al., 2020). Therefore, transcriptome analysis can possibly lead to the identification of alterations and consequently shed light on different processes associated with PD pathology.

The department of animal physiology performed a transcriptome analysis via NGS sequencing of two generated PD mouse models, Padel & Basyn, to identify changes in gene expression, caused by PD-associated transgenic alterations (Osenberg,2018). The NGS analysis revealed a substantial overlay of differently expressed genes in the *substantia nigra* of both PD mouse models, which did not occur in the other brain regions (152 genes).

Next-generation sequencing analyses can be a powerful tool in basic research, but it is essential to confirm revealed changes in gene expression with an independent method and a new set of sample material to validate these preliminary results. Once confirmed, PD-associated genes could be examined regarding their involvement in pathological processes.

1.7. Objectives

Parkinson’s disease is a common neurodegenerative disease with no cure and unknown molecular pathomechanisms. Investigation of its pathogenesis is essential for the development of diagnosis and treatment options in the long run.

To do so, this thesis aims to examine different aspects of PD pathology utilizing the Padel and Basyn mouse models. Firstly, this thesis aims to identify yet unknown PD key players to broaden the understanding of this poorly understood disease. The second aspect is the characterization of these mouse models regarding different postulated theories of PD pathogenesis.

The first objective of this thesis is the repetition of the bioinformatic analysis of the previously conducted transcriptome analysis. There have been advances in this research field and the algorithm used to align the generated reads to the reference genome has been replaced by a newer version. The previously used aligning algorithm Tophat will be exchanged by the newer version Hisat2. It might be beneficial to get an updated list of differentially expressed genes as a starting point for subsequent verification efforts.

That directly leads to the second objective of this thesis. The expression of potentially regulated genes from the NGS analysis shall be examined with an accurate independent method to confirm or disregard the postulated expression changes. The chosen method is the real-time polymerase chain reaction (qPCR), which will be applied to an independent sample set of RNAs from PD mouse models with a high sample size (n~10).

After the confirmation of differential expression, a systematic literature review will be performed on the candidate genes to get an overview of gene function, localization, and a possible link to PD. Subsequently, experiments will be designed to establish or broaden the link of these genes to PD pathology.

The other branch of this thesis is the characterization of the Padel mouse model regarding different published hypothesis of PD pathogenesis. A strong link between PD pathology and mitochondrial deficiencies has been reported in PD patients and PD mouse models in literature and previous experiments. One prominent hypothesis is the Pink1/Parkin mediated mitophagy (1.3). One aim of this thesis is the examination of autophagy/mitophagy under basal conditions utilizing the autophagosome marker LC3b in fibroblast primary culture. The readout for autophagy will be the ratio of cytosolic and autophagosome-membrane bound LC3b in western blot analysis. The examination of mitophagy will be conducted via a colocalization analysis of mitochondria and autophagosomes in living fibroblasts.

Mitochondrial-associated membranes have been implicated in PD pathology and have been discussed as the location, where Pink1/Parkin mediated mitophagy is initiated. Additionally, these sites are implicated in Calcium transfer between the ER and mitochondria. Parkin seems to influence mitochondrial – ER tethering but there is contradicting evidence in literature if Parkin increases or decreases MAM formation.

In this thesis, the number of MAMs in primary Padel fibroblasts will be visualized via immunocytochemistry and quantified with a bioinformatic image analysis pipeline to add data to the unanswered question of Parkin-dependent MAM tethering.

Although, it is not clear if how Parkin regulates the MAM amount, it is likely that it has an impact on MAM formation. Therefore, it is not implausible that the endoplasmic reticulum calcium dynamic could be altered in the Padel mouse line. This dynamic will be examined in primary Padel mesencephalic astrocytes to see if Parkin knockout influences calcium homeostasis.

The mechanism of mitochondrial exchange would provide a logical explanation for the observed damaged astrocytes in the THsyn mouse model, although this cell type does not even carry the mutated transgene. Recent publications have shown mechanisms, that mitochondrial exchange between neurons and astrocytes in the *cortex* and retinal ganglion cells can support stressed neurons by the donation of astrocytic mitochondria or the uptake of neuronal mitochondria in astrocytes for lysosomal degradation. This thesis aims to investigate a potential mitochondrial exchange between catecholaminergic midbrain neurons and midbrain astrocytes in a direct primary co-culture, utilizing reporter mouse lines to track the mitochondrial origin.

Previous experiments have shown that the differentiation of wild type cortical neurons was impaired in indirect co-culture with Padel astrocytes. This raises the question if Padel astrocytes will also fail to support catecholaminergic neuron differentiation. If so, it would be interesting to see, if wild type astrocytes can rescue differentiation of Padel neurons in an inverted experiment. A direct co-culture is better suited as an initial experiment for this objective because it better represents the *in vivo* situation. The conducted experiment will examine if the differentiation of mesencephalic, catecholaminergic neurons will be impacted by mesencephalic astrocytes in a direct co-culture.

2. Material and methods

2.1 Material

In this section, materials used in this thesis are listed to give transparency and make exact reproduction of performed experiments possible. Not listed material is considered basic laboratory research equipment, which could be exchanged by other material without endangering reproduction of experiments.

2.1.1 Animals

All animal experiments were conducted and approved using the German guidelines. The animals were cared for according to the guidelines of the animal welfare committee of North-Rhine-Westphalia (LANUV). Animals were housed in a 12/12 hrs light/dark cycle with access to food and water *ad libitum*. Ambient temperature was maintained at 24 °C.

Table 1: Mouse strains used in this thesis. *Official strain names and characteristics of mice, as well as their source of supply are listed.*

Mouse strain	Characteristics
Ai14	Floxed tdTomato, #007914; B6.Cg-*Gt(ROSA)26Sor*$^{tm14(CAG-tdTomato)Hze}$/J (Madisen et al., 2010)
Basyn	Overexpression of human mutated α-synuclein Ruhr-Universität Bochum [DE]
C57Bl/6N	Wild type strain NIH, 1999 [US]
GFAP-Cre line 77.6	Cre recombinase expression in GFAP positive cells University of California [US]
Padel	Loss of functional Parkin, exon 3 deletion (Zhu et al., 2007)
PhAM	Floxed Dendra2 mitochondrial photoconvertible eGFP #018385; B6;129S-*Gt(ROSA)26Sor*$^{tm1(CAG-COX8A/Dendra2)Dcc}$/J
Th-Cre1	Cre recombinase expression in catecholaminergic cells #008601; B6.Cg-7630403G23Rik$^{Tg(Th-cre)1Tmd}$/J (Savitt et al., 2005)

2.1.2 Antibodies

Table 2: List of antibodies used for immunocytochemistry and western blot experiments. *Working concentrations are listed in the methodology section.*

Antigen	Species	Manufacturer	Catalogue No.
ß-Actin	mouse	BD Bioscience	612656
ß-Tubulin III	mouse	Proteintech	66240-1-IG
Calreticulin	rabbit	Abcam	ab92516
Gfap	mouse	Invitrogen™	14-9892-82
Hsp60	chicken	Antibodies.com	A85438
Hsp90b1	mouse	Sigma Aldrich	AMAB91019
Lc3b	rabbit	Novus biology	NB100-2220
Mfn2	mouse	Abcam	ab56889
Rcn1	rabbit	Abcam	ab198996
Sdha	mouse	Abcam	ab14715
Alexa 488 a rb	goat	Invitrogen™	A27034
Alexa 546 a ms	goat	Invitrogen™	A11003
Alexa 647 a ch	goat	Invitrogen™	A21449
ECL a ms	sheep	Amersham™	NA931VS
ECL a rb	sheep	Amersham™	NA934VS

2.1.3 Chemicals

Table 3: List of frequently used chemicals. *Supplying company and location of their headquarter are listed as well.*

Chemical	Supplier
β-Mercaptoethanol	Applichem [DE]
5-FDU	Sigma Aldrich [US]
ECL™ Prime Luminol Enhancer	Amersham plc [UK]
Acetic acid	VWR Chemicals [US]
Acrylamide	Bio-Rad Laboratories Inc. [US]
Agarose	Sigma Aldrich [US]
Adenosine-Triphosphate	Sigma Aldrich [US]
Albumin Fraction V, bovine	Carl Roth® [DE]
Amidoblack	Applichem GmbH [DE]
Amphoterexin	Sigma Aldrich [US]
Ammoniumperoxidsulfate	Carl Roth® [DE]
B27-supplement	Life technologies [US]
Brilliant blue	Carl Roth® [DE]

…Table 3 continued.

Chemical	Supplier
BioTracker 655 Red	Sigma Aldrich [US]
Bromphenolblue	Sigma Aldrich [US]
Carbamoylcholinchloride	Acros Organics [US]
Colloidal gold total protein stain	Bio-Rad Laboratories Inc. [US]
cOmplete™, free protease inhibitor cocktail	Roche [US]
Dimethyl sulfoxide (DMSO)	Sigma Aldrich [US]
DNase I	Hoffmann-La Roche [CH]
Dulbecco's Modified Eagle Medium (DMEM)	Sigma Aldrich [US]
DMEM/F12 1:1	Life technologies [US]
Fetal calf serum, heat inactivated	Life technologies [US]
Formic acid	Chemical depository, RUB [DE]
Glial derived neurotrophic factor (GDNF)	Merck Millipore [DE]
GlutaMAX™ Supplement	Life technologies [US]
HEPES	VWR Chemicals [US]
Ethanol absolute	Sigma Aldrich [US]
Ethanol tech.	VWR Chemicals [US]
Ethidium Bromide	Carl Roth® [DE]
Fetal Calf Serum	Sigma Aldrich [US]
Formaldehyde, 30% Solution	Carl Roth® [DE]
Fura-2-AM	Abcam [UK]
Gelatin	Merck KGaA [DE]
Glycerin	Carl Roth® [DE]
Hank's Balanced Salt solution Ca_{2+} free	Sigma Aldrich [US]
Incidin® Plus	Ecolab Deutschland GmbH [DE]
Isopropanol	VWR Chemicals [US]
Kynurenic acid	Sigma Aldrich [US]
N,N,N,N'-Tetramethylendiamin (TEMED)	Merck Millipore [DE]
Laminin	Sigma Aldrich [US]
Mannitol	VWR Chemicals [US]
Milk powder	Carl Roth® [DE]
Methanol	VWR Chemicals [US]
MitoTracker™ RED CMXRos	Invitrogen™ [US]
Neurobasalmedium A	Life technologies [US]
Nuclease-Free Water	Promega [US]
Papain	Worthington biochemical corporation [US]
Penicillin/Streptomycin	Life technologies [US]
Percoll	Sigma Aldrich [US]
Phenol red	Sigma Aldrich [US]
Pre-stained Protein Ladder	Abcam [UK]
Poly-D-Lysine	Sigma Aldrich [US]
Pluronic® F-127 (20% in DMSO)	Invitrogen™ [US]
Phosphate Buffered Saline	Sigma Aldrich [US]

…Table 3 continued.

Chemical	Supplier
Proteinase K, recombinant PCR grade	Roche [US]
PVDF membrane	Carl Roth® [DE]
Restore western blot stripping buffer	Thermo Fischer Scientific [US]
Sodiumdodecylsulfate (SDS)	Carl Roth® [DE]
Sucrose	Applichem GmbH [DE]
Titriplex® (EDTA)	Merck KGaA [DE]
Titriplex® IV (EGTA)	Merck Millipore [DE]
Trichloric acid	Applichem [DE]
Tris-base	Carl Roth® [DE]
Tris-HCl	Carl Roth® [DE]
Triton-X	Sigma Aldrich [US]
Trypsin EDTA	ThermoFischer Scientific [US]
Trypsin inhibitor	Sigma Aldrich [US]
Tween20	VWR Chemicals [US]

2.1.4 Kits and products

Kits and products used in this thesis are listed in the table below. Products which are not listed are considered basic laboratory equipment.

Table 4: List of kits and products utilized in this thesis. *Supplier and location of their headquarter are listed in the central column, the catalogue numbers are listed in the right column.*

Kits and products	Supplier	Catalogue No.
GeneXPlus Transfection Reagent	ATCC [US]	ACS-4004
RNase-ZAP	Thermo Fischer Scientific Inc. [US]	AM9782
CellTiter 96 Aqueous One Solution Cell Proliferation Assay (MTS)	Promega GmbH [US]	G3582
GoTaq® qPCR Master Mix	Promega GmbH [US]	A6001
ReliaPrep Tissue RNA Miniprep Systems	Promega GmbH [US]	*Z6110*
RevertAid First Strand cDNA Synthesis Kit	Thermo Scientific™ [US]	K1622
ROTI® Mount FluorCare DAPI	Carl Roth® [DE]	HP20.1

…Table 4 continued.

Kits and products	Supplier	Catalogue No.
TC-Plate 24 Well, standard F	Sarstedt AG & Co [DE]	144530
TC-Plate 96 Well, standard F	Sarstedt AG & Co [DE]	20003796
Glass Bottom Dish 35 mm Sterile R	Ibidi [US]	81158
Open top polyclear centrifugation tubes	Seton scientific [US]	7031
Viromer RED	Lipocalyx [DE]	N/A
µ-Slide Luer I 0.8mm	Ibidi [US]	80196

2.1.5 Primer pairs

For the evaluation of the performed NGS analysis, a high number of primers had to be designed to be used in qPCR verification experiments. A complete list containing the sequence of used primers can be found in the attachment (table 19/20).

2.1.6 siRNA and plasmids

Table 5: Plasmids and SiRNAs used*. Catalogue number or sequence are listed as well as supplying company.*

Plasmid / siRNA	Catalogue No. / Sequence	Supplier
pEGFP-LC3	#21073	Addgene [US]
pCMV R-Cepia1er	#58216	Addgene [US]
Rcn1 Mouse untagged	# MC202694	Origene [IN]
Rcn1 siRNA 1	UUUAGCGACAUUAUCAUAG	Sigma Aldrich [US]
Rcn1 siRNA 2	UACCCUUGACAACUAUAGC	Sigma Aldrich [US]
Rcn1 siRNA 3	ACAUGUCCGCGAUGUACUC	Sigma Aldrich [US]
Trilencer-27 Universal scrambled negtive control siRNA duplex	SR30004	Origene [IN]

2.1.7 Solutions

Table 6: List of working solutions. *Solutions were prepared by the technical workersof the department and the composition is given in the right column.*

Solution	Content
Amidoblack discolor solution	Acetic Acid (20% v/v) Methanol (80% v/v)
Amidoblack staining solution	Amidoblack (0.24% w/v) Methanol (35% v/v) Acetic acid (10% v/v) in *A. dest.*
APS solution	Ammoniumperoxidsulfate (10% w/v) in *A. dest.*
Astrocyte digestion solution	DNase I (0.04 mg/ml) Trypsin (0.01 M) in PBS
Astrocyte growth medium	FCS (10% v/v) Penicillin (100 U/ml) Streptomycin (100 U/ml) Fungizone (2.5 mg/ml) in DMEM, high glucose
Astrocyte trituration solution	Trypsin inhibitor (0.5 mg/ml) DNase I (0.002 mg/ml) BSA (1mg/ml) in *A dest.*
Brain fractionation Buffer I	Mannitol (225 mM) Sucrose (75 mM) EGTA (0.5 mM) BSA (0.5% w/v) Tris-HCl (30 mM, pH 7.4) In *A.dest.*

…Table 6 continued.

Solution	Content
Brain fractionation buffer II	Mannitol (225 mM) Sucrose (75 mM) BSA (0.5% w/v) Tris-HCl (30 mM, pH 7.4) In *A.dest.*
Brain fractionation Buffer III	Mannitol (225 mM) Sucrose (75 mM) Tris-HCl (30 mM, pH 7.4) In *A.dest.*
Brain fractionation buffer IV	Mannitol (225 mM) EGTA (1 mM) HEPES/KOH (5 mM, pH 7.4) In *A.dest.*
Collection buffer	Tris (1 M), pH 6.8 *in A. dest.*
Collection gel	Acrylamid/Bisacrylamid (5% v/v) Collection buffer (13% v/v) SDS (0.1% w/v) TEMED (0.1% v/v) APS (0.2% w/v) in *A. dest.*
Gelatin solution	Gelatine (1% w/v) in *A. dest.*
Laminin solution	Laminin (2.7 µg/ml) in *A. dest.*

…Table 6 continued.

Solution	Content
Neuronal growth medium	FCS (1% v/V) B27 supplement (2% v/v) Glutamax (0.1% v/v) 5-FDU (16.5 µg/ml) GDNF (10 ng/ml) in Neurobasalmedium A
Papain solution	Cysteine (1 mM) $CaCl_2$ (1.52 mM) Papain (20 U/ml) Phenol red (0.001% v/v) Kynurenate (0.5 mM) HCl (differs, pH set to 7.4) NaCl (23.2 mM) KCl (1.08 mM) $NaHCO_3$ (5.2 mM) $NaH2PO_2$ (0.4 mM) $MgSO_4$ (0.2 mM) EDTA (0.1 mM) Glucose (5 mM) in *A. dest.*
PDL solution	Poly-D-Lysin (20 µg/ml) in *A. dest.*
Percoll solution	Percoll (30% v/v) Mannitol (157.5 mM) EGTA (0.7 mM) HEPES/KOH (17.5 mM, pH 7.4) In *A. dest*
Protein elution solution	Acetic acid (80% v/v) Formic acid (10% v/v) Trichloric acid (1% w/v) in *A. dest.*

…Table 6 continued.

Solution	Content
Proteinase K buffer	NaCl (100 mM) Tris (10 mM), pH 7.5 – 8.0 EDTA (25 mM) SDS (0.5% w/v) Proteinase-K In *A. dest.*
Separation buffer	Tris (1.5 M, pH 6.8) in *A. dest.*
Separation gel	Acrylamid/Bisacrylamid (10% v/v) Separation buffer (25% v/v) SDS (0.1% w/v) TEMED (0.04% v/v) APS (0.2% w/v) in *A. dest.*
TAE Buffer	Tris base (40 mM, pH 8.0) Acetic acid (20 mM) EDTA (1 mM)
TBST buffer	Tris (20 mM) NaCl (137 mM) Tween20 (0.1% v/v) in *A. dest.*
TE Buffer	Tris (10 mM) EDTA (1 mM) in *A. dest.*
Transfer buffer	Tris (20 mM) Glycin (192 mM) Methanol (20% v/v) in *A. dest.*
Trypsin-EDTA solution	Trypsin (2.5% w/v) EDTA (0.2% w/v) in *A. dest.*

2.1.8 Devices

This section contains the devices used in this thesis to perform experiments. Not listed devices are considered as basic research equipment.

Table 7: List of devices used. *The manufacturer and its country are also listed.*

Device	Manufacturer
Inverse Fluorescence-Microscope DMI4000	Leica Microsystems GmbH [DE]
Camera DFC350 FX	Leica Microsystems GmbH [DE]
Camera CoolSNAP EZ	Photometrics [US]
Camera EOS 600D	Canon [JP]
GloMax Discover Microplate Reader	Promega [US]
Gel Doc™ XR Imaging System	Bio-Rad [US]
Gene Pulser® II	Bio-Rad [US]
NanoDrop™ 2000 Spectralphotometer	Thermo Fischer Scientific [US]
Optima L-70K	Beckmann Coulter [US]
Robo Cycler 96	Stratagene [US]
Rotor-Gene Q	QIAGEN [DE]
SW40 rotor	Beckmann Coulter [US]
VisiChrome High Speed Polychromator System	Visitron Systems GmbH [DE]
Mikroskop LSM 510 Axiovert 200M	Carl Zeiss AG [DE]

2.1.9 Software

Table 8: List of commonly used software for analysis and data generation. *Software version, company, and type of application are also listed.*

Software / Version	Company	Application
Adobe Illustrator CS6 16.0.0	Adobe, 2012	Software to create figures
BLASTN	U.S: National Library of Medicine	Search for transcript sequences
Cell profiler™ 3.1.8	Carpenter lab 2003	Subcellular analysis
Cuffdiff 2.2.1	Trapnell Lab, Department of Genome Science, University of Washington [US]	Part of NGS analysis pipeline
Cufflinks 2.2.1 Hisat 2.2.1	Trapnell Lab, Department of Genome Science, University of Washington [US] Baruzzo et al., 2017	Part of NGS analysis pipeline Aligning algorithm
ImageJ 1.53c	National institute of Health [US]	Software to analyse image series
Integrative genomics viewer 2.3.91	National Cancer Institute 2013 [US]	SNP Analysis
Metafluor	Visitron Systems GmbH [DE]	Calcium imaging
Microsoft Excel 2016	Microsoft Cooperation 2016 [US]	Software to create tables
Microsoft Word 2016	Microsoft Cooperation, 2016 [US]	Text-writing tool
Nanodrop™ 2000 1.4	ThermoFischer Scientific 2014 [US]	Nucleic acid quantification and QC
Primer-BLAST	National Center for Biotechnology Information 2012 [US]	Algorithm to pick adequate primers
Rotor-Gene Q Series 2.1.0	QIAGEN, 2014 [DE]	Software to measure expression data
SamTools 0.1.19	Wellcome Trust Sanger Institute [UK]	Part of NGS analysis pipeline
SigmaPlot 12.5	SYSTAT, 2013 [US]	Statistical analysis and graphic design
Zen 2.3	Carl Zeiss Microscopy GmbH, 2011 [DE]	Capture and edit images

2.2 Methods

The following sections precisely describe the methods used in this project to allow data replication.

2.2.1 Optimization of the NGS analysis

In this thesis, a previously generated transcriptome dataset of *substantia nigra* tissue of adult Padel wild type, Padel homo, and Basyn mice (Osenberg, 2018) was reanalyzed with an updated methodology to ensure robust results as a basis for subsequent confirmation efforts.

The transcriptome sequencing of the samples was performed in cooperation with the Cologne Center of Genomics (CCG), which performed sequencing and quality control for the generated samples. The subsequent analysis of generated reads was performed by Katharina Osenberg in her thesis with the Tophat2 aligning tool and the Cuffdiff expression analysis tool. (Osenberg, 2018) The exact methodology of the whole analysis pipeline and quality control can be studied in her thesis. The key hallmarks of the analysis are summarized in the following section.

Briefly, paired-end reads were generated with the Illumina sequencing technology with an average yield of 34 million paired reads with an average length of 75 base pairs per sample. The reference genome used was the annotated igenome mm10 (GRCm38/mm10). The alignment was performed with the default settings of Tophat2. Transcriptome assembly was done with the Cufflinks algorithm, which estimates the expression of each gene per sample including parameters like the number of isoforms for the calculation, thereby generation FPKM values (fragments per kilobase per million mapped fragments) for every gene in every sample. The differential expression analysis was performed with Cuffdiff, a program comparing completely assembled transcriptomes against each other to identify differences in gene expression (2.2.1) via the assumption of the negative binomial distribution and the correction for the often-

underestimated dispersion rate of the dataset (Trapnell et al., 2013). A false discovery rate of 5% was allowed and the significance level was set to p<=0.05.

In this thesis, a new alignment tool on the market has been utilized to repeat the aligning process with higher accuracy and thereby optimizing the expression analysis to yield results of higher quality. The Tophat2 aligning algorithm has been replaced with the Hisat2 algorithm, which is basically a successor of the Tophat2 software (Pertea et al., 2016; Baruzzo et al., 2017; Kim et al., 2019).

The following command lines were used to replace the command lines in the previously performed NGS analysis of Osenberg:

```
hisat2 -x /home/admintb/bioinfo/mm10/genome -1 K002000102_56102_1.fq -2
K002000102_56102_2.fq -S accepted_hits.sam -q—rna-strandness RF
```

The command line above aligns the generated reads to a reference genome and generates a sam file for further processing. The subsequent analysis was replicated from Osenberg in the following fashion.

```
samtools view -bS accepted_hits.sam > accepted_hits.bam
samtools sort accepted_hits.sam > my_sorted_accepted_hits.bam
samtools index my_sorted_accepted_hits.bam
```

This command transforms the generated sam files into bam files.

```
cufflinks -o mm10 -G /home/admintb/bioinfo/mm10/genes.gtf
my_sorted_accepted_hits.bam
```

The transcripts get assembled and their abundance estimated with this command, finally assigning FPKM values to each gene.

cuffmerge -o /home/admintb/Schreibtisch/NGS_Parkinson_Auswertung/merged_asm_PWT_PHO_SN -g /home/admintb/bioinfo/mm10/genes.gtf /media/admintb/max/NGS_Parkinson_1B/Cuffmerge_assembly_list_PWT_PHO_SN.txt

The Cuffmerge then assigns group identifiers to all analyzed samples as a basis for subsequent differential expression analysis.

cuffdiff -p 4 -o /home/admintb/Schreibtisch/NGS_Parkinson_Auswertung/Cuffdiff_SN_PWT_PHO_PC -use-sample-sheet /home/admintb/Schreibtisch/NGS_Parkinson_Auswertung/merged_asm_PWT_PHO_SN/merged.gtf /media/admintb/max/NGS_Parkinson_1B/SN_sample_sheet_PWT_PHO.txt—library-type fr-firststrand—dispersion-method per-condition

The Cuffdiff command performs the actual differential expression analysis assuming a negative binomial distribution and corrects the dispersion rate of the data set.
These command lines were just one part of the analysis pipeline showing the workflow with one sample of the whole dataset.

2.2.2 Dissection of *substantia nigra* and *striatum* of one-year-old mice

To obtain samples from *substantia nigra* and *striatum*, the necks of one-year-old Padel WT, Padel homo, as well as Basyn were dislocated, the brain was removed from the skull and a brain slice matrix was used to slice the tissue. A razor was used to cut the *substantia nigra* and the *striatum* out of the slice and the samples were frozen in liquid nitrogen immediately to minimize RNA degradation.

2.2.3 RNA isolation and quantification

The RNA isolation from dissected brain regions was performed with the Relia Prep RNA Miniprep Systems according to the manufacturer's instructions. The isolated RNAs were analyzed photometrically using the Nanodrop™ 2000 device to obtain concentration and purity. The quality of used RNAs was assessed using the 280/260 and the 260/230 ratios.

2.2.4 cDNA synthesis

The cDNA synthesis of isolated RNA was performed with the RevertAid First Strand Synthesis Kit, following the instructions provided by the manufacturer. Random primers were used for reverse transcription to provide an unbiased basis for the following qPCR experiments.

2.2.5 Real-time semi-quantitative PCR

The method of real-time semi-quantitative PCR (RT-qPCR) was used to perform the expression analysis in this project as an independent method for verification of obtained NGS results.

RT-qPCR enables relative quantification of mRNAs within a sample utilizing a PCR reaction with implemented fluorescence measurement after each amplification cycle. The fluorescence signal is proportional to the generated PCR product due to a dye intercalating with double-stranded DNA which is added to the reaction mix. This results in a graph like the one depicted below. The normalized fluorescence is displayed against the amount of conducted PCR cycles.

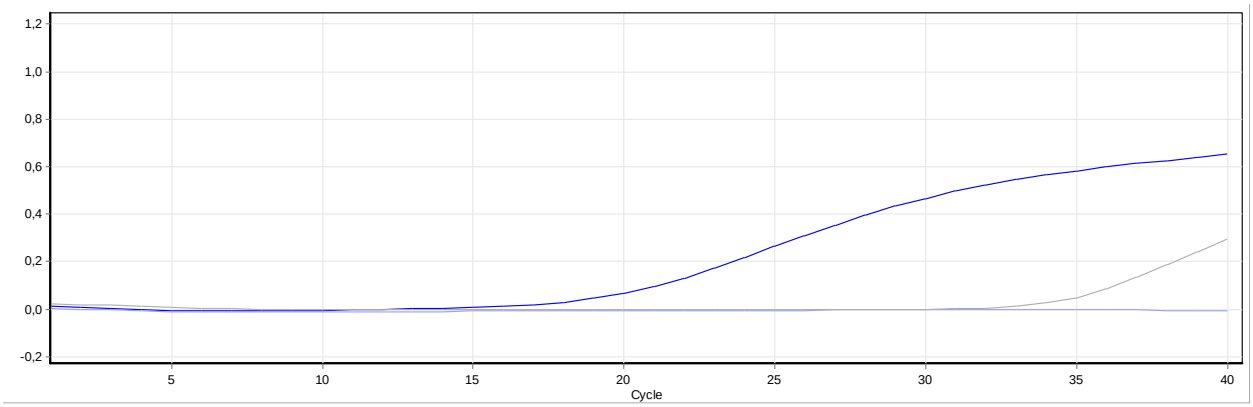

Figure 1: Exemplary fluorescence curve obtained during Rcn1-product amplification using SN RNA of a one-year-old Padel wild type mouse*. The normalized fluorescence is displayed against the corresponding cycle number (blue saturation curve). Non-template control (NTC) was run to test for nucleic acid contamination in the primer solution or the master mix (light blue). Control without reverse transcriptase (RT^-) in the cDNA synthesis step was run to check for genomic contamination (grey).*

To generate values, which can be compared between samples, a threshold must be defined. Although generally arbitrary, it is commonly chosen at the beginning of the logarithmic phase of the amplification curve. It is important to set the threshold for each gene at the same height between all samples to ensure comparability. In this thesis, a threshold of 0.1 was selected as default and corrected manually if the curve was not yet in its exponential phase. The amplification cycle, at which the defined threshold is crossed, represents the so-called CT value, which is an abstract value for the expression level of the target gene. To further enhance comparability between samples and correct for different amounts of starting cDNAs, reference genes are quantified beneath the genes of interest for every sample. It is assumed, that the expression level of reference genes is stable through all samples. To normalize expression values of the gene of interest, its CT value is put into relation to the CT value of the reference gene by subtraction, thereby generating a normalized, comparable number: the ΔCT value.

For the means of replicability, the specifications of the used qPCR program are described in the following table.

Table 9: Specification of the used RT-qPCR program. *The mentioned melting phase is part of the performed quality control and will be discussed in 2.2.6.*

Initial phase
2 minutes at 95° C
Amplification phase (40x)
15 seconds at 95° C 90 seconds at 60° C
Melting phase
Pre-melting for 90 seconds at 50° C Increase 0.5° C every 5 seconds to 99° C

In theory, the amount of PCR product should double in every amplification cycle, but this depends on multiple parameters like primer properties or the presence of PCR inhibitors from cDNA synthesis. Differences in amplification efficiency between target and reference genes can cause technical variance. Although these differences are small in relative quantification compared to a quantitative approach, oligo efficiencies of each primer pair were determined via cDNA dilution series and calibration curves. One example of such a curve is shown below.

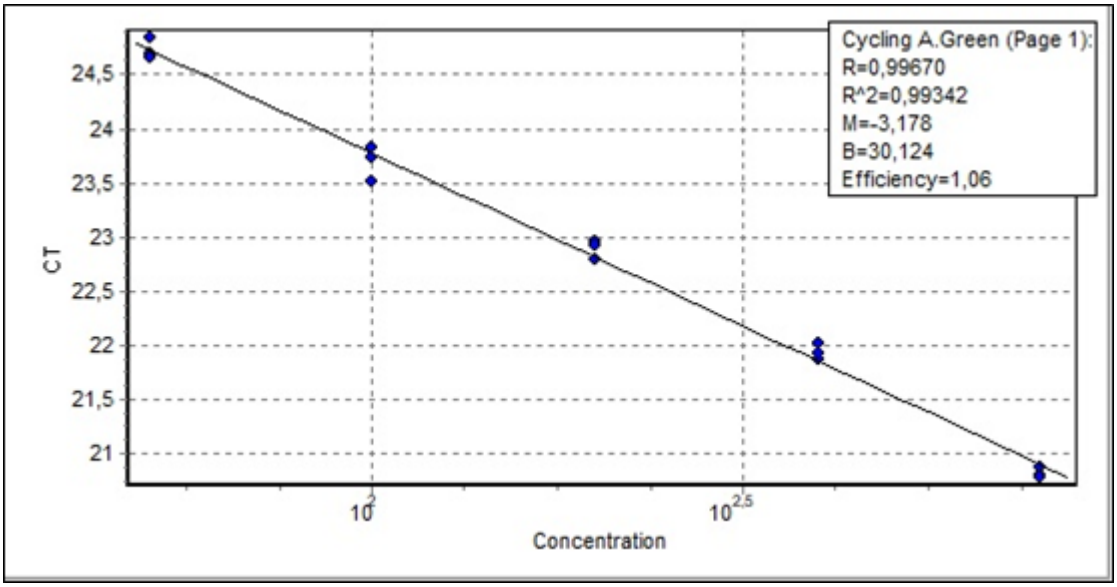

Figure 2: Example calibration curve for the determination of oligo efficiency (Rcn1). *Depicted is the CT value, which is plotted against the logarithmic concentration of cDNA. The box in the upper right shows slope, coefficient of determination, and efficiency of the primer pair.*

2.2.6 Strategy of experimental design and quality control for the qPCR analysis for the verification of candidate genes

Thoughtful quality control and analysis are essential for reliable data generation in the field of expression analysis. This section deals with different considerations to ensure the high quality of generated data.

Repetition of the transcriptome analysis to ensure an optimal starting point for verification

The starting point of this analysis was obtained transcriptome data of Padel, Basyn, and Padel wild type mice to potentially identify new key players in PD pathogenesis. Multiple quality control measures were performed to check the quality of used samples, like an RNA integrity analysis using a bioanalyzer. Additionally, generated transcriptome data were analyzed regarding its quality with the FastQC software (Osenberg, 2018).

To ensure an optimal starting point for qPCR verification, a new aligning algorithm was used to reanalyze NGS expression raw data (section 3.1).

The performed transcriptome analysis had a very low sample size (n=4), which is predestined to cause a high false-positive rate due to low statistical power (Button et al., 2013). This makes an evaluation of these differentially expressed genes (DEG) with an independent method essential before further analysis. Confirmation of changed gene expression in PD mouse models with two different methods is a robust approach to identify targets, which might be involved in PD pathology.

Identify priority targets for verification

The examination of 451 DEGs in the *substantia nigra* in Padel mice and 209 DEGs in the *substantia nigra* of Basyn mice is very time-consuming and expensive, therefore a strategy was developed to identify priority targets for qPCR verification. The first consideration to identify promising DEGs was to prioritize genes, which were differentially expressed in both mouse models, possibly representing essential genes

involved in both forms of PD. This approach condensed the priority list to 150 genes, which were tested in the Padel mouse model at first since its genetic alteration is closer to human PD pathogenesis.

This priority list was sorted using the variance of the different groups, beginning with genes, whose FPKM values were clearly separated between the different mouse models. This is the reason, why the candidate genes are not displayed in alphabetical order.

Choosing multiple reference genes for verification

Normalization of generated CT values is a critical part of qPCR analysis. It corrects variance caused by different amounts of starting material in the PCR reaction. Small differences can have a great impact on quantification, due to the exponential nature of this method. Reference genes are thought to have a stable expression through all samples, thereby allowing to compare the expression of genes of interest (GOI) in relation to those reference genes (Thellin et al., 1999). Unfortunately, different studies have demonstrated, that the expression of reference genes can vary between different tissues and conditions (Hsiao et al., 2001; De Jonge et al., 2007; Chari et al., 2010). Consequently, multiple reference genes were established to reliably test the differential expression of target genes (Vandesompele et al., 2002; Bustin et al., 2009).

To identify promising targets with efficient cost and time consumption, candidate genes will be tested against Hypoxanthin-Guanin-Phosphoribosyltransferase (Hprt) at first, which is a classical reference gene that should give a first orientation (de Kok et al., 2005; Martino et al., 2011). Every confirmed gene will be subsequently tested against a broad panel of reference genes as a measure of quality control. The common reference genes Acvrl1, Aes, Eif4g2, and Ube2d2a were chosen to bolster the confirmation panel (Eisenberg et al., 2003; Svingen et al., 1999; Velculescu et al., 1999). Two additional reference genes were selected manually utilizing the generated transcriptome data. Mgrn1 and Oxr1 exhibited only minimal variance in FPKM values between all three mouse lines indicating stable expression in the *substantia nigra* of the adult mouse brain.

Technical replicates to minimize the technical variance

The use of technical replicates is another basic form of quality control, minimizing technical variance in qPCR experiments. In this thesis, technical triplicates were used to minimize variation by averaging. If one value of the triplicate deviates strongly from the other two replicates (≥2CT), a methodical error is assumed, and the aberrant value was excluded from further analysis and, the other replicates were averaged.

Primer design considerations

Primers were designed to meet multiple criteria to ensure reliable results. If possible, 20 base pair long primers with a GC content of 50% were designed, resulting in a product of 130-170 base pairs. Each primer pair was intron spanning to prevent the amplification of genomic DNA residues in the qPCR reaction. The primers were chosen to amplify all known splice variants. A dilution series was conducted for each primer pair aiming for a PCR efficiency of 100%. However, this could not be achieved for every primer pair.

Contamination analysis with non-template controls and RT^- controls

It is important to check for contamination sources in reagents and cDNA samples, since unwanted nucleic acids could act as a template for the PCR, thereby altering the resulting CT values and consequently disrupting accurate expression analysis. In order to do so, non-template controls (NTC) were used, which contained nuclease-free water instead of a cDNA sample. If a fluorescence signal is measured during the qPCR, it must be caused by contaminated reagents. Fluorescence emitting NTCs are repeated once with new nuclease-free water to exclude the possibility of contaminated water or contamination of the tube by air particles. If fluorescence still occurs, the primer solution and qPCR master mix were replaced.

Another essential control check is for genomic contamination in the RNA sample. PCR amplification of genomic DNA is visible in the melting curve since all primers were designed intron-spanning and consequently the product of genomic templates has a higher product length and melting temperature. To prevent the amplification of genomic

DNA, a DNase digestion step was included in RNA isolation. However, the remaining genomic residue cannot be excluded. To further ensure uncontaminated RNAs, an RT control was run for each gene. These controls use samples in the qPCR reaction, which did not contain reverse transcriptase (RT-) in the cDNA synthesis step. Any fluorescence caused by these controls, if the NTCs are blank, must be caused by genomic templates in the sample.

Since PCR reactions are based on an exponential function, minimal traces of contamination can ultimately lead to fluorescence after 40 cycles. Therefore, fluorescent controls with CT values with a difference of 10 compared to their corresponding sample, were considered unproblematic since the expression is more than 1024 times lower and won't impact the analysis.

Melting analysis to ensure primer specificity

The melting analysis is a powerful tool to investigate if primer pairs only amplify the desired target in a qPCR reaction. This analysis step is routinely performed after each qPCR run as part of the basic protocol. A slowly increasing temperature ramp is performed with a fluorescence measurement after each increase. Each PCR product has a specific melting temperature, depending on product length, and GC content. Since the intercalating DNA dye needs double-stranded DNA to be fluorescent, the temperature ramp reveals the exact melting temperatures of each product in the sample. This control gives insight into the presence of unwanted amplicons or primer dimers, which could emit fluorescence and distort the measured CT values. Primer pairs causing an unclean melting curve were reordered until specificity could be guaranteed. A picture of a clean melting curve is shown below.

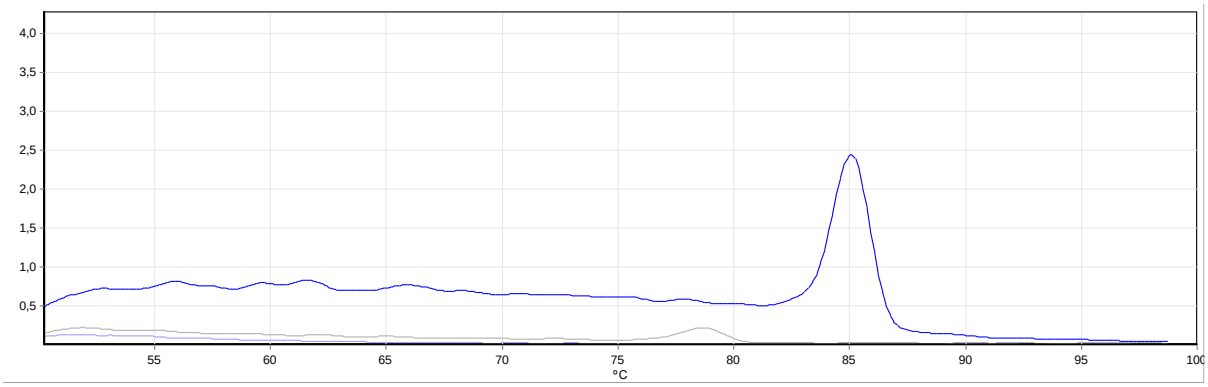

Figure 3: Melting curve for primer specificity confirmation. *Rcn1 amplicon of substantia nigra RNA of a Padel wild type mouse. Displayed is the change in fluorescence level depending on the temperature. The analysis revealed a single peak at ca. 85° C (blue), indicating the absence of undesired PCR products. The RT- is displayed in grey, NTC in light blue.*

As an additional measure to ensure primer specificity, the PCR product of each primer pair including NTC and RT- controls were placed onto an agarose gel (2% w/v in TAE buffer) and run at 80V for one hour.

Only primer pairs which did not produce additional bands on the gel were used in qPCR experiments. An example gel is shown below.

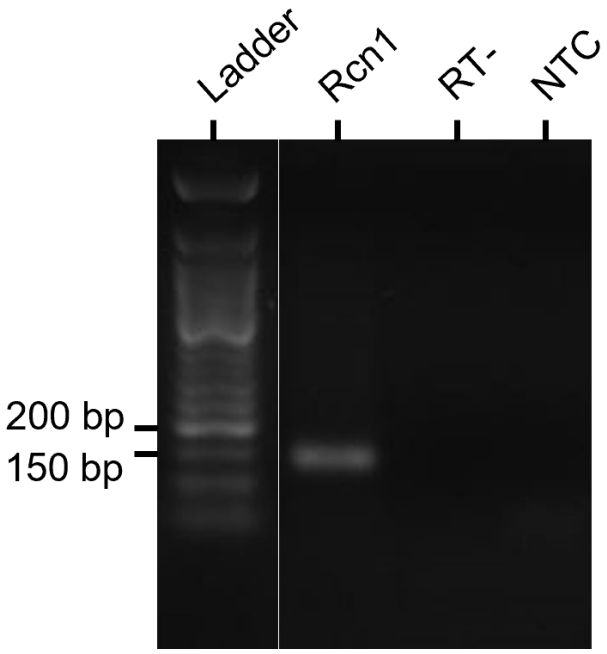

Figure 4: Exemplary gel electrophoresis image to further confirm primer specificity. *An agarose gel (2%) loaded with Rcn1, RT-, and NTC PCR products as a quality control measure for Rcn1 primer sensitivity and specificity. Expected band height: 142 base pairs. RT- and NTC controls need to be blank to proceed to qPCR experiments.*

The sum of all quality control measures should enable robust data generation. Generated ΔCT values of each group were tested for statistical significance with the Mann-Whitney rank-sum test with an α of 0.05 in the Sigmastat software.

2.2.7 Cell culture

Primary mesencephalic astrocytes

Astrocytes were prepared from the *mesencephalon* of neonatal Padel or Dendra pups and the corresponding littermates. To ensure a sufficient amount of cells for vital cultures, tissue of two pups was pooled following dissection. After removing the meninges, the *mesencephalon* was dissected, and diced into small fragments. The chunks were incubated in astrocyte digestion solution at 37°C for 15 min, followed by centrifugation (300g, 3min). The pellets were resuspended in trituration solution with perforated pipette tips, (22 Gauge, 23 Gauge, 27 Gauge). Cell suspensions were centrifuged (300g, 3min), and the pellets were resuspended in astrocyte growth medium and seeded on poly-D-lysine (20µg/ml) coated T25 cell culture flasks. Cultivation was performed at 37°C with 5% CO_2. Culture media were refreshed twice per week. After 14 days, cultures were shaken for 120 minutes at 37°C to remove unwanted cell types and subsequently seeded in 35 mm glass-bottom dishes for experiments (80.000 cells).

Primary postnatal ventral midbrain neurons

Postnatal instead of embryonic neurons were cultivated during this thesis since the number of already differentiated cells with dopaminergic character is much higher in the neonatal developmental state.

For the cultivation of postnatal ventral midbrain neurons, it is mandatory to seed freshly extracted cells on a mature astrocytic feeder layer to ensure neuronal survival. One day before preparation, cell culture dishes containing mature, confluent astrocytes

were preconditioned with neuronal growth medium to further increase neuronal survival after extraction.

In the preparation procedure, the mesencephalon of neonatal mouse pups was removed as described in the section above and sliced into small pieces. Subsequently, the tissue chunks got incubated in papain solution for 15 min, which was specifically designed to digest the tissue gently and avoid excitotoxicity. The solution was carefully removed, and the tissue was washed multiple times with neuronal growth medium. Trituration with perforated pipette tips was performed to create a cell suspension, which was subsequently centrifuged at 300g for 5 min. Cells were resuspended in a small amount of neuronal growth medium and counted in a Neubauer chamber. 100.000 cells were seeded in a small volume on the prepared preconditioned astrocytic feeder layers. Co-cultures were incubated at 37°C for 7 days and then used for experiments. Since neurons are very sensitive to media exchange, the only preconditioned medium was used for co-cultures and the medium was only exchanged partially (50%). To increase the medium/cell ratio, 30 mm dishes with small wells were used thereby slowing down medium consumption.

Cultivation and transfection of primary murine fibroblasts

The following sections contain the cultivation procedures for murine primary fibroblasts as well as their transfection protocol.

Thawing:

Frozen murine embryonal fibroblasts were thawed in a 37°C water bath and subsequently diluted in 10 ml DMEM/10% FCS to reduce DMSO concentration, which was added before freezing as cryoprotection. The liquid was removed through centrifugation (300g, 3min) and resuspended in 10 ml DMEM/10%FCS and transferred into a T75 flask for cultivation at 37°C with 5% CO_2. The medium was exchanged the next day to remove DMSO residue.

Passaging/ seeding:

For passaging of primary murine fibroblasts, flasks were washed with PBS (0.01M) to remove FCS, which can interfere with cell detachment. Afterward, cells were incubated with Trypsin/EDTA Solution for 1 min at room temperature for detachment and separation. The enzyme was inactivated with 9 ml DMEM/10% FCS and removed via centrifugation (300g, 3min). 30.000 cells were seeded into the inner well of gelatin (1% w/v) coated 35 mm glass-bottom dishes. After cell attachment, dishes were filled up with medium 2-5 hours after seeding.

Transfection:

For the transfection of murine primary fibroblasts, cells were used 24 hours after seeding to guarantee cell density, differentiation, and vitality. The Viromer Red transfection reagent was used according to the instructions of the manufacturer's manual. Plasmid amount was experimentally determined with the MTS Assay. 250 ng LC3b-eGFP plasmid produced a sufficient number of transfected cells by maintaining 90% vitality (data not shown).

Cultivation and transfection of SH-SY5Y neuroblastoma cell line

For transfection and subsequent calcium imaging, the SH-SY5Y neuroblastoma cell line was utilized. The frozen cells were thawed from liquid nitrogen storage and diluted into DMEM/F12 medium containing 10% FCS. The remaining DMSO from the freezing process was removed by centrifugation (300g, 3min). Cultivation was performed in T25 flasks at 37°C at 5% CO_2. Only cells under passage 20 were used in the experiments.

For transfection, SHSY-5Y cells were detached from the flasks with Trypsin/EDTA (2.5%, 0.2%), which was removed by centrifugation afterward (300g, 3 min). Cell suspension (40.000 cells) was seeded into channel slides with Luer adapters. 24 hours later, transfection was performed with the GeneXPlus transfection reagent according to the instructions of the manufacturer.

2.2.8 Immunocytochemistry

For immunocytochemical staining, cells were fixated with Formaldehyde (4% v/v) for 15 minutes. Culture dishes were washed twice with PBS (0.01M) and subsequently blocked and permeabilized with 5% normal goat serum and 0.2% Triton-X for 45 minutes at RT. The solution was removed, and cells were incubated with primary antibody (in 0.01M PBS) overnight at 4°C.

Table 10: Dilution of applied antibodies used for immunocytochemistry experiments *is listed in the table below. Details on the antibodies are given in section 2.2.*

Antibody	Dilution
ß-Tubulin III	1:500
Gfap	1:500
Hsp60	1:2000
Hsp90b1	1:200
Rcn1	1:200

The next day, the cells were washed in PBS (0.01M) three times, and fluorescent secondary antibodies corresponding to the species of the primary antibodies were applied (1:300) and incubated for 60 min at RT. The secondary antibodies were washed away with PBS (0.01M) three times and fluorescence protection (Fluorocare) was applied to maintain signal strength.

2.2.9 siRNA delivery by electroporation

For silencing of Rcn1 gene expression in primary astrocytes, an siRNA transfection was conducted. For that, the “gene pulser electroporation system” was chosen, because traditional transfection reagents have shown poor efficiency on primary murine astrocytes.

The cells were detached from their flasks with Trypsin/EDTA (2.5%, 0.2%), which was diluted with medium to stop the enzymatic reaction and removed by centrifugation

(300g, 3min). The cell pellet was resuspended in medium and diluted to a concentration of 1.000.000 cells/ml. Three different Rcn1 siRNAs (section 2.6) were added to a final concentration of 100nM and transferred to an electroporation cuvette. The control group was treated with a nonsense scramble siRNA instead. Cuvettes were shocked three times at 300V and 250µF with an exponential decay function. Afterward, the electroporated cells were seeded for subsequent experiments.

2.2.10 Viability measurement with the MTS Assay

The Cell Titer 96® Aqueous One Solution Cell Proliferation Assay (MTS) was used to measure the vitality of electroporated siRNA treated primary murine astrocytes to ensure, that the process did not damage cells before calcium imaging.

In this assay, a formazan precursor is added to living cells, which will subsequently produce formazan, that can be measured in a spectrometer. The amount of formazan is directly proportional to the number of viable cells in the chamber.

Astrocytes were electroporated as already described (2.2.9) and subsequently, 15.000 cells were seeded into Poly-D-Lysin (20µg/ml) coated 96 well plates and received a medium exchange 24 hours later (100µl) followed by 20µl MTS reagent. The absorbance was measured in triplicates 2 hours later in a plate reader at 490 nm. Control conditions with unshocked cells and empty wells were also included in the analysis.

2.2.11 Calcium imaging in cultivated cells

For calcium imaging experiments with astrocytes, cells were seeded into closed channel slides with Luer adapters which enable the possibility of a constant liquid flow. The ratiometric cytoplasmatic calcium indicator Fura2-AM was used to visualize

calcium responses. Calcium-loaded Fura2-AM emits at 380 nm wavelength, while calcium-free Fura2-AM emits at 340 nm.

The dye was incubated for 30 minutes (37°C) at a concentration of 5 µM in an astrocyte growth medium together with 0.5% Pluronic F-127 (20% DMSO) to ensure balanced loading of Fura2-AM. The calcium dye was washed out with calcium-free Hank's balanced salt solution (HBSS) and the slide was placed in the microscope (DMI4000). The cells were excited alternately at 340 nm and 380 nm with an exposure time of 100ms (Visichrome monochromator). Pictures were taken at an emission of 510 nm (Filter BP 520/35 nm, BS 505 nm) resulting in ~3 pictures per second.

When the baseline response of Fura2-AM was steady under calcium-free HBSS flow, the Astrocytes were stimulated with 100 µM adenosine triphosphate ATP for 15s. The flow rate of the system was 1.3 ml/min. Cells unresponsive to ATP stimulus were excluded from the analysis.

For the calcium imaging of SH-SY5Y cells, the endoplasmic reticulum (ER) resident calcium indicator R-Cepia1er was used to test, if Rcn1 manipulation would alter the calcium dynamic of the cells. For this, the cells were excited at 561 nm and the emission measured at 584 nm. Stimulation was performed with 100 µM Carbachol for 5 minutes. Prolonged stimulation time is a consequence of ER calcium indicator, which requires a large amount of calcium release until calcium saturation in the ER is broken.

2.2.12 Fractionation of cell compartments via differential centrifugation

For the subcellular localization of Proteins, the approach of differential centrifugation was selected as a complementary method along with immunocytochemistry. Differential centrifugation utilizes a density gradient to separate cell organelles from each other. Those fractions can be characterized via western blot analysis.

Starting material for fractionation required five brains of three months old mice per biological replicate. C57BL6 and Padel mice were used in this analysis to see if

genotype influences the subcellular localization of target proteins. One day before procedure brain fractionation buffer (BFB) I-IV and Percoll solution were prepared. On the day of the procedure, mice were sacrificed via cervical dislocation, brains extracted and transferred into BFB-I and the brains were sliced into small pieces. Blood was removed by washing the tissue stripes with 20 ml BFB-III and subsequently homogenized in BFB-I with 12 slow strokes of a motorized Teflon homogenizer at 10 rcf. Unbroken material was spun down at 800g for 5min at 4°C. The pellet contains the crude mitochondrial fraction, while the supernatant contains the ER fraction and MAMs. The supernatant was transferred into a new tube and centrifugated again in the same manner to clear additional debris. Afterward, the supernatant was centrifugated at 16.000g for 20min at 4°C. The supernatant was transferred again and centrifuged at 100.000g for one hour at 4°C. The pellet contained the purified ER fraction.

The crude mitochondrial pellet was resuspended in 12 ml ice-cold BFB-II and centrifugated at 10.000g for 10min at 4°C. The supernatant was discarded, and the pellet was resuspended in 12 ml ice-cold BFB-III with subsequent centrifugation at 10.000g for 10min at 4°C. The pellet was resuspended in 2 ml ice-cold BFB-IV in an ultracentrifugation tube and 9 ml Percoll solution was added. The tube was ultracentrifuged in an SW40 rotor at 95.000g for 30min at 4°C in slow brake mode. This step separates the pure mitochondrial fraction from the MAM fraction. The MAM band can be seen as a white cloudy band in the middle of the gradient, while the pure mitochondrial fraction is a yellow band close to the bottom of the tube. Fractions can be extracted with a thin Pasteur pipette and transferred into new centrifugation tubes.

To remove the remaining Percoll from the pure mitochondrial fraction, 13 ml ice-cold BFB-IV was added, and the solution was centrifuged at 6.000g for 10min at 4°C. The pellet contained the pure mitochondrial fraction. The Percoll contaminating the MAM fraction was removed by adding 13 ml BFB-IV with subsequent centrifugation at 100.000g for 1 hour at 4°C in the SW 40 rotor. The pure MAM fraction is visible as a white band at the bottom of the tube. Every isolated fraction is resuspended in TE buffer for protein yield determination and western blot analysis.

This protocol is based on the publication of Schreiner and Ankacrona with slight modifications. It is recommended to read the publication if reproduction of these experiments shall be achieved (Schreiner and Ankacrona, 2017).

2.2.13 Protein determination

The determination of protein concentration is a necessary step before every western blot analysis. 10µl samples were poured on a cellulose acetate membrane. After drying, the membrane was incubated in amido black solution to stain containing proteins. The discolor solution was used to remove the excessive color from the membrane until the background of the membrane was completely discolored. When dried out, the membrane was dissolved in elution solution and the extinction of the eluate was measured photometrically at 630nm. Protein concentrations were calculated utilizing a standard curve for bovine serum albumin.

2.2.14 Western blot analysis

The expression of the target proteins was evaluated in the corresponding protein samples by western blot analysis using enhanced chemiluminescence (ECL). Mice were decapitated and *substantia nigra* tissue was homogenized in homogenization buffer (50 mM HEPES, 150mM NaCl, 10mM EDTA, 1% NP-40, 0.5% Na-deoxycholate, 0.1% SDS) containing complete protease inhibitor cocktail (Roche, Germany) using a Teflon/glass homogenizer at 4°C. After homogenization, samples were incubated on ice for 30min, followed by centrifugation for 20min at 12.000g. The supernatant was collected, and proteins were separated by electrophoresis on 15% polyacrylamide gels containing 0.1% SDS and transferred with 200mA for 1.5hr at RT onto a PVDF membrane. Blocking was performed with 3 % milk powder and 2% BSA in TBS-Tween (0.1% Tween, 20mM TBS) at RT for 1 hr. Incubation with the primary antibodies was performed in blocking buffer overnight at 4°C.

Table 11: Dilution of applied antibodies used for western blot experiments.
Details on the antibodies can be found in section 2.2.

Antibody	Fraction / Sample type	Dilution
ß-Actin	Whole protein	1:10.000
Calreticulin	Whole protein	1:1000
	ER fraction	1:5000
	Crude mito fraction	1:1000
	MAM fraction	1:5000
Lc3b	Fibroblast cell lysate	
Mfn2	Whole protein	1:1000
	ER fraction	1:1000
	Crude mito fraction	1:2000
	MAM fraction	1:2000
	Pure mito Fraction	1:2000
Rcn1	Whole protein	1:250
	ER fraction	1:250
	Crude mito fraction	1:250
	MAM fraction	1:500
	Pure mito Fraction	1:500
Sdha	Whole protein	1:20.000
	Crude mito fraction	1:20.000
	Pure mito fraction	1:20.000

Subsequently, the blots were washed with TBS-Tween20 and incubated with HRP-coupled secondary antibodies (anti-mouse / anti-rabbit HRP, 1:20 000). For detection, the membrane was washed three times in TBS-Tween, and signals were detected using the ECL-Plus system (GE Healthcare, Germany). To monitor the amount of proteins bound to the blots, they were stripped using Restore TM Western Blot Stripping buffer (Pierce, Rockford, IL, USA) according to the manufacturer's recommendations, followed by detection with the antibody mouse anti-ß-actin (1:10.000, BD Bioscience, Germany) for testing equal protein loading. For normalization against the whole protein amount, Coomassie blue (0.1 % w/v) staining or colloidal gold total protein staining was performed on the PVDF membrane for 1 hour.

2.2.15 Subcellular localization and quantification of mitochondrial-associated membranes and Rcn1 amount in primary fibroblasts

For the subcellular localization and quantification of mitochondrial associated membranes and rcn1 amount, 4% Formaldehyde fixated primary murine fibroblasts (P3-P5) were immunocytochemically stained with an Rcn1 antibody, a mitochondrial marker (Hsp60), and an endoplasmic reticulum marker (Hsp90b1). 5 Pictures were taken from each culture (n=8) with a small pinhole (0.45 µm) and every image was analyzed in the Cell Profiler™ software using a self-written pipeline with an emphasis on pixel colocalization. The first step of the pipeline was individually thresholding every channel with the Otsu thresholding algorithm (2.2.16) to cut background noise from every image. Individual cells were marked by shape manually and the drawn shape was applied to each channel to inversely mask surrounding cells in the image. Subsequently, masked images were merged to perform a pixel analysis to identify pixels that are above the threshold in more than one channel, thereby establishing a colocalization analysis approach.

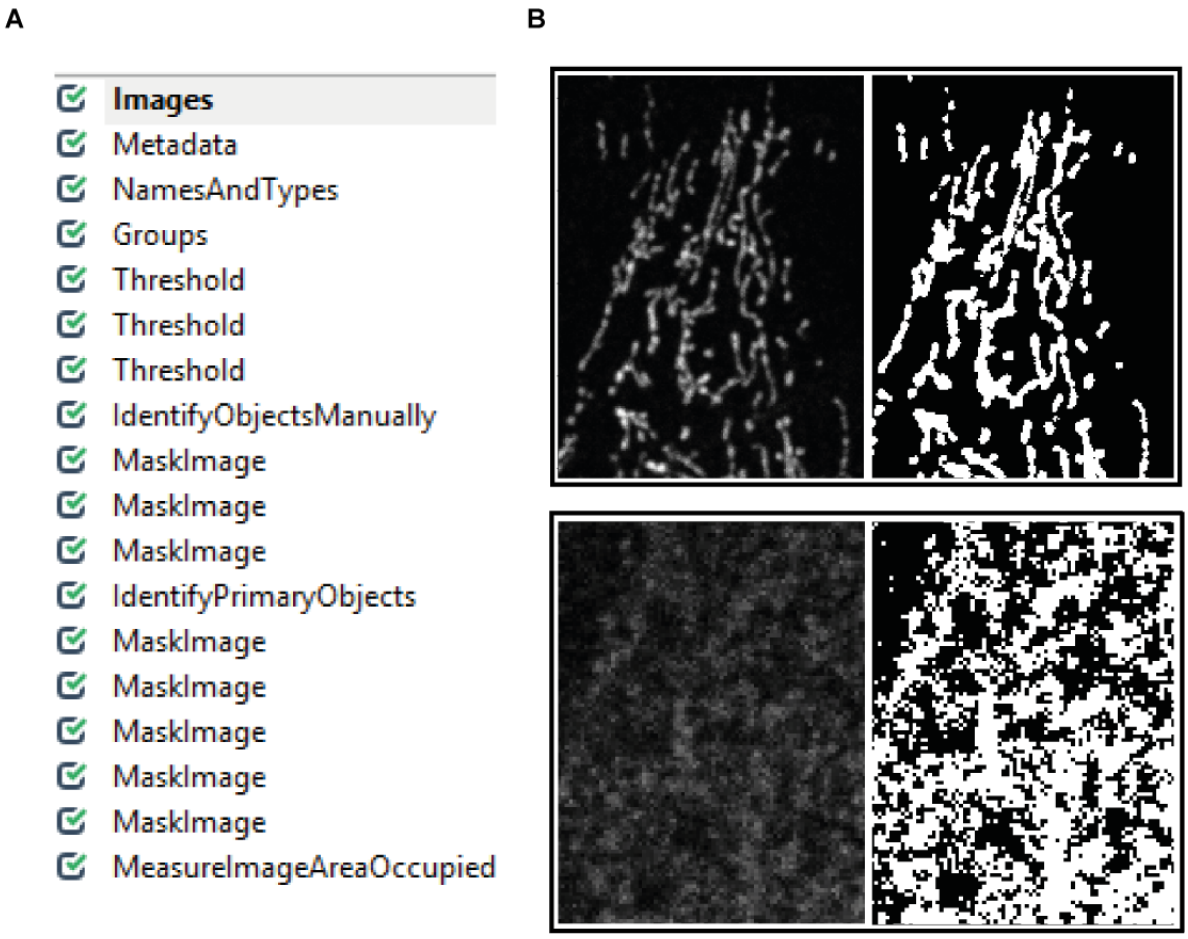

Figure 5: CellProfiler™ Image analysis pipeline for MAM identification and Rcn1 localization. *A: Displayed are the different modules for image processing. Key steps were thresholding to distinguish between signal and noise fluorescence, manually drawing the cell shapes around desired cells, and subsequently using different masks to identify signal locations present in different channels. B: Example images demonstrating the thresholding algorithm. Mitochondria were identified using object recognition utilizing, intensity, shape, and size of wanted objects (top images). The threshold of ER/Rcn1 was set based on image intensity because the staining pattern displayed no clear distinguishable shapes (bottom images).*

2.2.16 Mitophagy analysis in primary fibroblasts

For microscopic examination of mitophagy 80.000, Padel/WT fibroblasts were seeded into pdl/laminin (20µg/ml, 2.7µg/ml) coated cell culture chambers and transfected with 250ng LC3b-eGFP plasmid with the Viromer red kit according to the instructions of the manufacturer. On the next day, cultures were stained with the mitochondrial dye Mitotracker RED xmros (50nM) for 20min and subsequently washed 3 times with

DMEM/10% FCS. Transfected cells in living cultures were imaged in one focal plane (0.45µm) with a laser scanning microscope. Every n consists of 3-6 images.

The threshold in the LC3b channel (green) was selected manually in Zen2 to extinguish background staining leaving only green vesicular structures in the image. Mitochondria in the red channel were identified utilizing the object recognition algorithms of the cell profiler software. Objects between 5 and 50 pixels in diameter were accepted as possible candidates for recognition if they didn't touch the border of the image. The Otsu thresholding algorithm was chosen for object identification, which calculates the threshold by dividing pixels into three intensity categories by minimizing the variance in each category. The pixel intensity parameter was used to distinguish between clumped objects and a smoothing filter was applied to support object identification. After thresholding, every pixel not located in an identified object was set to black (inverse mask) and the number of mitochondrial pixels was counted. Both images were merged, and a pixel analysis was performed to identify and count co-localized green and red pixels.

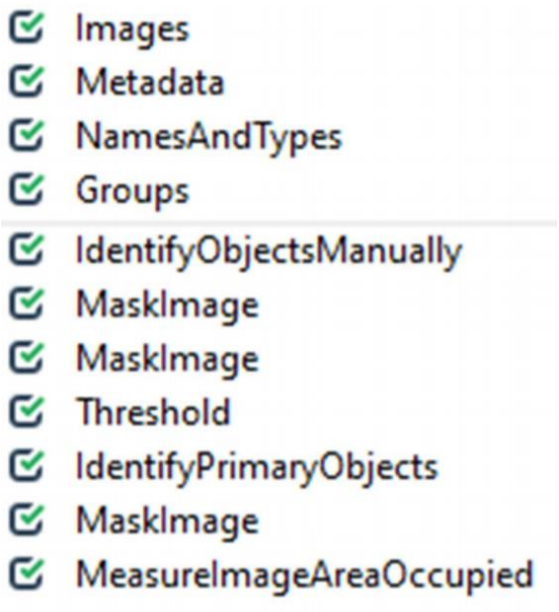

Figure 6: CellProfiler™ image analysis pipeline for mitophagy examination. *Images processed in this pipeline had already a threshold set to cut noise from the autophagosome marker LC3b. This pipeline's key features were manually identifying and drawing cell shapes of desired cells and mask the rest of the image in further analysis. Mitochondria were identified utilizing an object recognition algorithm considering, intensity, shape, and size of wanted objects. The last step was a colocalization analysis, identifying pixels, which displayed signals in both channels, indicating Mitochondrial and autophagosomal presence at the same location.*

2.2.17 Genotyping of used cells and tissue via DNA isolation and PCR

For the confirmation of genotypes, DNA isolations were realized from cultivated cells or mouse tail biopsies. Proteinase K buffer was used for lysis of sample material overnight at 55°C. Clearance of debris was achieved by a Centrifugation step at 18.400g for 15min. The supernatant was transferred, and the DNA precipitated with 0.7 volumes of isopropanol. Subsequently, centrifugation at 18.400g for 30min was performed. The pellet was washed two times with ethanol (70%) and dried for two hours at RT. The DNA was solved in an adequate amount of TE buffer and incubated overnight at 55°C. Afterward, the DNA was used as a template for PCR reactions, which result in different product lengths depending on the genotype of the sample. If the expected genotype could not be confirmed, the sample was removed from the corresponding dataset.

3 Results

3.1 Optimization of the previously conducted NGS analysis of PD mouse models with an aligning algorithm

The previous NGS analysis was conducted using the Tophat aligning algorithm. This old software has been replaced by an improved update (Hisat2) that is supposed to be much more sensible and much more reliable as well (Pertea et al., 2016; Baruzzo et al., 2017; Kim et al., 2019). Because of its outdated algorithm, the formerly conducted Tophat analysis might have resulted in some false positives, and some false negatives as well. In order to obtain differentially expressed genes that may have been missed by the original analysis, the Hisat2 aligning algorithm was used to perform a second analysis with the transcriptome data. The potentially differentially expressed genes should subsequently be analyzed via qPCR to confirm or dismiss the NGS results. The results of the new NGS analysis and qPCR verification efforts are depicted in the figure below.

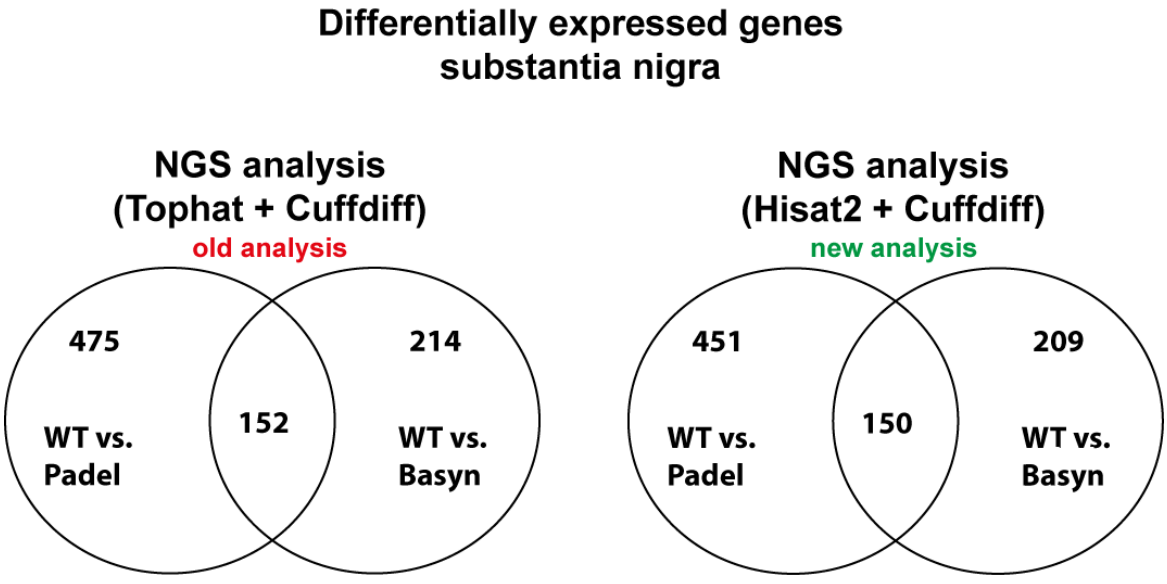

Figure 7: Comparison of the transcriptome analysis with the Tophat and Hisat2 aligning algorithm of PD mouse models in the substantia nigra of one-year-old animals. *Padel (left circles) and Basyn mice (right circles). The old NGS analysis (Tophat) revealed 475 altered genes in Padel, while the new NGS analysis (Hisat2) showed only 451 differentially expressed genes (DEGs). For Basyn mice, the DEGs were reduced from 214 to 209. Overlapping fields indicate DEGs that are regulated in both mouse lines. n = 4 for Padel WT, Padel Homo, Basyn each.*

The results of the old and the new NGS analysis are visualized in figure 7. The number of differentially expressed genes (DEGs) in both PD mouse models, and their overlay differs between both analyses. Differentially expressed genes in the Padel mouse line decreased by 24 with the new aligning algorithm, while DEGs in the Basyn group decreased by five. The overlay of both models decreased by two. However, the Hisat2 NGS analysis identified 15 new DEGs in the Basyn line and 10 new DEGs in the Padel mouse, which are displayed in the table below.

Table 12: List of newly emerged genes in Padel and Basyn models after optimization of the NGS analysis *with a new aligning algorithm.*

New genes for Basyn		New genes for Padel	
Ablim3	Kcnmb4	Ccnjl	Kcnmb4
Bhlhe22	P4ha3	Cdon	Pisd-ps3
Cyp2e1	Peak1	Erdr1	Srp54b
Fam171b	Prmt8	Itgbl1	St8sia5
Gm14296,Gm6182	Pyy	Itih3	Tph2
Hba-a1,Hba-a2	Sorl1		
Inpp5a	Tob2		
Zfp385c			

None of the genes listed were differentially expressed in both PD mouse models, therefore decreasing the priority list for NGS verification by two genes, instead of increasing this overlay fraction. The complete list of DEGs for both mouse models is depicted in the supplement of this thesis (6.2 + 6.3).

The 150 genes which seem differentially expressed in both PD mouse models in both analyses were subsequently chosen for qPCR verification in the Padel mouse model as a priority target.

3.2 qPCR verification efforts of prioritized candidate genes from the NGS analysis

Both NGS analysis programs identified 150 DEGs commonly regulated in Basyn and Padel mice, which were considered prioritized candidate genes. These genes were

analyzed with quantitative real-time PCR to verify potential regulation on an mRNA level. A summary of these confirmation efforts is depicted in Figure 8.

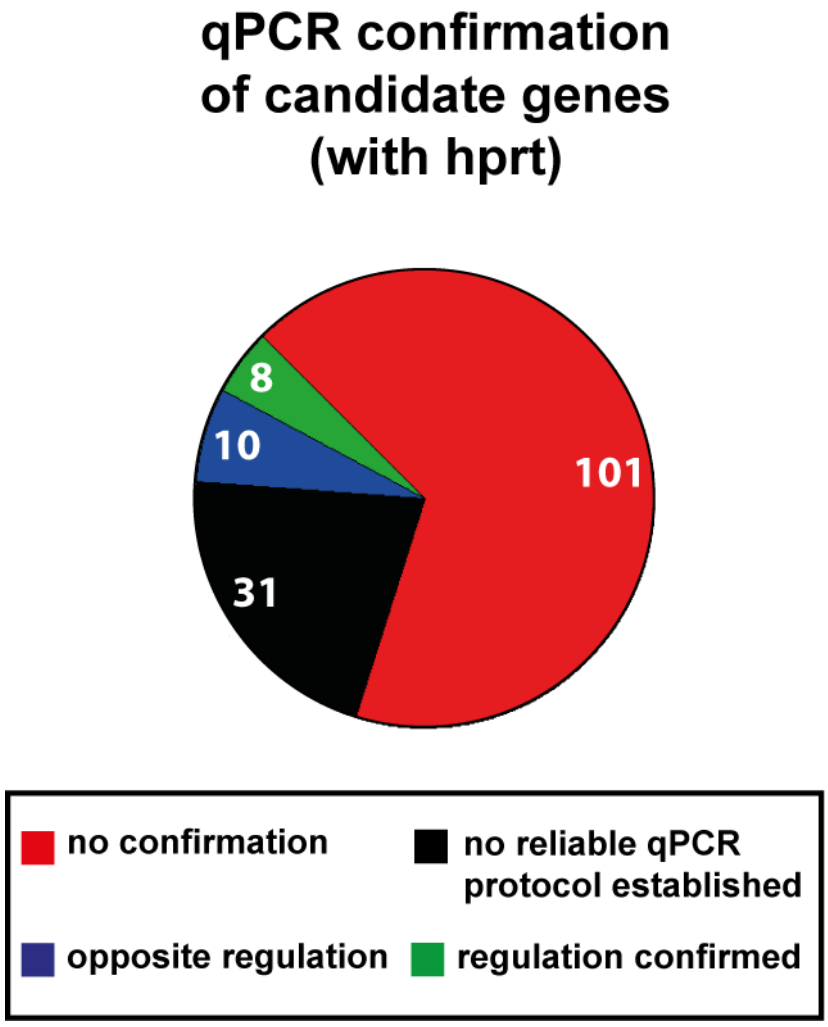

Figure 8: qPCR verification efforts to identify PD-associated genes. *qPCR confirmation of differentially expressed genes from the transcriptome analysis. Expression was examined in SN tissue of one-year-old Padel mice (n~10). Expression was normalized against Hprt as reference gene. The status of confirmation is color-coded, as indicated by the legend. 101 DEGs could not be confirmed in qPCR (red), 10 genes were differently regulated, but contrary to NGS prediction (blue). For 31 genes, no reliable qPCR protocol could be established. 8 of the 150 predicted DEGs from the NGS analysis were confirmed to be differentially expressed. Some of the qPCRs were performed from supervised students during their bachelor thesis (Steinkamp, 2018; Blasey, 2020; Lemhoefer, 2020).*

Figure 8 shows the status of qPCR verification efforts of these priority targets, separated in confirmation or no confirmation, opposite regulation compared to transcriptome data, or no qPCR protocol established, as indicated by the colors. For initial analysis, qPCR experiments were performed with the reference gene Hprt. It was not possible to establish a working qPCR protocol for 31 of the 150 candidate genes

due to the low quality of RT-qPCRs or low gene expression. Detailed Primer requirements are described in section 2.2.6. Low gene expression of candidate genes ($\Delta CT \geq 28$) can result in high variance or failed PCR reactions and therefore yield inaccurate results in qPCR analysis; thus, these genes were excluded from further analysis. 119 Genes were successfully examined in qPCR experiments. From these, 101 candidate genes could not be confirmed as differentially expressed by statistical analysis with the Mann-Whitney u-test. Their figures and ΔCT values are in the supplement of this thesis (6.2 – 6.5). 18 genes showed significantly changed expression in qPCR experiments, although only eight genes were regulated in the same direction as in the NGS analysis. Visualized data of the 18 genes will be displayed in the following figure.

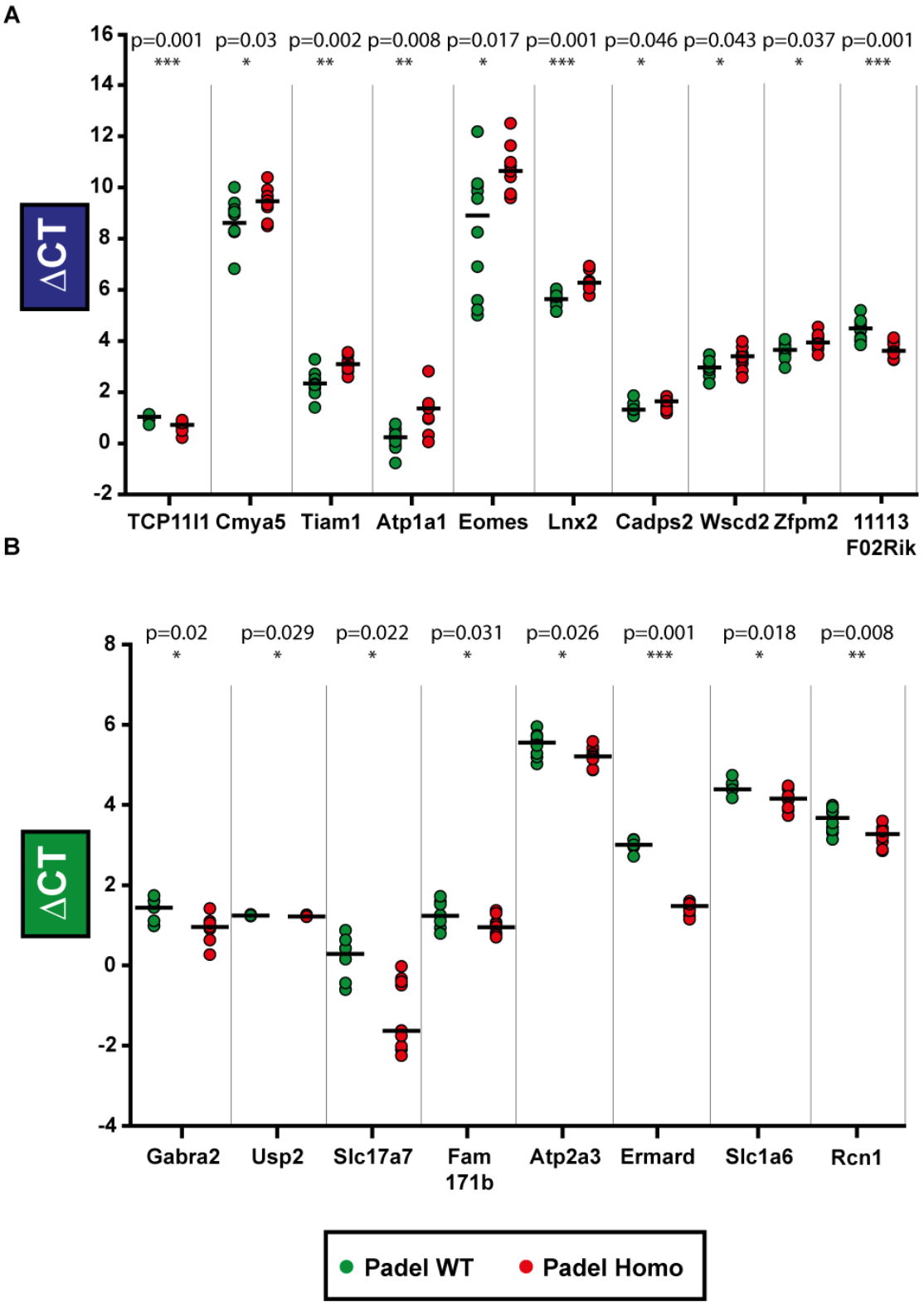

Figure 9: Statistically significant gene expression results of substantia nigra tissue of one-year-old Padel mice normalized with the reference gene Hprt (n=10). A: *List of genes regulated in the opposite direction compared to NGS results (displayed in blue).* ***B:*** *List of genes regulated in the same direction as the NGS analysis (displayed in green). Black bars represent the median of the corresponding groups. Statistical analysis was performed with the Mann-Whitney u-test. p-values are displayed above the scatter plots (* p< 0.05, ** p< 0.01, *** p< 0.001).*

The expression data of all genes shown in figure 9 indicate expression changes between the Padel homo and its WT littermates. However, confirmation of expression changes verified with only one reference gene does not deliver the desired certainty for the identification of PD-associated genes. Therefore, each gene was additionally tested with an independent sample set with a broad panel of selected reference genes to increase evidence for regulation, described in the section below.

3.3 Validation of Hprt confirmed genes with independent data sets and multiple reference genes

This section contains the evaluation of genes, which had significant changes in expression using the Hprt reference gene in qPCR experiments (18 genes). However, the direction of regulation for some of those genes was opposite to the NGS results (10 genes). Since the transcriptome analysis is prone to high false-positive rates due to technical variance and low sample size (n=4), qPCR data with increased sample size (n=10) is considered potentially more reliable and accurate. Therefore, detected expression changes will not be disregarded although they do not match previous transcriptome analysis.

Reproduction with an independent sample set would add a layer of proof to retrieved results. Additionally, normalization with multiple reference genes also increases the credibility of obtained expression data because it cannot be excluded that single reference genes are not stably expressed as expected. Therefore, qPCR experiments were repeated for the 18 identified genes with new samples and a whole reference gene panel. New reference genes included Acvri1, Aes, Eif4g2, Mgrn1, Oxr1, and Ube2d2a. Hrpt is included for reproduction purposes as well.

The results of the ten tested genes (regulated in the opposite direction in qPCR experiments compared to the NGS analysis) are displayed in the figures below.

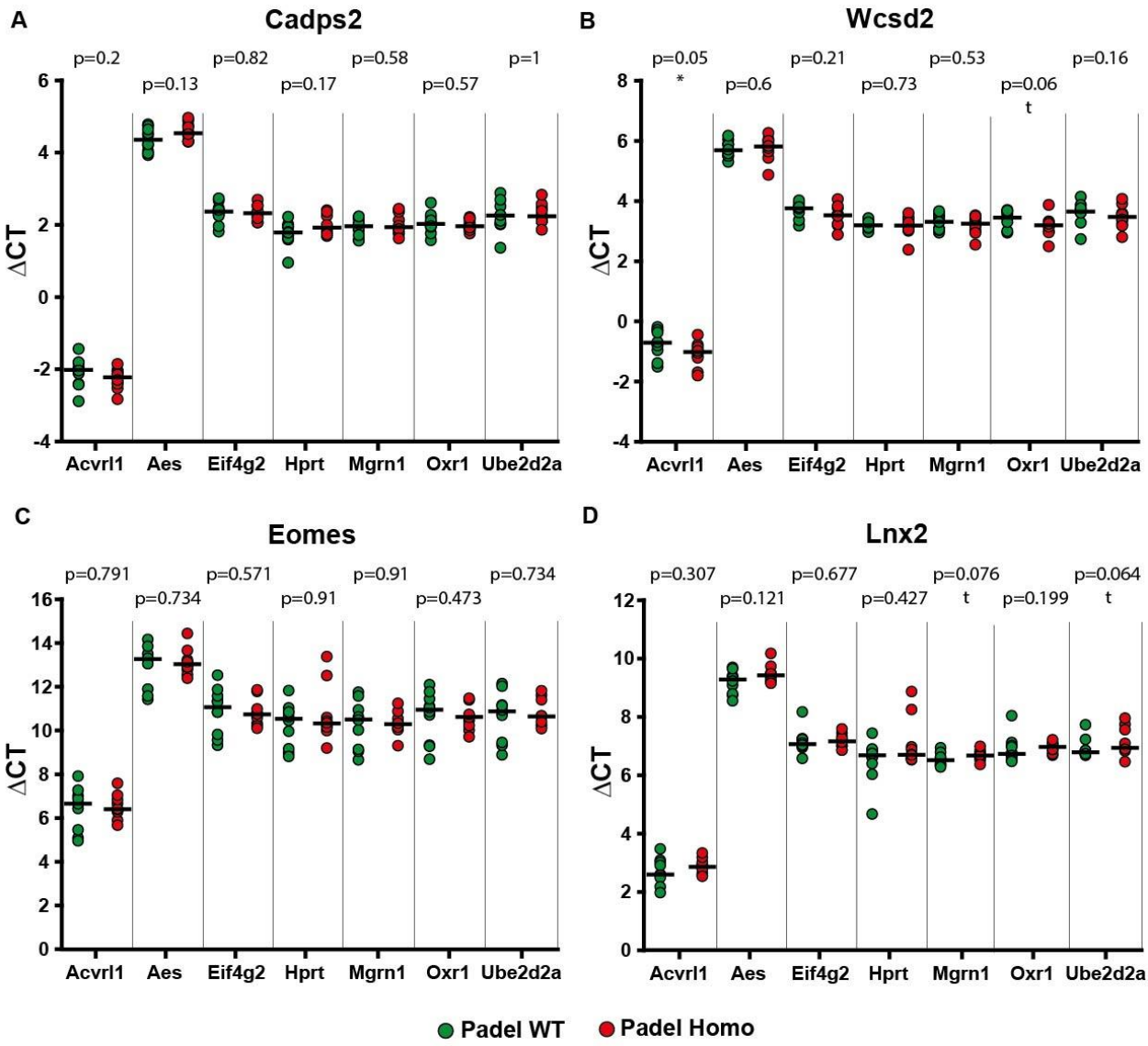

Figure 10: qPCR results of Hprt-confirmed genes with an independent sample set and multiple reference genes. *Displayed are the genes Cadps2 (**A**), Wcsd2 (**B**), Eomes (**C**) and Lnx2 (**D**), which were shown to have opposite regulation as indicated by qPCR compared to predicted NGS analysis (compare fig. 9)* ***A:*** *Regulation of Cadps2 could not be reproduced with Hprt or confirmed with multiple reference genes.* ***B:*** *Regulation of Wcsd2 could not be confirmed with most reference genes. Reproduction with Hprt was not significant (p=0.73). Normalization with Acvrl1 was significant (p=0.05), while Oxr1 displayed a trend (t p=0.06)* ***C:*** *Regulation of Eomes could not be reproduced with Hprt or confirmed with multiple reference genes.* ***D:*** *Regulation of Lnx2 could overall not be confirmed. Reproduction with Hprt was not significant, although it was highly significant in the first run (compare fig. 9, p=0.001). Normalization with Mgrn1 and Ube2d2a displayed a statistical trend (p=0.076 and p=0.064). n=10, SN tissue, one-year-old mice, littermates = green, Padel = red, black bar = median, * p< 0.05, ** p< 0.01, *** p< 0.001 Mann-Whitney u-test.*

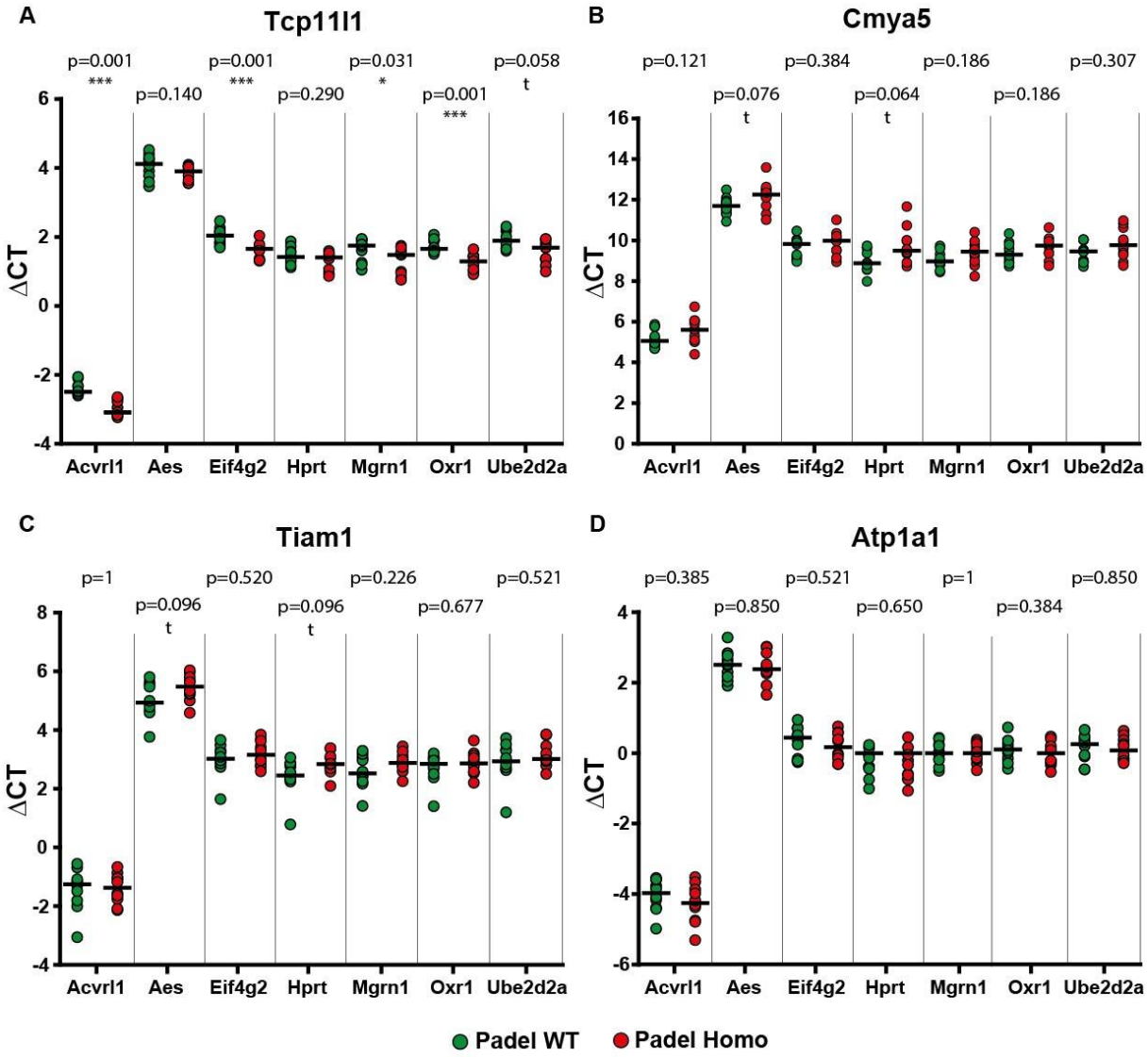

Figure 11: qPCR results of Hprt-confirmed genes with an independent sample set and multiple reference genes. *Displayed are the genes Tcp11l1 (**A**), Cmya5 (**B**), Tiam1 (**C**), and Atp1a1 (**D**), which were shown to have opposite regulation as indicated by qPCR compared to predicted NGS analysis (compare fig. 9).*
A: *Regulation of Tcp11l1 could not be reproduced with Hprt but was confirmed with multiple reference genes. Normalization with Acvrl1, Eif4g2, Mgrn1, and Oxr1 were statistically significant, while Ube2d2a displayed a trend (p=0.001, p=0.001, p=0.031, p=0.058, respectively).* ***B:*** *Regulation of Cmya5 could overall not be confirmed. Reproduction with Hprt yielded a statistical trend and normalization with Aes displayed a statistical trend also (p=0.076 and p=0.064)* ***C:*** *Regulation of Tiam1 could overall not be confirmed. Reproduction with Hprt yielded a statistical trend and normalization with Aes displayed a statistical trend also (p=0.096 and p=0.096)* ***D:*** *Regulation of Atp1a1 could neither be reproduced with Hprt nor confirmed with multiple reference genes. n=10, SN tissue, one-year-old mice, littermates = green, Padel = red, black bar = median * p< 0.05, ** p< 0.01, *** p< 0.001 Mann-Whitney u-test.*

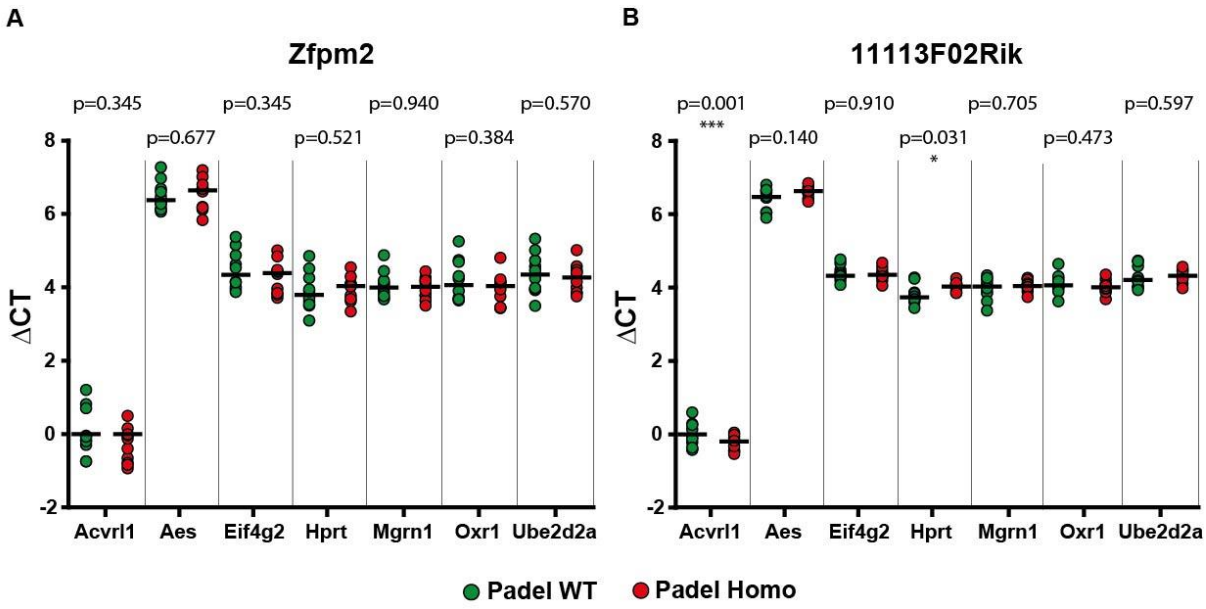

Figure 12: qPCR results of Hprt-confirmed genes with an independent sample set and multiple reference genes. *Displayed are the genes Zfpm2 (**A**), and 11113F02Rik (**B**), which were shown to have opposite regulation as indicated by qPCR compared to predicted NGS analysis (compare fig. 9)* ***A:*** *Regulation of Zfpm2 could not be reproduced with Hprt or confirmed with multiple reference genes.* ***B:*** *Regulation of 11113F02Rik could overall not be confirmed. Reproduction with Hprt was successful, and one other reference gene was significant (Acvrl1). (p=0.031 and p=0.001). n=10, SN tissue, one-year-old mice, littermates = green, Padel = red, black bar = median * p< 0.05, ** p< 0.01, *** p< 0.001 Mann-Whitney u-test.*

Ten genes have shown significant expression changes in SN Tissue of one-year-old homozygous Padel mice compared to their WT littermates in qPCR experiments with Hprt normalization. The subsequent reproduction of experiments with independent sample sets (n=10) could confirm significant expression changes with Hprt normalization only for the gene 11113F02Rik (p=0.031), while the genes Cmya5 and Tiam1 have shown a statistical trend (p=0.064 and p=0.096, Mann-Whitney u-test). Although some genes had statistically significant expression changes with single reference genes, only Tcp11l1 showed altered expression levels with multiple reference genes. Four out of seven reference genes yielded significant results (Acvrl1 p=0.001, Eif4g2 p=0.001, Mgrn1 p=0.031, Oxr1 p=0.001) and one reference gene displayed a statistical trend (Ube2d2a p=0.058). The average ΔCT difference between Padel and WT for all reference genes is 0.36, which translates into a foldchange of 1.28. Because most reference genes could confirm differential regulation, Tcp11l1 is considered a potential PD-associated candidate gene.

The next section contains the evaluation of genes, which had significant changes in expression using the Hprt reference gene in qPCR experiments. The direction of

regulation aligns with previously obtained transcriptome data. However, further evaluation with qPCR needs to be performed as a measure of quality control.

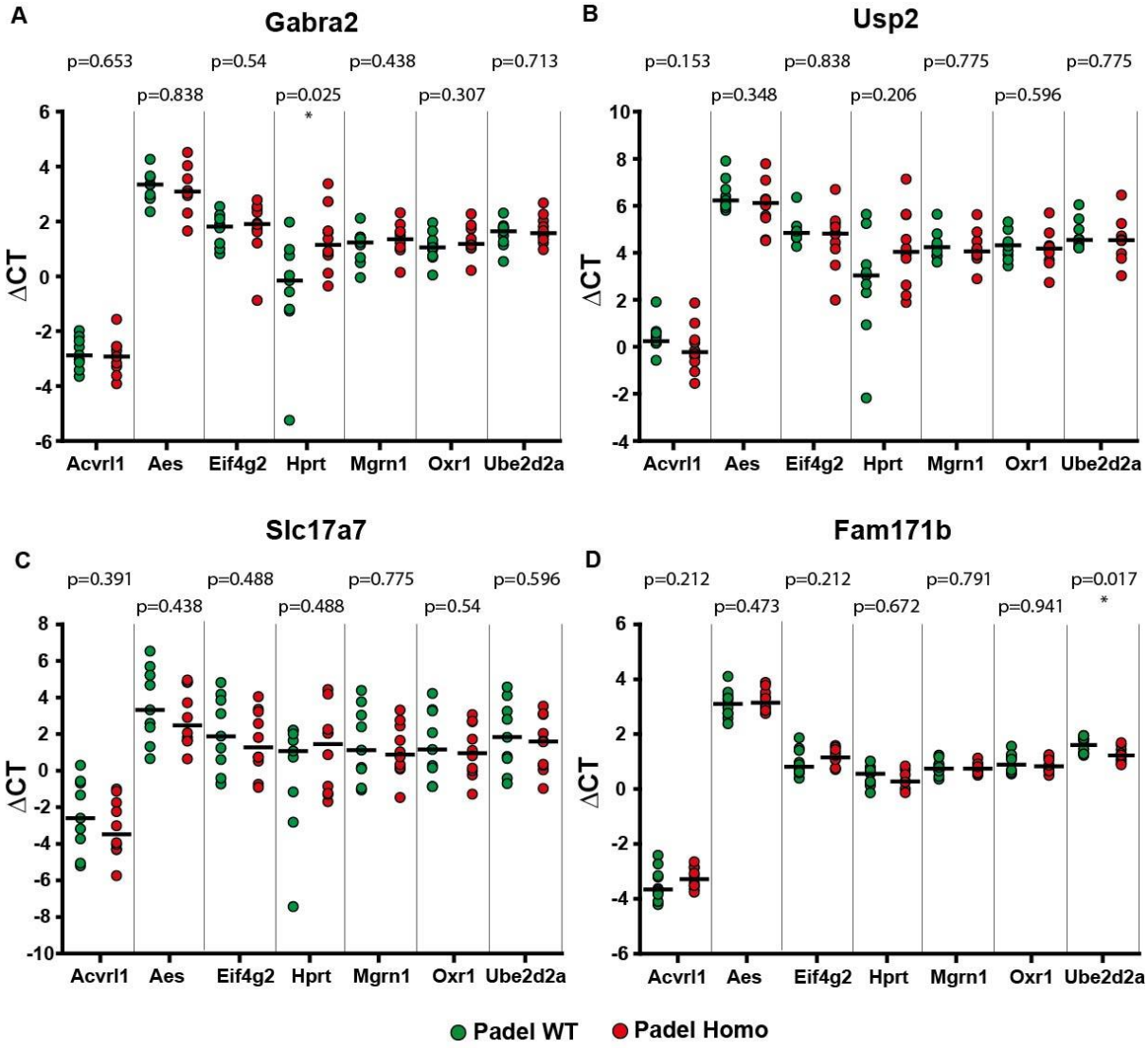

Figure 13: qPCR results of Hprt-confirmed with an independent sample set and multiple reference genes. *Displayed are the genes Gabra2(**A**), Usp2 (**B**), Slc17a7 (**C**), and Fam171b (**D**), whose differentially altered expression was predicted via NGS analysis and could be confirmed via qPCR (compare fig. 9)* ***A:*** *Regulation of Gabra2 could be reproduced with Hprt but not be confirmed with other reference genes. (p=0.025).* ***B:*** *Regulation of Usp2 could not be reproduced with Hprt or confirmed with other reference genes.* ***C:*** *Regulation of Slc17a7 could not be reproduced with Hprt or confirmed with other reference genes.* ***D:*** *Regulation of Fam171b could not be reproduced with Hprt and only be confirmed with the reference gene Ube2d2a (p=0.017). n=10, SN tissue, one-year-old mice, littermates = green, Padel = red, black bar = median * p<0.05, ** p< 0.01, *** p< 0.001 Mann-Whitney u-test.*

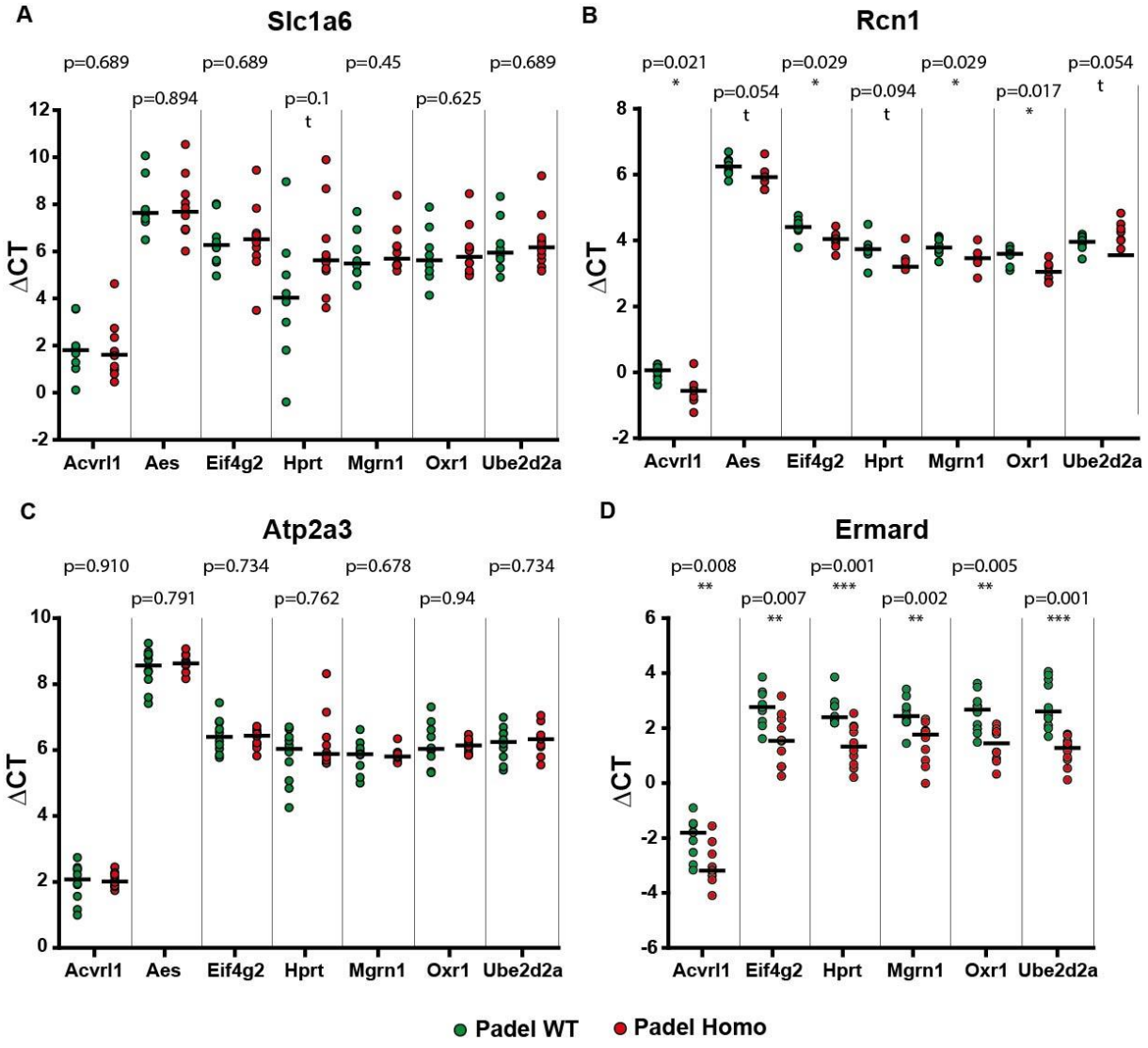

Figure 14: qPCR results of Hprt-confirmed with an independent sample set and multiple reference genes. *Displayed are the genes Slc1a6 (**A**), Rcn1 (**B**), Atp2a3 (**C**), and Ermard (**D**), whose differentially altered expression was determined via NGS analysis and could be confirmed via qPCR (compare fig. 9).* ***A:*** *Regulation of Slc1a6 could not be reproduced with Hprt of confirmed with other reference genes.* ***B:*** *Regulation of Rcn1 could be reproduced with Hprt as a statistical trend and confirmed with all other tested reference genes except Aes and Ube2d2a, which displayed a strong trend (p=0.021, p=0.054, p=0.029, p=0.094, p=0.029, p=0.017, p=0.054).* ***C:*** *Regulation of Atp2a3 could not be reproduced with Hprt of confirmed with other reference genes.* ***D:*** *Regulation of Ermard could be reproduced with Hprt and confirmed with all other tested reference genes (p=0.008, p=0.007, p=0.001, p=0.002, p=0.005, p=0.001). n=10, SN tissue, one-year-old mice, littermates = green, Padel = red, black bar = median*
** p< 0.05, ** p< 0.01, *** p< 0.001 Mann-Whitney u-test.*

The eight examined genes have previously shown statistically significant expression changes in the transcriptome analysis and in qPCR experiments utilizing Hprt as a reference gene. The reproduction of qPCR experiments with independent sample sets (n=10) confirmed two genes with significant expression changes (Gabra2 p=0.025, Ermard p=0.001) and two genes with statistical trends (Slc1a6 p=0.1, Rcn1 p=0.094). Analysis of the whole reference gene panel resulted in four genes with no statistically

significant expression changes in any reference gene (Usp2, Slc17a7, Atp2a3, Slc1a6), while Gabra2 and Fam171b were significantly regulated with only one reference gene (Hprt and Ube2d2a, respectively). Those six genes were dismissed due to lacking evidence of regulation. Ermard was tested against six reference genes, which all yielded significant results with an $\alpha \leq 1\%$, indicating very stable upregulation. The average ΔCT difference between Padel and WT is 1.25, which would represent a 2.38-fold increased expression in the Padel mouse. The Rcn1 gene displays at least a statistical trend in all reference genes, while four of them are statistically significant ($\alpha \leq 5\%$). Rcn1 is considered upregulated in the Padel mouse model. The average ΔCT difference is 0.88, which translates into a fold change of 1.84.
The following table sums up the qPCR verification efforts.

Table 13: Summary of candidate genes and their status after qPCR verification *using multiple reference genes and an independent sample set. Confirmed genes are displayed in green and the arrow indicates the direction of regulation in the Padel mouse model.*

differentially expressed genes (Hprt normalized)	Status after further evaluation with multiple reference genes
opposite regulation compared to NGS results	
11113F02Rik	-
Atp1a1	-
Cadps2	-
Cmya5	-
Eomes	-
Lnx2	-
Tcp11l1	↑ Confirmed, foldchange 1.28
Tiam1	-
Wscd2	-
Zfpm2	-
Same regulation compared to NGS results	
Atp2a3	-
Ermard	↑ Confirmed, foldchange 2.38
Fam171b	-
Gabra2	-
Rcn1	↑ Confirmed, foldchange 1.84
Slc17a7	-
Slc1a6	-
Usp2	-

After repeated qPCR experiments with independent sample sets and multiple reference genes, Tcp11l1, Ermard, and Rcn1 were confirmed to be upregulated in the *substantia nigra* of one-year-old Padel homozygous mice compared to their wild type littermates.

3.4 Characterization of identified candidate genes Tcp11l1, Ermard, and Rcn1 via literature review

Three candidate genes could successfully be confirmed in qPCR experiments regarding their upregulation in the SN of the Padel mouse model. A short characterization of each gene will be conducted to illuminate protein function and a possible PD association.

Tcp11l1:

The chromosome 2 located gene Tcp11l1 codes for the T-complex protein 11-like protein 1. There is not a single publication referring to this gene in the PubMed database. One publication was found on Tcp11, which displays sequence similarities to Tcp11l1. Tcp11 plays a role in murine sperm motility (Castaneda et al., 2019).

Ermard:

The Ermard gene is located on chromosome 17 and codes for the ER membrane-associated RNA degradation Protein. Its chromosomal location is in very close proximity to Parkin (<3 mb). The Padel mouse model has been generated utilizing the 129Sv/J mouse stem cell. Despite the fact, that the genetic background of Padel mice has been purified via backcrossing with C57BL/6 over twenty generations (homologous recombination), it was very likely, that this gene has a 129Sv/J origin. The differential expression could have been an artifact and not caused by Parkin deficiency.

Rcn1:

The Reticulocalbin (Rcn1) gene is located on chromosome two of *mus musculus* and its product was identified and characterized in 1993 to be an ER-resident calcium-binding protein. ER localization was hypothesized because of a C-terminal ER import sequence (HDEL) and immunocytochemical staining in Cos cells which displayed an ER-like staining pattern (Ozawa and Muramatsu, 1993). Rcn1 has six EF-hand motifs, some of which have retained calcium-binding capabilities (Tachikui et al., 1997). The physiological function of Rcn1 is not clear but expression manipulation experiments in cancer cell lines produced evidence for a protective function via ER stress mitigation (Xu et al., 2017). Rcn1 has been examined in a cancer context in multiple studies, but a connection to Parkinson's disease has not been reported (Liu et al., 2018; Chen et al., 2019; Ueda et al., 2020). In comparison to the other candidate genes, the upregulation of Rcn1 seems to be very consistent over all used reference genes and is, therefore, the most promising candidate for further evaluation

3.5 Investigation of Rcn1 expression in Basyn, neonatal Padel mesencephalon, and primary Padel astrocytes

The Rcn1 gene was originally selected for further verification of its differential expression in a Parkinson's disease mouse model because it was found in the Padel/Basyn overlay list from the NGS transcriptome analysis (figure 7). Since upregulation of Rcn1 was confirmed in the s*ubstantia nigra* of one-year-old Padel mice in qPCR experiments, it is of interest to check its expression in Basyn as well.

Additionally, Rcn1 expression in neonatal *mesencephalon* tissue of Padel mice was analyzed to examine, whether upregulation develops in an age-dependent manner or is already present at birth.

Lastly, the upregulation of Rcn1 was investigated in primary Padel astrocytes to potentially establish a cellular model system for subsequent manipulation experiments. The results can be seen below this section.

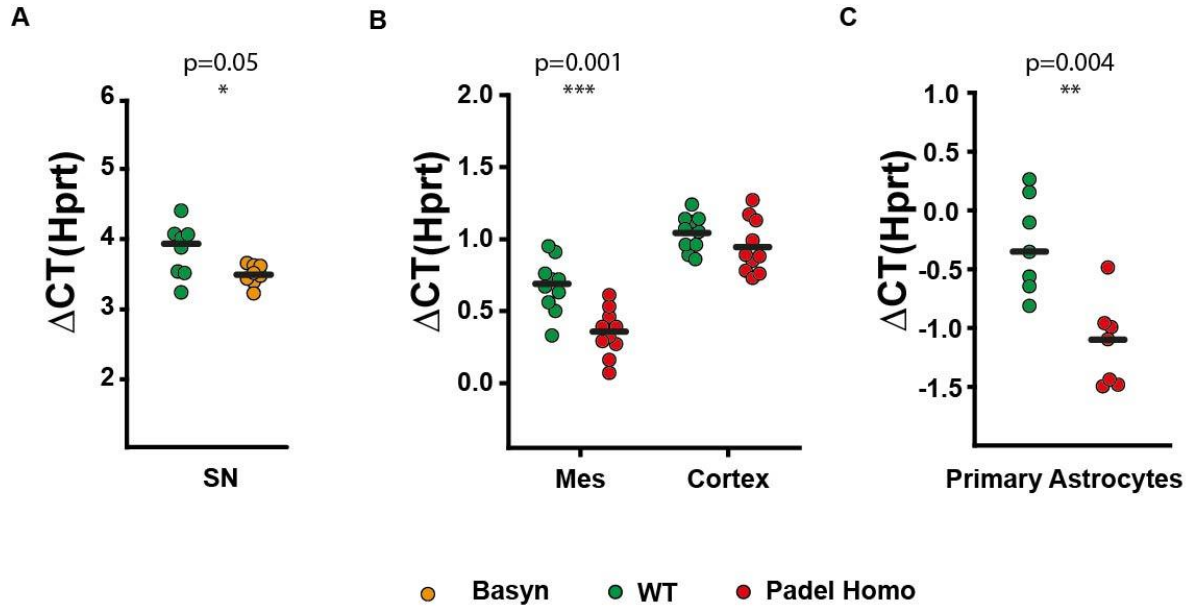

Figure 15: Investigation of Rcn1 expression in Basyn and different Padel regions (Hprt normalized). A: *Rcn1 expression in the substantia nigra of one-year-old Basyn mice revealed Rcn1 is significantly higher expressed in Basyn than WT (n=8, p=0.05).* ***B:*** *Rcn1 expression of neonatal mesencephalon (left) and cortex (right) tissue of Padel mice showed upregulation of Rcn1 in homozygous Padel mice in the mesencephalon, but not cortex (n=10, p=0.001).* ***C:*** *Rcn1 expression increases could be confirmed in neonatal primary mesencephalic Padel astrocytes (n=7, p=0.004). Color coding is explained in the legend below the graphs. Black bars represent the median of the corresponding groups. Statistical analysis was performed with the Mann-Whitney u-test (* p< 0.05, ** p< 0.01, *** p< 0.001). Practical work for this qPCR experiment was performed by supervised students in their bachelor thesis (Steinkamp, 2018; Schäning, 2019).*

The Rcn1 expression data from the Basyn mouse model (figure 15A) indicates a statistically significant upregulation compared to the wild type (p=0.05). This upregulation of Rcn1 in both Parkinson's disease mouse models introduces the possibility of its involvement in a shared pathomechanism.

The investigation of neonatal tissue of the Padel mouse model regarding its Rcn1 expression (figure 15B) confirmed upregulation in the *mesencephalon* (p=0.001, left), but not in the cortex (p=0.19, right). Therefore, altered Rcn1 expression levels are not likely to develop during the aging process, but are rather present since birth. Additionally, it might be possible to utilize primary culture to investigate the impact of this expression change. In fact, primary Padel astrocytes also possess differential Rcn1 expression (figure 15C, p=0.004).

3.6 Examination of intracellular calcium response in primary Padel astrocytes

Based on its upregulation in two Parkinson mouse models, its calcium-binding properties, and its postulated subcellular location in the ER, one could speculate, that Rcn1 may influence intracellular calcium dynamics by modulation of ER-mediated calcium release. To Investigate a possible modulation of ATP-dependent Endoplasmic reticulum calcium release, primary Padel astrocytes were used to conduct calcium imaging studies utilizing Fura2-AM as a calcium indicator.

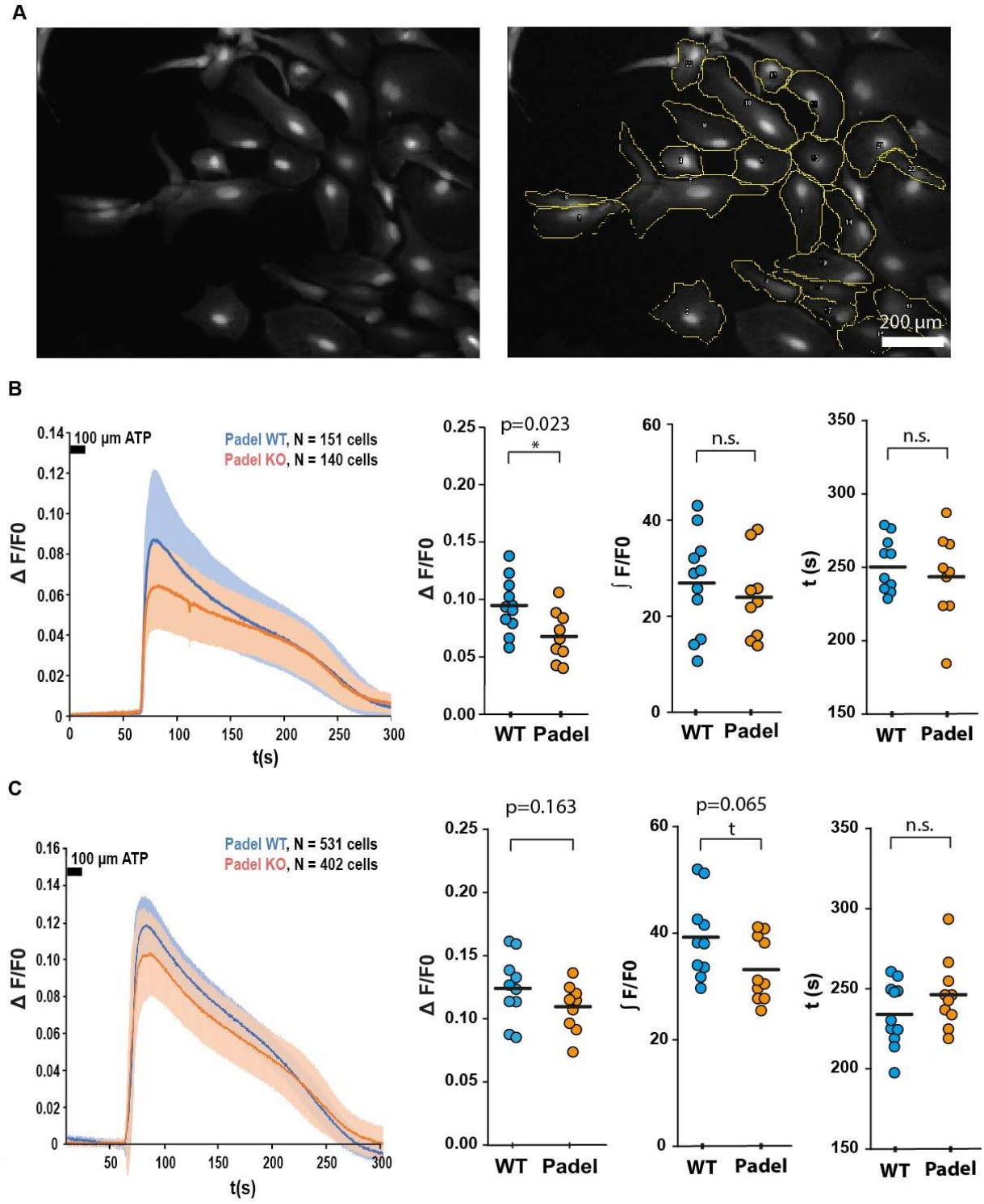

Figure 16: Investigation of intracellular calcium release in primary Padel astrocytes. *The ratiometric calcium indicator Fura2-AM was used together with ATP stimulation to visualize and evoke calcium responses.* ***A:*** *Representative recordings from an image series displaying the Fura2-AM calcium dye at the 380/340 nm ratio. Cells were manually selected before measurement (yellow regions). scale bar: 200 µm* ***B:*** *Results of the calcium imaging experiment (n=11/9; N=151/140). Displayed is the average response curve after 100µM ATP stimulus for 15 seconds from all measured cells including standard deviation (left). Statistical evaluation of peaks (ΔF/F0), integral (∫F/F0), and duration (t(s)). Statistically different response in peak height was measured (p=0.023), whilst integral and duration were not altered (p=447, p=0.82).* ***C:*** *The experiment was repeated as a quality control measure (n=10/9, N=531,402). The difference in peak height could not be reproduced (p=0.163), although the integral was reduced in the Padel group with a statistical trend (p=0.065). WT=blue, Padel=orange,*
** p< 0.05, ** p< 0.01, *** p< 0.001 Mann-Whitney u-test.*

Examination of intracellular calcium response in primary Padel astrocytes (n=11/9) has shown a reduced calcium peak signal with Fura2-AM measurement (figure 16B, p=0.023), hinting at either a reduced calcium release or a changed dynamic. A reduced calcium response would manifest as a reduced integral or a shortened response duration. Padel astrocytes displayed a smaller integral in the calcium response curve compared to the WT one, but the difference was statistically not significant. The calcium response durations of both groups were also very similar. This result indicates that the absence of Parkin seemed to change the dynamic of ER-mediated calcium release in primary astrocytes, without affecting their total amount of calcium release.

Since the p-value of the statistical analysis for the maximum calcium release signal was just slightly below 5%, this experiment (figure 16C) was repeated with an independent sample set (n=10/9). To enhance methodical accuracy, the number of measured cells per sample was increased ~3 fold. The intent was to reduce variance caused by differences of individual cells per measured slide (cell cycle, cell type, vitality). This strategy seemed to lead to an overall reduced standard deviation in the response curve (figure16C left). This experiment could not find a statistically significant difference in peak height, but a tendency in the same direction as in the first sample set could be observed (p=0.163). Also, a decrease in the integral was measured this time as a statistical trend (p=0.065), while the duration was not significantly altered. The average response duration was slightly elongated in the Padel group though, which could not be seen in the first experiment.

Taken together, it seems likely that the intracellular calcium dynamic is somehow altered in primary Padel astrocytes. A decreased initial calcium output into the cytoplasm seems more likely, than a slowed-down response because of the decrease in peak height and integral, while the response duration is largely unaffected. A further investigation of this phenomenon seems logical to shed light on ER-associated PD pathomechanisms.

3.7 Investigation of intracellular calcium dynamics of primary Padel astrocytes with Rcn1 siRNA knockdown

Previous experiments indicated a possible reduction of intracellular calcium release in primary Padel astrocytes (section 3.6). Furthermore, the conducted transcriptome analysis of adult Padel mice revealed upregulation of the calcium-binding protein Rcn1. This upregulation was confirmed in different contexts in these mice, including neonatal primary astrocytes. This upregulation would be a potential explanation for the altered calcium dynamic observed in previous experiments (figure 16).

Consequently, manipulation of Rcn1 expression via siRNA knockdown was performed in primary Padel astrocytes to investigate a functional connection between Rcn1 expression and ER-mediated calcium release that might contribute to PD pathology. The following figure shows experimental data regarding Rcn1 subcellular location and its impact on intracellular calcium dynamics.

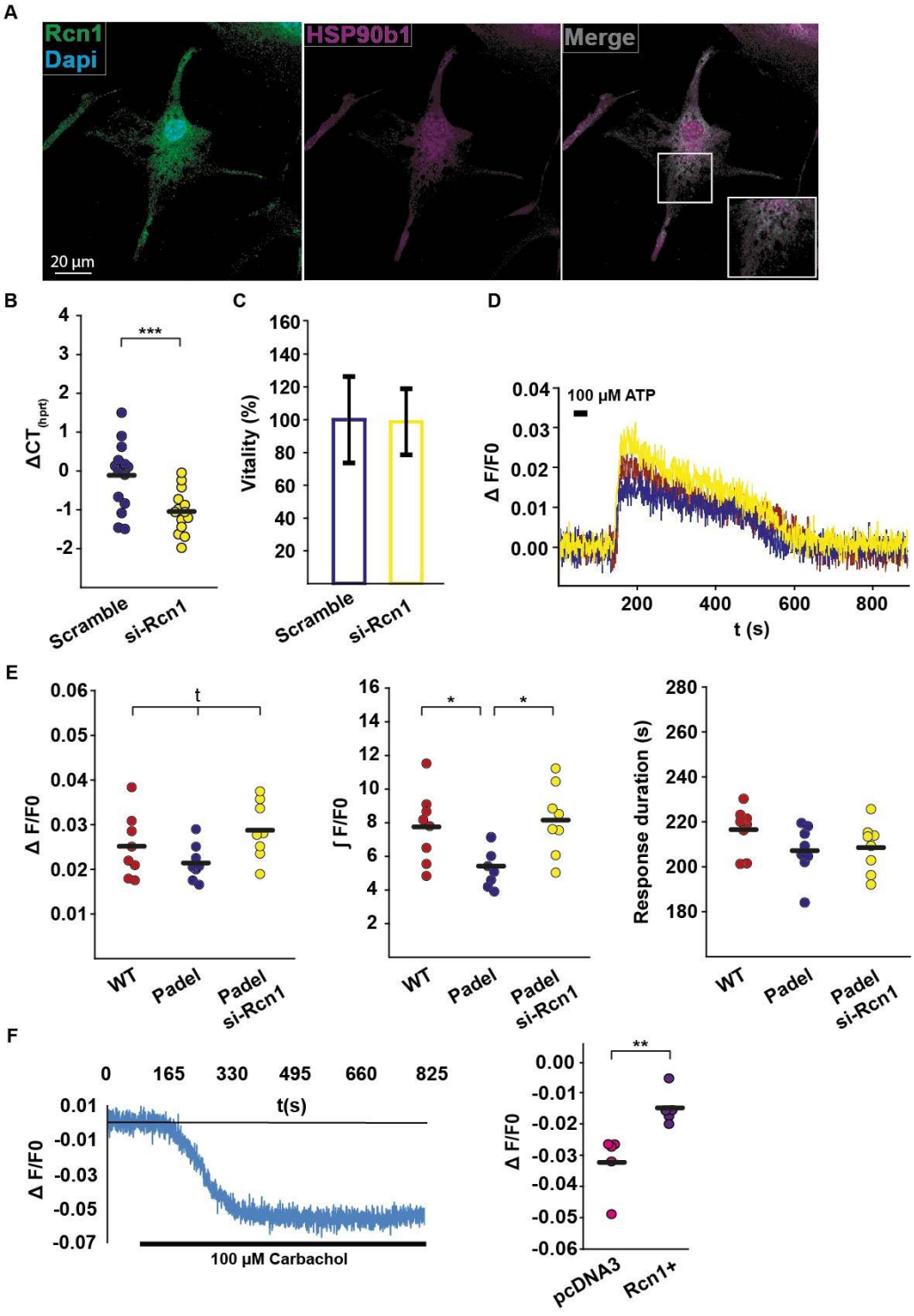

Figure 17: Rcn1 Localization and its impact on ER-mediated calcium dynamics in primary Padel astrocytes. ***A****: Immunocytochemical staining of a primary murine astrocyte with Rcn1 (green) and the ER-marker Hsp90b1 (magenta). Co-localization shows Rcn1 signal in the ER and is displayed in grey.* ***B****: Rcn1 siRNA treatment of murine Padel astrocytes reduces Rcn1 expression to ca. 55% (Gapdh normalized, n=15/14, Mann-Whitney u-test: p=0.001).* ***C****: Vitality of primary Padel astrocytes (n=9/14) measured with the MTS-test was not reduced by siRNA delivery (100nM).* ***D****: Averaged intracellular calcium response of siRNA treated wild type (scramble), Padel (scramble), and Padel (Rcn1 siRNAs) astrocytes (n=8, 100nM siRNA) after ATP stimulation for 15 sec (100 µM).* ***E****: Comparison of intracellular calcium peaks (ΔF/F0), integral (∫F/F0), and duration (t(s)) in the treatment groups (left to right). Peaks (ANOVA on ranks p=0.077). Integrals (ANOVA on ranks p=0.015, post hoc test: Dunn's method p≤0.05) Duration (ANOVA on ranks p=0.185).* ***F****: Calcium measurement in the ER lumen with R-Cepia1er in SH-SY5Y with Rcn1 overexpression (ΔF/F0). Stimulation with 100 µM carbachol. Rcn1 decreases ER-mediated calcium output (n=5, p=0.008 Mann-Whitney u-test). * p< 0.05, ** p< 0.01, *** p< 0.001.*

Rcn1 siRNA was chosen as a tool for expression manipulation to investigate if Rcn1 knock-down to wild type level might restore intracellular calcium response in Padel astrocytes.

To ensure an adequate siRNA knock-down, qPCR experiments were performed 3 days after electroporation (figure 17B). Rcn1 siRNA treatment could significantly reduce the ΔCT value compared to the Scramble siRNA group (foldchange -1.79, p=0.001, n=15/14), restoring expression to wild type levels (upregulation between WT and Padel: foldchange 1.84). It is essential to check the cell vitality if a complex manipulation on cellular systems is performed to ensure comparable measurements and generate data under physiological conditions. Vitality was measured utilizing the MTS assay (figure 17C). Neither electroporation nor siRNA treatment did reduce cell vitality in this pre-experiment (vitality ≥ 98% in Rcn1 and Scramble group, n=13/8).

For the investigation of Rcn1s impact on intracellular calcium release, three experimental groups were formed. Wild type astrocytes treated with scramble siRNA, Padel astrocytes treated with scramble siRNA, and Padel astrocytes treated with Rcn1 siRNA (figure 17E). The peak height of the calcium response showed a statistical trend in the ANOVA on ranks (p=0.077) but no statistical significance. However, the peak was lowest in the Padel group and distinctly higher in the wild type and siRNA group, which nearly had the same peak height, thereby matching the general hypothesis. The analysis of the integral, which represents the whole amount of calcium release after stimulation, showed the same distribution pattern as the peak analysis. Plus, the ANOVA on ranks was statistically significant (p=0.015) and the Dunn's post hoc test revealed significant changes between the Padel group and both other groups.

Although the exact function of Rcn1 is still unclear, this protein seems to reduce the calcium output from the Endoplasmic Reticulum. To add another layer of evidence to this mechanism, an Rcn1 overexpression experiment was performed in the neuroblastoma cell line SH-SY5Y (figure 17F). The ER located red calcium sensor R-cepia1er was co-transfected with the Rcn1 construct to directly measure calcium flow out of the ER (n=6). A decreased fluorescence signal of the ER-sensor indicates a higher calcium outflow. Rcn1 overexpression could decrease calcium output of the ER in a statistically significant fashion (p=0.008), thereby confirming the link between Rcn1 amount and intracellular calcium release.

This finding reinforces the previous calcium imaging experiments indicating reduced calcium release in Padel astrocytes and additionally shows, that Rcn1 knockdown can increase calcium output of Padel astrocytes to wild type levels.

Rcn1 has been reported as an ER calcium-binding protein in diverse tumor cell lines suggesting its direct involvement in calcium release pathways within the ER. Therefore, a potential ER localization of Rcn1 in primary astrocytes was investigated by immunocytochemical co-staining using an Rcn1 antibody and the ER marker Hsp90b1 (figure 17A). The staining pattern of Rcn1 and the ER marker merged to a very high degree, demonstrating ER localization of Rcn1 exclusively, thereby confirming localization information from literature also apply in murine astrocytes

3.8 Rcn1 amount, subcellular localization, and mitochondrial associated membranes in the Padel mouse model

The experiments conducted in this thesis have demonstrated an increased Rcn1 expression in the Padel mouse model. Consequently, information about this protein, including the exact subcellular localization is of great interest. Immunocytochemical staining of astrocytes has shown colocalization with an ER marker indicating ER residency. However, the exact subcellular localization is still unknown, and it is not clear if the Parkin knockout influences Rcn1 distribution or localization.
Since the Padel mice show signs of mitochondrial damage *in vivo* and an altered ER-mediated calcium release dynamic *in vitro*, both mitochondria and the ER seem to be affected by the Parkin knockout. It seems logical to examine Mitochondrial associated membranes (MAMs), which build the basis for ER mitochondrial interaction to investigate a possible link between both deficiencies. The following experiments utilize primary Padel fibroblasts as a model organism to investigate the amount of mitochondrial associated membranes and Rcn1 localization.

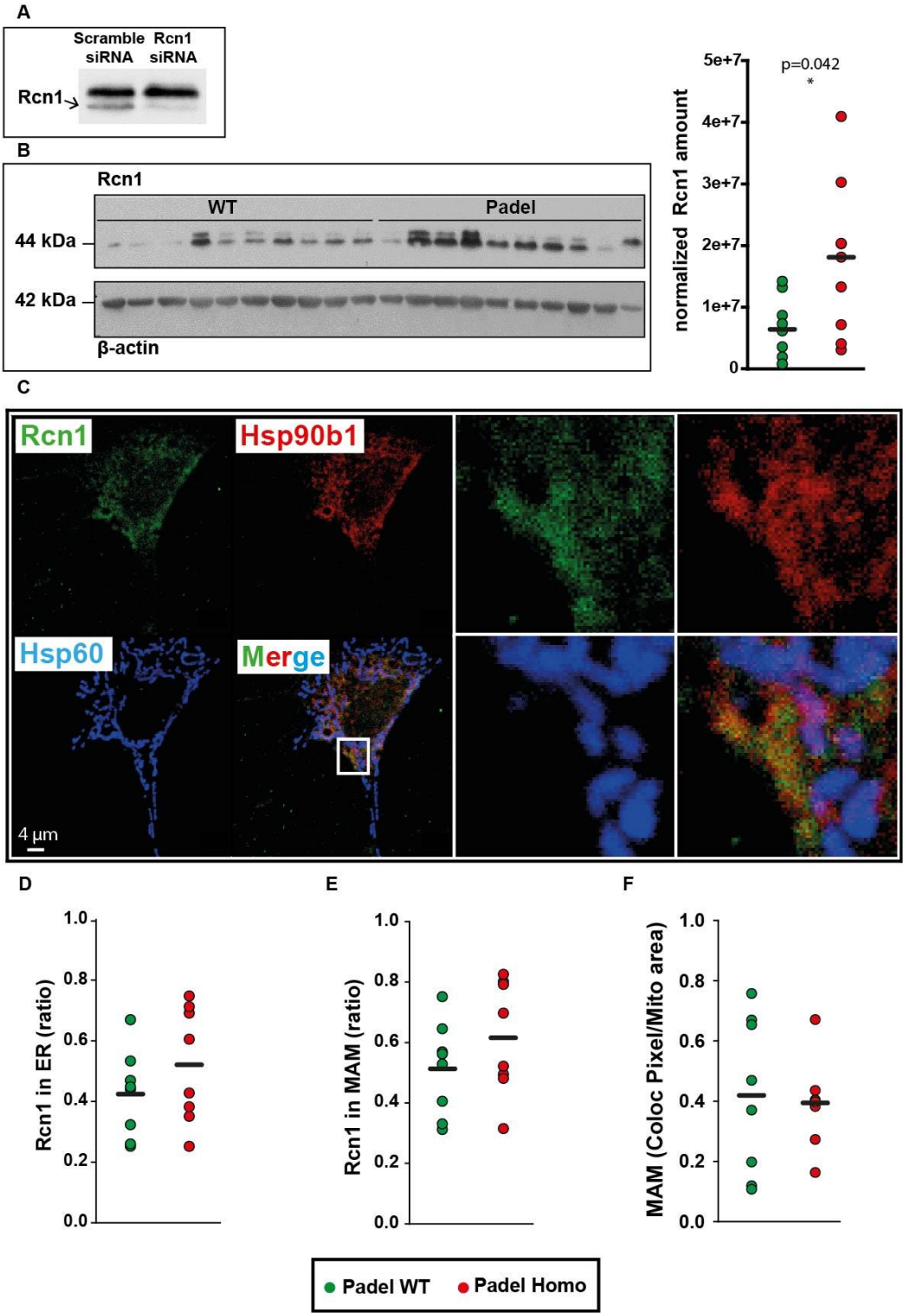

Figure 18: Rcn1 amount, subcellular localization, and amount of mitochondrial associated membranes in primary Padel fibroblasts. A: *Western blot analysis for the determination of the specific Rcn1 band with siRNA.* ***B:*** *Quantification of Rcn1 protein in primary fibroblasts via western blot (n=10) (performed by a supervised bachelor student: Behling,2021). Normalization was performed with β-actin (p=0.042).* ***C:*** *Immunocytochemical staining for image analysis (n=8) of a primary fibroblast with an ER-marker (red), a mitochondria-marker (blue), and Rcn1 (green).* ***D:*** *Rcn1-positive pixel co-localized with ER-positive pixel. No significant difference of Rcn1 amount was found between the genotypes (p=0.270 t-test).* ***E:*** *Rcn1-positive pixel co-localized with MAM-positive pixel. No significant difference of Rcn1 distribution in MAMs was found between the genotypes (p=0.251 t-test).* ***F:*** *MAM amount in relation to mitochondrial pixel. No difference in mitochondrial-ER tethering could be detected between Padel and WT (p=0.959 Mann-Whitney u-test). * p< 0.05, ** p< 0.01, *** p< 0.001.*

The western blot experiment (figure 18B) should confirm Rcn1 overexpression on protein level in primary Padel fibroblasts as a basis for Padel/wild type comparison. The Rcn1 antibody produces double bands as described in the antibody's datasheet. To determine, if both bands are actually representing signal from Rcn1 proteins, siRNA treatment (figure 18A) should identify the Rcn1 specific bands. Only the lower band was reduced after treatment with three different RCN1 siRNAs, indicating Rcn1 specificity only in the bottom band, which was consequently used for quantification with ImageJ (figure 18B). Padel fibroblasts express significantly more Rcn1 protein than their wild type counterpart ($p=0.042$), indicating its upregulation also takes place in Padel fibroblasts, thereby making them suitable for investigation of Rcn1 involvement in PD pathology.

For the examination of cellular Rcn1 location, an immunocytochemical staining was performed, allowing labeling of the ER, mitochondria, and Rcn1 (figure 18C). The observed Rcn1 staining pattern is similar to the previously stained primary astrocytes (see figure 17A), having high colocalization with the chosen ER marker indicating localization in all parts of the ER, likely including MAMs.

For MAM quantification and Rcn1 analysis, the image analysis software CellProfiler™ was utilized (section 2.2.15), comparing WT and Padel fibroblasts. No statistically significant alterations could be detected regarding Rcn1 intensity (figure 18D), mitochondrial ER contact sites (figure 19E), or Rcn1 localization in MAM or ER (Figure 18F+G). Nonetheless, the average Rcn1 intensity and the amount of Rcn1 positive pixels in MAM and ER were higher in the Padel group than in the wild type.

The observed variance in each group was quite substantial, indicating missing sensitivity of the chosen method. For the quantification of mitochondrial associated membranes, a newer method with higher sensitivity was chosen (proximity ligation assay) and conducted at the department of animal physiology in a master thesis (Pfeffel, 2021). The results will be evaluated in the discussion.

For subcellular localization of Rcn1, the more precise method of cell compartmentalization via ultracentrifugation was used to investigate a possible Rcn1 localization in mitochondrial associated membranes. The results are depicted in the following section.

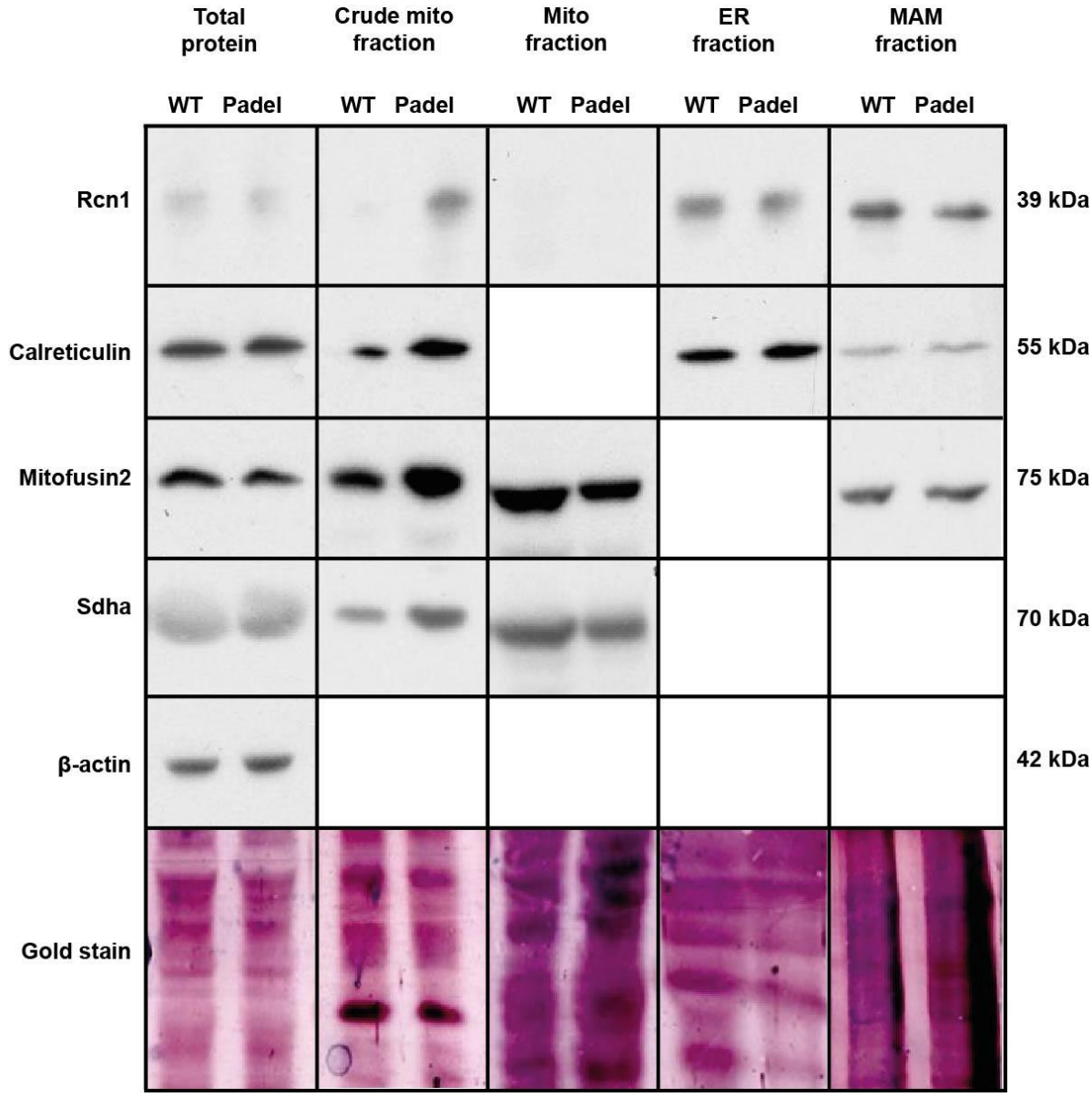

Figure 19: Cellular localization of Rcn1 examined via cell fractionation. *Western blot characterization of the cell compartment fractions of adult Padel and WT mouse brains. Fractions were generated by differential centrifugation. Organelle markers were used to confirm fraction identity. Calreticulin (55 kDa) was used as ER/MAM marker, Mitofusin2 (75 kDa) was used as a mitochondrial/MAM marker, Sdha (70 kDa) was used as a mitochondrial marker, β-Actin (42 kDa) was used as a cytoplasmatic marker, the gold staining was used to demonstrate sufficient protein content. Rcn1 (39 kDa) was tested for localization in the respective fractions. Rcn1 localization could be found in the endoplasmic reticulum and mitochondrial associated membranes. The crude mitochondrial fraction still contains MAMs, which explains the Rcn1 band in this fraction.*

All antibodies utilized in this experiment have been tested in multiple conditions to identify the optimal signal-to-noise ratio. Additionally, the fractions generated with the used protocol have been characterized and checked for contamination in a supervised master thesis (Lewendel, 2020). The gold-stained blots of every fraction indicate enough protein on every blot with a reasonably similar intensity. Each isolated fraction

contains all expected marker bands, indicating the desired fraction is indeed contained in the samples. The Rcn1 antibody produced bands on the expected height (39 kDa) in all fractions, except the purified mitochondrial fraction. This result would indicate Rcn1 is located in the ER and MAM since the crude mitochondrial fraction still contains the mitochondrial associated membranes. 5 wild type and 4 Padel mouse brain samples were analyzed to see if the Padel knockout could cause a change in organelle amount or distribution patterns (figure 19 shows one example of them). Variation between the samples in Western blot analysis seemed very high which might have masked small changes of Rcn1 distribution in those fractions caused by Parkin deficiency. The whole blots can be found in the attachment of this thesis (figure 41).

3.9 Examination of LC3b mediated autophagy in primary Padel and WT fibroblasts

One prevalent hypothesis of PD pathology is a defect in Parkin-mediated autophagy, which could lead to the accumulation of defect mitochondria, as observed in Padel mice. However, *in vivo* evidence of defect mitophagy is still missing. So far, this mechanism with defective autophagy by Parkin deficiency has only been demonstrated in tumor cell lines with artificial Parkin overexpression and autophagy-inducing substances. Thus, the following experiments aimed to explore the basal Parkin-dependent autophagy/mitophagy to allow conclusions as to whether the Padel phenotype is sufficient to negatively impact cellular autophagy in primary cells.

Because of their very high basal autophagy levels in a cultured environment, astrocytes seemed unsuitable for this kind of investigation (Violou, 2019). Unlike astrocytes, fibroblasts have often been used for studies of mitophagy (Martín-Maestro et al., 2017; Ramakrishnan et al., 2020). Therefore, mitophagy in Padel fibroblasts was investigated by using western blot and immunocytochemistry.

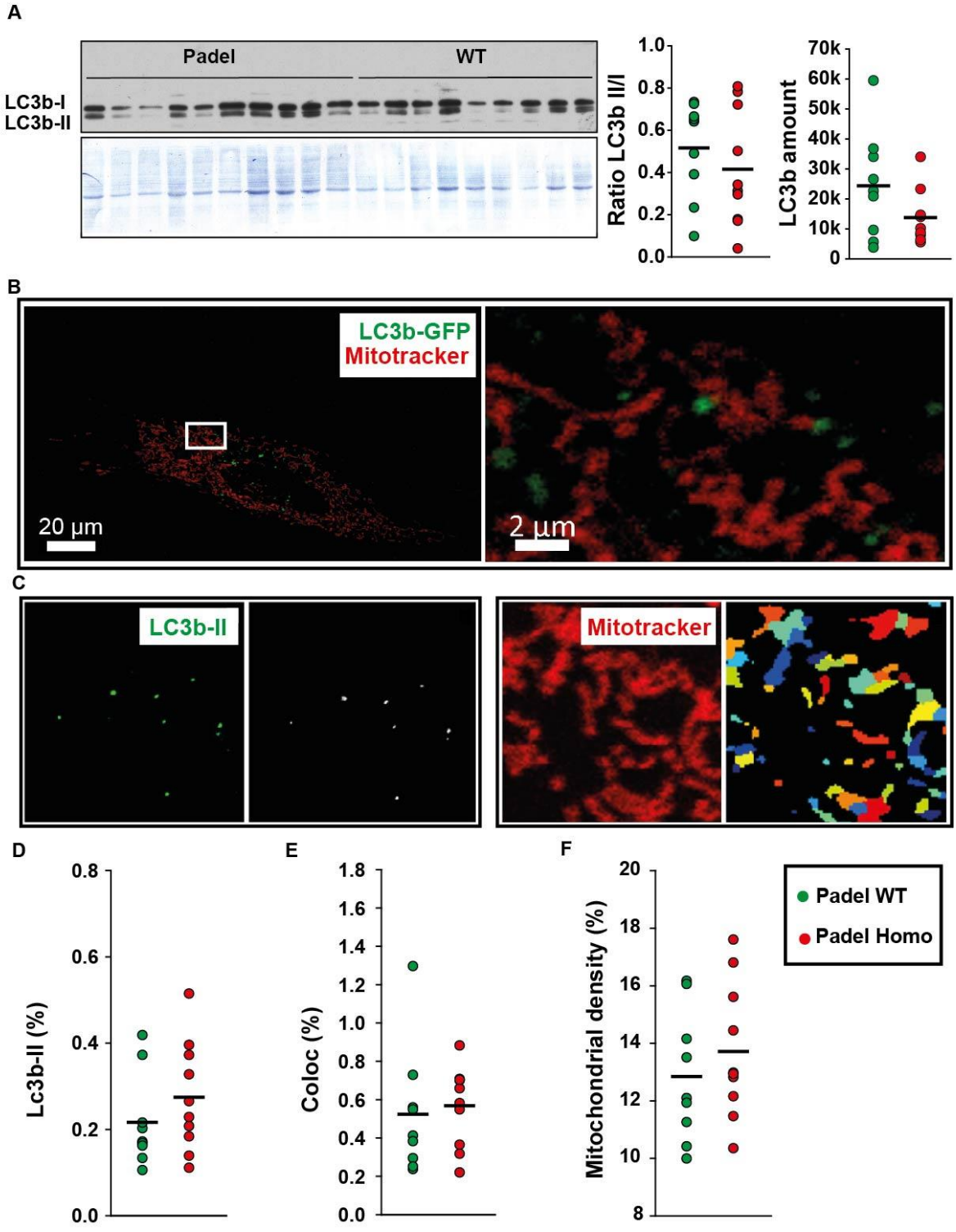

Figure 20: Examination of basal LC3b mediated autophagy and mitophagy in primary Padel fibroblasts. ***A:*** *Autophagy measurement via LC3b conversion in western blot analysis (n=10/9). No significant difference in LC3b II/I ratio was observed (p=0.406), normalized LC3b amount with whole protein did not show a significant difference (p=0.114), indicating no detectable change of basal autophagy.* ***B:*** *Image of a living LC3b-eGFP transfected primary fibroblast with dyed mitochondria. Practical work for this experiment was performed by a supervised bachelor student (Lössl, 2020)* ***C:*** *Examples of the thresholding algorithm for vesicular LC3b (left) and mitochondria (right) for co-localization analysis to detect mitophagy.* ***D:*** *Vesicular LC3b pixel in relation to the cell surface area. No difference in LC3b containing vesicles was detected (p=0.296).* ***E:*** *Vesicular LC3b pixel co-localized with mitochondrial pixel. No statistical difference in mitophagy was found in Padel fibroblasts (p=0.725).* ***F:*** *Mitochondrial density of the cells was unaltered between the genotypes (p=0.421).*
** p< 0.05, ** p< 0.01, *** p< 0.001 Mann-Whitney u-test.*

The LC3b antibody has been validated in previous experiments conducted by the department of animal physiology (Violou, 2019). The exposure time of the western blot was optimized to prevent saturated bands on the blot, thereby preventing biased analysis. However, variance in total protein amount between the samples could be observed in the Coomassie blue staining. This should not affect analysis, since normalization occurs within the sample lanes. The ratio of cytosolic and vesicular LC3b between Padel and wild type fibroblasts did not show a statistically significant effect (figure 20A right p=0.406). The normalized vesicular LC3b amount with the whole protein content of the sample did not produce a significant alteration in autophagy as well (p=0.114). Although, both analyses show a slight tendency for reduced autophagy in Padel fibroblasts.

The subsequent experiment (figure 20B) focuses on mitophagy especially, ignoring other autophagic processes. The experiment was designed to minimize technical variance to identify a possibly small biological difference in basal mitochondrial recycling. Images were taken from living fibroblasts to exclude the possibility of fixation or staining artifacts. Visualization of Organelles for colocalization analysis can be seen in figure 20B. Thresholding for colocalization analysis is displayed in figure 20C. Identification of vesicular autophagosomes could be achieved with high precision via manual thresholding. The object recognition for mitochondrial structures by the cell profiler algorithm is a possible source for technical variance. Due to intensity variation, not all mitochondria could be identified as objects by the algorithm, but the overall identification rate was very high. Quantification and comparison of vesicular LC3b amount between Padel and wild type fibroblasts (figure 20D) did not result in a statistically significant difference (p=0.296). The mean comparison displayed even an increased autophagosome amount in the Padel group. The results of mitophagy analysis via colocalization (figure 20E) did not show a significant alteration as well (p=0.725). The amount of mitochondria was quantified as well because a potentially impaired mitophagy in Parkin deficient cells could lead to mitochondrial accumulation (figure 20F). This hypothesis could not be confirmed in this experimental setup, though (p=0.421). Similar experiments with different cell types and means of mitochondrial visualization examined this as well and also could not confirm an increased amount of mitochondria in Parkin deficient cells (Wittenberg 2018, Pfeffel, 2019).

3.10 Investigation of mitochondrial exchange between mesencephalic astrocytes *in vitro*

Previous experiments of the department of animal physiology indirectly hinted at a possible mitochondrial exchange in the *substantia nigra in vivo*. The mitochondrial exchange has been published in different cell types and settings since (Ahmad et al., 2014; Dong et al., 2017; Diaz-Carballo et al., 2015), but exchange in mesencephalic astrocytes has not been reported. To demonstrate the capability of mitochondrial release and uptake in mesencephalic astrocytes, a proof of principle experiment was designed.

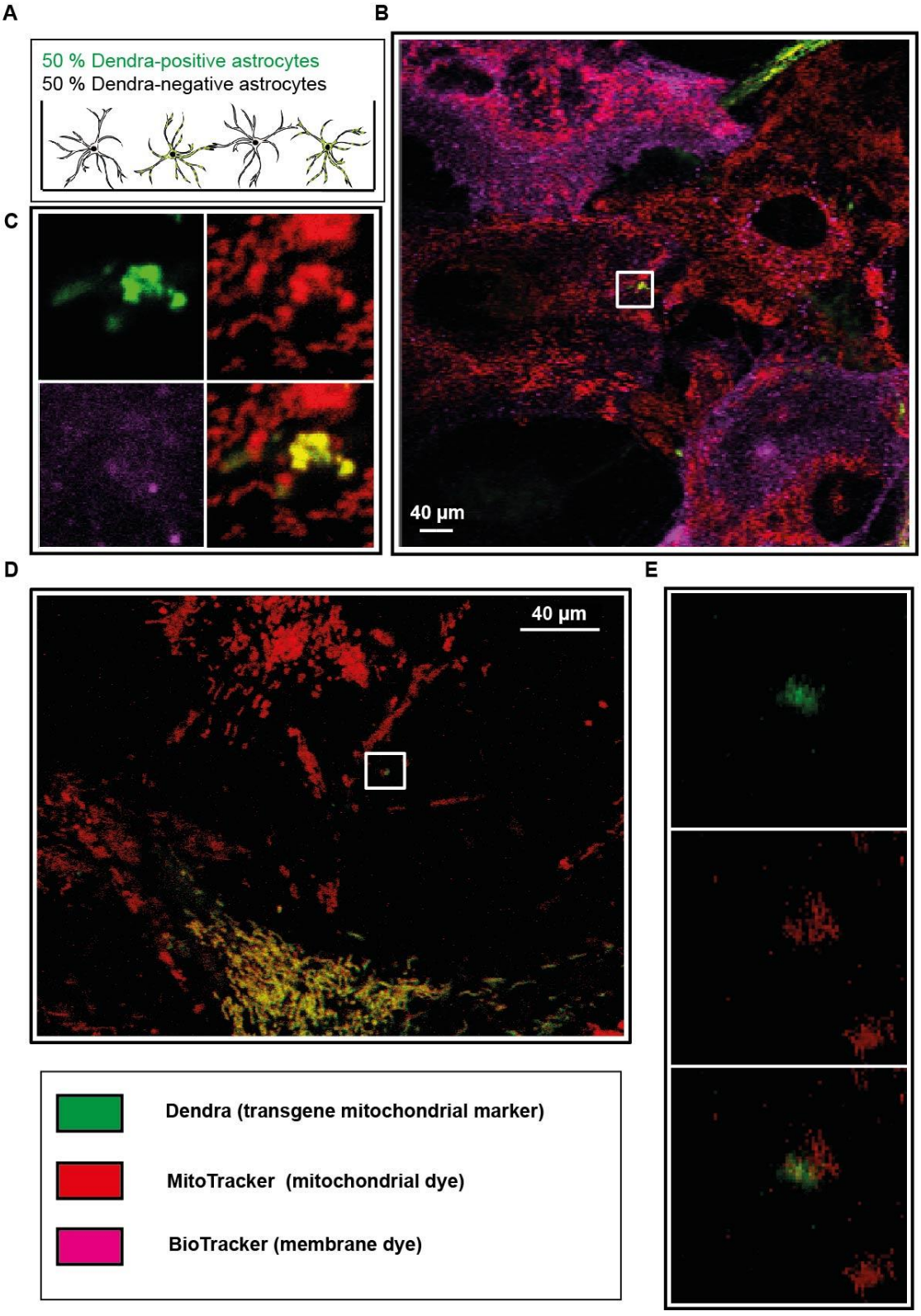

Figure 21: Intercellular mitochondrial exchange between living mesencephalic astrocytes in vitro. A: *Image of the experimental design. Mesencephalic astrocytes with marked mitochondria (Dendra) were co-cultured with astrocytes without marked mitochondria.* ***B:*** *living co-cultures were stained with a mitochondrial (red) and membrane dye (magenta) to visualize all mitochondria and cell borders.* ***C:*** *Dendra-positive structures in Dendra-negative cells exhibiting mitochondrial morphology were found indicating mitochondrial exchange (example image).* ***D:*** *Image shows a Dendra-positive structure in a Dendra-negative cell as part of a bigger MitoTracker positive structure indicating fusion with an exchanged mitochondrion.* ***E:*** *Video of a fused exchanged mitochondrion (Video on the CD).*

Figure 21A displays the principle of experimental design. Primary mesencephalic astrocytes were labeled with a transgenic, green fluorophore with a mitochondrial location tag and co-cultured with wild type astrocytes in a one-to-one ratio. These cultures were subsequently stained with a mitochondrial and a membrane dye (figure 21B). The staining off all mitochondria in the culture was performed to clearly identify exchanged mitochondria. Those mitochondria would have to be located in Dendra-negative cells, displaying a mitochondrial shape, integration in the mitochondrial network, same focal plane as endogenous mitochondria, and green + red fluorescence. These parameters should ensure the mitochondrial identity of exchanged green, fluorescent structures, since just relying on fluorescence can cause false positives (dust particles, autofluorescence). The membrane dye should visualize long protrusions from Dendra-positive cells, piercing or overlaying Dendra-negative cells as an additional control for their location.

Figure 21C shows a green+ red fluorescent structure with mitochondrial morphology, embedded in the mitochondrial network of an only red fluorescent cell. The focal plane of the green structure is identical with surrounding red mitochondria and the membrane dye does not indicate any form of protrusions from other cells. Additionally, no Dendra-positive cell is in the near proximity of the green, fluorescent structure. Taken together, it is highly probable, that the green structure consists of exchanged, Dendra-positive mitochondria, which were integrated into the host cells mitochondrial network. This phenomenon could be observed in different cells and cultures, but the frequency was very low.

The next image (figure 21D) displays an exchanged mitochondrion, which is not fully embedded in the host cell’s mitochondrial network. However, this Dendra-positive mitochondrion seems to have fused with a Dendra-negative mitochondrion, indicated by figure 21E. A video of the fused mitochondria can be found in the digital supplement of this thesis.

Taken together, it seems clear that primary murine mesencephalic astrocytes do exchange mitochondria and integrate them into their mitochondrial network *in vitro.*

3.11 Exchange of mitochondria from mesencephalic astrocytes to postnatal catecholaminergic midbrain neurons

It has been demonstrated that primary murine mesencephalic astrocytes are capable of intercellular mitochondrial exchange *in vitro*. The next logical is step is the investigation of a possible mitochondrial exchange between those astrocytes and catecholaminergic midbrain neurons to illuminate a potential mechanism, which might be associated with PD pathology. The following experiments investigate an exchange from astrocytes into neurons.

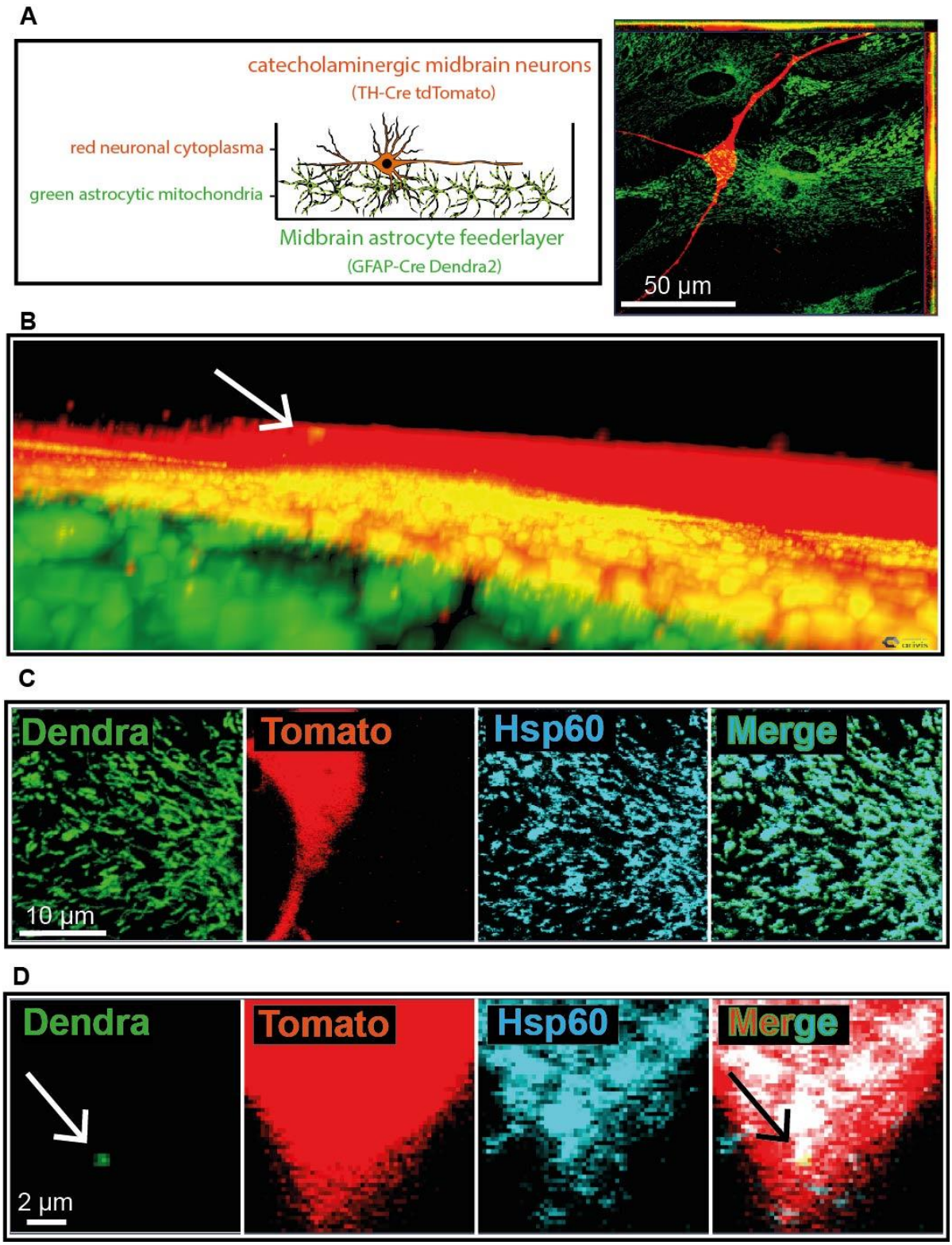

Figure 22: Mitochondrial exchange from primary murine midbrain astrocytes to postnatal catecholaminergic midbrain neurons in a direct co-culture in vitro. A: *Image of the experimental design. Red, fluorescent catecholaminergic midbrain neurons (tdTomato) were seeded on an astrocytic feeder layer with green, fluorescent mitochondria (Dendra).* ***B:*** *A 3D reconstruction of a confocal image stack shows a green, fluorescent structure in the red cytoplasm of the catecholaminergic neuron.* ***C:*** *Co-cultures were immunocytochemically stained with the mitochondrial marker Hsp60 (blue). The merge with the Dendra channel in the focal plane of the astrocytic feeder layer shows high co-localization, which indicates the mitochondrial specificity of the antibody.* ***D:*** *Image slice of the 3D reconstruction in the focal plane of the green, fluorescent structure in the neuronal soma. The structure is immunoreactive for Hsp60 indicating mitochondrial identity.*

Figure 22A shows the experimental strategy utilized for the examination of a mitochondrial exchange from mesencephalic astrocytes to catecholaminergic midbrain neurons. The neurons carried the tomato transgene, thereby enabling the search of Dendra-positive structures in red cells. Z-stacks with a minimal pinhole were chosen to increase z-resolution to distinguish between objects in or on catecholaminergic neurons. Figure 22B shows an example of a green, fluorescent structure in red cytoplasm. The z-stack ended before the soma could be completely reconstructed indicating the cytoplasmatic location of the green structure. To further check for mitochondrial identity, the co-cultures were immunocytochemically stained with the mitochondrial marker Hsp60. MitoTracker could not be utilized due to overlap with the tomato fluorophore. The antibody was able to achieve a high colocalization with the Dendra transgene on the focal plane of the astrocytic feeder layer (figure 22C). On the focal plane of the catecholaminergic neuron, the green, fluorescent structure was also immunoreactive for Hsp60, although the overall quality of mitochondrial staining of the antibody revealed less distinct morphology (figure 22D). Taken together, it is likely that the observed green, fluorescent structures in catecholaminergic neurons are Dendra-positive mitochondria of astrocytic origin. Events like this could be observed in different cultures (Padel and WT), but the frequency was very low. In fact, this phenomenon seemed to be too rare to investigate a possible impact of the Parkin knockout.

3.12 Possible mechanisms for intercellular mitochondrial exchange *in vitro*

During co-culture experiments with murine cells in primary culture, evidence of possible mitochondrial transport mechanisms emerged. They are displayed in the following figure.

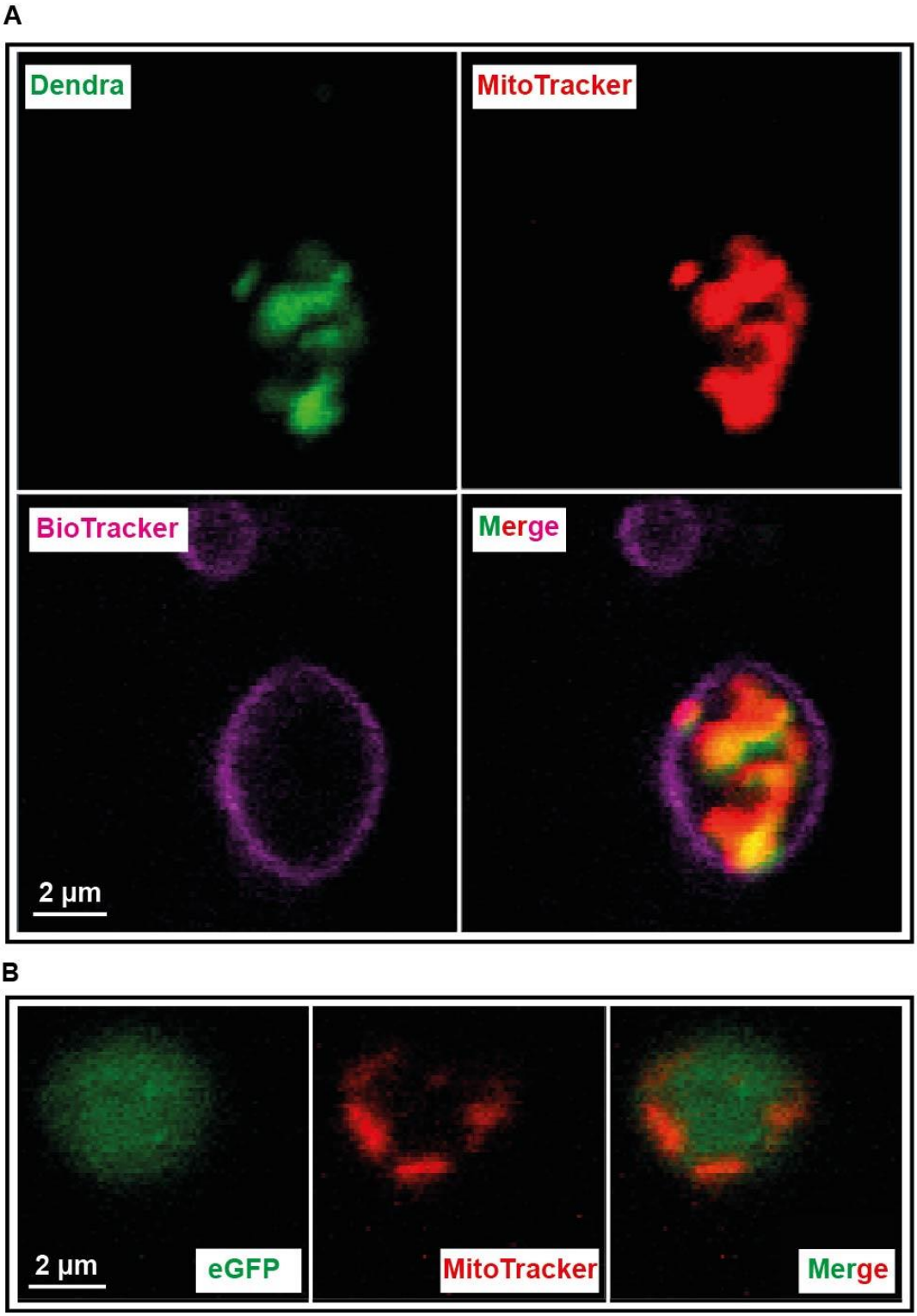

Figure 23: Mechanisms of murine mitochondrial exchange in vitro. A: *Image of a living, primary, mesencephalic astrocyte culture with transgenic green mitochondria (Dendra), treated with a red mitochondrial dye (MitoTracker) and a magenta membrane dye (BioTracker). A membrane-encapsulated structure between 4-8 µm diameter containing Dendra-positive mitochondria was found between the cells. This indicates vesicular transport of mitochondria as one mechanism of exchange in primary mesencephalic astrocytes in vitro.* ***B:*** *An image of a living primary murine fibroblast culture with eGFP-transfected cells was treated with MitoTracker. A round vesicular structure containing cytosol and mitochondria was found between the cells, indicating the same mechanism exists in primary murine fibroblasts.*

Figure 23A shows fluorescence images from a living primary murine astrocyte culture containing cells expressing the Dendra transgene. Cultures were additionally treated with two dyes to visualize all mitochondria and lipid membranes. The picture shows an oval structure with a 4-6 µm diameter surrounded by a lipid double membrane. The vesicle contains structures exhibiting mitochondrial morphology, which are fluorescent in the Dendra and MitoTracker channel, indicating mitochondrial identity. This object was located between cells in the culture. Taken together with the observation, that many exchanged mitochondria did not have Dendra-positive cells in the near proximity, indicates a primarily indirect transport mechanism like vesicular transport in this *in vitro* environment.

The second image was taken from a living primary murine fibroblast culture, which was transfected with an eGFP construct and treated with MitoTracker (figure 23B). A round object with a 3 µm diameter containing cytosolic eGFP can be observed between cells, indicating vesicular identity. It contains MitoTracker-positive structures with mitochondrial morphology. It seems plausible, that mitochondrial exchange also takes place in primary murine fibroblasts via vesicular mechanisms.

3.13 Induction of mitochondrial exchange from mesencephalic astrocytes to postnatal catecholaminergic midbrain neurons with hypoxia and stroke simulation

Mitochondrial exchange from primary, murine, mesencephalic astrocytes has been demonstrated *in vitro*, but those events seemed to be too rare for quantification. An increase of mitochondrial exchange frequency has been described from astrocytes into cortical neurons after oxygen and glucose deprivation in the literature. The following experiment aims to increase mitochondrial exchange to enable Padel/WT comparison.

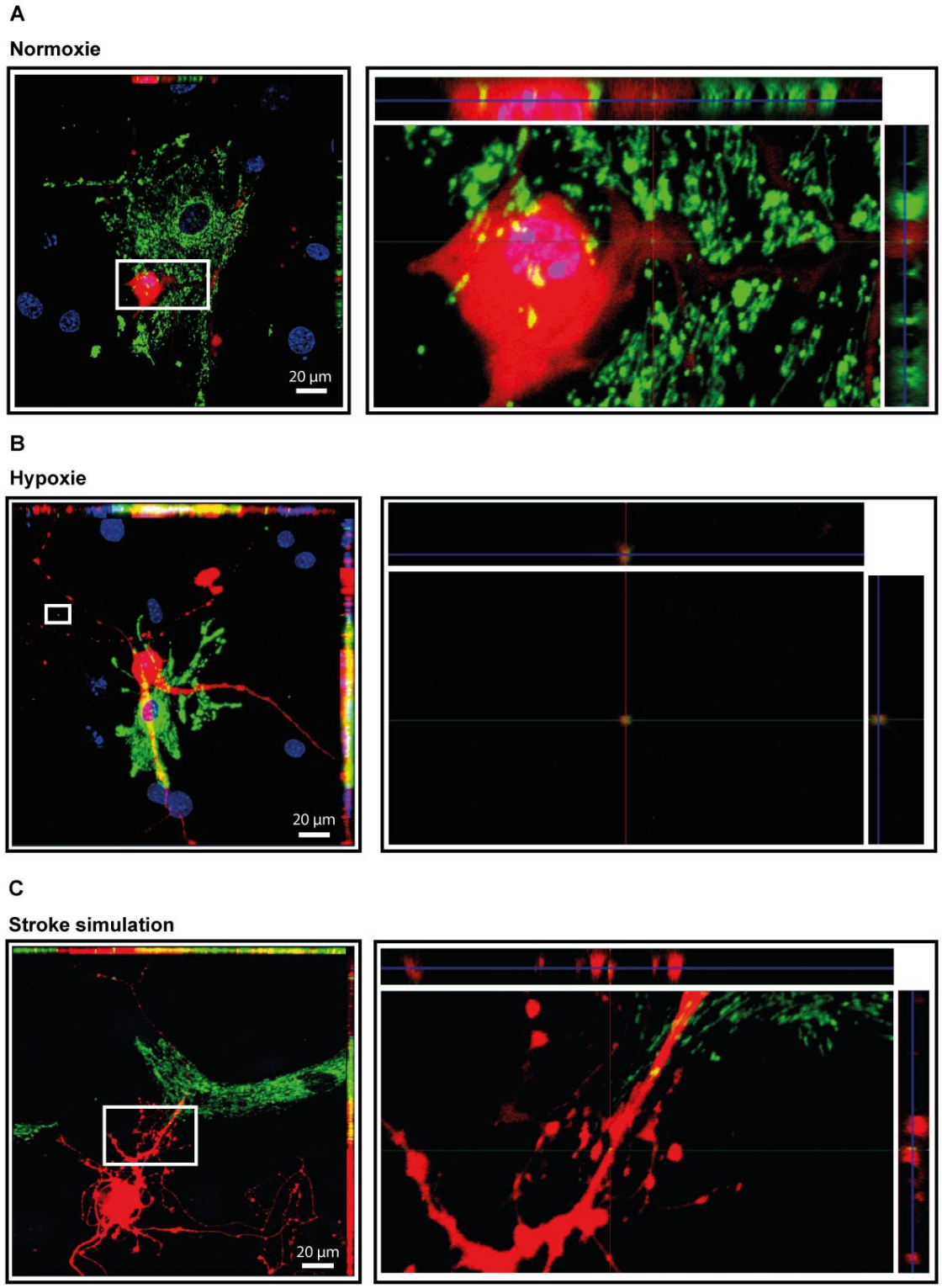

Figure 24: Induction of intercellular mitochondrial exchange from murine mesencephalic astrocytes to catecholaminergic midbrain neurons in vitro *(n=4).* ***A:*** *Image of a mesencephalic catecholaminergic neuron without oxygen or glucose deprivation. The mitochondrial exchange could be observed as a rare event, in this case into a dendrite near the soma.* ***B:*** *Hypoxia treatment: The co-cultures were placed in a hypoxic chamber for two hours (5% O_2, 5% CO_2, 90% N_2). The mitochondrial exchange frequency did not increase as a consequence. One exchanged mitochondrion is displayed in the axon.* ***C:*** *Stroke simulation: co-cultures were glucose deprived and placed in a chamber without oxygen for two hours (5% CO_2, 95% N_2). The intercellular mitochondrial exchange did not increase as a result, but neuronal morphology was affected. An exchanged mitochondrion is displayed in the dendrite. Note: Mitochondrial exchange into axons and dendrites was also observed in unstressed co-cultures.*

The previously established co-culture model for the examination of mitochondrial exchange between astrocytes and neurons has been utilized in this experiment. Co-cultures received a hypoxia treatment (5% O_2, 1 hour) to induce mitochondrial exchange (image 24B). The treatment did not visually alter neuronal morphology or seemed to increase the number of exchanged mitochondria. To further increase the stress on catecholaminergic neurons, a stroke was simulated (0% Glucose, 0% O_2,1 hour), which allegedly induced mitochondrial exchange into cortical neurons (figure 24C). Treatment changed neuronal morphology and led to axonal and dendritic beading, as well as swelling. An increased number of exchanged mitochondria was not detected.

3.14 Impact of Parkin knockout on the differentiation of primary mesencephalic midbrain neurons *in vitro*

Previous experiments indicated Padel astrocytes failed to support differentiation of WT cortical neurons in indirect co-culture (Schmidt et al., 2011). This experiment examines the impact of Parkin deficiency on the differentiation capabilities of mesencephalic neurons, that are more closely related to PD pathogenesis. Besides the effect of Parkin deficiency in astrocytes, its impact on mesencephalic neurons should also be investigated in this experiment.

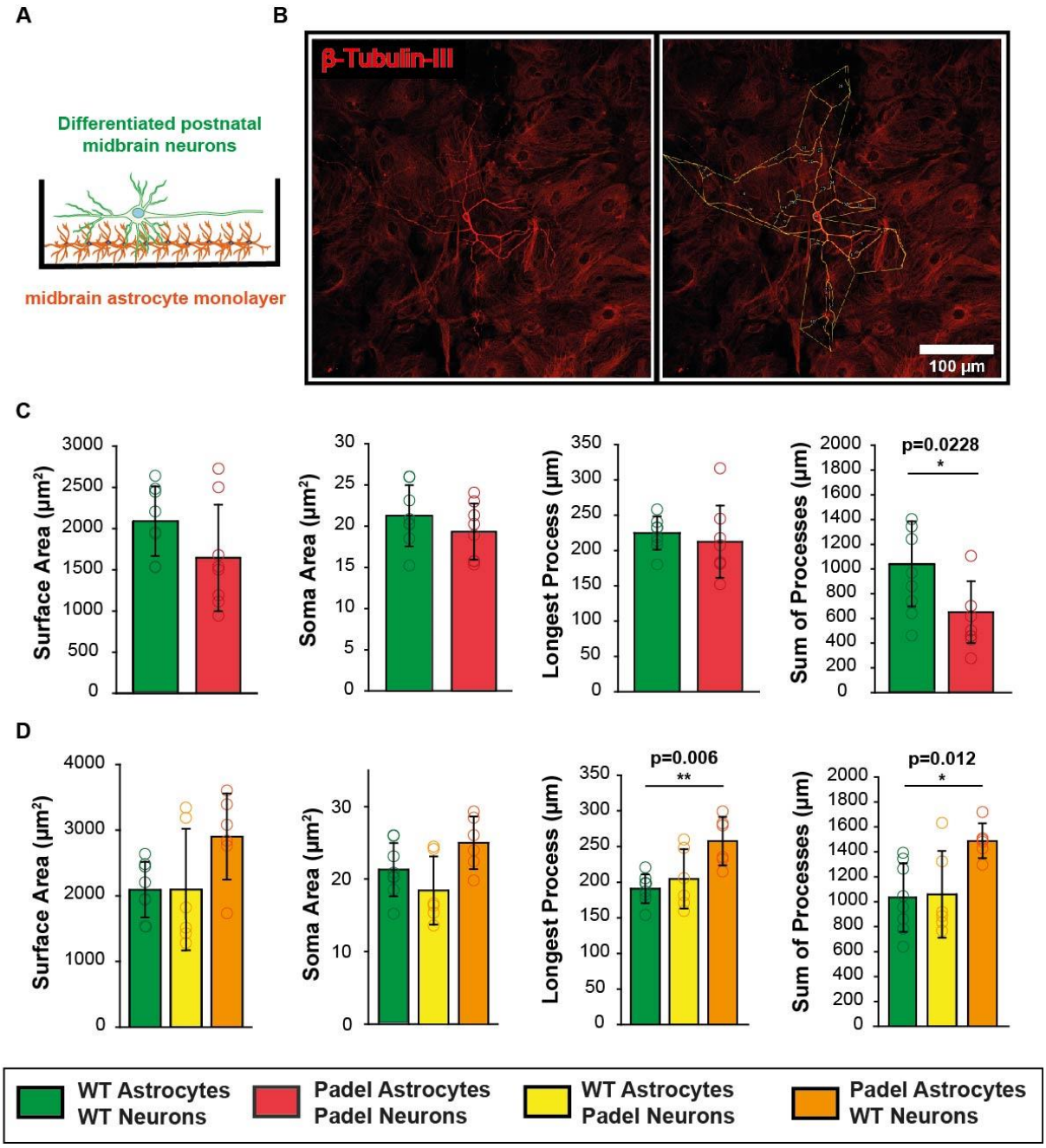

Figure 25: Impact of the Padel knock-out on the differentiation of postnatal mesencephalic neurons in vitro. ***A:*** *Principle of experimental design. Primary murine midbrain neurons were seeded on a mesencephalic astrocytic feeder layer and had 7 days to differentiate.* ***B:*** *Neurons were visualized with β-Tubulin-III, which stained neurons homogenously and with sufficient intensity for quantification. Morphological features were determined with the ImageJ software.* ***C:*** *Comparison of morphological parameters between Parkin deficient and wild type co-cultures. The sum of processes was reduced in the Parkin-deficient group (p=0.0228, Mann-Whitney u-test).* ***D:*** *Examination of hybrid cultures to find out if one Parkin-deficient cell type in co-culture is enough to cause morphological impairment. Morphological deficiencies could not be observed compared to the WT/WT culture, indicating both cell types need to carry the Parkin mutation and neuron-glia interaction is required to cause reduced neuronal differentiation. Interestingly, the co-culture with Padel astrocytes and WT neurons displayed even longer processes than the WT/WT group (p=0.006, p=0.012 ANOVA on Ranks).*
*n=8,6,6-8 left to right, * p< 0.05, ** p< 0.01, *** p< 0.001.*

This experiment again utilizes the two-step co-culture with an astrocytic feeder layer and subsequent neuronal seeding (figure 25A). This allows different genotype combinations of cells in the culture experiment. Mesencephalic neurons were visualized via immunocytochemical β-Tubulin-III staining, and afterward morphologically characterized with the ImageJ software (figure 25B). The first comparison was performed between the WT/WT and Padel/Padel, which is more related to the real situation in PD patients (figure 25C). Despite no observed statistically significance in surface area, soma area, and the longest process the Padel/Padel group exhibited a significantly lower sum of neuronal processes ($p=0.028$), demonstrating differentiation impairment of mesencephalic neurons similar to the previously described impairment of cortical neurons.

To examine if one Parkin deficient cell type in co-culture is sufficient to cause impairment of differentiation, combinations of Padel and WT cells were used for co-culture (figure 25D). Compared to the WT/WT group, neither combination has shown an impairment in morphology in any category. Interestingly, the group with Padel astrocytes and WT neurons had significantly longer processes than the WT/WT group ($p=0.006$, $p= 0.012$ Mann-Whitney u-test).

Taken together, Parkin deficient mesencephalic neurons co-cultured with Parkin mutated astrocytes displayed significant impairment in their differentiation. This impairment seems to be dependent on the interaction between neurons and astrocytes, which both must carry the Parkin deletion.

3.15 Close examination of identified PD-associated genes via SNP analysis revealed impurities in the genetic background of Padel WT mice

In this thesis, a transcriptome analysis of PD mouse lines was repeated with a new aligning algorithm to identify PD-associated genes. qPCR experiments confirmed three upregulated genes (Ermard, Tcp11l1, Rcn1). The gene Ermard was not further investigated, because its chromosomal location was directly neighboring Parkin and therefore, likely had a 129Sv/J background, representing a rudiment from mouse line

generation (section 3.4). Tcp11l1 and Rcn1 were considered possible PD-associated genes and Rcn1 was picked as a primary target because its hypothesized function aligned with obtained calcium measurement data in Padel mice.

However, a later conducted SNP analysis, which should function as an additional control for publication, revealed impurities in our Padel WT line despite backcrossing for over 20 generations. The results of the SNP analyses can be seen below.

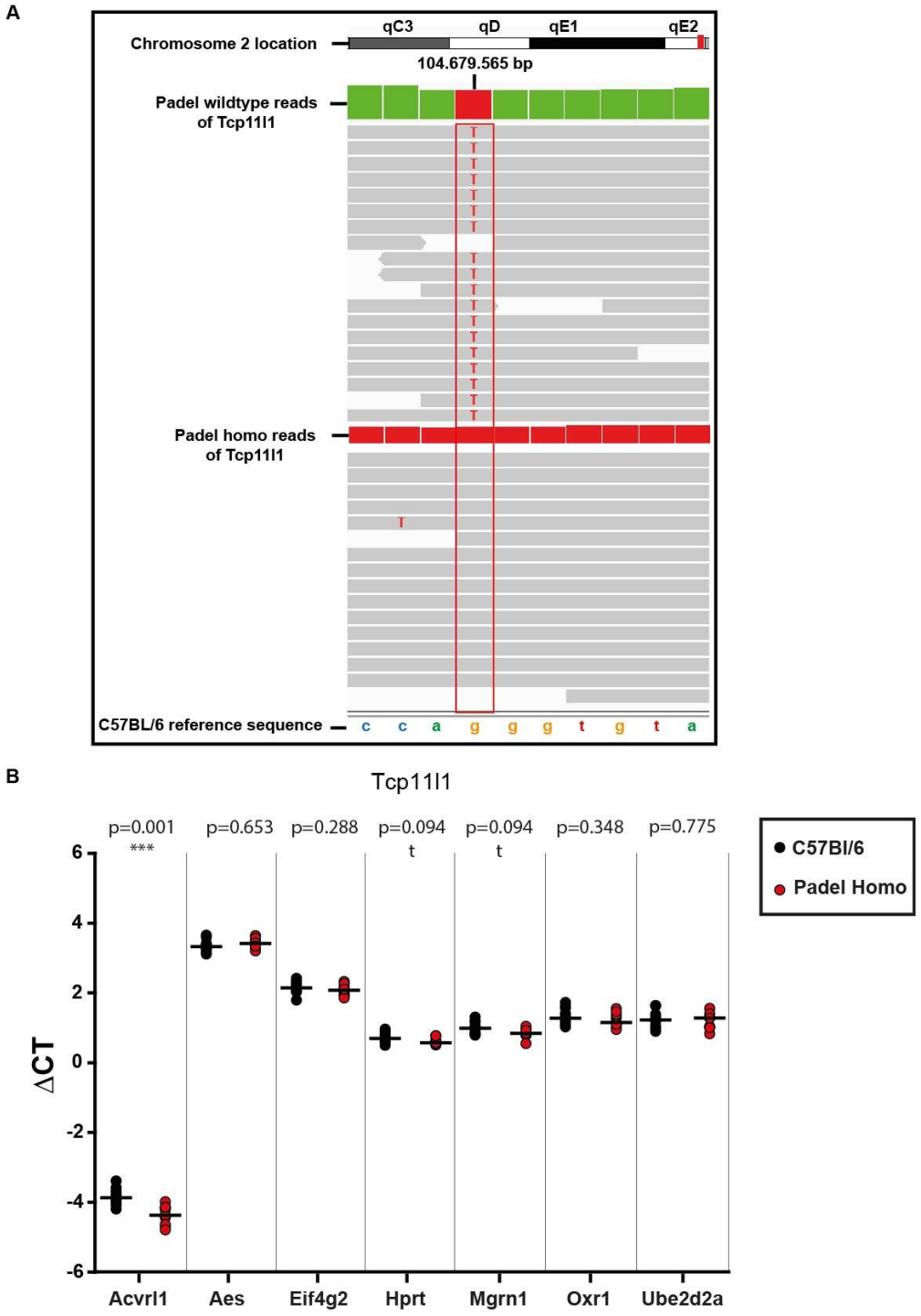

Figure 26: Single Nucleotide Polymorphism (SNP) analysis of Padel and their littermates for the Tcp11l1 gene. A: *A SNP analysis of reads from the transcriptome dataset revealed a different genomic background for Tcp11l1 between Padel mice and their littermates. Littermates exhibit over 20 SNPs in the TCP11l1 gene not aligning with the C57BL/6 reference sequence.* ***B:*** *To investigate if the previously detected expression changes are a result from the different genomic background instead of the Parkin knock-out, qPCR experiments with Padel mice and C57BL/6 were performed, replacing Littermates as the control group. The upregulation of Tcp11l1 could not be confirmed in most reference genes, indicating no upregulation in the Padel mouse model. * p< 0.05, ** p< 0.01, *** p< 0.001 Mann-Whitney u-test.*

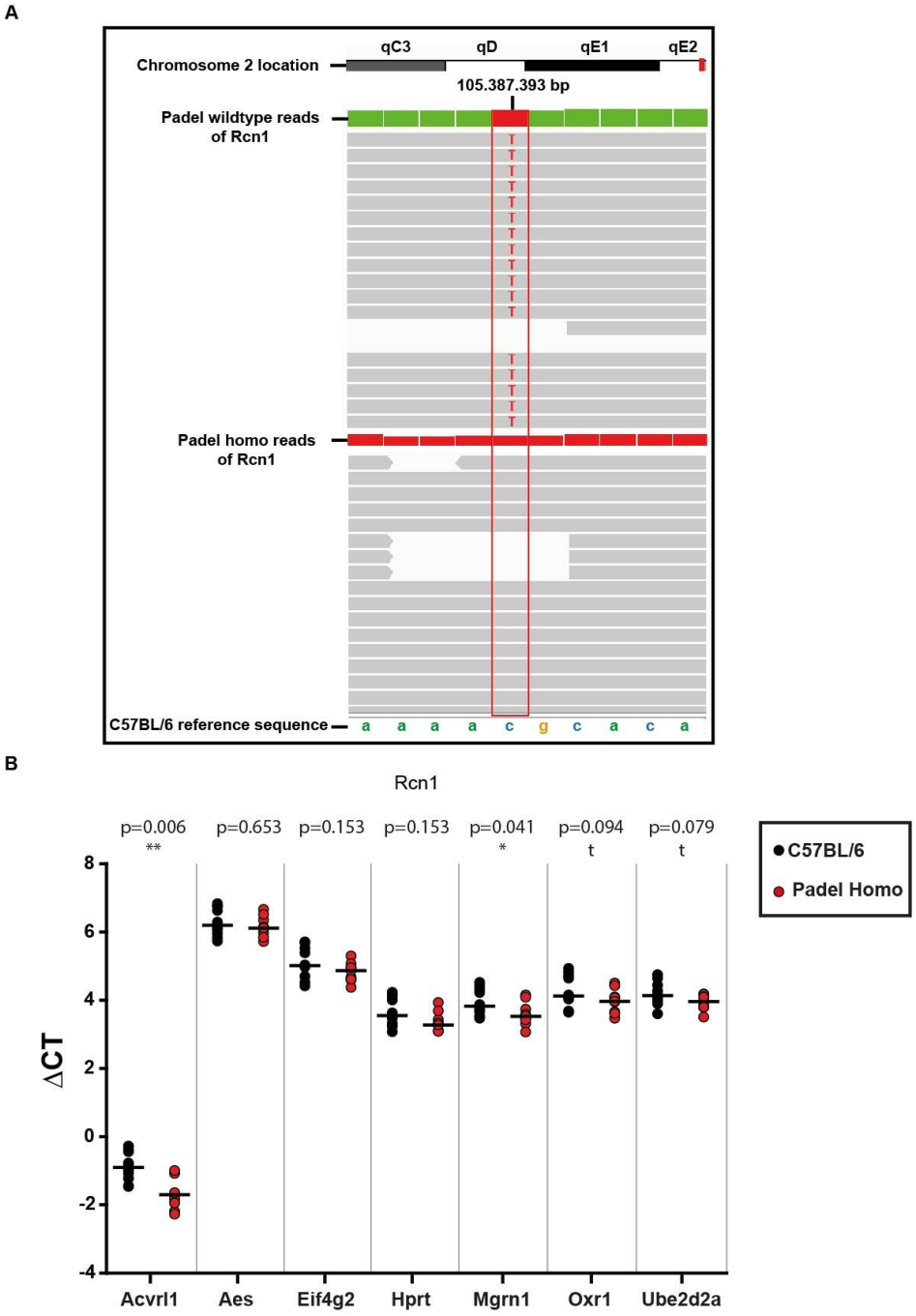

Figure 27: Single Nucleotide Polymorphism (SNP) analysis of Padel and their littermates for the Rcn1 gene. ***A:*** *A SNP analysis of reads from the transcriptome dataset revealed a different genomic background for Tcp11l1 between Padel mice and their littermates. Littermates exhibit one SNP in the Rcn1 gene not aligning with the C57BL/6 reference sequence.* ***B:*** *To investigate if the previously detected expression changes are a result from the different genomic background instead of the Parkin knock-out, qPCR experiments with Padel mice and C57BL/6 were performed, replacing Littermates as the control group. The median of the Padel group indicates higher expression of Rcn1 with all reference genes. Two reference genes (Acvrl1, Mgrn1) showed a significant difference (p=0.006, p=0.041, respectively). Two reference genes (Oxr1, Ube2d2a) showed a statistical trend (p=0.094, p=0.079, respectively) and two reference genes (Eif4g2, Hprt) showed a tendency (p=0.153, p=0.153 respectively). Taken together, Rcn1 still seems to be upregulated in the Padel mouse model, although the effect size seems to be reduced slightly. * p< 0.05, ** p< 0.01, *** p< 0.001 Mann-Whitney u-test.*

The conducted SNP analyses for Tcp11l1 and Rcn1 revealed SNPs in both genes in all four Padel WT samples, deviating from the C57BL/6 sequence (figure 26A, 27A). Tcp11l1 contained over 20 SNPs, which were spread over the whole gene, while Rcn1 just contained one SNP in the untranslated region.

This finding challenges previously conducted experiments with the Padel littermate because expression differences could be caused by the different genetic background instead of the Parkin knock-out. Therefore, mice with pure C57BL/6 background were used as a control group and qPCR experiments were repeated to examine differential expression of Tcp11l1 and Rcn1 with multiple reference genes. Tcp11l1 did not show convincing evidence of upregulation in repeated qPCR experiments and was therefore excluded from further analysis (figure 26B). Rcn1 on the other hand, still shows signs of upregulation in one-year-old SN tissue. The median of the Padel group is higher than the control group with seven reference genes (figure 27B). 6 reference genes showed a tendency for upregulation ($p \leq 0.153$), 4 showed at least a statistical trend ($p \leq 0.094$), and two were statistically significant ($p \leq 0.041$). Overall, the upregulation of Rcn1 expression in one-year-old SN tissue of Padel mice was still visible. It is essential to evaluate if this expression change is also present in neonatal animals to back up cell culture experiments. qPCR evaluation of neonatal mesencephalic tissue of Padel and C57BL/6 mice can be seen in the next figure.

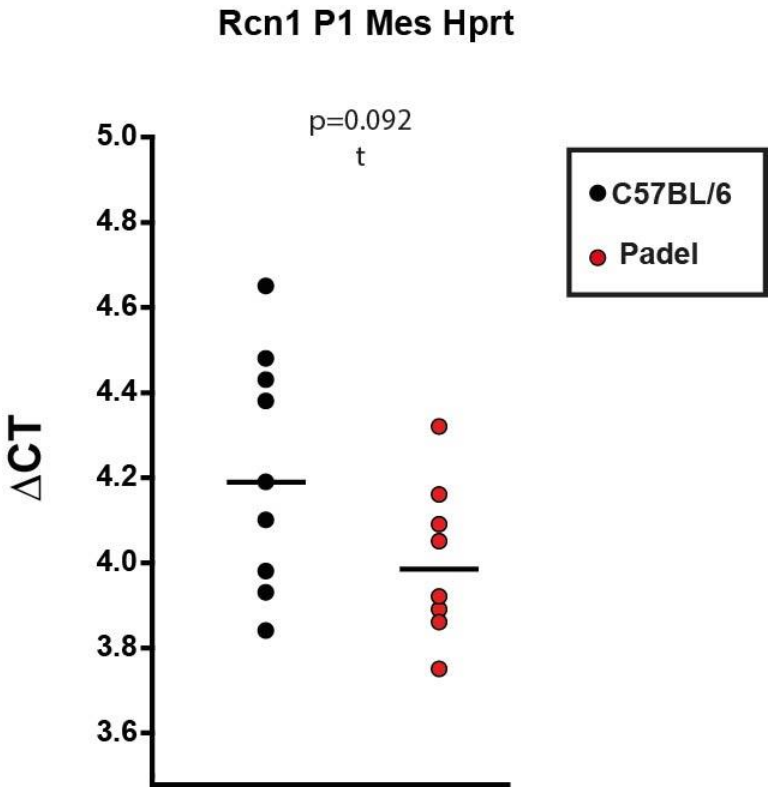

Figure 28: Examination of Rcn1 expression differences between neonatal Padel and C57BL/6 mesencephalic tissue. *Normalization was performed with Hprt as a reference gene. A statistical trend for its upregulation could be observed (p=0.092). Together with the previous experiment, it seems like Rcn1 can still be considered overexpressed in the Padel mouse model, but the effect size is smaller compared to the Padel wild type. n=10/8 * p< 0.05, ** p< 0.01, *** p< 0.001 Mann-Whitney u-test.*

The qPCR examination of neonatal mesencephalic tissue (figure 28) shows a statistical trend for Rcn1 upregulation in Padel compared to C57BL/6 (p=0.092). Like with one-year-old SN tissue, upregulation seems to be smaller but is very consistent among all experiments. Therefore, upregulation of Rcn1 in Parkin deficient mice should be biologically relevant.

3.16 Transcriptome analysis of expression differences between two PD mouse models prevalent in both SN and ST

The conducted SNP analysis revealed impurities in the genetic background of the littermate WT mice from Padel breeding, which have been used as a control group in the transcriptome analysis to identify DEGs. It seems plausible to change the strategy

for the identification of new PD-associated genes since the control group has potentially been compromised. The old strategy focused on common pathomechanisms between the Padel and Basyn mouse model, using DEGs contained in the SN of both mice for qPCR verification. The new approach aims to identify PD-associated genes, which are only relevant in one of these mouse models. This strategy removes the compromised Padel WT line from the equation as well.

The transcriptome analysis will be repeated by testing one PD model using the other PD model as the control group. The Basyn mouse as a control group has a pure C57BL/6 background, that was different from the blastocysts injected with the 129Sv/J stem cells for the Parkin knockout approach. It is important to emphasize, the aim of this comparison between Padel and Basyn was to identify genes that are differentially expressed between both mutants. In this approach, one part of these identified genes could be caused by the difference between Padel and C57BL/6, and the other part should be originated solely from Basyn transgene influence. Subsequent qPCRs analysis with Padel, Basyn, and C57BL/6 mice will make clear which genes are differentially expressed in Padel and which in Basyn.

To identify priority targets for evaluation, the transcriptome analysis will be performed in the *substantia nigra* and the *striatum*, utilizing their overlay to find genes regulated in both areas. The results of this newly performed transcriptome analysis are depicted in the following figure.

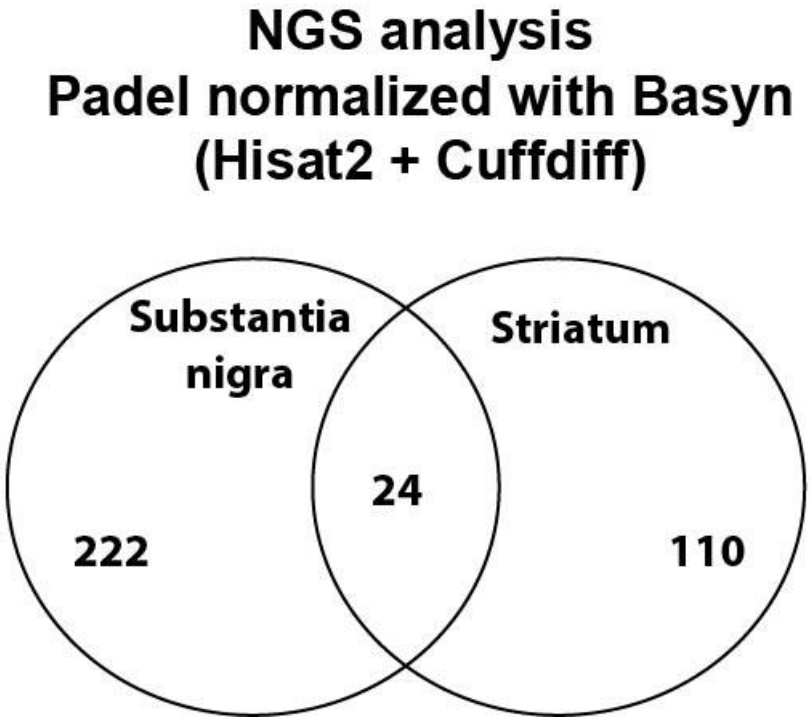

Figure 29: New NGS approach to identify PD-associated genes, which differ between both PD mouse models. *The NGS analysis was repeated with the Hisat2 aligning algorithm and the Cuffdiff expression analysis tool with the Padel mouse line, utilizing Basyn as the control group (see section 3.16). This approach should identify genes, which are just relevant in the PD pathogenesis of one of these mouse models. The substantia nigra was analyzed, as well as the striatum, which led to 222 DEGs in the SN and 110 DEGs in the ST. The overlay between the SN and ST (24 genes) was assumed to be more likely relevant to PD than the single brain regions and will be examined in Padel and Basyn with qPCR using C57Bl/6 as control group to investigate differential expression.*

Figure 29 shows the results of the new transcriptome analysis. 222 DEGs could be identified in the SN between Padel and Basyn, while 110 DEGs could be found in the *striatum*. SN and *striatum* share 24 DEGs, which seem more likely to be regulated in these mutant mice and were examined with qPCR with priority. These genes are listed in the following table with their fold change and their q-value to show regulation and statistical significance.

Table 14: List of differentially expressed genes from the SN/ST overlay produced by the new NGS analysis of Padel mice, which used Basyn mice as a control group. *Foldchange (log2, Padel against Basyn) and q-values are listed.*

Gene	Fold change	q-value	Gene	Fold change	q-value
31100 35E1ik	-0.363972	0.0101366	**Miat**	0.320264	0.0457991
Ankrd33b	-0.351828	0.0352794	**Mpped1**	-0.30892	0.0399833
Crym	-0.363644	0.0101366	**Park2**	0.89265	0.0101366
Ctsc	0.83679	0.0101366	**Pde1a**	-0.37473	0.0254012
Dlx5	-0.841519	0.0101366	**Rprml**	-0.407881	0.0101366
Dlx6os1	-0.701028	0.0101366	**Rtn4rl2**	-0.391587	0.0182203
Erdr1	1.78038	0.0101366	**Sgk1**	-0.363227	0.0101366
Gm11549	-0.515815	0.0352794	**Slc18a2**	0.627454	0.0101366
Hba-a1, Hba-a2	0.761792	0.0101366	**Snhg11**	0.415494	0.0101366
Icam5	-0.330981	0.0101366	**Tbr1**	-0.424295	0.0101366
Itpka	-0.312776	0.0352794	**Tcf7l2**	0.404449	0.0101366
Kcng2	-0.430838	0.0101366	**Xist**	0.658862	0.0101366

Before confirming a possible regulation of their expression with qPCR experiments, all their reads from NGS data have been compared to C57Bl/6 genomic sequences, thereby confirming the absence of SNPs.

To confirm expression changes, genes had to be tested in qPCR experiments with both PD models and C57Bl/6 mice. The summarized results of qPCR status are displayed on the next page.

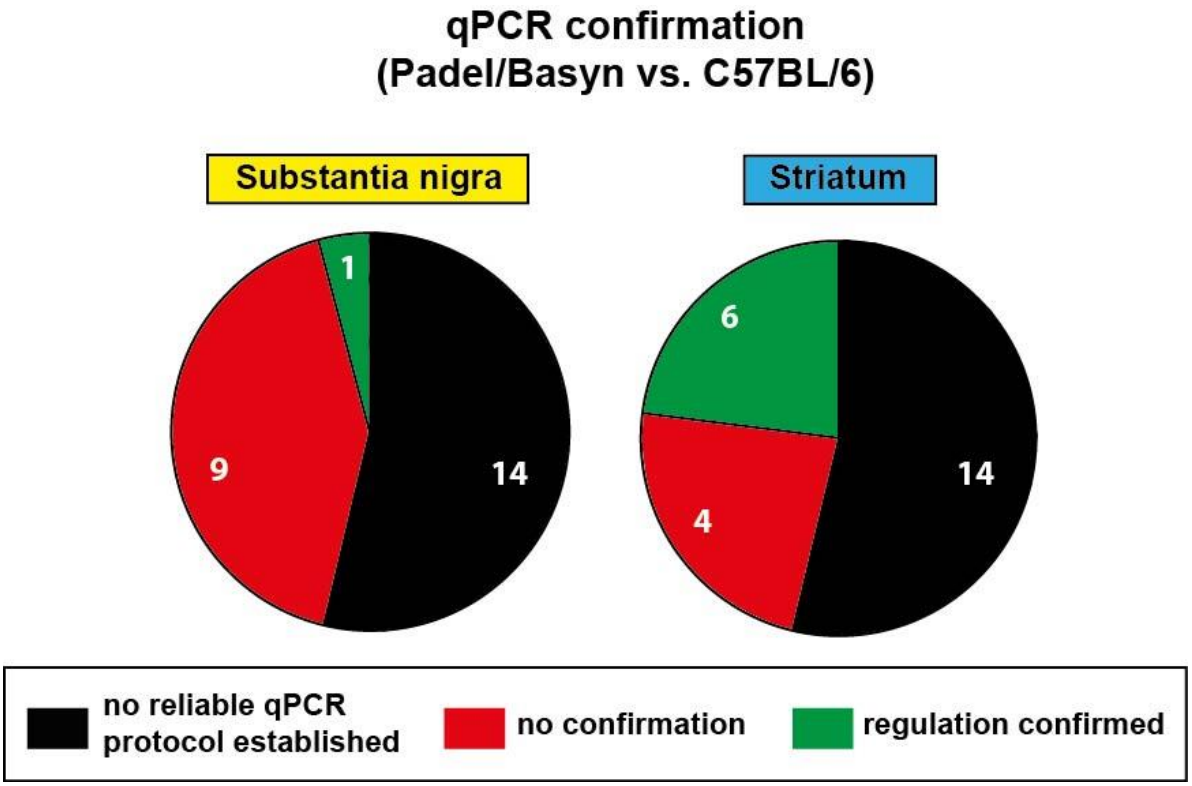

Figure 30: Summary of the qPCR verification efforts of newly identified DEGs from transcriptome analysis of Padel mice using Basyn as control group. *The gene expression was examined in the SN (left) and the ST (right) of one-year-old Padel and Basyn mice (n=8-10). The expression was normalized using Hprt as a reference gene. The status of confirmation is color-coded, as indicated by the legend. For 14 genes, no reliable qPCR protocol could be established. Ten genes could successfully be tested, resulting in one confirmed gene in the SN and six confirmed genes in the Striatum. The corresponding scatter plots and statistical analysis can be seen in the following two figures.*

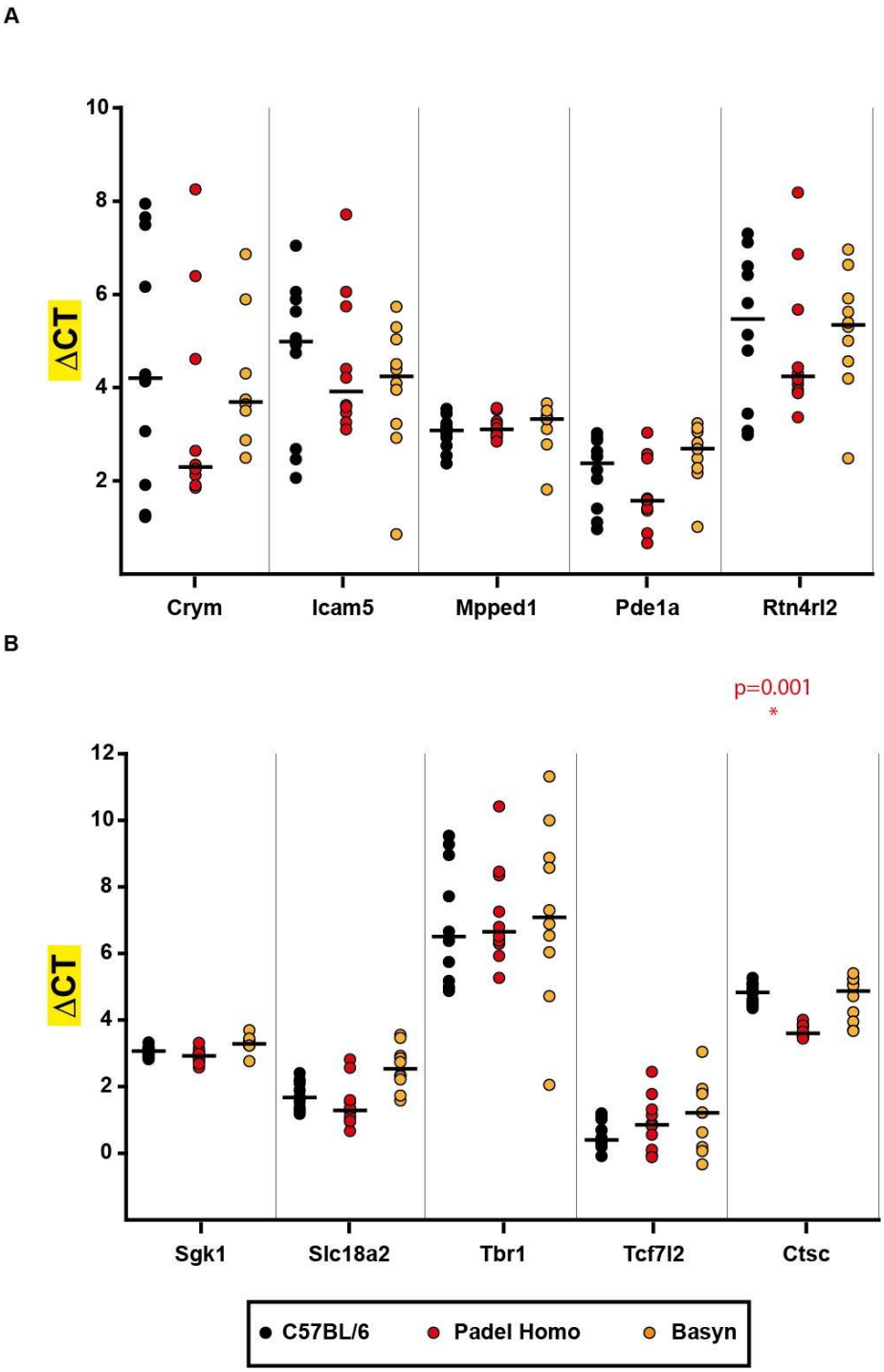

Figure 31: Statistically significant gene expression results of substantia nigra tissue of one-year-old Padel and Basyn mice. *The expression was normalized with the reference gene Hprt. Displayed are genes from the new NGS analysis of Padel mice using Basyn as control group.* ***A:*** *The genes Crym, Icam5, Mpped1, Pde1a, and Rtn4rl2 did not confirm differential regulation in the Padel or Basyn mouse model compared to C57BL/6.* ***B:*** *The genes Sgk1 Slc18a2, Tbr, and Tcf7l2 did not confirm differential regulation in Padel or Basyn compared to C57BL/6 either. Ctsc could be confirmed as upregulated in the Padel mouse model with high certainty (p=0.001). n=10/10/8/ * p< 0.05, ** p< 0.01, *** p< 0.001 Mann-Whitney u-test.*

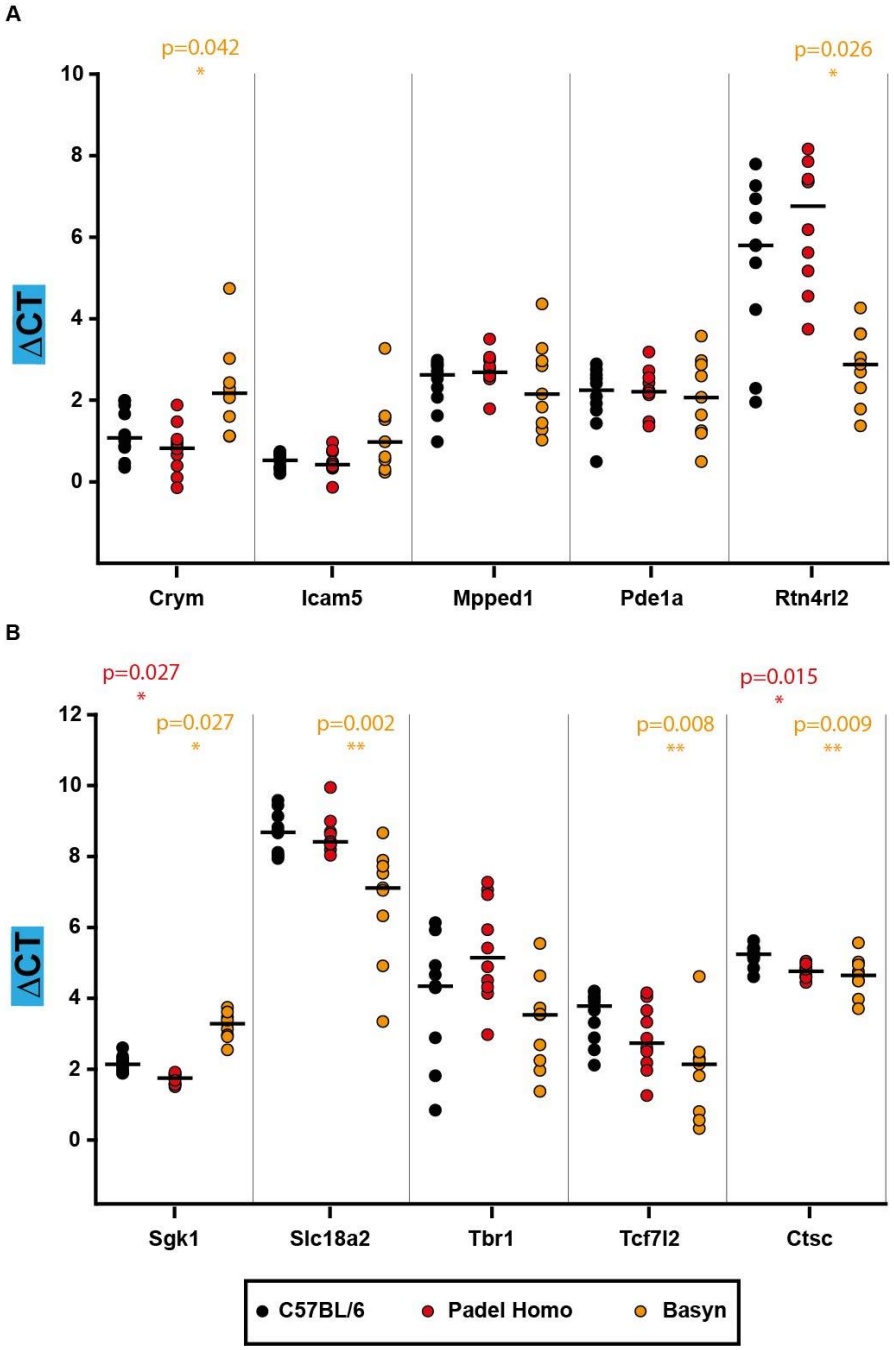

Figure 32: Statistically significant gene expression results of striatum tissue of one-year-old Padel and Basyn mice. *The expression was normalized with the reference gene Hprt. Displayed are genes from the new NGS analysis of Padel mice using Basyn as control group.* ***A:*** *The genes Icam5, Mpped1, and Pde1a did not confirm differential regulation in Padel or Basyn compared to C57BL/6 mice. However, the genes Crym and Rtn4rl2 could be confirmed as differentially expressed in the Basyn mouse model (p=0.042 ↓, p=0.026 ↑).* ***B:*** *The gene Tbr did not confirm differential regulation in Padel or Basyn compared to C57BL/6. The genes Sgk1 and Ctsc could be confirmed as upregulated in the striatum of the Padel mouse model (p=0.027, p=0.015, respectively). The genes Crym, Rtn4rl2, Sgk1, Slc18a2, Tcf7l2, and Ctsc could be confirmed as upregulated in the striatum of the Basyn mouse model (p=0.042, p=0.026, p=0.027, p=0.002, p=0.008, p=0.009, respectively).*
*n=9/10/8 * p< 0.05, ** p< 0.01, *** p< 0.001 Mann-Whitney u-test.*

Figure 31 shows the qPCR verification status of the new candidate genes in the *substantia nigra* of one-year-old animals. While the C57BL/6 comparison with Basyn yielded no statistically different expression results for all ten genes, comparison with Padel showed a clear upregulation for the gene Ctsc (p=0.001), making it a promising candidate for further evaluation.

Figure 32 displays the qPCR verification results of the new candidate genes in the *striatum* of one-year-old animals. A Comparison to wild type mice demonstrates significant upregulation of Sgk1 and Ctsc in the Padel mouse line (p= 0.027, p=0.015). Ctsc is the only gene, which is statistically significantly overexpressed in SN as well as ST tissue, making it interesting for further evaluation. The Basyn model exhibits six upregulated DEGs in this comparison (Crym, Rtn4rl2, Sgk1, Slc18a2, Tcf7l2, Ctsc). None of them were significantly regulated in the *substantia nigra* in the previous analysis. Interestingly, the gene Ctsc was regulated in the same direction in both PD mouse models, which was unlikely to be detected, since common alterations in both PD mouse models should decrease the chance of significance in this unconventional transcriptome analysis. The upregulation in must has had a different effect size between Padel and Basyn in the NGS analysis to still produce significant differences. However, the Ctsc upregulation in this qPCR experiment is nearly identical.
Multiple DEGs could be confirmed in different brain areas of two PD mouse lines with this new strategy. A summary of the examined genes is displayed in the next table.

Table 15: Summary of the gene expression status from qPCR examined genes emerged from the new transcriptome analysis. *Genes are normalized with the reference gene Hprt.*
SN =substantia nigra, ST=striatum, ↑=upregulated (green), ↓=downregulated (red).

qPCR tested genes from the new transcriptome analysis (with Hprt)	Expression status in Padel		Expression status in Basyn	
Regulated in:	**SN**	**ST**	**SN**	**ST**
Crym	-	-	-	↓
Icam5	-	-	-	-
Mpped1	-	-	-	-
Pde1a	-	-	-	-
Rtn4rl2	-	-	-	↑
Sgk1	-	↑	-	↓
Slc18a2	-	-	-	↑
Tbr1	-	-	-	-
Tcf7l2	-	-	-	↑
Ctsc	↑	↑	-	↑

However, only one gene (Ctsc) in one mouse model (Padel) was confirmed to be differentially regulated in both brain areas associated with PD pathology. This makes Ctsc the most promising candidate for further evaluation. It was tested with the whole reference gene panel to confirm differential expression. The results can be spectated in the following figure.

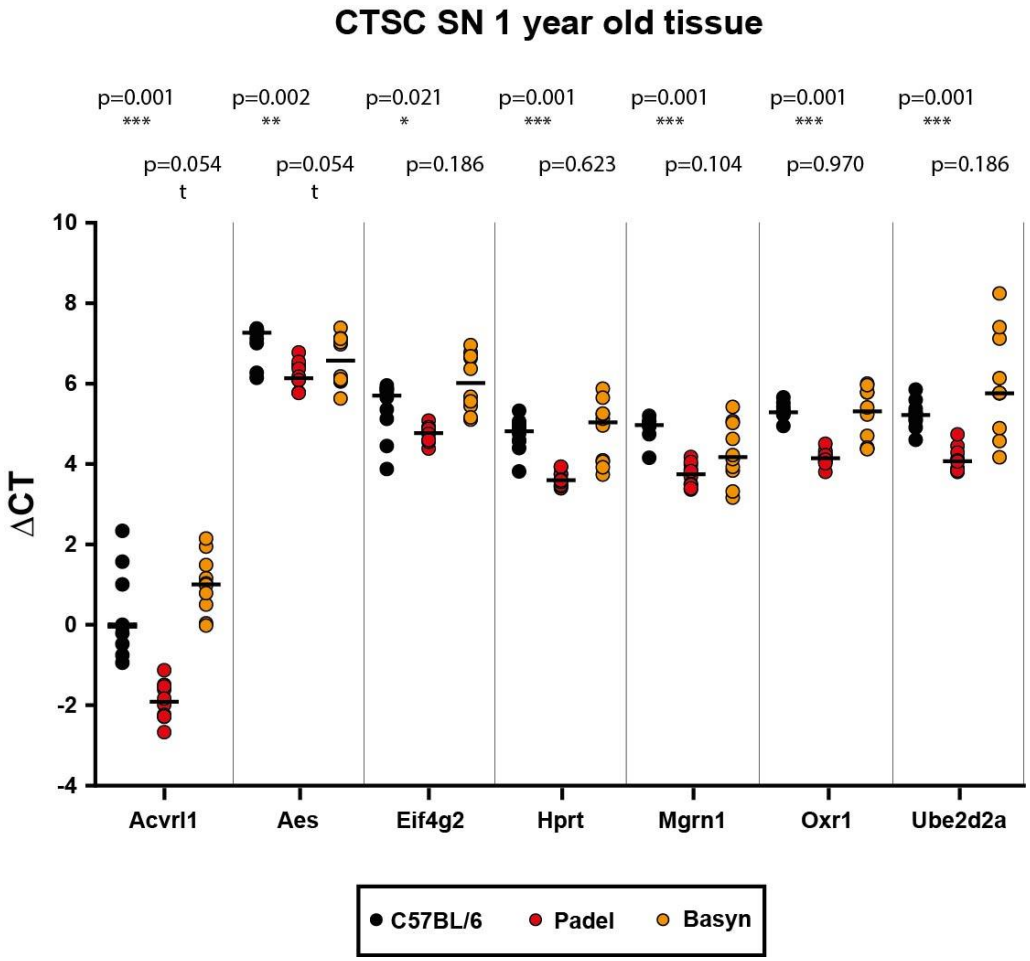

Figure 33: qPCR results of Ctsc expression in one-year-old Padel/Basyn SN tissue normalized with multiple reference genes. *Upregulation of Ctsc in the Padel mouse model could be confirmed with all reference genes with high certainty (p=0.001, p=0.002, p=0.021, p=0.001, p=0.001, p=0.001, p=0.001). Upregulation of Ctsc in the Basyn mouse model could not be confirmed. Reference genes Acvrl1 and Aes displayed a statistical trend (p=0.054, p=0.054). n=10, * p< 0.05, ** p< 0.01, *** p< 0.001, Mann-Whitney u-test.*

Evaluation of the qPCR expression analysis with multiple reference genes (figure 33) did not find a clear upregulation of Ctsc in the Basyn mouse model in any reference gene. The Padel mouse model, on the other hand, has shown clear upregulation of Ctsc with any tested reference gene, thereby confirming the hypothesized upregulation from previous experiments. The average expression foldchange between C57BL/6 and Padel is 2.36.

To investigate, if the increase in Ctsc expression is acquired over a lifetime or existent from birth, its expression was evaluated in neonatal mesencephalic tissue from Padel mice. The experiment did not show a clear result, since normalization with different reference genes resulted in either up-or downregulation and should be repeated (data not shown).

Taken together, this new approach identified multiple new potentially PD-associated candidate genes. The gene Ctsc was confirmed overexpressed with high statistical certainty with all reference genes and is particularly interesting since it is overexpressed in the Padel mouse model in both brain regions, which are affected in PD pathology.

4 Discussion

After experimental work and data generation, it is essential to analyze obtained results regarding their methodical aspects and content. This analysis is necessary to examine their validity and significance.

4.1 Repetition of transcriptome analysis and qPCR verification efforts in PD mouse models

The molecular basis of PD pathogenesis is still poorly understood. To gain insight into its mechanisms, the department of animal physiology performed a transcriptome analysis to find Parkinson's disease-associated genes in *the substantia nigra* and the *striatum* of Padel and Basyn mice. NGS analysis can be a powerful tool in basic research, but the scientific method requires replication of experiments to preliminary belief obtained results. Reproduction of results with an independent method (qPCR) further increases credibility because it excludes the possibility of methodical bias from one method (Plesser et al., 2018).
While the transcriptome analysis has the advantage of examining the whole transcriptome at the same time, its disadvantage is reduced sensitivity and reliability because of the limited sample size (Rocke et al., 2015). The qPCR can only examine one gene at a time, which makes it unsuitable for the genome-wide identification of new disease-associated genes, but it can detect expression changes with high accuracy. The combination of both methods enables a preselection of candidate genes via NGS analysis and an accurate method of confirmation via qPCR analysis.

Before the confirmation process, the transcriptome analysis was repeated replacing the aligning algorithm with a new one, which should align the generated reads to a reference genome with higher accuracy and calculation efficiency (Pertea et al., 2016; Baruzzo et al., 2017; Kim et al., 2019). Quality control of samples and methodical considerations of this NGS analysis were discussed thoroughly in the Ph.D. thesis of Katharina Osenberg and won't be further examined in this section (Osenberg, 2018).

The results of the repeated NGS analysis did indeed differ from the previous analysis indicating changes in the alignment process since the other parameters were not changed (10 new genes in Padel, 15 new genes in Basyn). However, the priority list of genes, which should be confirmed with qPCR, should consist of SN genes regulated in the Padel as well as in the Basyn mouse model as a priority. Genes regulated in both mouse models were considered more likely to be associated with PD pathogenesis. The genes identified with the new aligning algorithm did not fall into that category, but two genes previously contained in this overlay were not found in the new analysis, thereby reducing the number of priority genes to 150.

For the evaluation of these target genes, qPCR experiments were designed to check their differential expression. Multiple quality control measures were taken to ensure reliable expression results (section 2.2.6). Briefly, primers were evaluated regarding their specificity and efficiency, it was controlled for genomic contamination, RNA purity was photometrically assessed, and technical triplicates were used to balance technical variance. Additionally, a relatively high sample size (n=10) was picked to increase the statistical power of the experiments. 119 genes were examined in qPCR experiments with SN samples of the Padel mouse model, normalized with the reference gene Hprt, which has often been used for mouse brain tissue (Gubern et al., 2009; Gong et al., 2016; Kang et al., 2018), and has been shown as a suitable reference gene for Padel brain tissue by several previous experiments (Dr. Xhu, unpublished data). Confirmed genes were subsequently tested again with an independent sample set and a broad panel of reference genes to confirm differential expression. The strategy to test genes only with one reference gene at the beginning has the advantage to get a first selection on the regulation status of the candidate genes in a reasonable amount of time. The following reproduction and confirmation with multiple reference genes should eliminate false-positive results from the first confirmation experiments. Only three out of the 119 examined genes were confirmed upregulated in the Padel mouse model, which represents only 2.5% (Ermard, Tcp11l1, Rcn1).

Due to described quality control measures and much higher sample size, those results are considered credible to a high degree, indicating a high false-positive rate of the transcriptome analysis. It is likely caused by the small sample size (n=4), which necessarily generates group differences for stochastic reasons. This phenomenon is commonly described in the literature. Low sample size in combination with technical

variance in transcriptome analysis often leads to lacking reproducibility and high false-positive rates (Tsai et al., 2004; Faber and Conseca., 2014; Stretch et al., 2014). The workgroup of Maleki demonstrated, that gene set analysis with a sample size ≤ 5 per group is unlikely to be reproducible (Maleki et al., 2019). One analysis even concluded that at least 20 samples per treatment would be required for reproducible expression results (Schurch et al., 2016).

Interestingly, Osenberg tested some DEGs from the original NGS analysis in qPCR experiments using the same RNAs, which were used to build the transcriptome. The differential expression could be confirmed in 7 of 17 genes, which represents a confirmation rate of 39% (Osenberg, 2018). This indicates a strong reproduction capability of qPCR while using the same sample material. However, most of these genes failed to be confirmed as regulated genes when new samples with a larger sample size were used. Therefore, the observed high false-positive rate in the performed qPCR experiments is likely caused by biological variance, which was not extracted representatively from the transcriptome analysis due to the low sample size.

The three confirmed genes were reviewed regarding their function and localization to examine a potential connection to PD pathology. The genomic background of the Ermard gene in Padel is still 129Sv/J origin, despite the backcrossing for 20 generations with C57BL6 (Dr. Zhu, unpublished data). Since Ermard is in close proximity to Parkin on chromosome 17 with less than 3 mb distance, it is almost not possible to replace this genomic area with C57BL6 by backcrossing. Therefore, the final confirmation of Ermard regulation in the Padel mice should be performed by using 129Sv/J mice as control, which is currently not available.

The SNP analysis was also conducted for the other confirmed genes, which are in direct proximity on chromosome two (Tcp11l1, Rcn1), and revealed SNPs in the Padel Wild type not matching genetic C57BL/6 background. This finding challenged the suitability of the Padel wild type as a control group for experiments concerning the respective genes. The most plausible source of a genetic impurity would be the 129Sv/J mouse model since it was used to generate the precursor mouse model PaKO, although it was backcrossed over 20 generations with C57BL/6.

The origin of the SNPs was examined utilizing the Jackson lab SNP database to find the source of this genetic contamination. The results can be seen in the table below.

Table 16: SNP origin analysis to find the source of genetic impurity. *Displayed are SNP-containing genes, SNP location, mutation (C57BL/6 sequence has a cytosine), and a comparison with SNPs of potential strains, which caused this impurity. SNP=single nucleotide polymorphism, Chr=chromosome.*

Gene	SNP Location Chr. 2	SNP	Mouse strains					
			129Sv/ J	A/ J	AKR/ J	BALB/ cByJ	DBA/ 2J	FVB/ NJ
Rcn1	105.387.393	C/T	C	T	T	T	T	T
Tcp11l1	104.688.393	C/T	T	C	C	C	C	T
	104.681.631	C/T	T	T	T	T	T	T
SNP origin			-	-	-	-	-	+

The SNP analysis identified one SNP on the Rcn1 gene sequence, which was present in only 5 mouse strains in the Jackson lab database, thereby reducing possible candidates to five. The 129Sv/J mouse did not exhibit the SNP contained in Rcn1, which leads to the conclusion, that these genetic impurities must originate from the Deleter mouse used to remove the neomycin cassette in the old PaKO animal model. The Deleter mouse was backcrossed multiple generations with C57BL/6, like our Padel mouse, but seemed to still carry genetic impurities from its generation, which was likely carried out with FVB/NJ oocytes (table 16). Another explanation would be a mistake in the breeding process. However, this is highly unlikely due to the distinctly different phenotype between these mouse lines. Only one SNP was identified on the whole Rcn1 transcript sequence, located in the untranslated region. The Tcp11l1 gene contained more than 22 SNPs, which were distributed over the whole transcript.

The genes Tcp11l1 and Rcn1 were found to be differentially expressed in Padel homo mice compared to their littermates. Since those genes have another genetic background in littermates, the question arises, if upregulation is a result of Parkin deficiency or genetic impurity.

Upregulation of Tcp11l1 in adult Padel SN tissue vanished after repetition of qPCR experiments with C57BL/6 as control group indicating previous regulation was caused by the genetic impurity of the control group. It is not implausible, that over 20 SNPs distributed over the transcript can affect regulatory regions or mRNA conformation, thereby influencing mRNA expression or stability (Shastry et al., 2009; Keane et al., 2012; Robert and Pelletier, 2018).

Consequently, different genomic backgrounds should be accounted for during the identification of differentially expressed genes in congenic mouse lines, even when they were backcrossed for more than 20 generations.

The evaluation of Rcn1 expression of one-year-old SN tissue of Padel mice compared to C57BL/6 still showed a constant trend for upregulation, although the effect seems to be smaller compared to littermate. However, the Rcn1 qPCR experiment with neonatal Padel mesencephalic tissue also resulted in a statistical trend. Taken together, Rcn1 is carefully considered still upregulated and might still be a worthwhile target in PD research. If this postulated differential expression gets falsified in future experiments, general information about Rcn1 function and localization can still be utilized, since Rcn1 is thoroughly investigated in context with malignancy (Chen et al., 2019; Liu et al., 2018; Ueda et al., 2020).

Taken together, the examination of 119 candidate genes of a conducted transcriptome analysis in the substantia nigra resulted in the confirmation of three genes in the Padel mouse model (Ermard, Tcp11l1, Rcn1). An SNP analysis revealed a different genomic background in the Padel wild type for all three genes and subsequent qPCR experiments with C57BL/6 as a control group could confirm upregulation for the Rcn1 gene. It seems like after backcrossing the Padel mouse for over 20 generations, it was still possible to detect traces of strain contamination. By now, more modern methods have been developed to create transgene mouse models without utilizing mice like 129Sv/J for genetic manipulation of stem cells. CRISPR/Cas-based methods can precisely generate mouse models with pure C57BL/6 background, which seem to be more favorable for NGS analysis. However, unwanted genomic alterations via integration at a random genomic location can occur with CRISPR/Cas, which makes the exact characterization of these mouse strains crucial before experiments.

Because of the low qPCR confirmation rate and the genetic deviation in the Padel wild type, a new approach for the identification of PD-associated genes was designed. While the first NGS analysis focused on genes, which were commonly regulated in both Padel and Basyn, the new approach targeted genes that were specifically regulated in just one of the two mouse models (section 3.16).

Although PD ultimately results in neurodegeneration in the *substantia nigra*, there might be multiple different pathways leading to the same result. This analysis aimed to

identify genes that are involved in the pathogenesis in either Padel or Basyn mice, not both. The obtained NGS data were reanalyzed utilizing Basyn as the control group for the Padel mice, which possess pure C57BL/6 background (Maskri et al., 2004). This has the disadvantage of not identifying genes, which are commonly regulated as a result of the different PD mutations. Additionally, DEGs from this analysis could either be abnormally expressed in Padel or Basyn mice. This makes it essential to confirm obtained results in qPCR experiments with both PD mouse models and C57BL/6 animals as the control group. It is clear, that this experiment would not be designed *de novo* because of its mentioned disadvantages, but it can harness additional information from the already generated NGS dataset and at the same time remove the variable of the problematic Padel wild type from the equation.
To further increase the chance to identify PD-related genes, the transcriptome dataset of the *striatum* was also analyzed in this fashion and only DEGs identified in both brain regions were chosen for qPCR confirmation (24 genes). qPCR experiments confirmed multiple genes, but the gene Ctsc was particularly interesting because it was the only DEG upregulated in the *substantia nigra* as well as in the *striatum* of the Padel mouse model. Consequently, it was chosen as a priority target, and upregulation was confirmed with all seven reference genes in an independent sample set of SN tissue or one-year-old Padel mice, thereby confirming upregulation with high certainty.

Ctsc is a lysosomal exo-cysteine protease belonging to the papain superfamily (Kominami et al., 1992; Berti et al., 1995; Pham et al., 1997). It plays a role in intracellular lysosomal protein degradation and can remove dipeptides from different peptides and proteins (Coffey and de Duve, 1968; Metrione et al., 1970; Katunuma, 1989). There is no published connection to Parkinson’s disease, but Ctsc has been implicated in the activation process of immune cells, where it resides in cytotoxic granules and is the main activator of serine proteases by cleaving their N-terminal dipeptide before secretion (Thiele and Lipsky, 1990; Brown et al., 1993; Mcguire et al., 1993). Recent studies found Ctsc’s involvement in neuroinflammation, where its selective overexpression in microglia worsened demyelination in a multiple sclerosis mouse model (Shimizu et al., 2017). Additionally, microglia in Ctsc overexpressing mice have been shown to develop a neurotoxic phenotype after Lipopolysaccharide injection, in contrast to the wild type mice (Liu et al., 2019).

A connection between microglial mediated neuroinflammation and Parkinson's disease has been postulated by numerous studies (He et al., 2002; Grabert et al., 2016; Lopez Gonzales et al., 2016; Liddelow et al., 2017). Because of the upregulation of Ctsc in the *substantia nigra* of the Padel mouse and its function in microglial activation, Ctsc should be examined regarding its role in neuroinflammation in a PD context.

Taken together, the new NGS analysis approach was able to preliminary confirm six DEGs in the *striatum* of Basyn mice and two genes in the *striatum* of Padel mice. One differentially expressed gene (Ctsc) could be found in the *substantia nigra* of the Padel mouse model. This gene was upregulated in both brain regions of the Padel mouse and could successfully be confirmed with a new sample set and multiple reference genes implicating its upregulation with PD pathology.

The other promising genes from this analysis also should be tested with an independent sample set and multiple reference genes to further increase evidence of their regulation. Additionally, Ctsc should be further examined to investigate a functional connection to PD pathogenesis.

4.2 Examination of autophagy/mitophagy in Parkin deficient primary fibroblasts

In this thesis, the basal autophagy and mitophagy of primary Padel fibroblasts was examined to identify a possible Parkin-dependent effect (figure 20). Background for this experiment was the postulated mechanism of Parkin/Pink1 mediated mitophagy, which has been linked to the autophagosomal degradation of defective mitochondria in an LC3-dependent manner. However, this mechanism has only been demonstrated *in vitro* with Parkin overexpression or strong autophagy-inducing chemicals (Cai et al., 2012; Ashrafi et al., 2014; Bingol et al., 2014). Previous experiments in our department have tried to examine basal mitophagy in primary Padel astrocytes utilizing immunocytochemistry to visualize mitochondria and autophagosomes with no significant Parkin-dependent difference in colocalization of both organelles (Pfeffel, 2019). This approach with antibodies can detect targets without altering their protein and organelle status in cells, however, unspecific binding can introduce

technical variation to experiments. To minimize this kind of technical variance, a different experimental design was chosen to measure mitophagy to examine the validity of previous findings.

This approach used transfection of LC3b-eGFP and subsequent staining with a mitochondrial dye and confocal live imaging to generate images for a colocalization analysis, thereby eliminating the problem of unspecific antibody binding and fixation artifacts. Quantification of LC3-II positive puncta is considered the gold standard for autophagosomal quantification (Runwal et al., 2019). Due to the hard-to-transfect nature of primary astrocytes, easily manipulatable primary fibroblasts were used to examine Parkin-dependent mitophagy effects. However, it should be considered that transfection with LC3b-eGFP may cause cellular stress, which would be disadvantageous compared to the approach of immunocytochemistry.

Additionally, neither immunocytochemistry nor transfection with LC3b-eGFP can offer the information which LC3b isoform is co-localized with mitochondria. In general, the LC3 conversion can be measured via western blot analysis only. However, this analysis examines the total LC3b-mediated autophagy including mitophagy and cannot distinguish between both. Therefore, mitophagy should be assessed from these two perspectives parallelly by using a combination of immunocytochemical colocalization and LC3b conversion.

The experiment for the examination of basal mitophagy via LC3b transfection produced fluorescence images showing distinct green vesicular structures with a low, homogenous background staining, thereby exhibiting a plausible visualization pattern of autophagosomes (figure 20B). The cytoplasmatic background fluorescence represents the cytosolic LC3b-I protein before processing, while distinct vesicular structures with strong fluorescence should represent processed LC3b-II in the autophagosome membrane.

Mitochondrial dyes get actively transported in the lumen of mitochondria and get covalently linked to thiol groups, thereby visualizing these organelles stably and with high specificity (Chazotte, 2011). The used dye required a negative membrane potential to get imported into the mitochondrial lumen. This raises the question if observed damaged mitochondria could still be labeled with this method. Multiple studies indicate that mitochondrial membrane potentials get more negative under the

context of cellular stress (Iijima et al., 2003; Nagy et al., 2003). Additionally, it has been demonstrated, that some defective mitochondria can exhibit normal membrane potential, nevertheless leading to apoptosis (Krohn et al., 1999). A recent study has also revealed that cristae from the same mitochondrion can display different membrane potentials and act functionally independent (Wolf et al., 2019). Taken together, it seems that the MitoTracker dye will most likely accumulate in all mitochondria, thereby enabling the examination of mitophagy in this experimental context.

The observed fluorescence caused by MitoTracker distinctly marked mitochondrial structures in all cells with nearly no background fluorescence (figure 20B). Not transfected cells did not show signs of autofluorescence in the chosen image settings indicating no presence of interfering fluorescence signals in both channels in the analysis.

The pinhole setting was set at 0.45 µm to visualize just a thin section of the cell to prevent wrong colocalization signals from bleeding through from other focal planes. Autophagosomes are between 0.5 and 1.5 µm in size, while mitochondria vary between 0.75 and 3 µm, which makes a false colocalization via fluorescent bleed through unlikely (Mizushima et al., 2002; Wiemerslage et al., 2016).

An essential parameter for the subsequent colocalization analysis is the threshold. This intensity value differentiates between noise and signal in the fluorescence images. The threshold in the LC3b channel was set manually, thereby ensuring all vesicular structures were still present after the cutoff (figure 20C left). This was feasible because the intensity values of vesicular LC3b-II exceeded the values of cytoplasmatic background LC3b-I to a great extent. The identification of mitochondrial structures was more complicated since its intensity was not homogenous like the LC3b vesicles. The object recognition algorithm of the analysis software was utilized to guarantee a signal identification based on the same parameters in every image. On close examination, the software did not recognize all mitochondrial structures in the image, but the success rate was estimated at ≥ 95% (figure 20C right). This parameter introduced a low amount of technical variance to the experiment, which could not be reduced further.

The results of the analysis did not show a statistically significant difference in LC3b amount between primary Padel and WT fibroblasts, exactly as in the LC3b conversion

experiment (figure 20A). the combination of both results indicates no difference in basal mitophagy capabilities in primary Padel fibroblasts. This finding of unaltered LC3b conversion aligns with other LC3 conversion experiments of the department of animal physiology in primary astrocytes, neonatal mesencephalic tissue, and one-year-old SN tissue (Vilou, 2019). However, LC3 conversion investigates the sum of all autophagic processes in the cell. Plenty of ubiquitin ligases besides Parkin have been identified and it is possible, that these proteins can compensate for Parkin deficiency at a basal level (Cherra et al., 2009). Additionally, mitophagy is just a small fraction of all autophagic processes and if only mitophagy is altered in a Parkin-dependent manner, this small effect might not be detectable with the overall measurement of autophagy due to lacking sensitivity.

The examination of mitochondrion-autophagosome colocalization, which specifically targets mitophagy, did not show a statistically significant difference in primary Padel fibroblasts as well (figure 20E). This finding aligns with the previously performed experiment of Pfeffel, which found an unaltered basal mitophagy in primary astrocytes with immunocytochemistry (Pfeffel, 2018). Both approaches show the same result with different methodology thereby strengthen the evidence for their validity.

In theory, the mechanism of Parkin-dependent mitophagy has been demonstrated in multiple contexts and is considered credible in this field of research. However, this pathway is not believed to be the main mechanism of mitochondrial macroautophagy (Mcwilliams et al., 2018). Alternative mechanisms could balance out Parkin deficiency on a basal level and just fail to compensate under enormous stress levels (Allen et al., 2013; Kageyama et al., 2014; Szargel et al., 2016). This would also explain the findings of multiple *in vitro* studies, which demonstrated Parkin-dependent mitophagy with Parkin overexpression and/or autophagy inducing substances (Narendra et al., 2008; Geisler et al., 2010; Matsuda et al., 2010; Narendra et al., 2010; Vives-Bauza et al., 2010). It is possible, that defects in basal mitophagy are age-dependent and young cells in primary culture do not display this effect yet. In fact, it has been shown, that autophagy does decline with age, including in neuronal cells (Liang et al., 2020; Stavoe and Holzbauer, 2020; Karabiyik et al., 2021). However, it cannot be excluded, that a small difference in basal mitophagy was masked by technical variance, although the experiment was specifically designed to minimize disturbing parameters.

The mitochondrial density of primary Padel and WT fibroblasts was also quantified to evaluate a potential deficiency in mitophagy leading to mitochondrial accumulation. No statistically significant difference in mitochondrial amount could be measured in Padel fibroblasts (figure 20F).

This result aligns with previous fluorescence-based measurements of mitochondrial density from primary Padel astrocytes *in vitro* (Schmidt et al., 2011; Wittenberg, 2018; Pfeffel, 2019). However, morphologically abnormal mitochondria have been found in electron microscopy images from Padel astrocytes *in vitro* and *in vivo,* while the number of intact mitochondria was not altered (Schmidt et al., 2011; Hemmersbach, 2016). If this effect is also present in Padel fibroblasts, it could not be detected with this measurement approach. Although there is evidence in the literature that deficient mitochondria will still import mitochondrial dyes into their lumen, it is possible that this capability will be diminished when mitochondrial damage exceeds a certain point, thereby potentially masking heavily damaged mitochondria in this analysis.

Taken together, the examination of mitophagy in primary Padel fibroblasts did not result in the detection of an impaired basal mitophagy or accumulation of detected mitochondria. Although the existence of the Parkin/Pink1 dependent mitophagy mechanism seems clear, it does not seem to affect basal mitochondrial turnover in neonatal fibroblasts, or the effect was too small for reliable detection. qPCR evaluation of Parkin expression in primary fibroblasts compared to neonatal brain tissue revealed a distinctly lower Parkin expression in fibroblasts, which could potentially result in a smaller difference of Parkin-dependent mitophagy, compared to other cell types where Parkin is expressed on a higher level (data not shown).

4.3 Quantification of mitochondrial associated membranes in Padel fibroblasts

In this thesis, a Parkin-dependent effect on the formation of mitochondrial associated membranes (MAM) was examined in primary Padel fibroblasts. Altered crosstalk between these organelles has been implicated in different neurodegenerative

diseases, including PD (Paillusson et al., 2016). MAM's can influence multiple PD-associated processes as mitochondrial dynamics, Ca2+ homeostasis, and autophagy (Sala-Vila et al., 2016; Tagaya et al., 2017; Morciano et al., 2018). However, so far it is not clear, whether MAM dysregulation is part of the cause or consequence of PD pathogenesis (Cali et al., 2012; Ottolini et al., 2013).

For the quantification of MAMs, primary Padel and WT fibroblasts were stained via immunocytochemistry to visualize mitochondria (Hsp60) and the endoplasmic reticulum (Hsp90b1) with antibody markers (figure 18C). The visualization of mitochondria produced distinct and intense staining of mitochondrial shapes with sharp borders and nearly no background fluorescence, suitable for subsequent colocalization analysis. The ER marker produced a porous staining pattern with intense fluorescence around the nucleus, which gradually decreased in direction of the cell borders. The observed staining is typical for ER morphology, so both antibodies were considered suitable for colocalization. However, it was difficult to set a threshold for the fluorescence signal for the endoplasmic reticulum, because of the intensity decline between cell center and cell borders. High thresholds would eliminate ER structures in the cell periphery, while low thresholds would count all ER pixels near the nucleus as signal, due to bleed through from other focal planes. This thesis contains the results generated with the higher threshold because missing ER structures in the cell periphery in every image still yields accurate results for center ER structures. The low threshold would have generated a homogenous mass of signal pixels without physiological relevance.

The image analysis of mitochondrial and endoplasmic reticulum pixels in primary Padel and WT fibroblasts did not yield a statistically significant change in colocalization of mitochondrial and ER signal between the genotypes (figure 18E). Although, the mean MAM amount in the Padel fibroblasts was slightly reduced compared to the wild type. It seems the high variance may have masked a potential reduction in this experiment. The tendency for a reduced MAM amount in Parkin deficient cells is in alignment with published results with cancer cell lines, where Parkin overexpression increased mitochondrial-ER crosstalk, while Parkin siRNA reduced signal transmission (Cali et al., 2012). Another study confirms decreased MAMs in Parkin deficient human primary fibroblasts (Basso et al., 2018). However, a contradicting publication found an increased number of mitochondrial associated membranes in human Parkin deficient

fibroblasts (Gautier et al., 2016). All studies used a transfection approach to visualize the organelles with ER/mitochondrial transport tags attached to fluorescent reporter proteins. The deviation in results compared to the experiment in this thesis could have been caused by differences in methodology.

The published transfection experiments could have influenced physiological parameters by artificial overexpression of fluorescence proteins, which could have led to cell stress and thereby affecting MAM formation (Bravo et al., 2011). However, the immunocytochemistry approach which was used here could have caused technical variance via unspecific binding of primary or secondary antibodies, possibly influencing the colocalization analysis.

Cali examined the cancerous cell line SH-SY5Y, which is likely to exhibit much less biological variation due to their clonal origin, which makes it easier to detect small changes potentially. Furthermore, the published experiments used a 3D rendered cell reconstruction analysis, while the experiment in this thesis analyzed single images. The pinhole of the used confocal microscope was set to 0.22 µm to generate very thin focal planes to prevent signal bleed-through from below and above.

Taken together, close examination of small structures like MAMs with this method did not result in a significant change in MAM amount between Padel and WT fibroblasts, however, a small biological change could have been masked by technical variance. Consequently, the department of animal physiology conducted a subsequent experiment for MAM quantification in Padel astrocytes with a method, which inherently possesses higher sensitivity and specificity – the proximity ligation assay (PLA).

This analysis was conducted after the completion of this colocalization experiment as a master thesis under supervision (Pfeffel, 2021). PLA utilizes two antibodies against protein interaction partners from both sides of the mitochondrial-ER tethering. The corresponding secondary antibodies have complementary oligonucleotides attached, which can only hybridize if the primary antibodies are in less than 40 nm distance. The nucleotide can be ligated, amplified, and then visualized with fluorescently labeled oligonucleotides. This mechanism has the great advantage of just visualizing colocalization points between the two targeted proteins, leaving antibody-bound target proteins without the desired interaction partner invisible, thereby eliminating unspecific signal. This comparison between Padel and WT primary astrocytes with this method

identified a tendency for reduced MAM amount in Padel astrocytes (p=0.17, Mann-Whitney u-test). This reduction aligns with the tendency of the fibroblast experiment from this thesis.

Considering both published and generated results, the evidence seems to point at a reduced mitochondrial-ER tethering caused by Parkin's absence. One main function of MAMs is the coordination of intracellular calcium transfer, which could be impaired because of MAM reduction (Basso et al., 2018). Accordingly, multiple publications have demonstrated deficient calcium homeostasis in cell culture models with Parkin or Pink1 knockout (Sandebring et al., 2009; Heeman et al., 2010; Gandhi et al., 2011). *In vitro* experiments with SH-SY5Y cells treated with Parkin SiRNA have shown a 10% decrease in mitochondria-ER contact sites and reduced calcium exchange between mitochondria and the endoplasmic reticulum (Cali et al., 2013).

Taken together, it seems likely that a loss of Parkin impairs MAM formation in primary Padel astrocytes and thereby potentially altering mitochondria-ER crosstalk and calcium homeostasis.

4.4 Cellular localization of Rcn1

The calcium-binding protein Rcn1 was associated with PD pathogenesis in this thesis, which made its cellular localization in the Padel mouse model relevant for further experiments. Rcn1 was postulated to be in the endoplasmic reticulum due to a rare C-terminal ER import sequence and an Rcn1 antibody staining with an ER-like staining pattern in a monkey cell line (Ozawa and Muramatsu, 1993). To verify its ER residency in *mus musculus*, the method of immunocytochemistry was performed.

The Rcn1 antibody, which was co-stained with an ER and mitochondrial marker, produced a similar staining pattern in primary fibroblasts and astrocytes, displaying almost complete colocalization with the ER marker. There was no fluorescence pattern indicating Rcn1 presence in other organelles than the ER. This indicates a homogenous Rcn1 distribution in the endoplasmic reticulum, which would also include

mitochondrial associated membranes. To examine this closer, the mitochondrial channel was compared to both the ER and Rcn1 channel to detect possible differences in colocalization. Rcn1 signal was clearly detected in locations, which were positive for the ER marker as well as the mitochondrial marker, indicating MAM localization. However, immunocytochemistry has limitations regarding microscopic resolution and potential unspecific signal, therefore the method of cell fractionation, which possesses higher specificity, was performed to confirm Rcn1 localization in mitochondrial associated membranes. MAMs possess a lower density than the rest of the endoplasmic reticulum, which enables organelle separation via differential centrifugation (Area-Gomez, 2014).

The organelle fractionation was performed with mouse brain tissue and also confirmed ER residency of Rcn1 and additionally demonstrated its expression in mitochondrial associated membranes.

Taken together, both methods indicated Rcn1 localization in the endoplasmic reticulum and mitochondrial associated membranes. To see, if the Parkin knockout causes a change in the Rcn1 distribution pattern in primary fibroblasts, the immunocytochemical triple staining has been utilized to examine Rcn1 amount in the different. The analysis of Padel and WT fibroblasts with immunocytochemistry did not find statistically significant differences in Rcn1 amount in the different organelles. Although, the average Rcn1 signal was higher in the ER and the MAM in Padel fibroblasts compared to the WT. The increased Rcn1 signal in both organelles of the Padel genotype fits the result of the significantly increased Rcn1 expression in Padel fibroblasts, demonstrated by western blot analysis.

4.5 Investigation of intracellular calcium dynamics in primary Padel astrocytes and Rcn1 connection

ER-mediated calcium release in primary Padel astrocytes was examined in this thesis.

A close connection between endoplasmic reticulum calcium homeostasis, ER-stress and Parkinson's disease has been described in multiple publications (Shimura et al., 2000; Ko et al., 2009; Ding and Goldberg., 2009) For example, Parkin expression increases in response to ER-stress inducing substances, indicating its protective function in this context (Imai et al., 2000). Another factor enhancing the interest in ER-calcium dynamics besides the published associations between ER and PD was the identification of the Ca-binding protein Rcn1. This ER-resident protein was shown to be upregulated in the SN of Parkin deficient mice, and also in primary Padel astrocytes. Differential Rcn1 expression in astrocytes enabled their use as a cellular model for the examination of endoplasmic reticulum calcium dynamics.

The calcium imaging experiment with primary Padel astrocytes was designed utilizing the ratiometric calcium indicator dye Fura2-AM. Its ratiometric characteristics have the advantage of removing potential disturbing factors in the image analysis, like bleaching artifacts, changes in focus, or varying concentrations of the indicator. The dye enters the cells via diffusion and gets subsequently processed by endogenous esterase enzymes, thereby trapping the dye inside the cells. Fura2 also accumulates in the Endoplasmic reticulum, but even after ER calcium release, the ER-resident calcium dye should still be saturated due to calcium excess, thereby not affecting the cytosolic measurement.

Astrocyte cultivation was performed in channels with Luer adapters to ensure a homogenous liquid flow without turbulence during the imaging experiment. To produce a relatively pure astrocyte culture, flasks were shaken for 120 minutes before seeding to detach and remove unwanted cell types. ATP stimulation has been shown to elicit ER-mediated calcium release in astrocytes and was therefore chosen as a stimulus for the experiments (Arcuino et al., 2002). To ensure the measurement of calcium responses, which exclusively originate from intracellular calcium stores, the buffered salt solution for washing and stimulation contained no calcium. 100 µM ATP stimulation

for 15 seconds evoked a calcium response in nearly all cells during the experiments (≥98%). Nonresponsive cells were excluded from the analysis, assuming lacking vitality or the wrong cell type.

The first measurement of ER-mediated calcium release in Padel astrocytes did show a statistically significant reduction in the peak of the calcium response curve, while its integral and duration was not altered. A replication of this experiment with an independent sample set and an increased number of measured cells also demonstrated a reduced ER calcium release in Padel astrocytes. However, the reduction of peak height in the response curve just showed a tendency this time ($p=0.163$, Mann-Whitney u-test), while the integral showed a reduction with a statistical trend ($p=0.065$, Mann-Whitney u-test). Both experiments show a reduced calcium response in primary Padel astrocytes. Additionally, the later performed calcium imaging experiment examining effects of Rcn1 siRNA contained Padel and WT astrocytes with scramble siRNA as control groups, which replicated the effect of a reduced ER-mediated calcium response.

Taken together, the three experiments clearly indicate a reduced ER-mediated calcium response in Padel astrocytes that seems to be unaffected in its duration. A Connection between PD and disturbed calcium homeostasis has been postulated in different publications, although a direct link between Parkin and a reduced ER calcium release is not known yet (Marongiu et al., 2009; Akundi et al., 2011). However, Parkin has been postulated to facilitate mitochondrial-ER tethering and its deficiency caused reduced calcium flux from the ER to mitochondria (Cali et al., 2013). Other publications and findings or the department of animal physiology support this mechanism of Parkin-dependent mitochondrial tethering (section 4.3.). It is known, that Fura2-AM also accumulates in mitochondria, and it would be theoretically possible, that this calcium imaging experiment detected changes in mitochondrial calcium dynamics and not changes in the cytosol (Allen et al., 1992).

On the other hand, a different mechanism could also be at play explaining the observed reduction in ER-mediated calcium release. The calcium-binding protein Rcn1 has been shown to be upregulated in Padel astrocytes with high probability. It is plausible, that differential expression of a calcium-binding protein can affect cellular calcium dynamics. To investigate a potential Rcn1 dependent effect, its expression in Padel

astrocytes was reduced with siRNA and the calcium dynamics measured in the previously described setup. siRNA knockdown was confirmed with qPCR experiments indicating a reduction of Rcn1 expression to ~55 %, thereby restoring wild type expression levels in Padel astrocytes. siRNA treatment did not reduce the vitality of astrocytes, indicated by MTS test measurement. Non-coding siRNAs were used as a control in Padel and WT astrocytes to ensure that measured effects are based on Rcn1 knockdown and not mRNA treatment.

The Rcn1 siRNA treatment in Padel astrocytes was able to restore the integral of the calcium response curve back to wild type levels in a statistically significant fashion ($p=0.0015$, ANOVA on Ranks). The peak of the calcium response curve showed the same effect with a statistical trend ($p=0.077$, ANOVA on Ranks). Conclusively, Rcn1 seems to reduce ER-mediated calcium output and can plausibly explain the previously measured difference in calcium release between Padel and WT astrocytes.

In accordance with this, the workgroup of Xu found an increased ER-mediated calcium release after Rcn1 knockdown in response to ATP stimulation in HEK293T cells (Xu et al., 2017). A protective role of Rcn1 was observed during ER stress in different cancer cells by the inhibition of apoptosis (Huang et al., 2020). This mechanism was also examined in prostate cancer cells, where Rcn1 depletion induced ER stress and CaMK-II activation. CaMKs usually get activated in response to increased cytosolic calcium concentration, which further indicates that Rcn1 reduces ER-mediated calcium release (Liu et al., 2018). A possible mechanism for this might be the interaction between Rcn1 and the major calcium release channel IP_3R1 of the ER membrane, which was demonstrated via immunoprecipitation (Xu et al., 2017). This interaction could modulate IP_3R1 dependent calcium output.

Conclusively, the observed results together with published data regarding Rcn1 function indicate a protective role during ER stress via reduction of ER-mediated calcium output, thereby inhibiting apoptotic pathways. The increased Rcn1 expression in the Padel mouse model might be a compensation mechanism working against effects caused by Parkin deficiency.

4.6 Cultivation of postnatal catecholaminergic midbrain neurons

For a long time, *in vitro* studies of catecholaminergic neurons were conducted with prenatal dissociated neuronal cultures, which usually contained less than 1% catecholaminergic neurons, because their phenotype has not been developed for the most part (Sulzer et al., 2011). The Cultivation of postnatal catecholaminergic neurons has the advantage, that much more of these neurons have obtained their destined catecholaminergic characteristics. Unfortunately, postnatal dopaminergic neurons are very sensitive and cannot survive in dissociated culture conditions, which makes their cultivation challenging. It has been demonstrated that it is essential for postnatal dopaminergic neurons to grow together with primary astrocytes, which provide necessary factors for their survival and differentiation (Takeshima et al., 1994; Fasano et al., 2008). It has been shown that basal astrocytic Fibroblast growth factor (FGF) expression is essential for the development of neurons with dopaminergic characteristics in a direct coculture (Forget et al., 2006). Additionally, from astrocytes secreted glial-derived neurotrophic factor (GDNF) stimulates the survival, differentiation, and synaptic efficiency of dopaminergic neurons (Bourque and Trudeau; 1998). Consequently, an astrocytic feeder layer was utilized to enable the cultivation of postnatal catecholaminergic neurons.

After a substantial effort of parameter calibration, it was successful to establish a stable co-culture system with differentiated postnatal catecholaminergic neurons. The importance of neuron-glia interaction for neuronal survival in this primary culture system was further emphasized by the findings of this thesis. It was shown that astrocytes can donate mitochondria to catecholaminergic neurons (section 3.10), and direct neuron-glia crosstalk can impact the differentiation of neuronal processes (section 3.13).

It was observed that catecholaminergic neurons responded very sensitive to medium exchange and could die as a result. Neurobasal medium toxicity to postnatal neurons is a well-documented effect in the corresponding literature (Hogins et al., 2011; Maggioni et al., 2015). To overcome this problem, big dishes with small wells were used for the cultivation process to increase the medium/cell ratio, thereby reducing medium exchange frequency. Additionally, Medium was always preconditioned 24 hours on an astrocyte culture and only partially changed on the co-culture (25%).

This methodology achieved differentiation of catecholaminergic neurons for subsequent analysis purposes.

The observed neuronal density was constant between cultures, but the number of catecholaminergic neurons varied substantially between cultures (0 - >20 neurons). Some catecholaminergic neurons likely died in the preparation and cultivation process since this neuronal subtype is considered to be very sensitive to external stimuli. Another source for this variance might be the preparation process of the postnatal mesencephalic brain tissue. It cannot be guaranteed to dissect the exact same brain region in every preparation. Additionally, incomplete tissue digestion and the fact, that just a subset of cells gets seeded onto the astrocytic feeder layer increases the chance of unevenly distribute catecholaminergic neurons.

All in all, it was ultimately possible to establish a working protocol for the cultivation of postnatal catecholaminergic neurons, which stably differentiated in cell culture conditions, although the low amount of differentiated catecholaminergic neurons per well complicated further analysis objectives.

4.7 Examination of mitochondrial exchange in mesencephalic astrocytes and catecholaminergic neurons

This thesis aimed to investigate a potential mitochondrial exchange in mesencephalic astrocytes and catecholaminergic midbrain neurons. A previous study delivered a strong indication of *substantia nigra* mitochondrial exchange in PD mouse models *in vivo* (Schmidt et al., 2011). In recent years, mitochondrial exchange was demonstrated as a means of tissue revitalization or as a support mechanism during cell stress like ischemia (Hayakawa et al., 2017; Cheng et al., 2020; English et al., 2020; Liu et al., 2021). A potential connection between mitochondrial transfer and PD pathology was found in the TH-Syn mouse line, which had damaged mitochondria in SN astrocytes *in vivo*, although the α-synuclein transgene was just expressed in catecholaminergic neurons (Schmidt et al., 2011). It would instead be

possible, that pathological alterations in synuclein expressing neurons indirectly influence surrounding astrocytes and lead to mitochondrial damage, but the demonstrated mechanism of intercellular mitochondrial transfer between brain cells justifies the examination of this effect as a potential explanation. To investigate mitochondrial exchange in a PD context, this mechanism was investigated in mesencephalic astrocytes and catecholaminergic midbrain neurons, the suspected area of PD pathogenesis. The first step aimed to demonstrate the capability of mesencephalic astrocytes to release and take up mitochondria in a simplified culture environment without neurons. Images were taken from a living astrocyte co-culture (50% Dendra/50% WT) to prevent fixation or staining artifacts causing fluorescence, thereby producing potentially false-positive signals.

It was possible to detect green, fluorescent objects in non-transgenic astrocytes in this co-culture setup. To confirm their mitochondrial identity, multiple parameters were examined. Structures, which were suspected to be exchange mitochondria had to exhibit mitochondrial morphology, Dendra fluorescence, and MitoTracker fluorescence. Additionally, some of the observed structures were in the same focal plane as the cell's other mitochondria and were visibly integrated into the cell's mitochondrial network, indicating mitochondrial identity. Furthermore, videos have shown the typical mitochondrial movement of these structures and some of them even fused with non-transgenic mitochondria. A membrane tracker dye was used to make sure, that the observed objects were not part of transgenic cells with long appendixes reaching into non-transgenic cells.

Another observation indicating mitochondrial exchange was membrane surrounded vesicular objects containing MitoTracker and Dendra positive mitochondrial shaped structures (4-8 µm). Vesicular transport as a means of mitochondrial exchange was also described in multiple studies (Hayakawa et al., 2017; Cheng et al., 2020).

All observations combined, it can be concluded that the observed structures are exchanged mitochondria, which can be transported by vesicles and integrate into their new host cells mitochondrial network. Consequently, mesencephalic murine astrocytes are capable of releasing and incorporating mitochondria *in vitro*.

This finding enables the examination of a potential mitochondrial exchange between mesencephalic astrocytes and catecholaminergic midbrain neurons. The previously

described cultivation of postnatal catecholaminergic neurons on an astrocytic feeder layer was utilized (2.2.7).

At first, the mitochondrial exchange from mesencephalic astrocytes into catecholaminergic midbrain neurons was examined utilizing the transgene combination of Gfap-Dendra astrocytes and Th-Cre tdTomato neurons. However, this combination prevented the use of Mitotracker red due to its similar emission spectrum as tdTomato. Therefore, mitochondria were visualized via antibody staining with a deep red secondary antibody, which had to replace the membrane visualization dye BioTracker. The mitochondrial antibody should confirm mitochondria identity of green structures in red neuronal cells, while z-stacks with very thin focal planes were utilized to reconstruct 2.5D images of neurons with high resolution to confirm their location within the cells. While it was relatively easy to find exchanged mitochondria between astrocytes in these cultures, the amount of green, fluorescent structures in the catecholaminergic neurons was very rare (0-1 per culture). However, exchanged mitochondria could be detected in neuronal somas, dendrites, and axons. The effect size seemed too small for reliable quantification and establishment of this parameter as a readout for following experiments with Padel mice. Nevertheless, a pilot experiment with Padel astrocytes or neurons was performed to see, if there would be a strong difference in exchange, which would have enabled quantification. The exchange frequency did not seem to be affected.

Taken together, this study demonstrated for the first time intercellular mitochondrial exchange from mesencephalic astrocytes to midbrain catecholaminergic neurons in primary culture. This finding aligns with previously published data which found an astrocyte to neuron mitochondrial transfer in cortical neurons (Hayakawa et al., 2017; English et al., 2020).

The number of exchanged mitochondria after stroke simulation was substantially higher than in the experiments performed in this thesis (Hayakawa et al., 2017). This was desirable because quantification purposes require a certain effect size. Therefore, hypoxia and stroke simulation treatments were applied on the co-cultures to potentially increase the number of exchanged mitochondria. The treatment did not affect the mitochondrial exchange, although morphological changes of neurons could be observed after stroke simulation. It might be possible, that this mechanism does not apply in mesencephalic cells. However, the spatial resolution of the image in the

publication was not optimal and it is hard to confirm if the displayed mitochondria were really located in neuronal cells or just in astrocytes surrounding these neurons.

One recent publication further confirms the observed findings of mesencephalic mitochondrial exchange and is of great interest due to their similar objective. The workgroup of Cheng found donation of functional mitochondria from human iPSC-derived astrocytes to iPSC-derived dopaminergic neurons to protect them from substance-induced mitochondrial damage (Cheng et al., 2020). This strengthens the evidence for the role of mitochondrial exchange in dopaminergic neurons in a diseased context. Although the use of human cells like in this study can be an advantage because it better represents human PD pathology, the utilization of iPSC-derived cells comes with certain limitations. The cells differentiate chemically without a physiological *in vivo* context, which could lead to differences in phenotype and differentiation (Marchetto et al., 2010; Dolmetsch et al., 2011).

It seems advantageous to pursue the established co-culture system for examination of PD pathology because it represents the *in vivo* situation more closely. The utilization of postnatal neurons enables long differentiation of catecholaminergic neurons in a physiological context and their phenotype is characterized much better than their iPSC-derived counterpart (Mateos-Aparicio et al., 2020).

Conclusively, this study demonstrates for the first time, that primary murine mesencephalic astrocytes release mitochondrial particles, which can be taken up by other astrocytes or catecholaminergic midbrain neurons *in vitro* without artificially inducing cellular stress.

Extracellular vesicles with double-lipid membranes were identified, which contained cytoplasm and mitochondria, indicating vesicular transport as at least one mechanism for intercellular mitochondrial exchange in *vitro.* This release mechanism has been demonstrated to be calcium-dependent in cortical astrocytes, which is interesting given the fact that altered calcium dynamics have been found in mesencephalic astrocytes in the Padel mouse model (Hayakawa et al., 2017). Released mitochondria can be incorporated into the host cell’s mitochondrial network and are able to fuse with other mitochondria.

However, the observed frequency of mitochondrial exchange between astrocytes and catecholaminergic neurons was very low and thereby not suited as a readout for the investigation of a potential Parkin-mediated influence. Efforts to increase mitochondrial exchange frequency via stroke simulation, as described in the literature, had no effect. However, other chemical inducers have been recently described to enhance mitochondrial exchange between astrocytes and neurons, including in iPSC-derived dopaminergic neurons (English et al., 2020, Cheng et al.,2020). It would be interesting to apply these substances to the co-culture model established in this thesis to potentially increase mitochondrial exchange frequency to use it as a readout to examine Parkin-dependent effects.

Lastly, it would have been interesting to examine a possible mitochondrial exchange from catecholaminergic neurons into mesencephalic astrocytes. This exchange has been described as a mechanism for transcellular mitophagy, where astrocytes degraded mitochondria from unmyelinated axons at the optical nerve head (Davis et al., 2014). Unfortunately, the utilized transgenic mouse Th-Dendra exhibited a leaky expression of the Dendra transgene in all neurons thereby masking mitochondrial origin. The examination of this mechanism would also be a prospect for future research to associate the mechanism of Parkin-dependent mitophagy with an intercellular mitochondrial exchange.

4.8 Impact of Parkin deficiency on neuronal morphology in a primary co-culture model

In this thesis, the established mesencephalic astrocyte-neuron co-culture model was utilized to examine the potential impact of Parkin deficiency on the differentiation capabilities of postnatal mesencephalic neurons (figure 25). Background for this experiment were previous findings, that Parkin deficient mesencephalic astrocytes were not able to support the differentiation of dissociated prenatal cortical neurons in indirect co-culture as wild type astrocytes could. The length of the longest neuronal process was significantly reduced indicating an impaired, Parkin-dependent astrocytic

support mediated by soluble factors (Schmidt et al., 2011). Although the experimental design revealed a negative impact on cortical neurons, it remained unclear, if this effect also influences mesencephalic neurons, which are more likely to be affected in a real PD context. Furthermore, it does not examine the effect of Parkin expression in neurons itself or includes possible effects requiring direct cell to cell contact. The chosen membrane with 0.4 µm pore size would also block a potential vesicular mitochondrial exchange because mitochondrial size usually varies between 0.75 and 3 μm^2 (Wiemerslage and Lee, 2016).

The experiment performed in this thesis was designed to imitate the *in vivo* situation to the degree it was possible. Dissociated cortical neurons were replaced by postnatal mesencephalic neurons, which had more time to grow in physiological context and were thought to better represent the *in vivo* situation because of their midbrain origin. A direct co-culture was utilized to ensure direct, physiological interaction between the cell types. It would have been optimal to examine Parkin-dependent effects on TH+ positive neurons instead of mesencephalic neurons, but the challenge to cultivate postnatal catecholaminergic neurons in sufficient numbers per culture (section 4.6) made quantification with robust statistical power difficult.

Beneath quantification of neuronal processes, the soma size was also examined, because another study has found a reduced soma size of Parkin deficient dopaminergic neurons in drosophila *in vivo* (Cha et al., 2005).

The comparison of WT/WT with Padel/Padel co-cultures resulted in a statistically significant reduction of overall neuronal process length in the Padel culture, while other morphological parameters were unaffected (soma size, longest process, surface area). This finding indicates Parkin-dependent effects, which influence mesencephalic neuronal differentiation *in vitro* (figure 25C). To further examine, whether this reduced differentiation is only dependent on the mutated neuron or on the mutated astrocyte, or both, hybrid co-cultures were utilized, where only one cell type was Parkin deficient (figure 25D). Deficiencies in neuronal differentiation could not be observed, when comparing hybrid cultures to the WT co-culture, indicating that both cell types must carry the Parkin mutation to result in a measurable effect in this setup, indicating an interaction between mesencephalic neurons and astrocytes.

The first experiment seems to confirm an impairment of neuronal differentiation in the absence of Parkin, but the second experiment, which's experimental design is much closer to the original experiment of Schmidt, could not confirm the postulated reduction of supportive capabilities in Padel astrocytes. However, there were big differences in the culture setup, which could explain the contradictory findings. It is possible, that Parkin deficiency causes a reduced capability of astrocytes regarding soluble factors, which could be measured in Schmidt's indirect co-culture experiment, which were balanced out in this direct co-culture via mechanisms requiring cell to cell contact or a potential mitochondrial exchange. These mechanisms could even be enhanced in Padel astrocytes as a countermeasure to compensate for Parkin-knockout, thereby explaining improved neuronal differentiation in the Padel/WT co-culture.

This hypothesis, together with the fact, that Padel/Padel cultures have shown an impaired process differentiation, seems to indicate that differentiation impairment requires Parkin knockout in both cell types, demonstrating the importance of neuron-glia interaction

Indeed, Parkin-dependent effects on neuronal morphology have been demonstrated in TH+ and TH- iPSC-derived human neurons, where the complexity of neuronal processes had been reduced, exactly as observed in this thesis (Ren et al., 2015). Another study has found Parkin-dependent alterations on the organization of the cellular cytoskeleton, that influences the spatial organization of actin filaments, thereby changing cellular morphology (Vergara et al., 2015). This mechanism could help explain observed changes in neuronal process formation.

Taken together, Parkin-dependent effects on mesencephalic neuronal process differentiation could be observed in the conducted experiment, aligning with similar published results. It is still not clear if or to which extent astrocytes are involved in this process. The experiment should be reproduced with an increased sample size to confirm observed effects and the co-culture model should be improved to be applied to catecholaminergic midbrain neurons in the future to get even closer to the simulation of actual PD pathology.

4.9 Summary and prospects

This thesis had the objective to investigate Parkinson's Disease-associated pathomechanisms in different PD mouse models to gain a deeper understanding of this highly prevalent disease as a basis for future development of diagnosis and treatment options.

One branch of this thesis was the conduction of a transcriptome analysis with subsequent qPCR verification, that led to the identification of two genes, which are differentially expressed in the Padel mouse model. The first gene is Cathepsin C, a lysosomal cysteine protease, which was confirmed upregulated in the substantia nigra and the striatum of one-year-old Padel mice. Although not associated with Parkinson's disease yet, it has a role in autophagic degradation of cellular proteins, which might be impaired in PD, and was implicated in neuroinflammation, where it can promote the neurotoxic phenotype of microglia. The consequences of its upregulation in Padel should be examined regarding its relevance in PD pathology. The second gene was Reticulocalbin1, an ER-resident calcium-binding protein, which was demonstrated to enact a protective function during ER stress. Localization experiments confirmed its location to the ER and mitochondrial-associated membranes.

It was shown, that Padel mice exhibit a reduced ER-mediated calcium release in primary astrocytes. Rcn1 siRNA was able to rescue calcium responses in Padel astrocytes to wild type levels, indicating its functional connection with the observed alteration. Although PD has been implicated with dysfunctional calcium homeostasis, proteins modulating this process have not been identified. Rcn1 is the first discovered ER protein that mediates a Parkin-dependent ER Ca_{2+} release.

It would be interesting to examine intracellular calcium dynamics with higher precision, utilizing ER-resident and mitochondrial-resident calcium sensors to find out, which part of the calcium response is altered by Rcn1. Interestingly, one study has shown its action as a microglial phagocytosis ligand, which gets secreted by healthy cells and is selectively bound to apoptotic neurons. (Ding et al., 2015). Both identified genes have been associated with microglial activation. Future experiments should include the investigation of this connection in a Parkin-dependent context.

The other branch of this thesis was the characterization of the Padel mouse model regarding different published theories of PD pathogenesis. Defective mitochondria have been implicated in PD pathogenesis in a variety of publications and the utilized mouse models in this thesis also displayed mitochondrial damage in previous experiments. The conducted experiments examined a potentially impaired mitophagy capability, a reduced mitochondrial ER crosstalk, a potential mitochondrial exchange to support stressed cells, and the capability of neuronal differentiation.

No significant Parkin-dependent changes in basal mitophagy could be observed in the experiments, although the tendencies, which aligned with the literature, pointed at a slightly reduced capability of Parkin-deficient cells regarding their mitophagy. A promising approach to increase a potentially small effect would be treatment with bafilomycin in this experimental setup. Bafilomycin is no autophagy inducer, instead, it prevents autophagosome fusion to the lysosome, thereby preventing their degradation. This method may allow for the quantification of autophagosomes, which were synthesized over multiple hours, instead of just quantifying a single time point as a snapshot.

The quantification analysis of mitochondrial-associated membranes did not result in a statistically significant change between Padel and wild type fibroblasts, although a slight reduction could be observed, which was also seen by Pfeffel in her experiments by using the proximity ligation assay. Because of contradicting findings in the literature, it might be worthwhile to repeat the proximity ligation assay for MAM quantification with increased sample size. The “SPLICS” method, which utilizes split GFPs with organellar location tags, could be used as an alternative approach to achieve MAM quantification (Cieri et al., 2018).
The high sensitivity of these approaches should be able to detect small differences when technical variation is minimized.

The possibility of an intercellular mitochondrial exchange in a mesencephalic context was examined in this thesis. This examination required the establishment of a stable

postnatal catecholaminergic neuronal culture system. It was successful to generate healthy, differentiated postnatal catecholaminergic neurons in this environment.
For the first time, an intercellular mitochondrial exchange between mesencephalic astrocytes and catecholaminergic midbrain neurons could be demonstrated *in vitro*. Mitochondrial containing vesicles were found indicating vesicular transport as one exchange mechanism. These exchange events were very rare and future experiments should utilize different substances to potentially increase this phenomenon as a basis for subsequent quantification.

One experiment examined the impact of Parkin-deficiency on the differentiation of mesencephalic neurons in an astrocyte-neuron co-culture model. Parkin-deficient astrocytes cultured with Parkin-deficient showed a statistically significant reduction of neuronal processes compared to the wild type co-culture. Hybrid cultures did not show any sign of impairment indicating that both cell types need to carry the Parkin mutation and impaired differentiation requires neuron-glia communication. The next step would be to apply the differentiation analysis on catecholaminergic neurons instead of mesencephalic neurons to simulate the PD context even better.

Acknowledgement

I want to thank Prof. Dr. Hermann Lübbert for the opportunity to write PhD thesis in his department and for providing such an interesting topic to work on.

I also want to thank Prof. Dr. Melanie Mark, who kindly agreed to act as the second supervisor of my project and gave me productive input and interesting cooperation opportunities.

Special thanks to my tutor Dr. Xinran Zhu, who always took time for my problems and supported me in every matter during the last 4 Years.

Appreciation goes to Dr. Frank Paris, Dr. Michael Andriske and Dr. Ben Novak, who answered all my questions and gave me good advice when I needed it.

Props shall be given to my Co-worker in the project: David Mrohs, for the motivation, inspiration, and interesting discussions.

Additional thanks to Nicole Schary and Felix Krause who i could always talk to in times of need.

I also want to thank Dr. Verian Bader, who was patient with me and taught me a lot.

I want to express gratitude to Katja Schmidtke, Tanja Behning, Katrin Schuster, Holger Schlierenkamp, Silvia Schweer, Uwe Hilsmann, and Manfred Ebbinghaus for the support, the distraction, and the bright atmosphere at the department.

Some final thanks go to my parents and my girlfriend, who supported me in any situation. Without them, this project might not have been possible.

Declaration

Ich versichere an Eides statt, dass ich die eingereichte Dissertation selbstständig und ohne unzulässige fremde Hilfe verfasst, andere als die in ihr angegebene Literatur nicht benutzt und dass ich alle ganz oder annähernd übernommenen Textstellen sowie verwendete Grafiken und Tabellen kenntlich gemacht habe. Weiterhin erkläre ich, dass digitale Abbildungen nur die originalen Daten enthalten oder eine eindeutige Dokumentation von Art und Umfang der inhaltsverändernden Bildbearbeitung vorliegt. Außerdem versichere ich, dass es sich bei der von mir vorgelegten Dissertation (elektronische und gedruckte Version) um völlig übereinstimmende Exemplare handelt und die Dissertation in dieser oder ähnlicher Form noch nicht anderweitig als Promotionsleistung vorgelegt und bewertet wurde.

Es wurden keine anderen als die angegebenen Hilfsmittel verwendet.

Die Dissertation wurde gemäß der Promotionsordnung und der Betreuungsvereinbarung angefertigt.

Bochum, den

_____

(Unterschrift)

Lebenslauf

Max Oliver Rybarski

15.08.1990
Gelsenkirchen, Deutschland

Oktober, 2021

MOMENTANES BESCHÄFTIGUNGSVERHÄLTNIS

Befristeter wissenschaftlicher Mitarbeiter der Ruhr-Universität Bochum (50 %)
mit Aussicht auf Promotion am Lehrstuhl für Tierphysiologie

ABGESCHLOSSENE AUSBILDUNG UND QUALIFIKATIONEN

2015–2018	M.Sc. der Biologie Lehrstuhl für Tierphysiologie “mit Auszeichnung”, (1,0)	Ruhr-Universität, Bochum
2012–2015	B.Sc. der Biologie Lehrstuhl für Tierphysiologie “gut”, (1,9)	Ruhr-Universität, Bochum
2011-2011	Ausbildung zum Rettungssanitäter “sehr gut“	RCS-Center, Gelsenkirchen
2001–2010	Allgemeine Hochschulreife “befriedigend”, (2,4)	Max Planck Gymnasium, Gelsenkirchen

PUBLIKATIONEN

Daylight photodynamic therapy for field cancerization: lessons from molecular biology

Max Rybarski, Lutz Schmitz, Ben Novak, Thomas Dirschka

2018, Giornale Italiano di Dermatologica e Venereologica; 153(6):806-10

LEHRE UND FÜHRUNGSERFAHRUNG

Betreuung des biologischen Tutoriums im Wintersemester 2014/2015
Betreuung der tierphysiologischen Übungen im Sommersemester 2016 und 2017
Betreuung von Bachelorstudenten (2019, 2020, 2021)
Betreuug von Masterstudenten (2019, 2020, 2021)

5. References

Aarsland, Dag, Elise Tandberg, Jan P Larsen, and Jeffrey L Cummings. 1996. “Frequency of Dementia in Parkinson Disease.” Arch Neurol. Vol. 53. http://archneur.jamanetwork.com/.

Abbas, Nacer, Christoph B Lücking, Sylvain Ricard, Alexandra Dürr, Vincenzo Bonifati, Giuseppe de Michele, Sandrine Bouley, et al. 1999. “A Wide Variety of Mutations in the Parkin Gene Are Responsible for Autosomal Recessive Parkinsonism in Europe.” Human Molecular Genetics. Vol. 8. https://academic.oup.com/hmg/article/8/4/567/2896763.

Ahmad, Tanveer, Shravani Mukherjee, Bijay Pattnaik, Manish Kumar, Suchita Singh, Rakhshinda Rehman, Brijendra K. Tiwari, et al. 2014. “Miro1 Regulates Intercellular Mitochondrial Transport & Enhances Mesenchymal Stem Cell Rescue Efficacy.” EMBO Journal 33 (9): 994–1010. https://doi.org/10.1002/embj.201386030.

Akundi, Ravi S., Zhenyu Huang, Joshua Eason, Jignesh D. Pandya, Lianteng Zhi, Wayne A. Cass, Patrick G. Sullivan, and Hansruedi Büeler. 2011. “Increased Mitochondrial Calcium Sensitivity and Abnormal Expression of Innate Immunity Genes Precede Dopaminergic Defects in Pink1-Deficient Mice.” PLoS ONE 6 (1). https://doi.org/10.1371/journal.pone.0016038.

Allen, George F.G., Rachel Toth, John James, and Ian G. Ganley. 2013. “Loss of Iron Triggers PINK1/Parkin-Independent Mitophagy.” EMBO Reports 14 (12): 1127–35. https://doi.org/10.1038/embor.2013.168.

Anwar, Arsalan, Sidra Saleem, Aisha Akhtar, Sara Ashraf, and Mirza Fawad Ahmed. 2019. “Juvenile Parkinson Disease.” Cureus, August. https://doi.org/10.7759/cureus.5409.

Arcuino, Gregory, Jane H-C Lin, Takahiro Takano, Collins Liu, Li Jiang, Qun Gao, Jian Kang, and Maiken Nedergaard. 2002. “Intercellular Calcium Signaling Mediated by Point-Source Burst Release of ATP.” PNAS 99: 9840–45. www.pnas.orgcgidoi10.1073pnas.152588599.

Area-Gomez, Estela. 2014. “Assessing the Function of Mitochondria-Associated ER Membranes.” In Methods in Enzymology, 547:181–97. Academic Press Inc. https://doi.org/10.1016/B978-0-12-801415-8.00011-4.

Ashrafi, Ghazaleh, Julia S. Schlehe, Matthew J. LaVoie, and Thomas L. Schwarz. 2014. “Mitophagy of Damaged Mitochondria Occurs Locally in Distal Neuronal Axons and Requires PINK1 and Parkin.” Journal of Cell Biology 206 (5): 655–70. https://doi.org/10.1083/jcb.201401070.

Baruzzo, Giacomo, Katharina E. Hayer, Eun Ji Kim, Barbara di Camillo, Garret A. Fitzgerald, and Gregory R. Grant. 2017. “Simulation-Based Comprehensive Benchmarking of RNA-Seq Aligners.” Nature Methods 14 (2): 135–39. https://doi.org/10.1038/nmeth.4106.

Basso, Valentina, Elena Marchesan, Caterina Peggion, Joy Chakraborty, Sophia von Stockum, Marta Giacomello, Denis Ottolini, et al. 2018. “Regulation of ER-Mitochondria Contacts by Parkin via Mfn2.” Pharmacological Research 138 (December): 43–56. https://doi.org/10.1016/j.phrs.2018.09.006.

Behling, R. 2021. “Etablierung Eines ER-Stress-Panels in Maus-Astrozyten Establishment of an ER Stress Panel in Mouse Astrocytes.”

Bendor, Jacob T., Todd P. Logan, and Robert H. Edwards. 2013. “The Function of α-Synuclein.” Neuron. https://doi.org/10.1016/j.neuron.2013.09.004.

Berti, Paul J, and Andrew C Storer. 1995. “Alignment / Phylogeny of the Papain Superfamily of Cystein Proteases.” J. Mol. Biol. Vol. 246.

Betarbet, Ranjita, Todd B. Sherer, Gillian MacKenzie, Monica Garcia-Osuna, Alexander V. Panovand, and J. Timothy Greenamyre. 2000. “Chronic Systemic Pesticide Exposure Reproduces Features of Parkinson’s Disease.” Nature Neuroscience 3: 1301–6.

Bingol, Baris, Joy S. Tea, Lilian Phu, Mike Reichelt, Corey E. Bakalarski, Qinghua Song, Oded Foreman, Donald S. Kirkpatrick, and Morgan Sheng. 2014. “The Mitochondrial Deubiquitinase USP30 Opposes Parkin-Mediated Mitophagy.” Nature 510 (7505): 370–75. https://doi.org/10.1038/nature13418.

Blasey, Nadja. 2020. “Genexpressionsanalyse Eines Mausmodells Für Morbus Parkinson Gene Expression Analysis of a Mouse Model for Parkinson´s Disease.”

Bodis-Wollner I. Neuropsychological and perceptual defects in Parkinson's disease. Parkinsonism Relat Disord. 2003 Aug;9 Suppl 2:S83-9. doi: 10.1016/s1353-8020(03)00022-1. PMID: 12915072.

Bonifati, Vincenzo, Patrizia Rizzu, Marijke J van Baren, Onno Schaap, Guido J Breedveld, Elmar Krieger, Marieke C J Dekker, et al. 1995. “Mutations in the DJ-1 Gene Associated with Autosomal Recessive Early-Onset Parkinsonism.” Proc. Natl. Acad. Sci. U.S.A. Vol. 270. https://www.science.org.

Bourque, Marie-Jose Â E, and Louis-Eric Trudeau. 2000. “GDNF Enhances the Synaptic Efficacy of Dopaminergic Neurons in Culture.” European Journal of Neuroscience 12: 3172–80.

Braak, Heiko, Kelly del Tredici, Udo Rüb, Rob A I de Vos, Ernst N H Jansen Steur, and Eva Braak. 2003. “Staging of Brain Pathology Related to Sporadic Parkinson’s Disease.” Neurobiology of Aging. Vol. 24.

Bravo, Roberto, Jose Miguel Vicencio, Valentina Parra, Rodrigo Troncoso, Juan Pablo Munoz, Michael Bui, Clara Quiroga, et al. 2011. “Increased ER-Mitochondrial Coupling Promotes Mitochondrial Respiration and Bioenergetics during Early Phases of ER Stress.” Journal of Cell Science. https://doi.org/10.1242/jcs.095455.

Brown GR, McGuire MJ, Thiele DL. Dipeptidyl peptidase I is enriched in granules of in vitro- and in vivo-activated cytotoxic T lymphocytes. J Immunol. 1993 Jun 1;150(11):4733-42. PMID: 8496587.

Bustin, Stephen A., Vladimir Benes, Jeremy A. Garson, Jan Hellemans, Jim Huggett, Mikael Kubista, Reinhold Mueller, et al. 2009. “The MIQE Guidelines: Minimum Information for Publication of Quantitative Real-Time PCR Experiments.” Clinical Chemistry 55 (4): 611–22. https://doi.org/10.1373/clinchem.2008.112797.

Button, Katherine S., John P.A. Ioannidis, Claire Mokrysz, Brian A. Nosek, Jonathan Flint, Emma S.J. Robinson, and Marcus R. Munafò. 2013. “Power Failure: Why Small Sample Size Undermines the Reliability of Neuroscience.” Nature Reviews Neuroscience 14 (5): 365–76. https://doi.org/10.1038/nrn3475.

Cai, Qian, Hesham Mostafa Zakaria, Anthony Simone, and Zu Hang Sheng. 2012. “Spatial Parkin Translocation and Degradation of Damaged Mitochondria via Mitophagy in Live Cortical Neurons.” Current Biology 22 (6): 545–52. https://doi.org/10.1016/j.cub.2012.02.005.

Calì, Tito, Denis Ottolini, Alessandro Negro, and Marisa Brini. 2013a. “Enhanced Parkin Levels Favor ER-Mitochondria Crosstalk and Guarantee Ca2+ Transfer to Sustain Cell Bioenergetics.” Biochimica et Biophysica Acta - Molecular Basis of Disease 1832 (4): 495–508. https://doi.org/10.1016/j.bbadis.2013.01.004.

———. 2013b. “Enhanced Parkin Levels Favor ER-Mitochondria Crosstalk and Guarantee Ca2+ Transfer to Sustain Cell Bioenergetics.” Biochimica et Biophysica Acta - Molecular Basis of Disease 1832 (4): 495–508. https://doi.org/10.1016/j.bbadis.2013.01.004.

Castaneda, Julio M., Haruhiko Miyata, Denise R. Archambeault, Yuhkoh Satouh, Zhifeng Yu, Masahito Ikawa, and Martin M. Matzuk. 2020. “Mouse T-Complex Protein 11 Is Important for Progressive Motility in Sperm.” Biology of Reproduction 102 (4): 852–62. https://doi.org/10.1093/biolre/ioz226.

Cha, Guang-Ho, Sunhong Kim, Jeehye Park, Eunji Lee, Myungjin Kim, Sung Bae Lee, Jin Man Kim, Jongkyeong Chung, and Kyoung Sang Cho. 2005. “Parkin Negatively Regulates JNK Pathway in the Dopaminergic Neurons of Drosophila.” PNAS 102: 10345–50. www.pnas.orgcgidoi10.1073pnas.0500346102.

Chari, Raj, Kim M. Lonergan, Larissa A. Pikor, Bradley P. Coe, Chang Qi Zhu, Timothy Hw Chan, Calum E. MacAulay, et al. 2010. “A Sequence-Based Approach to Identify Reference Genes for Gene Expression Analysis.” BMC Medical Genomics 3. https://doi.org/10.1186/1755-8794-3-32.

Chazotte, Brad. 2011. “Labeling Mitochondria with Mitotracker Dyes.” Cold Spring Harbor Protocols 6 (8): 990–92. https://doi.org/10.1101/pdb.prot5648.

Chen, Jialong, Yixian Ren, Chen Gui, Menglan Zhao, Xian Wu, Kanmin Mao, Wenjun Li, and Fei Zou. 2018. “Phosphorylation of Parkin at Serine 131 by P38 MAPK Promotes Mitochondrial Dysfunction and Neuronal Death in Mutant A53T α-Synuclein Model of Parkinson’s Disease.” Cell Death and Disease 9 (6). https://doi.org/10.1038/s41419-018-0722-7.

Chen, Xinming, Weiwei Shao, Hua Huang, Xiaochun Feng, Sumei Yao, and Honggang Ke. 2019. “Overexpression of RCN1 Correlates with Poor Prognosis and Progression in Non–Small Cell Lung Cancer.” Human Pathology 83 (January): 140–48. https://doi.org/10.1016/j.humpath.2018.08.014.

Cheng, Xiao Yu, Sangita Biswas, Juan Li, Cheng Jie Mao, Olga Chechneva, Jing Chen, Kai Li, et al. 2020. “Human IPSCs Derived Astrocytes Rescue Rotenone-Induced Mitochondrial Dysfunction and Dopaminergic Neurodegeneration in Vitro by Donating Functional Mitochondria.” Translational Neurodegeneration 9 (1). https://doi.org/10.1186/s40035-020-00190-6.

Cheong, Raymond, Alex Rhee, Chiaochun Joanne Wang, Ilya Nemenman, and Andre Levchenko. 2011. “Information Transduction Capacity of Noisy Biochemical Signaling Networks.” Science 334 (6054): 354–58. https://doi.org/10.1126/science.1204553.

Cieri, D., Vicario, M., Giacomello, M. *et al.* SPLICS: a split green fluorescent protein-based contact site sensor for narrow and wide heterotypic organelle juxtaposition. *Cell Death Differ* **25,** 1131–1145 (2018). https://doi.org/10.1038/s41418-017-0033-z

Coffey, J. W., and C. de Duve. 1968. “Digestive Activity of Lysosomes. I. The Digestion of Proteins by Extracts of Rat Liver Lysosomes.” Journal of Biological Chemistry 243 (12): 3255–63. https://doi.org/10.1016/S0021-9258(18)93301-6.

Cotzias, G, P Papavasiliou, and R Gellene. 1969. “Modification of Parkinsonism - Chronic Treatment with L-DOPA.” The New England Journal of Medicine 280: 337–45.

Dagda, Ruben K., Salvatore J. Cherra, Scott M. Kulich, Anurag Tandon, David Park, and Charleen T. Chu. 2009. “Loss of PINK1 Function Promotes Mitophagy through Effects on Oxidative Stress and Mitochondrial Fission.” Journal of Biological Chemistry 284 (20): 13843–55. https://doi.org/10.1074/jbc.M808515200.

Damier, P, E C Hirsch, Y Agid, and A M Graybiel. 1999. “The Substantia Nigra of the Human Brain I. Nigrosomes and the Nigral Matrix, a Compartmental Organization Based on Calbindin D 28K Immunohistochemistry.” Brain. Vol. 122.

Davis, Chung Ha O., Keun Young Kim, Eric A. Bushong, Elizabeth A. Mills, Daniela Boassa, Tiffany Shih, Mira Kinebuchi, et al. 2014. “Transcellular Degradation of Axonal Mitochondria.” Proceedings of the National Academy of Sciences of the United States of America 111 (26): 9633–38. https://doi.org/10.1073/pnas.1404651111.

Davis, Glenn C, Adrian C Williams, Sanford P Markey, Michael H Ebert, Eric D Caine, Cheryl M Reichert, and Irwin J Kopin. 1979. “Chronic Parkinsonism Secondary to Intravenous Injection of Meperidine Analogues Case Report.” Psychiatry Research. Vol. 1.

Díaz-Carballo, David, Jacqueline Klein, Ali H Acikelli, Camilla Wilk, Sahitya Saka, Holger Jastrow, Gunther Wennemuth, et al. 2017. “Cytotoxic Stress Induces Transfer of Mitochondria-Associated Human Endogenous Retroviral RNA and Proteins between Cancer Cells.” Oncotarget 8: 95945–64. www.impactjournals.com/oncotarget.

Ding, Xiaodong, and Matthew S. Goldberg. 2009. “Regulation of LRRK2 Stability by the E3 Ubiquitin Ligase CHIP.” PLoS ONE 4 (6). https://doi.org/10.1371/journal.pone.0005949.

Ding, Y., Caberoy, N. B., Guo, F., LeBlanc, M. E., Zhang, C., Wang, W., Wang, F., Chen, R., & Li, W. (2015). Reticulocalbin-1 facilitates microglial phagocytosis. *PloS one*, *10*(5), e0126993. https://doi.org/10.1371/journal.pone.0126993

Dolmetsch, Ricardo, and Daniel H. Geschwind. 2011. “The Human Brain in a Dish: The Promise of IPSC-Derived Neurons.” Cell. Elsevier B.V. https://doi.org/10.1016/j.cell.2011.05.034.

Dong, Lan-Feng, Jaromira Kovarova, Martina Bajzikova, Ayenachew Bezawork-Geleta, David Svec, Berwini Endaya, Karishma Sachaphibulkij, et al. 2017. “Horizontal Transfer of Whole Mitochondria Restores Tumorigenic Potential in Mitochondrial DNA-Deficient Cancer Cells.” ELife. https://doi.org/10.7554/eLife.22187.001.

Dorsey, E. Ray, Todd Sherer, Michael S. Okun, and Bastiaan R. Bloemd. 2018. “The Emerging Evidence of the Parkinson Pandemic.” Journal of Parkinson’s Disease. IOS Press. https://doi.org/10.3233/JPD-181474.

Doss-Pepe, Ellen W., Li Chen, and Kiran Madura. 2005. “α-Synuclein and Parkin Contribute to the Assembly of Ubiquitin Lysine 63-Linked Multiubiquitin Chains.” Journal of Biological Chemistry 280 (17): 16619–24. https://doi.org/10.1074/jbc.M413591200.

Doupé, David P., Maria P. Alcolea, Amit Roshan, Gen Zhang, Allon M. Klein, Benjamin D. Simons, and Philip H. Jones. 2012. “A Single Progenitor Population Switches Behavior to Maintain and Repair Esophageal Epithelium.” Science 337 (6098): 1091–93. https://doi.org/10.1126/science.1218835.

Eisenberg, Eli, and Erez Y. Levanon. 2003. “Human Housekeeping Genes Are Compact.” Trends in Genetics. Elsevier Ltd. https://doi.org/10.1016/S0168-9525(03)00140-9.

English, Krystal, Andrew Shepherd, Ndidi Ese Uzor, Ronnie Trinh, Annemieke Kavelaars, and Cobi J. Heijnen. 2020. “Astrocytes Rescue Neuronal Health after Cisplatin Treatment through Mitochondrial Transfer.” Acta Neuropathologica Communications 8 (1). https://doi.org/10.1186/s40478-020-00897-7.

Fahn, Stanley. 2003. “Description of Parkinson’s Disease as a Clinical Syndrome.” Ann. N.Y. Acad. Sci. Vol. 991.

Fasano, Caroline, Dominic Thibault, and Louis Éric Trudeau. 2008. “Culture of Postnatal Mesencephalic Dopamine Neurons on an Astrocyte Monolayer.” Current Protocols in Neuroscience. John Wiley and Sons Inc. https://doi.org/10.1002/0471142301.ns0321s44.

Forget, Caroline, Jane Stewart, and Louis Éric Trudeau. 2006. “Impact of Basic FGF Expression in Astrocytes on Dopamine Neuron Synaptic Function and Development.” European Journal of Neuroscience 23 (3): 608–16. https://doi.org/10.1111/j.1460-9568.2006.04570.x.

Gandhi, Sonia, Annika Vaarmann, Zhi Yao, Michael R. Duchen, Nicholas W. Wood, and Andrey Y. Abramov. 2012. “Dopamine Induced Neurodegeneration in a PINK1 Model of Parkinson’s Disease.” PLoS ONE 7 (5). https://doi.org/10.1371/journal.pone.0037564.

Gautier, Clément A., Zoi Erpapazoglou, François Mouton-Liger, Marie Paule Muriel, Florence Cormier, Stéphanie Bigou, Sophie Duffaure, et al. 2016. “The Endoplasmic Reticulum-Mitochondria Interface Is Perturbed in PARK2 Knockout Mice and Patients with PARK2 Mutations.” Human Molecular Genetics 25 (14): 2972–84. https://doi.org/10.1093/hmg/ddw148.

Geisler, Sven, Kira M. Holmström, Diana Skujat, Fabienne C. Fiesel, Oliver C. Rothfuss, Philipp J. Kahle, and Wolfdieter Springer. 2010. “PINK1/Parkin-Mediated Mitophagy Is Dependent on VDAC1 and P62/SQSTM1.” Nature Cell Biology 12 (2): 119–31. https://doi.org/10.1038/ncb2012.

Goldberg, Matthew S., Sheila M. Fleming, James J. Palacino, Carlos Cepeda, Hoa A. Lam, Anushree Bhatnagar, Edward G. Meloni, et al. 2003. “Parkin-Deficient Mice Exhibit Nigrostriatal Deficits but Not Loss of Dopaminergic Neurons.” Journal of Biological Chemistry 278 (44): 43628–35. https://doi.org/10.1074/jbc.M308947200.

Goldman, James E., Shu Hui Yen, Fung Chow Chiu, and Nancy S. Peress. 1983. “Lewy Bodies of Parkinson’s Disease Contain Neurofilament Antigens.” Science 221 (4615): 1082–84. https://doi.org/10.1126/science.6308771.

Gómez-Suaga, Patricia, José M. Bravo-San Pedro, Rosa A. González-Polo, J. M. Fuentes, and Mireia Niso-Santano. 2018. “ER-Mitochondria Signaling in Parkinson’s Disease Review-Article.” Cell Death and Disease. Nature Publishing Group. https://doi.org/10.1038/s41419-017-0079-3.

Gong, Huan, Liang Sun, Beidong Chen, Yiwen Han, Jing Pang, Wei Wu, Ruomei Qi, and Tie Mei Zhang. 2016. “Evaluation of Candidate Reference Genes for RT-QPCR Studies in Three Metabolism Related

Tissues of Mice after Caloric Restriction." Scientific Reports 6 (December). https://doi.org/10.1038/srep38513.

Grabert, Kathleen, Tom Michoel, Michail H. Karavolos, Sara Clohisey, J. Kenneth Baillie, Mark P. Stevens, Tom C. Freeman, Kim M. Summers, and Barry W. McColl. 2016. "Microglial Brain Regionâ 'dependent Diversity and Selective Regional Sensitivities to Aging." Nature Neuroscience 19 (3): 504–16. https://doi.org/10.1038/nn.4222.

Guardia-Laguarta, Cristina, Estela Area-Gomez, Cornelia Rüb, Yuhui Liu, Jordi Magrané, Dorothea Becker, Wolfgang Voos, Eric A. Schon, and Serge Przedborski. 2014. "α-Synuclein Is Localized to Mitochondria-Associated ER Membranes." Journal of Neuroscience 34 (1): 249–59. https://doi.org/10.1523/JNEUROSCI.2507-13.2014.

Gubern, Carme, Olivia Hurtado, Rocío Rodríguez, Jesús R. Morales, Víctor G. Romera, María A. Moro, Ignacio Lizasoain, Joaquín Serena, and Judith Mallolas. 2009. "Validation of Housekeeping Genes for Quantitative Real-Time PCR in in-Vivo and in-Vitro Models of Cerebral Ischaemia." BMC Molecular Biology 10 (June). https://doi.org/10.1186/1471-2199-10-57.

Haas, Richard H, Fatemeh Nasirian, Kazutoshi Nakano, David Ward, Mary Pay, Robert Hill, and Clifford W Shults. 1995. "Low Platelet Mitochondrial Complex I and Complex II/III Activity in Early Untreated Parhnson's Disease." Ann Neurol. Vol. 37.

Hajian-Tilaki, Karimollah. 2014. "Sample Size Estimation in Diagnostic Test Studies of Biomedical Informatics." Journal of Biomedical Informatics. Academic Press Inc. https://doi.org/10.1016/j.jbi.2014.02.013.

Hayakawa, Kazuhide, Elga Esposito, Xiaohua Wang, Yasukazu Terasaki, Yi Liu, Changhong Xing, Xunming Ji, and Eng H. Lo. 2016. "Transfer of Mitochondria from Astrocytes to Neurons after Stroke." Nature 535 (7613): 551–55. https://doi.org/10.1038/nature18928.

He, Yi, Wei Dong Le, and Stanley H. Appel. 2002. "Role of Fcγ Receptors in Nigral Cell Injury Induced by Parkinson Disease Immunoglobulin Injection into Mouse Substantia Nigra." Experimental Neurology 176 (2): 322–27. https://doi.org/10.1006/exnr.2002.7946.

Heeman, Bavo, Chris van den Haute, Sarah Ann Aelvoet, Federica Valsecchi, Richard J. Rodenburg, Veerle Reumers, Zeger Debyser, et al. 2011. "Depletion of PINK1 Affects Mitochondrial Metabolism, Calcium Homeostasis and Energy Maintenance." Journal of Cell Science 124 (7): 1115–25. https://doi.org/10.1242/jcs.078303.

Hemmersbach, Maren. 2016. "Characterization of Mitochondrial Morphology and Function in a New Parkinson-Mouse-Model."

Hogins, Joshua, Devon C. Crawford, Charles F. Zorumski, and Steven Mennerick. 2011. "Excitotoxicity Triggered by Neurobasal Culture Medium." PLoS ONE 6 (9). https://doi.org/10.1371/journal.pone.0025633.

Hristoph, C, B L Ücking, A Lexandra, D Ürr, V Incenzo, B Onifati, J Enny, et al. 2000. "ASSOCIATION BETWEEN EARLY-ONSET PARKINSON'S DISEASE AND MUTATIONS IN THE PARKIN GENE A BSTRACT Background Mutations in the Parkin Gene Have." The New England Journal of Medicine 342: 1560–67.

Hsiao, Li-Li, Fernando Dangond, Takumi Yoshida, Robert Hong, Roderick v Jensen, Jatin Misra, William Dillon, et al. 2001. "A Compendium of Gene Expression in Normal Human Tissues." Physiol. Genomics 7: 97–104. https://doi.org/10.1152/physiol.

Huang, Ze Hao, Jun Qiao, Yi Yang Feng, Meng Ting Qiu, Ting Cheng, Jia Wang, Chao Feng Zheng, Zhi Qin Lv, and Cai Hong Wang. 2020. "Reticulocalbin-1 Knockdown Increases the Sensitivity of Cells to Adriamycin in Nasopharyngeal Carcinoma and Promotes Endoplasmic Reticulum Stress-Induced Cell Apoptosis." Cell Cycle 19 (13): 1576–89. https://doi.org/10.1080/15384101.2020.1733750.

Iijima, Takehiko, Tatsuya Mishima, Kimio Akagawa, and Yasuhide Iwao. 2003. "Mitochondrial Hyperpolarization after Transient Oxygen-Glucose Deprivation and Subsequent Apoptosis in Cultured Rat Hippocampal Neurons." Brain Research 993 (1–2): 140–45. https://doi.org/10.1016/j.brainres.2003.09.041.

Imai, Y., M. Soda, and R. Takahashi. 2000. “Parkin Suppresses Unfolded Protein Stress-Induced Cell Death through Its E3 Ubiquitin-Protein Ligase Activity.” Journal of Biological Chemistry 275 (46): 35661–64. https://doi.org/10.1074/jbc.C000447200.

Ishikawa A, Tsuji S. Clinical analysis of 17 patients in 12 Japanese families with autosomal-recessive type juvenile Parkinsonism. Neurology. 1996 Jul;47(1):160-6. doi: 10.1212/wnl.47.1.160. PMID: 8710071.

Itier, Jean Michel, Pablo Ibáñez, Maria Angeles Mena, Nacer Abbas, Charles Cohen-Salmon, Georg Andrees Bohme, Michel Laville, et al. 2003. “Parkin Gene Inactivation Alters Behaviour and Dopamine Neurotransmission in the Mouse.” Human Molecular Genetics. https://doi.org/10.1093/hmg/ddg239.

James, Andrew M, and Michael P Murphy. 2002. “How Mitochondrial Damage Affects Cell Function.” J Biomed Sci. Vol. 9. www.karger.com/journals/jbs.

Javitch, Jonathan A, Robert J D’amato, Stephen M Strittmatter, and Solomon H Snyder. 1985. “Parkinsonism-Inducing Neurotoxin, N-Methyl-4-Phenyl-1,2,3,6-Tetrahydropyridine: Uptake of the Metabolite N-Methyl-4-Phenylpyridine by Dopamine Neurons Explains Selective Toxicity (Substantia Nigra/Caudate-Putamen/Nucleus Accumbens/Locus Ceruleus/[3H]Mazindol Autoradiography).” Proc. Nail. Acad. Sci. USA. Vol. 82.

Jonge, Hendrik J.M. de, Rudolf S.N. Fehrmann, Eveline S.J.M. de Bont, Robert M.W. Hofstra, Frans Gerbens, Willem A. Kamps, Elisabeth G.E. de Vries, Ate G.J. van der Zee, Gerard J. te Meerman, and Arja ter Elst. 2007. “Evidence Based Selection of Housekeeping Genes.” PLoS ONE 2 (9). https://doi.org/10.1371/journal.pone.0000898.

Kabeya, Yukiko, Noboru Mizushima, Takashi Ueno, Akitsugu Yamamoto, Takayoshi Kirisako, Takeshi Noda, Eiki Kominami, Yoshinori Ohsumi, and Tamotsu Yoshimori. 2000. “LC3, a Mammalian Homologue of Yeast Apg8p,Is Localized in Autophagosome Membranes Afterprocessing.” The EMBO Journal 19: 5720–28.

Kageyama, Yusuke, Masahiko Hoshijima, Kinya Seo, Djahida Bedja, Polina Sysa-Shah, Shaida A Andrabi, Weiran Chen, et al. 2014. “ Parkin-independent Mitophagy Requires D Rp1 and Maintains the Integrity of Mammalian Heart and Brain .” The EMBO Journal 33 (23): 2798–2813. https://doi.org/10.15252/embj.201488658.

Kang, Yingbo, Zhuomin Wu, De Cai, and Binger Lu. 2018. “Evaluation of Reference Genes for Gene Expression Studies in Mouse and N2a Cell Ischemic Stroke Models Using Quantitative Real-Time PCR.” BMC Neuroscience 19 (1). https://doi.org/10.1186/s12868-018-0403-6.

Karabiyik, Cansu, Rebecca A. Frake, So Jung Park, Mariana Pavel, and David C. Rubinsztein. 2021. “Autophagy in Ageing and Ageing-Related Neurodegenerative Diseases.” Ageing and Neurodegenerative Diseases. https://doi.org/10.20517/and.2021.05.

Katunuma N. Mechanisms and regulation of lysosomal proteolysis. Revis Biol Celular. 1989;20:35-61. PMID: 2700097.

Kawajiri, Sumihiro, Shinji Saiki, Shigeto Sato, Fumiaki Sato, Taku Hatano, Hiroto Eguchi, and Nobutaka Hattori. 2010. “PINK1 Is Recruited to Mitochondria with Parkin and Associates with LC3 in Mitophagy.” FEBS Letters 584 (6): 1073–79. https://doi.org/10.1016/j.febslet.2010.02.016.

Keane, Thomas M., Leo Goodstadt, Petr Danecek, Michael A. White, Kim Wong, Binnaz Yalcin, Andreas Heger, et al. 2011. “Mouse Genomic Variation and Its Effect on Phenotypes and Gene Regulation.” Nature 477 (7364): 289–94. https://doi.org/10.1038/nature10413.

Kim, Daehwan, Joseph M. Paggi, Chanhee Park, Christopher Bennett, and Steven L. Salzberg. 2019. “Graph-Based Genome Alignment and Genotyping with HISAT2 and HISAT-Genotype.” Nature Biotechnology 37 (8): 907–15. https://doi.org/10.1038/s41587-019-0201-4.

Kim, Hye Suk, Sang Myung Cheon, Jung Wook Seo, Hyun Ju Ryu, Kyung Won Park, and Jae Woo Kim. 2013. “Nonmotor Symptoms More Closely Related to Parkinson’s Disease: Comparison with Normal Elderly.” Journal of the Neurological Sciences 324 (1–2): 70–73. https://doi.org/10.1016/j.jns.2012.10.004.

Ko, Han Seok, Rachel Bailey, Wanli W Smith, Zhaohui Liu, Joo-Ho Shin, Yun-Il Lee, Yong-Jie Zhang, et al. 2009. “CHIP Regulates Leucine-Rich Repeat Kinase-2 Ubiquitination, Degradation, and Toxicity.” PNAS 106: 2897–2902.

Kok, Jacques B. de, Rian W. Roelofs, Belinda A. Giesendorf, Jeroen L. Pennings, Erwin T. Waas, Ton Feuth, Dorine W. Swinkels, and Paul N. Span. 2005. “Normalization of Gene Expression Measurements in Tumor Tissues: Comparison of 13 Endogenous Control Genes.” Laboratory Investigation 85 (1): 154–59. https://doi.org/10.1038/labinvest.3700208.

Kominami E, Ishido K, Muno D, Sato N. The primary structure and tissue distribution of cathepsin C. Biol Chem Hoppe Seyler. 1992 Jul;373(7):367-73. doi: 10.1515/bchm3.1992.373.2.367. PMID: 1515062.

Kordower, Jeffrey H., C. Warren Olanow, Hemraj B. Dodiya, Yaping Chu, Thomas G. Beach, Charles H. Adler, Glenda M. Halliday, and Raymond T. Bartus. 2013. “Disease Duration and the Integrity of the Nigrostriatal System in Parkinson’s Disease.” Brain 136 (8): 2419–31. https://doi.org/10.1093/brain/awt192.

Krohn, Aaron J, Tanja Wahlbrink, and Jochen H M Prehn. 1999. “Mitochondrial Depolarization Is Not Required for Neuronal Apoptosis.” Journal of Neuroscience 19: 7394–7404.

Langston JW, Ballard P, Tetrud JW, Irwin I. Chronic Parkinsonism in humans due to a product of meperidine-analog synthesis. Science. 1983 Feb 25;219(4587):979-80. doi: 10.1126/science.6823561. PMID: 6823561.

Lee, Tong Ihn, and Richard A. Young. 2013. “Transcriptional Regulation and Its Misregulation in Disease.” Cell. Elsevier B.V. https://doi.org/10.1016/j.cell.2013.02.014.

Lemasters, John J. 2005. “Perspective Selective Mitochondrial Autophagy, or Mitophagy, as a Targeted Defense Against Oxidative Stress, Mitochondrial Dysfunction, and Aging.” REJUVENATION RESEARCH. Vol. 8.

Lemhoefer, Katharina Inge Elisabeth. 2020. “Analysis of Changes in Gene Expression in Parkin-Deficient-Mice Using Semiquantitative Real-Time PCR.”

Lesage, Suzanne, Mathieu Anheim, Franck Letournel, Luc Bousset, Aurélie Honoré, Nelly Rozas, Laura Pieri, et al. 2013. “G51D α-Synuclein Mutation Causes a Novel Parkinsonian-Pyramidal Syndrome.” Annals of Neurology 73 (4): 459–71. https://doi.org/10.1002/ana.23894.

Lewendel, Aylin. 2020. “Investigations on the Subcellular Localisation of RCN1 within the Mouse Brain.”

Lian, Teng Hong, Peng Guo, Li Jun Zuo, Yang Hu, Shu Yang Yu, Li Liu, Zhao Jin, et al. 2019. “An Investigation on the Clinical Features and Neurochemical Changes in Parkinson’s Disease with Depression.” Frontiers in Psychiatry 10 (JAN). https://doi.org/10.3389/fpsyt.2018.00723.

Liang, Wenjing, Alexandra G. Moyzis, Mark A. Lampert, Rachel Y. Diao, Rita H. Najor, and Åsa B. Gustafsson. 2020. “Aging Is Associated with a Decline in Atg9b-Mediated Autophagosome Formation and Appearance of Enlarged Mitochondria in the Heart.” Aging Cell 19 (8). https://doi.org/10.1111/acel.13187.

Liddelow, Shane A., Kevin A. Guttenplan, Laura E. Clarke, Frederick C. Bennett, Christopher J. Bohlen, Lucas Schirmer, Mariko L. Bennett, et al. 2017. “Neurotoxic Reactive Astrocytes Are Induced by Activated Microglia.” Nature 541 (7638): 481–87. https://doi.org/10.1038/nature21029.

Lill, Christina M. 2016. “Genetics of Parkinson’s Disease.” Molecular and Cellular Probes. Academic Press. https://doi.org/10.1016/j.mcp.2016.11.001.

Lin, Leu-Fen H., H. Doherty Daniel, D. Lile Jack, Bektesh Susan, and Collins Frank. 1993. “GDNF: A Glial Cell Line-Derived Neurotrophic Factor for Midbrain Dopaminergic Neurons.” Science 260: 1130–32. www.sciencemag.org.

Liu, Delin, Youshui Gao, Jiao Liu, Yigang Huang, Junhui Yin, Yuyao Feng, Linjing Shi, et al. 2021. “Intercellular Mitochondrial Transfer as a Means of Tissue Revitalization.” Signal Transduction and Targeted Therapy. Springer Nature. https://doi.org/10.1038/s41392-020-00440-z.

Liu, Qing, Yanli Zhang, Shuang Liu, Yanna Liu, Xiaohan Yang, Gang Liu, Takahiro Shimizu, Kazuhiro Ikenaka, Kai Fan, and Jianmei Ma. 2019. “Cathepsin C Promotes Microglia M1 Polarization and Aggravates Neuroinflammation via Activation of Ca 2+ -Dependent PKC/P38MAPK/NF-KB Pathway.” Journal of Neuroinflammation 16 (1). https://doi.org/10.1186/s12974-019-1398-3.

Liu, Xiaofei, Nianzhao Zhang, Dawei Wang, Deyu Zhu, Quan Yuan, Xiulei Zhang, Lilin Qian, et al. 2018. “Downregulation of Reticulocalbin-1 Differentially Facilitates Apoptosis and Necroptosis in Human Prostate Cancer Cells.” Cancer Science 109 (4): 1147–57. https://doi.org/10.1111/cas.13541.

Lonneke M L de Lau, and Monique M B Breteler. 2006. “Epidemiology of Parkinson’s Disease.” The Lancet 5: 525–35. http://neurology.thelancet.comVol.

López González, Irene, Paula Garcia-Esparcia, Franc Llorens, and Isidre Ferrer. 2016. “Genetic and Transcriptomic Profiles of Inflammation in Neurodegenerative Diseases: Alzheimer, Parkinson, Creutzfeldt-Jakob and Tauopathies.” International Journal of Molecular Sciences. MDPI AG. https://doi.org/10.3390/ijms17020206.

Lössl, Patricia. 2020. “Untersuchung Der PINK1/Parkin-Abhängigen Mitophagie in Primären Fibroblasten Parkin-Defizienter Mäuse Investigation of the PINK1/Parkin-Dependent Mitophagy in Primary Fibroblasts of Parkin-Deficient Mice.”

Madisen, Linda, Theresa A. Zwingman, Susan M. Sunkin, Seung Wook Oh, Hatim A. Zariwala, Hong Gu, Lydia L. Ng, et al. 2010. “A Robust and High-Throughput Cre Reporting and Characterization System for the Whole Mouse Brain.” Nature Neuroscience 13 (1): 133–40. https://doi.org/10.1038/nn.2467.

Maggioni, Daniele, Marianna Monfrini, Maddalena Ravasi, Giovanni Tredici, and Arianna Scuteri. 2015. “Neurobasal Medium Toxicity on Mature Cortical Neurons.” NeuroReport 26 (6): 320–24. https://doi.org/10.1097/WNR.0000000000000343.

Maleki, Farhad, Katie Ovens, Ian McQuillan, and Anthony J. Kusalik. 2019. “Size Matters: How Sample Size Affects the Reproducibility and Specificity of Gene Set Analysis.” Human Genomics 13 (October): 42. https://doi.org/10.1186/s40246-019-0226-2.

Malkemper, Pascal. 2011. “The Role of Neurotrophic Factors and Mitochondrial Calcium Storage in Mouse Models of Parkinson’s Disease.-Die Rolle Neurotropher Faktoren Und Mitochondrialer Calciumspeicher in Mausmodellen Des Morbus Parkinson.”

Marchetto, Maria C.N., Cassiano Carromeu, Allan Acab, Diana Yu, Gene W. Yeo, Yangling Mu, Gong Chen, Fred H. Gage, and Alysson R. Muotri. 2010. “A Model for Neural Development and Treatment of Rett Syndrome Using Human Induced Pluripotent Stem Cells.” Cell 143 (4): 527–39. https://doi.org/10.1016/j.cell.2010.10.016.

Marongiu, Roberta, Brian Spencer, Leslie Crews, Anthony Adame, Christina Patrick, Margarita Trejo, Bruno Dallapiccola, Enza Maria Valente, and Eliezer Masliah. 2009. “Mutant Pink1 Induces Mitochondrial Dysfunction in a Neuronal Cell Model of Parkinson’s Disease by Disturbing Calcium Flux.” Journal of Neurochemistry 108 (6): 1561–74. https://doi.org/10.1111/j.1471-4159.2009.05932.x.

Martín-Maestro, Patricia, Ricardo Gargini, Andrew A. Sproul, Esther García, Luis C. Antón, Scott Noggle, Ottavio Arancio, Jesús Avila, and Vega García-Escudero. 2017. “Mitophagy Failure in Fibroblasts and IPSC-Derived Neurons of Alzheimer’s Disease-Associated Presenilin 1 Mutation.” Frontiers in Molecular Neuroscience 10 (September). https://doi.org/10.3389/fnmol.2017.00291.

Martino, Alessandro, Manuela Cabiati, Manuela Campan, Tommaso Prescimone, Daiana Minocci, Chiara Caselli, Anna Maria Rossi, Daniela Giannessi, and Silvia del Ry. 2011. “Selection of Reference Genes for Normalization of Real-Time PCR Data in Minipig Heart Failure Model and Evaluation of TNF-α MRNA Expression.” Journal of Biotechnology 153 (3–4): 92–99. https://doi.org/10.1016/j.jbiotec.2011.04.002.

Maskri, Lyutha, Xin Ran Zhu, Sabrina Fritzen, Kati Kühn, Christoph Ullmer, Peter Engels, Michael Andriske, Christine C. Stichel, and Hermann Lübbert. 2004. “Influence of Different Promoters on the

Expression Pattern of Mutated Human α-Synuclein in Transgenic Mice." Neurodegenerative Diseases 1 (6): 255–65. https://doi.org/10.1159/000085064.

Mateos-Aparicio, Pedro, Sabina A. Bello, and Antonio Rodríguez-Moreno. 2020. "Challenges in Physiological Phenotyping of HiPSC-Derived Neurons: From 2D Cultures to 3D Brain Organoids." Frontiers in Cell and Developmental Biology 8 (August). https://doi.org/10.3389/fcell.2020.00797.

Matsuda, Noriyuki, Shigeto Sato, Kahori Shiba, Kei Okatsu, Keiko Saisho, Clement A. Gautier, Yu Shin Sou, et al. 2010. "PINK1 Stabilized by Mitochondrial Depolarization Recruits Parkin to Damaged Mitochondria and Activates Latent Parkin for Mitophagy." Journal of Cell Biology 189 (2): 211–21. https://doi.org/10.1083/jcb.200910140.

McGuire, M. J., P. E. Lipsky, and D. L. Thiele. 1993. "Generation of Active Myeloid and Lymphoid Granule Serine Proteases Requires Processing by the Granule Thiol Protease Dipeptidyl Peptidase I." Journal of Biological Chemistry 268 (4): 2458–67. https://doi.org/10.1016/s0021-9258(18)53798-4.

McKeon, Jeanne E., Di Sha, Lian Li, and Lih Shen Chin. 2015. "Parkin-Mediated K63-Polyubiquitination Targets Ubiquitin C-Terminal Hydrolase L1 for Degradation by the Autophagy-Lysosome System." Cellular and Molecular Life Sciences 72 (9): 1811–24. https://doi.org/10.1007/s00018-014-1781-2.

McWilliams, Thomas G., Alan R. Prescott, Lambert Montava-Garriga, Graeme Ball, François Singh, Erica Barini, Miratul M.K. Muqit, Simon P. Brooks, and Ian G. Ganley. 2018. "Basal Mitophagy Occurs Independently of PINK1 in Mouse Tissues of High Metabolic Demand." Cell Metabolism 27 (2): 439-449.e5. https://doi.org/10.1016/j.cmet.2017.12.008.

Metrione RM, Okuda Y, Fairclough GF Jr. Subunit structure of dipeptidyl transferase. Biochemistry. 1970 Jun 9;9(12):2427-32. doi: 10.1021/bi00814a006. PMID: 5423262.

Mizuno', Yoshikuni, Shigeo Ohta, Masashi Tanaka3, Shinzaburo Takamiya4, Hiroshi Oya4, Keiji Suzuki', Takeshi Satol, Takayuki Ozawa3, and Yasuo Kagawa. 1989. "DEFICIENCIES IN COMPLEX I SUBUNITS OF THE RESPIRATORY CHAIN IN PARKINSON'S DISEASE." Biochemical and Biophysical Research Communications 163 (3): 1450–55.

Mizushima, Noboru, Yoshinori Ohsumi, and Tamotsu Yoshimori. 2002. "Autophagosome Formation in Mammalian Cells." CELL STRUCTURE AND FUNCTION. Vol. 27.

Moisoi, Nicoleta, Valentina Fedele, Jennifer Edwards, and L. Miguel Martins. 2014. "Loss of PINK1 Enhances Neurodegeneration in a Mouse Model of Parkinson's Disease Triggered by Mitochondrial Stress." Neuropharmacology 77: 350–57. https://doi.org/10.1016/j.neuropharm.2013.10.009.

Morciano, Giampaolo, Saverio Marchi, Claudia Morganti, Luigi Sbano, Mart Bittremieux, Martijn Kerkhofs, Mariangela Corricelli, et al. 2018. "Role of Mitochondria-Associated ER Membranes in Calcium Regulation in Cancer-Specific Settings." Neoplasia (United States). Neoplasia Press, Inc. https://doi.org/10.1016/j.neo.2018.03.005.

Mrohs, David. 2017. "Investigations of Locomotor Dysfunctions and Cellular Damages in a Pakinson's Disease Mouse Model."

Nagy, Gyorgy, Agnes Koncz, and Andras Perl. 2003. "T Cell Activation-Induced Mitochondrial Hyperpolarization Is Mediated by Ca 2+-and Redox-Dependent Production of Nitric Oxide 1." J Immunol. Vol. 171.

Naon, Deborah, and Luca Scorrano. 2014. "At the Right Distance: ER-Mitochondria Juxtaposition in Cell Life and Death." Biochimica et Biophysica Acta - Molecular Cell Research. Elsevier B.V. https://doi.org/10.1016/j.bbamcr.2014.05.011.

Narendra, Derek P., Seok Min Jin, Atsushi Tanaka, Der Fen Suen, Clement A. Gautier, Jie Shen, Mark R. Cookson, and Richard J. Youle. 2010. "PINK1 Is Selectively Stabilized on Impaired Mitochondria to Activate Parkin." PLoS Biology 8 (1). https://doi.org/10.1371/journal.pbio.1000298.

Narendra, Derek, Atsushi Tanaka, Der Fen Suen, and Richard J. Youle. 2008. "Parkin Is Recruited Selectively to Impaired Mitochondria and Promotes Their Autophagy." Journal of Cell Biology 183 (5): 795–803. https://doi.org/10.1083/jcb.200809125.

Nido, Gonzalo S., Fiona Dick, Lilah Toker, Kjell Petersen, Guido Alves, Ole Bjørn Tysnes, Inge Jonassen, Kristoffer Haugarvoll, and Charalampos Tzoulis. 2020. “Common Gene Expression Signatures in Parkinson’s Disease Are Driven by Changes in Cell Composition.” Acta Neuropathologica Communications 8 (1). https://doi.org/10.1186/s40478-020-00932-7.

Nussbaum, Robert L, Alan E Guttmacher, Francis S Collins, and Christopher E Ellis. 2003. “Alzheimer’s Disease and Parkinson’s Disease.” Genomic Medicine 348: 1356–64. www.nejm.org.

Olanow, C W, and W G Tatton. 1999. “ETIOLOGY AND PATHOGENESIS OF PARKINSON’S DISEASE.” Annu. Rev. Neurosci. Vol. 22.

Osenberg, Katharina. 2018. “Next-Generation Sequencing-Basierte Transkriptomanalysen in Experimentellen Mausmodellen.”

Ottolini, Denis, Tito Calì, Alessandro Negro, and Marisa Brini. 2013. “The Parkinson Disease-Related Protein DJ-1 Counteracts Mitochondrial Impairment Induced by the Tumour Suppressor Protein P53 by Enhancing Endoplasmic Reticulum-Mitochondria Tethering.” Human Molecular Genetics 22 (11): 2152–68. https://doi.org/10.1093/hmg/ddt068.

Ozawa, M., and T. Muramatsu. 1993. “Reticulocalbin, a Novel Endoplasmic Reticulum Resident Ca2+-Binding Protein with Multiple EF-Hand Motifs and a Carboxyl-Terminal HDEL Sequence.” Journal of Biological Chemistry 268 (1): 699–705. https://doi.org/10.1016/s0021-9258(18)54208-3.

Paillusson, Sebastien, Radu Stoica, Patricia Gomez-Suaga, Dawn H.W. Lau, Sarah Mueller, Tanya Miller, and Christopher C.J. Miller. 2016. “There’s Something Wrong with My MAM; the ER-Mitochondria Axis and Neurodegenerative Diseases.” Trends in Neurosciences. Elsevier Ltd. https://doi.org/10.1016/j.tins.2016.01.008.

Palacino, James J., Dijana Sagi, Matthew S. Goldberg, Stefan Krauss, Claudia Motz, Maik Wacker, Joachim Klose, and Jie Shen. 2004. “Mitochondrial Dysfunction and Oxidative Damage in Parkin-Deficient Mice.” Journal of Biological Chemistry 279 (18): 18614–22. https://doi.org/10.1074/jbc.M401135200.

Pertea, Mihaela, Daehwan Kim, Geo M. Pertea, Jeffrey T. Leek, and Steven L. Salzberg. 2016. “Transcript-Level Expression Analysis of RNA-Seq Experiments with HISAT, StringTie and Ballgown.” Nature Protocols 11 (9): 1650–67. https://doi.org/10.1038/nprot.2016.095.

Pfeffel, Katharina. 2019. “Investigation of Mitophagy in Mouse Astrocytes with Parkin Deletion in Vitro.”

———. 2021. “Untersuchung Der Kontaktstellen Zwischen Dem Endoplasmatischen Retikulum Und Der Mitochondrien in Einem Zellulären Parkinson-Maus-Modell.”

Pham, Christine T.N., Randall J. Armstrong, Drazen B. Zimonjie, Nicholas C. Popescu, Donald G. Payan, and Timothy J. Ley. 1997. “Molecular Cloning, Chromosomal Localization, and Expression of Murine Dipeptidyl Peptidase I.” Journal of Biological Chemistry 272 (16): 10695–703. https://doi.org/10.1074/jbc.272.16.10695.

Pinto, Milena, Nadee Nissanka, and Carlos T. Moraes. 2018. “Lack of Parkin Anticipates the Phenotype and Affects Mitochondrial Morphology and MtDNA Levels in a Mouse Model of Parkinson’s Disease.” Journal of Neuroscience 38 (4): 1042–53. https://doi.org/10.1523/JNEUROSCI.1384-17.2017.

Plesser, Hans E. 2018. “Reproducibility vs. Replicability: A Brief History of a Confused Terminology.” Frontiers in Neuroinformatics 11 (January). https://doi.org/10.3389/fninf.2017.00076.

Polymeropoulos, Mihael H., Joseph J.Higgins, Lawrence Golbe, William G. Johnson, Susan E. Ide, Giuseppe Dilorio, Giuseppe Sanges, et al. 1996. “Mapping of a Gene for Parkinson’s Disease to Chromosome 4q21-Q23.” Science 274: 1197–1999.

Polymeropoulos, Mihael H., Christian Lavedan, Elisabeth Leroy, Susan E. Ide, Anindya Dehejia, Amalia Dutra, Brian Pike, et al. 1997. “Mutation in the α-Synuclein Gene Identified in Families with Parkinson’s Disease.” Science 276 (5321): 2045–47. https://doi.org/10.1126/science.276.5321.2045.

Ramakrishnan, Rakhee K., Khuloud Bajbouj, Mahmood Y. Hachim, Andrea K. Mogas, Bassam Mahboub, Ronald Olivenstein, Rifat Hamoudi, Rabih Halwani, and Qutayba Hamid. 2020. “Enhanced

Mitophagy in Bronchial Fibroblasts from Severe Asthmatic Patients." PLoS ONE 15 (11 November). https://doi.org/10.1371/journal.pone.0242695.

Raps, Stephen P, James C K Lai, Leif Hertz, and Arthur J L Cooper. 1989. "Glutathione Is Present in High Concentrations in Cultured Astrocytes but Not in Cultured Neurons." Brain Research 493: 398–401.

Rejko Kruger, Wilfried Kuhn, Thomas Muller, Dirk Woitalla, Manuel Graeber, Sigfried Kosel, Horst Przuntek, Jorg T. Epplen, Ludger Schols, and Olaf Riess. 1998. "Ala30Pro Mutation in the Gene Encoding A-Synuclein in Parkinson's Disease." Nature Genetics 18: 106–8.

Ren, Yong, Houbo Jiang, Zhixing Hu, Kevin Fan, Jun Wang, Stephen Janoschka, Xiaomin Wang, Shaoyu Ge, and Jian Feng. 2015. "Parkin Mutations Reduce the Complexity of Neuronal Processes in IPSC-Derived Human Neurons." Stem Cells 33 (1): 68–78. https://doi.org/10.1002/stem.1854.

Rieker, Claus, David Engblom, Grzegorz Kreiner, Andrii Domanskyi, Andreas Schober, Stefanie Stotz, Manuela Neumann, et al. 2011. "Nucleolar Disruption in Dopaminergic Neurons Leads to Oxidative Damage and Parkinsonism through Repression of Mammalian Target of Rapamycin Signaling." Journal of Neuroscience 31 (2): 453–60. https://doi.org/10.1523/JNEUROSCI.0590-10.2011.

Robert, Francis, and Jerry Pelletier. 2018. "Exploring the Impact of Single-Nucleotide Polymorphisms on Translation." Frontiers in Genetics 9 (October). https://doi.org/10.3389/fgene.2018.00507.

Rocke, David, Luyao Ruan, Yilun Zhang, J. Jared Gossett, Blythe Durbin-Johnson, and Sharon Aviran. 2015. "Excess False Positive Rates in Methods for Differential Gene Expression Analysis Using RNA-Seq Data." BioRxiv, 020784. https://doi.org/10.1101/020784.

Rodríguez-Leyva, Ildefonso, Ana Laura Calderón-Garcidueñas, María E. Jiménez-Capdeville, Ana Arely Rentería-Palomo, Héctor Gerardo Hernandez-Rodriguez, Rodrigo Valdés-Rodríguez, Cornelia Fuentes-Ahumada, et al. 2014. "α-Synuclein Inclusions in the Skin of Parkinson's Disease and Parkinsonism." Annals of Clinical and Translational Neurology 1 (7): 471–78. https://doi.org/10.1002/acn3.78.

Runwal, Gautam, Eleanna Stamatakou, Farah H. Siddiqi, Claudia Puri, Ye Zhu, and David C. Rubinsztein. 2019. "LC3-Positive Structures Are Prominent in Autophagy-Deficient Cells." Scientific Reports 9 (1). https://doi.org/10.1038/s41598-019-46657-z.

Sala-Vila, Aleix, Inmaculada Navarro-Lérida, Miguel Sánchez-Alvarez, Marta Bosch, Carlos Calvo, Juan Antonio López, Enrique Calvo, et al. 2016. "Interplay between Hepatic Mitochondria-Associated Membranes, Lipid Metabolism and Caveolin-1 in Mice." Scientific Reports 6 (June). https://doi.org/10.1038/srep27351.

Sandebring, Anna, Nodi Dehvari, Monica Perez-Manso, Kelly Jean Thomas, Elena Karpilovski, Mark R. Cookson, Richard F. Cowburn, and Angel Cedazo-Mínguez. 2009. "Parkin Deficiency Disrupts Calcium Homeostasis by Modulating Phospholipase C Signalling." FEBS Journal 276 (18): 5041–52. https://doi.org/10.1111/j.1742-4658.2009.07201.x.

Savitt, Joseph M., Susie S. Jang, Weitong Mu, Valina L. Dawson, and Ted M. Dawson. 2005. "Bcl-x Is Required for Proper Development of the Mouse: Substantia Nigra." Journal of Neuroscience 25 (29): 6721–28. https://doi.org/10.1523/JNEUROSCI.0760-05.2005.

Schaar, D, B Sieber, C Dreyfus, and I Black. 1993. "Regional and Cell-Specific Expression of GDNF in Rat Brain." Experimental Neurology 124: 368–71.

Schapira AH, Cooper JM, Dexter D, Clark JB, Jenner P, Marsden CD. Mitochondrial complex I deficiency in Parkinson's disease. J Neurochem. 1990 Mar;54(3):823-7. doi: 10.1111/j.1471-4159.1990.tb02325.x. PMID: 2154550.

Schäning, Ruth. 2019. "Analysis of RCN1-Expression in a Mouse Model and Cellular Model for Parkinson's Disease."

Schmidt, Saskia, Bettina Linnartz, Sonja Mendritzki, Teresa Sczepan, Matthias Lübbert, Christine C. Stichel, and Hermann Lübbert. 2011. "Genetic Mouse Models for Parkinson's Disease Display Severe

Pathology in Glial Cell Mitochondria." Human Molecular Genetics 20 (6): 1197–1211. https://doi.org/10.1093/hmg/ddq564.

Schreiner, Bernadette, and Maria Ankarcrona. 2017. "Isolation of Mitochondria-Associated Membranes (MAM) from Mouse Brain Tissue." In Methods in Molecular Biology, 1567:53–68. Humana Press Inc. https://doi.org/10.1007/978-1-4939-6824-4_5.

Schurch, Nicholas J., Pietá Schofield, Marek Gierliński, Christian Cole, Alexander Sherstnev, Vijender Singh, Nicola Wrobel, et al. 2016. "How Many Biological Replicates Are Needed in an RNA-Seq Experiment and Which Differential Expression Tool Should You Use?" RNA 22 (6): 839–51. https://doi.org/10.1261/rna.053959.115.

Schwenk, Frieder, Udo Baron1, and Klaus Rajewsky. 1995. "A Cremtransgenic Mouse Strain for Te Ubiquitous Deletion of Ioxflanked Gene Segments Including Deletion in Germ Cells." Nucleic Acids Research. Vol. 23.

Shamim, Ejaz A., Jason Chu, Linda H. Scheider, Joseph Savitt, H. A. Jinnah, and Mark Hallett. 2011. "Extreme Task Specificity in Writer's Cramp." Movement Disorders 26 (11): 2107–9. https://doi.org/10.1002/mds.23827.

Shimura, Hideki, Nobutaka Hattori, Shin-Ichiro Kubo, Yoshikuni Mizuno, Shuichi Asakawa, Shinsei Minoshima, Nobuyoshi Shimizu, et al. 2000. "Familial Parkinson Disease Gene Product, Parkin, Is a Ubiquitin-Protein Ligase." Nature Genetivs 25: 302–5. http://genetics.nature.com.

Sonninen, Tuuli Maria, Riikka H. Hämäläinen, Marja Koskuvi, Minna Oksanen, Anastasia Shakirzyanova, Sara Wojciechowski, Katja Puttonen, et al. 2020. "Metabolic Alterations in Parkinson's Disease Astrocytes." Scientific Reports 10 (1). https://doi.org/10.1038/s41598-020-71329-8.

Spillantini, Maria Grazia, R Anthony Crowther, Ross Jakes, Masato Hasegawa, and Michel Goedert. 1998. "Synuclein in Filamentous Inclusions of Lewy Bodies from Parkinson's Disease and Dementia with Lewy Bodies (Ubiquitinsarkosyl-Insoluble Filamentsimmunoelectron Microscopy)." Neurobiology Communicated by Max F. Perutz, Medical Research Council. Vol. 95. www.pnas.org.

Stavoe, Andrea K.H., and Erika L.F. Holzbaur. 2020. "Neuronal Autophagy Declines Substantially with Age and Is Rescued by Overexpression of WIPI2." Autophagy. Taylor and Francis Inc. https://doi.org/10.1080/15548627.2019.1695401.

Stefanis, Leonidas. 2012. "α-Synuclein in Parkinson's Disease." Cold Spring Harbor Perspectives in Medicine 2 (2). https://doi.org/10.1101/cshperspect.a009399.

Steinkamp, Joy. 2018. "Analysis of Gene Expression in Substantia Nigra and Astrocytes of a Parkin-Deficient Mouse Mutant (PaDel) by Semiquantitative Real-Time PCR."

Stichel, Christine C., Xin Ran Zhu, Verian Bader, Bettina Linnartz, Saskia Schmidt, and Hermann Lübbert. 2007. "Mono- and Double-Mutant Mouse Models of Parkinson's Disease Display Severe Mitochondrial Damage." Human Molecular Genetics 16 (20): 2377–93. https://doi.org/10.1093/hmg/ddm083.

Subramaniam, Sudhakar Raja, Laurent Vergnes, Nicholas R. Franich, Karen Reue, and Marie Francoise Chesselet. 2014. "Region Specific Mitochondrial Impairment in Mice with Widespread Overexpression of Alpha-Synuclein." Neurobiology of Disease 70: 204–13. https://doi.org/10.1016/j.nbd.2014.06.017.

Sulzer, D. 2011. "Postnatal Ventral Midbrain Dopamine Neuronal Culture Protocols Sulzer Lab Postnatal Ventral Midbrain Dopamine Neuronal Culture Protocols."

Sveinbjornsdottir, Sigurlaug. 2016. "The Clinical Symptoms of Parkinson's Disease." Journal of Neurochemistry. Blackwell Publishing Ltd. https://doi.org/10.1111/jnc.13691.

Svingen, Terje, Heidi Letting, Niels Hadrup, Ulla Hass, and Anne Marie Vinggaard. 2015. "Selection of Reference Genes for Quantitative RT-PCR (RT-QPCR) Analysis of Rat Tissues under Physiological and Toxicological Conditions." PeerJ 2015 (3). https://doi.org/10.7717/peerj.855.

Swatschek, Maren. 2016. "Analysis of the Nucleolar Integrity in the Parkinson Mousemodel."

Szargel, Raymonde, Vered Shani, Fatimah Abd Elghani, Lucy N. Mekies, Esti Liani, Ruth Rott, and Simone Engelender. 2016. “The PINK1, Synphilin-1 and SIAH-1 Complex Constitutes a Novel Mitophagy Pathway.” Human Molecular Genetics 25 (16): 3476–90. https://doi.org/10.1093/hmg/ddw189.

Tachikui, Hiroshi, Apala Farhat, and Masayuki Ozawa4. 1997. “Identification of the Ca"-Binding Domains in Reticulocalbin , an E Ndoplasmic Reticulum Resident Cat+-Binding Protein with Multiple EF-Hand Motifs1.” J. Biochem. Vol. 121.

Tagaya, Mitsuo, and Kohei Arasaki. 2017. “Regulation of Mitochondrial Dynamics and Autophagy by the Mitochondria-Associated Membrane.” In Advances in Experimental Medicine and Biology, 997:33–47. Springer New York LLC. https://doi.org/10.1007/978-981-10-4567-7_3.

Takeshima, Takao, Jane M Johnston, and John W Commissiong. 1994. “Mesencephalic Type 1 Astrocytes Rescue Dopaminergic Neurons from Death Induced by Serum Deprivation.” The Journal of Neuroscience.

Thellin, O, W Zorzi, B Lakaye, B de Borman, B Coumans, G Hennen, T Grisar, A Igout, and E Heinen. 1999. “Housekeeping Genes as Internal Standards: Use and Limits.” Journal of Biotechnology. Vol. 75. www.elsevier.com/locate/jbiotec.

Tohru Kitada, Shuichi Asakawa, Nobutaka Hattori, Hiroto Matsumine, Yasuhiro Yamamura, Shinsei Minoshima, Masayuki Yokochi, Yoshikuni Mizuno, and Nobuyoshi Shimizu. 1998. “A Hippocampal GluR5 Kainate Receptor Regulating Inhibitory Synaptic Transmission.” Nature 392: 605–8.

Trapnell, Cole, David G. Hendrickson, Martin Sauvageau, Loyal Goff, John L. Rinn, and Lior Pachter. 2013. “Differential Analysis of Gene Regulation at Transcript Resolution with RNA-Seq.” Nature Biotechnology 31 (1): 46–53. https://doi.org/10.1038/nbt.2450.

Tsunemi, Taiji, Yuta Ishiguro, Asako Yoroisaka, Clarissa Valdez, Kengo Miyamoto, Keiichi Ishikawa, Shinji Saiki, Wado Akamatsu, Nobutaka Hattori, and Dimitri Krainc. 2020. “Astrocytes Protect Human Dopaminergic Neurons from α-Synuclein Accumulation and Propagation.” Journal of Neuroscience 40 (45): 8618–28. https://doi.org/10.1523/JNEUROSCI.0954-20.2020.

UEDA, SEI, KENGO HASHIMOTO, SATORU MIYABE, SHOGO HASEGAWA, MITSUO GOTO, DAI SHIMIZU, ICHIRO OH-IWA, KAZUO SHIMOZATO, TORU NAGAO, and SHUJI NOMOTO. 2020. “Salivary NUS1 and RCN1 Levels as Biomarkers for Oral Squamous Cell Carcinoma Diagnosis.” In Vivo 34 (5): 2353–61. https://doi.org/10.21873/invivo.12048.

Valente, Eriza Maria, Patrick M. Abou-Sleiman, Viviana Caputo, Miratul M.K. Muqit, Kirsten Harvey, Suzana Gispert, Zeeshan Ali, et al. 2004. “Hereditary Early-Onset Parkinson’s Disease Caused by Mutations in PINK1.” Science 304 (5674): 1158–60. https://doi.org/10.1126/science.1096284.

Vance, Jean E. 2014. “MAM (Mitochondria-Associated Membranes) in Mammalian Cells: Lipids and Beyond.” Biochimica et Biophysica Acta - Molecular and Cell Biology of Lipids. https://doi.org/10.1016/j.bbalip.2013.11.014.

Vandesompele, Jo, Katleen de Preter, ilip Pattyn, Bruce Poppe, Nadine van Roy, Anne de Paepe, and rank Speleman. 2002. “Accurate Normalization of Real-Time Quantitative RT-PCR Data by Geometric Averaging of Multiple Internal Control Genes.” Genome Biology 3. http://genomebiology.com/2002/3/7/research/0034.1Correspondence:.rankSpeleman.

Vergara, Daniele, Marzia M. Ferraro, Mariafrancesca Cascione, Loretta L. del Mercato, Stefano Leporatti, Anna Ferretta, Paola Tanzarella, et al. 2015. “Cytoskeletal Alterations and Biomechanical Properties of Parkin-Mutant Human Primary Fibroblasts.” Cell Biochemistry and Biophysics 71 (3): 1395–1404. https://doi.org/10.1007/s12013-014-0362-1.

Victor E. Velculescu, Stephen L. Madden, Lin Zhang, Alex E. Lash, Jian Yu, Carlo Rago, Anita Lal, et al. 1999. “Analysis of Human Transcriptomes.” Nature Genetics 23: 387–88.

Vives-Bauza, Cristofol, Chun Zhou, Yong Huang, Mei Cui, Rosa L.A. de Vries, Jiho Kim, Jessica May, et al. 2010. “PINK1-Dependent Recruitment of Parkin to Mitochondria in Mitophagy.” Proceedings of the National Academy of Sciences of the United States of America 107 (1): 378–83. https://doi.org/10.1073/pnas.0911187107.

Vyas I, Heikkila RE, Nicklas WJ. Studies on the neurotoxicity of 1-methyl-4-phenyl-1,2,3,6-tetrahydropyridine: inhibition of NAD-linked substrate oxidation by its metabolite, 1-methyl-4-phenylpyridinium. J Neurochem. 1986 May;46(5):1501-7. doi: 10.1111/j.1471-4159.1986.tb01768.x. PMID: 3485701.

Wiemerslage, Lyle, and Daewoo Lee. 2016. “Quantification of Mitochondrial Morphology in Neurites of Dopaminergic Neurons Using Multiple Parameters.” Journal of Neuroscience Methods 262 (March): 56–65. https://doi.org/10.1016/j.jneumeth.2016.01.008.

Wittenberg, Olga. 2018. “Pathophysiology of Mitochondria and Gene Expression in Substantia Nigra in Parkinson Animal Model.”

Wolf, Dane M, Mayuko Segawa, Arun Kumar Kondadi, Ruchika Anand, Sean T Bailey, Andreas S Reichert, Alexander M Bliek, David B Shackelford, Marc Liesa, and Orian S Shirihai. 2019. “Individual Cristae within the Same Mitochondrion Display Different Membrane Potentials and Are Functionally Independent.” The EMBO Journal 38 (22). https://doi.org/10.15252/embj.2018101056.

Xu, S., Y. Xu, L. Chen, Q. Fang, S. Song, J. Chen, and J. Teng. 2017. “RCN1 Suppresses ER Stress-Induced Apoptosis via Calcium Homeostasis and PERK-CHOP Signaling.” Oncogenesis 6 (3). https://doi.org/10.1038/oncsis.2017.6.

Yang, Jin Yi, and Wei Yuan Yang. 2013. “Bit-by-Bit Autophagic Removal of Parkin-Labelled Mitochondria.” Nature Communications 4 (September). https://doi.org/10.1038/ncomms3428.

Yang, Ming, Chenrui Li, Shikun Yang, Ying Xiao, Xiaofen Xiong, Wei Chen, Hao Zhao, Qin Zhang, Yachun Han, and Lin Sun. 2020. “Mitochondria-Associated ER Membranes – The Origin Site of Autophagy.” Frontiers in Cell and Developmental Biology. Frontiers Media S.A. https://doi.org/10.3389/fcell.2020.00595.

Yoshimori, Tamotsu. 2004. “Autophagy: A Regulated Bulk Degradation Process inside Cells.” In Biochemical and Biophysical Research Communications, 313:453–58. Academic Press Inc. https://doi.org/10.1016/j.bbrc.2003.07.023.

Yoshinobu Ichimura, Takayoshi Kirisako, oshifumi Takaoß, Yoshinori Satomiß, Yasutsugu Shimonishiß, Naotada Ishihara, Noboru Mizushima, et al. 2000. “A Ubiquitin-like System Mediatesprotein Lipidation.” Nature 408: 488–92.

Youle, Richard J., and Alexander M. van der Bliek. 2012. “Mitochondrial Fission, Fusion, and Stress.” Science. American Association for the Advancement of Science. https://doi.org/10.1126/science.1219855.

Youle, Richard J., and Derek P. Narendra. 2011. “Mechanisms of Mitophagy.” Nature Reviews Molecular Cell Biology 12 (1): 9–14. https://doi.org/10.1038/nrm3028.

Zarranz, Juan J, Javier Alegre, Juan C Gómez-Esteban, Elena Lezcano, Raquel Ros, Israel Ampuero, Lídice Vidal, et al. 2004. “The New Mutation, E46K, of-Synuclein Causes Parkinson and Lewy Body Dementia.” Ann Neurol. Vol. 55. www.ncbi.nlm.nih.gov.

Zhu, Xin Ran, Lyutha Maskri, Christina Herold, Verian Bader, Christine C. Stichel, Onur Güntürkün, and Hermann Lübbert. 2007. “Non-Motor Behavioural Impairments in Parkin-Deficient Mice.” European Journal of Neuroscience 26 (7): 1902–11. https://doi.org/10.1111/j.1460-9568.2007.05812.x.

6. Attachment

Table 17: Complete list of differentially expressed genes in the substantia nigra of Padel and Basyn mice. *(n=4) Transcriptome analysis with the Hisat2 aligning algorithm and the Cuffdiff expression analysis software. Displayed are gene name, log2 fold change (Padel/WT), and significance value.*

Padel *substantia nigra*			Basyn *substantia nigra*		
Gene	Foldchange Padel/WT	q value	Gene	Foldchange Basyn/WT	q value
1110037F02Rik	-0.563196	0.0028375	1110037F02Rik	-0.480127	0.00527664
1700086L19Rik	-0.96042	0.00741225	1190002N15Rik	-0.40561	0.0138134
2010300C02Rik	-1.07423	0.0028375	2810002D19Rik	-1.02005	0.00527664
2810002D19Rik	-1.06254	0.0028375	Ablim3	-0.388584	0.0281128
4933412E12Rik	-1.18836	0.041117	Adcy1	-0.767835	0.00527664
6330403A02Rik	-1.15958	0.0028375	Als2, Mpp4	-0.450635	0.00527664
9030025P20Rik	-2.01785	0.0499299	Aqp6	-0.955116	0.00527664
Actn1	-0.467227	0.0294238	Arhgef33	-1.39156	0.00527664
Actn2	-0.902826	0.0422326	Asgr1	-0.87371	0.0178494
Adamts10	-0.743288	0.0028375	Atp1a1	-0.425771	0.00527664
Adamts18	-1.206	0.0165561	Atp2a3	-1.13977	0.00527664
Adcy1	-1.00923	0.0028375	Avil	-0.814539	0.0342426
Afap1l2	-0.510787	0.0216542	B3gnt5	-1.38168	0.00527664
Agap2	-0.834114	0.0028375	Barhl2	-1.19887	0.00527664
Ak4	-0.419783	0.0364938	Bcl2l15	-1.43525	0.00527664
Akap5	-0.764013	0.0028375	Bcl6	-0.393349	0.0366954
Aloxe3	-0.694594	0.043417	Bhlhe22	-0.464822	0.0342426
Als2,Mpp4	-0.469106	0.0131674	Bsn	-0.366838	0.00527664
Ankrd33b	-0.941906	0.0028375	Btg1	-0.481443	0.00527664
Ankrd63	-3.8757	0.0028375	Btg2	-0.511316	0.0281128
Ano2	-2.52873	0.0028375	Cacna1a	-0.42552	0.00527664
Aqp6	-0.852303	0.0248505	Cacna1g	-0.524961	0.00527664
Arhgap33	-0.683533	0.0028375	Cadps2	-0.375807	0.0342426
Arhgef33	-1.11825	0.0028375	Calb1	-1.04675	0.00527664
Arntl	-0.44523	0.0499299	Camk4	-0.828473	0.00527664
Arpp21	-0.941612	0.0028375	Car8	-1.41218	0.00527664
Arx	-2.81305	0.0028375	Cartpt	0.810499	0.00527664
Asgr1	-0.775189	0.019956	Cbln1	-0.865319	0.00527664
Atp1a1	-0.476392	0.0028375	Cbln3	-1.80236	0.00527664
Atp2a3	-1.03147	0.0028375	Ccl28	1.18518	0.00527664
Auts2	-0.452103	0.0165561	Cd52	0.921388	0.00527664

Padel *substantia nigra*			Basyn *substantia nigra*		
Gene	Foldchange Padel/WT	q value	Gene	Foldchange Basyn/WT	q value
B3gnt5	-1.14196	0.0028375	Cd74, Mir5107	0.548371	0.0138134
Baiap2	-0.876128	0.0028375	Cdc42bpg	-0.515271	0.0178494
Barhl1	-0.695327	0.00940324	Cdh15	-1.20508	0.00527664
Barhl2	-1.16937	0.0028375	Cep76	-0.910278	0.00527664
Bcl11b	-0.707873	0.0028375	Chd7	-0.599891	0.00527664
Bcl2l15	-1.38562	0.0028375	Chn2	-0.823727	0.00527664
Bcl6	-0.425738	0.0499299	Clec7a	0.887208	0.0449651
Bhlhe22	-109989	0.0028375	Cmya5	-0.955095	0.00527664
Bmp1	-0.583136	0.0028375	Cnksr2	-0.437716	0.00963867
Bmp3	-0.967676	0.026278	Cnksr3	-0.495564	0.0449651
Boc	-0.52987	0.0131674	Cnr1	-0.530519	0.00527664
Bsn	-0.483909	0.0028375	Col18a1	-0.685475	0.00527664
Btg1	-0.577779	0.0028375	Coro2b	-0.343027	0.0138134
C1qtnf4	-0.397544	0.043417	Crtam	-1.49698	0.00527664
Cacna1e	-0.430645	0.0149114	Ctsc	0.731799	0.00527664
Cacnb3	-0.539861	0.0028375	Cyp2e1	1.19801	0.0250717
Cadps2	-0.522193	0.00526377	Dact1	-0.582738	0.0281128
Calb1	-1.02183	0.0028375	Ddx3y	-1.69088	0.00527664
Camk2a	-1.42651	0.0028375	Dgkg	-0.383041	0.00963867
Camk4	-0.915344	0.0028375	Dgkz	-0.508417	0.00527664
Camkv	-0.957892	0.0028375	Diras2	-0.476467	0.00527664
Car12	-1.4805	0.0028375	Dner	-0.365149	0.00527664
Car4	-0.483148	0.030872	Dpysl4	-0.402439	0.0342426
Car8	-1.25778	0.0028375	Dusp1	-0.455073	0.0138134
Car9	-1.48899	0.0322844	Dusp5	-1.54122	0.00527664
Cartpt	-1.10316	0.0028375	Ebf1	-0.403994	0.0397595
Cbfa2t3	-0.619463	0.0028375	Eif2s3y	-1.40947	0.00527664
Cbln1	-0.740462	0.0028375	Eln	-0.592096	0.0212618
Cbln3	-1.74206	0.0028375	En2	-0.60631	0.00527664
Cbx6, Npcd, Nptxr	-0.522523	0.00741225	Eomes	-1.93846	0.00527664
Ccdc63	-1.38656	0.019956	Epb4.1	-0.475982	0.00527664
Cck	-1.26914	0.0028375	Epha8	-0.46311	0.0310925
Ccl28	1.17601	0.0248505	Exph5	-1.42461	0.00527664
Ccnjl	-0.764312	0.048861	Fam107b	-0.596216	0.00527664
Ccsap	-0.895171	0.0028375	Fam171b	-0.40773	0.00527664
Cd83	0.403918	0.0350918	Fat1	-0.424358	0.00527664
Cdc42bpg	-0.575247	0.0149114	Fat2	-2.00109	0.00527664

Padel *substantia nigra*			Basyn *substantia nigra*		
Gene	Foldchange Padel/WT	q value	Gene	Foldchange Basyn/WT	q value
Cdh1	-0.705427	0.00940324	Gabra2	-0.496457	0.00527664
Cdh15	-112201	0.0028375	Gabra6	-1.6198	0.00527664
Cdh9	-0.64878	0.0233694	Gabrd	-1.02661	0.00527664
Cdk17	-0.409787	0.043417	Garnl3	-0.39137	0.00963867
Cdkl4	-0.715441	0.0183126	Gas7	-0.436831	0.00527664
Cdon	-0.512674	0.0364938	Gdf10	-1.19103	0.00527664
Cecr6	-0.815386	0.0028375	Gm14296, Gm6182	1.18699	0.00527664
Celf2	-0.470518	0.00940324	Gm15446	-inf	0.00527664
Celf3	-0.627852	0.0028375	Gm2694	-0.99753	0.00527664
Celf5	-0.67942	0.0028375	Gm5083	-1.38975	0.00527664
Cemip	-0.630939	0.0131674	Gm7120	0.866853	0.00527664
Cep76	-0.821229	0.0028375	Gm996	-0.340017	0.0366954
Chd7	-0.580492	0.0028375	Gng13	-0.682231	0.00527664
Chn2	-0.752831	0.0028375	Gpr63	-1.07129	0.00527664
Chodl	0.738188	0.00741225	Gprc5c	-0.954895	0.00527664
Chrd	-0.573351	0.0322844	Grid2	-0.726801	0.00527664
Chrm1	-182903	0.0028375	Grid2ip	-1.0439	0.00527664
Chrna2	108756	0.0380495	Grin2c	-0.408926	0.00527664
Cmya5	-0.965124	0.0028375	Grm1	-0.423409	0.00527664
Cnih3	-0.893318	0.0028375	Grm4	-0.64549	0.00527664
Cnksr2	-0.897269	0.0028375	H2-Aa	0.650392	0.0310925
Cnpy1	-146215	0.00741224	Hba-a1, Hba-a2	-0.634575	0.00527664
Cnr1	-0.770726	0.0028375	Hes3	-1.51783	0.00527664
Col18a1	-0.595139	0.00526377	Homer3	-1.00164	0.00527664
Col23a1	-0.726035	0.0028375	Hr	-0.347233	0.0397595
Col27a1	-0.837428	0.0028375	Hspa1a	-0.76753	0.00527664
Col5a1	-0.612777	0.0499299	Hspa1b	-1.16148	0.00527664
Col6a1	-0.561594	0.027867	Icmt	-0.692069	0.00527664
Col6a2	-0.560952	0.0322844	Ier2	-0.718244	0.00527664
Coro2b	-0.39751	0.0216542	Il16	-1.63435	0.00527664
Cort	-289114	0.026278	Il20rb	-1.22897	0.00963867
Cplx3	-151573	0.00526377	Iltifb	-1.49158	0.0178494
Cpne2	-0.635861	0.0028375	Inpp5a	-0.5089	0.0281128
Cpne6	-0.521993	0.0028375	Itpka	-0.578413	0.00527664
Cpne7	-118757	0.0028375	Itpr1	-1.16152	0.00527664
Crb1	-292041	0.0028375	Jchain	1.95266	0.00527664
Crtam	-140724	0.0028375	Kank2	-0.650315	0.00527664
Crtc1	-0.386446	0.0476597	Kcng4	-0.330218	0.0366954

Padel *substantia nigra*			Basyn *substantia nigra*		
Gene	Foldchange Padel/WT	q value	Gene	Foldchange Basyn/WT	q value
Crym	-2982	0.0028375	Kcnmb4	-0.830106	0.00527664
Ctgf	-0.521049	0.027867	Kdm5d	-1.40552	0.00527664
Ctxn1	-0.971151	0.0028375	Kit	-0.815897	0.00527664
Cyp4f15	-0.785416	0.0183126	Kitl	-0.608229	0.00527664
D430019H16Rik	-0.44289	0.0335805	Lamb1	-0.585555	0.0212618
Dact1	-0.65766	0.0149114	Lhx1	-0.574245	0.00963867
Dbh	0.76231	0.0028375	Lin7a	-0.448917	0.00527664
Dbpht2	-0.744716	0.0165561	Lingo3	-0.455744	0.0138134
Dcn	-0.67902	0.0028375	Lnx2	-0.6215	0.0178494
Ddn	-231959	0.0028375	Ltbp2	-1.46297	0.00527664
Ddx3y	-22083	0.0028375	Megf11	-0.444366	0.00527664
Dgkg	-0.69949	0.0028375	Mical2	-0.36043	0.0366954
Dgkz	-0.749463	0.0028375	Mir22, Mir22hg	1.82205	0.00527664
Dio3	-48507	0.00526377	Mpp3	-0.420366	0.0212618
Diras2	-0.483765	0.01135	Mrgprf	-0.850777	0.0310925
Dlgap1	-0.620703	0.0028375	Mtcl1	-0.536539	0.00527664
Dlx6os1	-316503	0.0028375	Mybpc1	-1.72742	0.00527664
Doc2b	-0.420487	0.030872	Mybpc3	-1.62169	0.00527664
Doc2g	-0.833925	0.030872	Nek2	-1.03962	0.00963867
Dock4	-0.393357	0.027867	Neurod1	-1.76098	0.00527664
Dot1l	-0.475667	0.0294238	Neurod2	-0.927597	0.00527664
Dpysl4	-0.552131	0.0028375	Nptx1	-0.528081	0.00527664
Dusp14	-0.642524	0.0233694	Nr4a1	-0.497592	0.00963867
Dusp5	-143786	0.0028375	Nr4a3	-0.540255	0.0212618
Dyrk2	-0.647465	0.0131674	Nrep	-0.669557	0.00527664
E130012A19Rik	-0.609668	0.01135	Nrk	-1.34494	0.00527664
Efnb2	-0.72315	0.0028375	Nrxn1	-0.424806	0.00527664
Egr3	-172602	0.0028375	P4ha3	0.484358	0.0310925
Egr4	-137063	0.0028375	Pcp2	-1.48973	0.00527664
Eif2s3x	0.445295	0.01135	Pde5a	-1.01728	0.00527664
Eif2s3y	-200989	0.0028375	Peak1	-0.370969	0.0449651
Emx1	-192932	0.00741225	Phf21b	-0.703391	0.0212618
En2	-0.498054	0.027867	Phyhip	-0.342583	0.0250717
Enc1	-0.631326	0.0028375	Pkp3	-1.42298	0.00527664
Eomes	-20203	0.0028375	Plcb4	-0.321614	0.0366954
Epb4.1	-0.442874	0.0395905	Plch2	-0.485913	0.00527664
Erdr1	-290771	0.0028375	Plekhd1	-0.410369	0.00963867
Exph5	-148067	0.0028375	Ppp1r17	-1.38455	0.00527664
Fam107a	-0.441853	0.00940324	Prkcg	-1.19041	0.00527664

Padel *substantia nigra*			Basyn *substantia nigra*		
Gene	Foldchange Padel/WT	q value	Gene	Foldchange Basyn/WT	q value
Fam107b	-0.50733	0.0165561	Prmt8	-0.381776	0.0429446
Fam131a	-0.857165	0.00526377	Ptpn22	-1.09446	0.0397595
Fam171b	-0.613741	0.0028375	Ptprr	-0.626698	0.00527664
Fam212b	-0.648902	0.0028375	Pvalb	-0.380926	0.00527664
Fam81a	-0.887326	0.0028375	Pyy	inf	0.00527664
Fat2	-192659	0.0028375	Rala	0.543696	0.00527664
Fbxl16	-0.54193	0.0028375	Rcn1	-0.418717	0.0281128
Fezf2	-342012	0.0028375	Reln	-0.854501	0.00527664
Fibcd1	-0.52492	0.019956	Rgs8	-0.751241	0.00527664
Figf	-207811	0.026278	Rnf19b	-0.348196	0.0138134
Fmod	-0.523917	0.00940324	Rora	-0.383124	0.00527664
Fosl2	-0.689988	0.0028375	Ryr1	-1.24482	0.00527664
Foxg1	-256816	0.0028375	Sbk1	-0.660829	0.00527664
Gabra2	-0.720204	0.0028375	Sel1l3	-0.478014	0.00963867
Gabra4	-0.59349	0.0028375	Serinc2	-0.945442	0.0366954
Gabra6	-165159	0.0028375	Sestd1	-0.397086	0.0212618
Gabrd	-135086	0.0028375	Shf	-0.545541	0.00527664
Gabrq	0.483851	0.0461206	Shisa6	-0.76562	0.00527664
Gal3st3	-0.599664	0.0028375	Skor2	-1.04809	0.0138134
Gas7	-0.798679	0.0028375	Sla	-0.608662	0.0429446
Gda	-1.99496	0.0028375	Slc17a7	-0.436955	0.00527664
Gdf10	-1.11855	0.0028375	Slc1a6	-0.668996	0.00527664
Gldc	-1.05052	0.0028375	Slc5a1	-1.84992	0.00527664
Gm11549	-2.74185	0.0028375	Slc8a2	-0.359482	0.0366954
Gm2694	-0.979137	0.00526377	Soga1	-0.549855	0.00527664
Gm5083	-1.13045	0.030872	Sorl1	-0.313263	0.0449651
Gm7120	0.926674	0.0028375	Sphkap	-0.480722	0.00527664
Gm996	-0.475011	0.01135	Sptbn2	-0.368506	0.00963867
Gng13	-0.57261	0.00940324	Stk17b	-0.846943	0.00527664
Gng7	-0.424723	0.0422326	Strip2	-0.49089	0.00527664
Gpc4	-0.78023	0.00526377	Svep1	-1.24153	0.00527664
Gpr63	-1.04828	0.0028375	Sycp1	-2.00438	0.00527664
Gpr88	-0.797116	0.00526377	Syne1	-0.432197	0.0178494
Gprc5c	-0.854871	0.0028375	Tbata	-1.3627	0.0449651
Gprin1	-0.571266	0.0028375	Tcp11l1	0.526602	0.00527664
Gpx3	0.439566	0.0248505	Tfap2b	-0.667499	0.00527664
Grasp	-0.632265	0.019956	Tiam1	-0.622133	0.00527664
Grhl1	-0.901192	0.0028375	Tmem132a	-0.420353	0.00527664
Gria2	-0.494593	0.00741225	Tmem178	-0.494214	0.00527664
Grid2	-0.573578	0.0028375	Tmem181b-ps	-0.671484	0.00527664

Padel *substantia nigra*			Basyn *substantia nigra*		
Gene	Foldchange Padel/WT	q value	Gene	Foldchange Basyn/WT	q value
Grid2ip	-0.971346	0.0028375	Tmem200b	-0.794043	0.00963867
Grin2b	-0.536342	0.019956	Tob2	-0.363216	0.0449651
Grin2c	-0.59327	0.0028375	Trabd2b	-0.804361	0.00963867
Grm4	-0.501496	0.01135	Trim62	-0.60887	0.00527664
Hes3	-1.19475	0.0028375	Trim67	-0.529294	0.00527664
Hivep2	-0.456493	0.00940324	Trpc3	-0.629019	0.00527664
Homer3	-0.983826	0.00741225	Tspan11	-0.872892	0.00527664
Hpcal4	-1.23651	0.0028375	Tspan9	-0.376023	0.00963867
Hrk	-10.2495	0.0028375	Ttr	-1.34757	0.00527664
Hspa1b	-1.16049	0.0028375	Tuba8	-0.514131	0.0250717
Htr3a	-0.895592	0.00741225	Usp2	-0.423803	0.0212618
Icam5	-201481	0.0028375	Ust	-0.410457	0.0310925
Icmt	-0.565449	0.0028375	Uty	-1.77544	0.00527664
Igfbp6	-0.59668	0.0322844	Wdfy1	-0.683514	0.00527664
Il16	-1.72099	0.0028375	Wscd2	-0.668016	0.00527664
Il20rb	-1.90435	0.0028375	Zbtb18	-0.488686	0.00527664
Ipcef1	-0.83805	0.0028375	Zbtb46	-0.62472	0.0281128
Iqgap2	-0.987457	0.00526377	Zfp385b	-0.437953	0.0212618
Iqsec2	-0.562968	0.0028375	Zfp385c	-1.57662	0.00527664
Islr2	-1.11906	0.0028375	Zfp521	-0.345128	0.0310925
Itga4	-0.62572	0.0248505	Zfpm2	-0.378548	0.0449651
Itgbl1	-0.990114	0.0131674	Zic1	-1.12203	0.00527664
Itih3	0.385127	0.048861	Zic2	-0.891148	0.00527664
Itpka	-1.77662	0.0028375	Zic5	-0.955755	0.0281128
Padel *substantia nigra*					
Itpr1	-1.09522	0.0028375	Reln	-0.83938	0.0028375
Jchain	2.17537	0.00940324	Rfx3	-0.601282	0.0028375
Jph4	-0.394329	0.0216542	Rgl3	-0.66813	0.00741225
Junb	-0.579386	0.00741225	Rgs14	-1.90612	0.0028375
Kalrn	-1.05712	0.0028375	Rgs8	-0.638991	0.0028375
Kank2	-0.643377	0.0028375	Rims1	-0.477301	0.026278
Kcnf1	-1.01568	0.0028375	Rin1	-2.16558	0.0028375
Kcng1	-1.07774	0.0028375	Rln3	2.01117	0.0028375
Kcng2	-0.927438	0.0028375	Rnf165	-0.504328	0.0149114
Kcnh1	-0.417952	0.0422326	Ror1	-1.07835	0.0131674
Kcnip2	-1.24131	0.0028375	Rprml	-1.39275	0.0028375
Kcnj4	-2.37917	0.0028375	Rreb1	-0.60591	0.0028375
Kcnmb4	-1.03525	0.0028375	Rspo2	-1.1112	0.0028375

Padel *substantia nigra*					
Gene	Foldchange Padel/WT	q value	Gene	Foldchange Basyn/WT	q value
Kcnv1	-1.5362	0.0028375	Rspo3	-0.711462	0.0131674
Kdm5d	-2.09167	0.0028375	Rtn4r	-0.687657	0.0028375
Kit	-0.94814	0.0028375	Rtn4rl1	-0.999608	0.0028375
Kitl	-0.624901	0.0028375	Rtn4rl2	-2.29485	0.0028375
Klf16	-0.495768	0.0364938	Ryr1	-1.1508	0.0028375
Klhl3	-0.83323	0.0028375	Satb2	-1.05448	0.0149114
Krt12	-2.06774	0.00526377	Sbk1	-0.620735	0.0028375
Krt2	-1.71693	0.0028375	Sec14l1	-0.462582	0.00940324
Krt77	-1.08739	0.0248505	Sel1l3	-0.536349	0.00741225
Krt9	-1.19338	0.0233694	Serinc2	-0.99575	0.01135
Lamb1	-0.847814	0.0028375	Sertm1	-0.546947	0.0165561
Leng8	-0.501592	0.01135	Sfrp5	0.516092	0.0183126
Lhx2	-1.39093	0.0028375	Sgk1	0.507013	0.0028375
Lhx6	-2.73816	0.0028375	Shank2	-0.714524	0.0248505
Limd2	-0.459347	0.0395905	Shank3	-0.516456	0.0028375
Lin7a	-0.485034	0.00741225	Shf	-0.601853	0.00526377
Lmo4	-0.511352	0.00526377	Shisa6	-0.676629	0.0028375
Lmo7	-0.696199	0.0028375	Shisa7	-0.658841	0.0028375
Lnx2	-0.673025	0.01135	Sidt1	-0.64473	0.0028375
Lpl	-0.683862	0.0028375	Sipa1l1	-0.425944	0.0165561
Lppr4	-0.663212	0.0028375	Ski	-0.404643	0.0380495
Lrrc10b	-0.881974	0.0350918	Sla	-0.745178	0.00940324
Lrrc7	-0.527779	0.0165561	Slc10a4	0.495807	0.0165561
Ltbp2	-1.75514	0.0028375	Slc13a4	-0.48586	0.0248505
Marveld2	-0.920263	0.043417	Slc16a2	-0.562162	0.00940324
Mef2c	-1.20048	0.0028375	Slc17a7	-1.31108	0.0028375
Mfge8	-0.610127	0.0028375	Slc18a2	0.453706	0.0149114
Mgp	-0.516707	0.01135	Slc1a3	-0.49295	0.0028375
Miat	-0.62768	0.0028375	Slc1a6	-0.473835	0.030872
Mical2	-0.789013	0.0028375	Slc22a6	-0.538737	0.0149114
Mir124a-1, Mir124a-1hg, Mir3078	-1.21603	0.0028375	Slc24a4	-0.75036	0.0028375
Mir22, Mir22hg	1.81067	0.0028375	Slc26a4	-1.87227	0.00526377
Mmd	-0.490899	0.01135	Slc47a1	-0.670902	0.0422326
Moxd1	-1.50233	0.0028375	Slc5a1	-1.74819	0.0028375
Mpp3	-0.597832	0.0028375	Slc5a7	0.642528	0.0028375
Mpped1	-0.566663	0.0028375	Slc6a2	0.775031	0.0028375
Mpzl2	-0.699914	0.026278	Slc7a8	-0.503562	0.00940324

Padel *substantia nigra*					
Gene	Foldchange Padel/WT	q value	Gene	Foldchange Basyn/WT	q value
Mrap2	0.428232	0.0461206	Slc8a2	-0.828596	0.0028375
Mrgprf	-0.931288	0.0028375	Slc9a4	-2.56588	0.0028375
Msx2	-1.25756	0.0335805	Slit3	-0.649237	0.0028375
Mtcl1	-0.490712	0.00526377	Smad3	-0.553584	0.0028375
Mybpc1	-1.10566	0.0028375	Smoc2	-0.935941	0.0028375
Mybpc3	-1.73118	0.0028375	Snca	-0.475534	0.0165561
Myo5b	-0.746264	0.0028375	Sncg	0.419441	0.026278
Nab2	-0.686952	0.0028375	Snhg11	-0.600295	0.0028375
Ndst3	-0.547246	0.00741225	Sorbs2	-0.41438	0.0499299
Nek2	-0.987954	0.0322844	Sowaha	-1.1328	0.0028375
Nell2	-0.524734	0.0028375	Sphkap	-0.474566	0.0028375
Neurl1a	-0.443873	0.0216542	Sprn	-0.773607	0.0028375
Neurl1b	-1.36861	0.0028375	Sptbn2	-0.565573	0.0028375
Neurod1	-1.86153	0.0028375	Srp54b	0.724329	0.026278
Neurod2	-1.29373	0.0028375	Sstr1	-0.497481	0.0149114
Neurod6	-1.21941	0.0028375	Sstr4	-0.906674	0.00741225
Nfib	-0.482906	0.00940324	St6galnac5	-0.936823	0.0028375
Nfix	-0.405491	0.0335805	St8sia5	-0.417015	0.0461206
Nov	-1.86277	0.0028375	Stk17b	-0.830035	0.0028375
Npas2	-0.779411	0.0028375	Stx1a	-0.632106	0.0028375
Npr3	-0.735835	0.0028375	Stxbp2	-0.612757	0.0183126
Nptx1	-0.749825	0.0028375	Svep1	-0.921784	0.0028375
Npy	-0.934192	0.0028375	Sycp1	-1.72814	0.01135
Npy2r	-0.695673	0.00940324	Syne1	-0.813293	0.0028375
Nr2e1	-1.27591	0.0028375	Syngap1	-0.683164	0.0028375
Nr4a1	-0.610195	0.0028375	Synpo	-0.960129	0.0028375
Nr4a2	-0.580564	0.00526377	Tac2	-1.5056	0.00741225
Nr4a3	-1.10564	0.0028375	Tbata	-1.82119	0.0028375
Nrep	-0.538785	0.00526377	Tbr1	-2.0688	0.0028375
Nrgn	-1.418	0.0028375	Tcf4	-0.433128	0.0131674
Nrk	-1.22938	0.0028375	Tcf7l2	-0.644596	0.0028375
Nsmf	-0.49423	0.00940324	Tcp11l1	0.657326	0.0028375
Ntn5	-1.68594	0.0294238	Thbd	-0.44726	0.043417
Ntrk1	1.26365	0.00526377	Tiam1	-0.825265	0.0028375
Olfm1	-0.526173	0.0183126	Tmem132a	-0.642333	0.0028375
Otp	104673	0.0028375	Tmem178	-0.723591	0.0028375
Pak6	-0.432177	0.0448805	Tmem181b-ps	-0.583327	0.00526377
Park2	-0.952681	0.0028375	Tnfaip8l3	-0.988292	0.0028375
Pcdh1	-0.437951	0.0149114	Tph2	0.453137	0.048861
Pcdh20	-0.525369	0.00741225	Trabd2b	-1.17963	0.0028375

Padel *substantia nigra*					
Gene	Foldchange Padel/WT	q value	Gene	Foldchange Basyn/WT	q value
Pde1a	-0.782876	0.0028375	Trh	-0.886389	0.0028375
Pde2a	-0.608049	0.0028375	Trim62	-0.57232	0.0028375
Pde5a	-0.817225	0.0028375	Trpc4	-0.679044	0.00526377
Pdzrn3	-0.622799	0.0461206	Tspan11	-0.850536	0.0028375
Phf21b	-0.728721	0.0131674	Tspan9	-0.427742	0.0131674
Phyhip	-0.568826	0.0028375	Ucn	-0.990422	0.0448806
Pisd-ps3	0.496805	0.0028375	Unc13b	-0.527741	0.0294238
Pkp3	-1.18559	0.00741225	Unc5c	-0.430781	0.0350918
Plch2	-0.811219	0.0028375	Usp2	-0.447434	0.0422326
Plk2	-0.60704	0.0028375	Ust	-0.5042	0.0165561
Plxnd1	-0.723653	0.0028375	Uts2	1.68178	0.048861
Ppp1r17	-1.19061	0.0028375	Uty	-2.26358	0.0028375
Ppp1r1a	-0.490703	0.0216542	Vgll3	-0.899515	0.00741225
Prdm8	-1.10282	0.0028375	Vip	-1.00449	0.0028375
Prkcg	-1.6684	0.0028375	Vipr1	-1.84657	0.0028375
Prmt8	-0.6496	0.0028375	Vsx2	1.01433	0.0028375
Prrt1	-0.476709	0.0422326	Vwa3a	-0.907772	0.0149114
Psd	-0.568169	0.0028375	Wasf1	-0.57913	0.0028375
Psd3	-0.447715	0.0183126	Wfs1	-0.401087	0.041117
Ptgs2	-1.16983	0.0028375	Wipf3	-0.933119	0.0028375
Ptk2b	-1.61147	0.0028375	Wnt4	-0.717304	0.00526377
Ptpn14	-0.679849	0.0028375	Wscd2	-0.725266	0.0028375
Ptpn22	-1.40741	0.0028375	Xist	0.887543	0.0028375
Ptprr	-0.485069	0.019956	Zbtb18	-0.751697	0.0028375
Pxdn	-0.475381	0.0364938	Zfp365	-0.4282	0.0233694
Rab40b	-0.935208	0.0028375	Zfp831	-1.33966	0.0028375
Ranbp3l	-0.564964	0.0335805	Zfpm2	-0.441231	0.0335805
Rasal1	-0.868362	0.0028375	Zic1	-1.1421	0.0028375
Rasgef1a	-0.447043	0.019956	Zic2	-0.997744	0.0028375
Rasgrp1	-0.887247	0.0028375	Zic4	-0.722801	0.0131674
Rcn1	-0.456576	0.0335805	Zic5	-1.02523	0.0028375

Table 18: List of all used candidate gene primers for qPCR experiments. *Corresponding gene name, sequences, and product length are listed.*

Gene name	Forward primer	Reverse primer	product length
Sec14l1	CCAGTGCGGGTGTATAAACA	CGATGACATGAAGAGCCCCA	145 bp
Pisd-ps1	ATCCTCCACTACCTCCTGCC	ACTTTGTTGAGGCGACCACA	137 bp
1110037 F02Rik	CAGACATGGCGGTGGACTC	GGGGTATAACTCGGACTTCATTG	138 bp
Adcy1	CCTCGCACTTACTGGTCACA	CTCTGTCAAGATCCGCACGA	129 bp
Atp1a1	GAACGCCTACCTAGAGCTGG	GACCCACGAAGCAGAGGTTA	146 bp
Atp2a3	GGATGGTGTTCTCGGGACAT	GCCTGGATGCTCTCAGTCTG	154 bp
Bcl6	ACCCAGTCAGAGTATTCGGA	TGGTTTGTCACTGTGCGTCT	126 bp
Bsn	TCTCTGTCCGACCCTAAGCC	TTCACCTTGCGGACCAGG	137 bp
Btg1	CATCTCCAAGTTCCTCCGCA	TAACCTGATCCCTTGCACGG	138 bp
Cadps2	AAGAACGGTTCCAGGCCTTT	AGCATCCTCCACTTTGAACCA	138 bp
Calb1	GCGCACTCTCAAACTAGCC	CCTGGATCAAGTTCTGCAGC	154 bp
Camk4	CTGGTGGGATGAAGTGTCTT	ATGTGAACAAAGTTGGCCGC	138 bp
Car8	CCTTGCAGCGAAGGAGTTAC	GTCTCCCAAAATCCCATCGC	141 bp
Cartpt	ACGAGAAGAAGTACGGCCAA	CGTCCCTTCACAAGCACTTC	144 bp
Cbln1	GAACGCAGCACTTTCATCGC	GTCTTGGTCACCGGCGAAG	144 bp
Cbln3	CCCAGGACGAGTGGCGTTT	CAGCCCGAGGTCCGATCAAA	141 bp
Cep76	ACTTGAAATGTACCCACCGCT	ATACTCCCTCCACCACTGCT	136 bp
Chd7	CACCCGTCACCCCAGAATAC	GGCAGGTAATCGTCGCTCTT	143 bp
Chn2	AGGTGCCTACATCCTTCGAG	TCGAACCTCTTCTCACCCAC	132 bp
Cmya5	CTCTCCAGATCTCCGCGAAC	TCGATAGGCTGGACTGTCTGC	145 bp
Cnksr2	TGGAACCGGTGAGCAAATGG	GCTCCTGATGTGTAATGCGT	141 bp
Cnr1	TCTCCACTTCTTTTCCGCCT	TGCTACAAGGAAATTTGCCCC	128 bp
Coro2b	GGATCCCCATCACCAAGAATG	TGGGGTAGTTTGGCTCGATT	147 bp
Crym	TCGGTGCTTCTCTTTGATCCC	GCACATCACTGCCTGGGG	133 bp
Ctsc	TGCAGCACATCTTGGAGGTCTC	GCAGTCCAAGACTTCTGAACGG	105 bp
Dgkg	TGAGCGAAGAACAATGGGTC	ATGGGCTTGTGTGGGTCATA	148 bp
Dgkz	CGAATCAGGCTCCAGGAATG	ATGGCTACGATCTCCTTGCT	144 bp
Diras2	CTGGAGACCTGCGGCTCT	CTCTTGCCAACACCGCCT	133 bp
Dpysl4	TGGAAGACGGTCTGATTAAACA	ATCATCAGCTGGGGTCATGC	155 bp
Dusp5	ACAGACCAGCCTATGACCAG	GGGAAACATTCAGCAGGGC	129 bp
Eln	CCAGGCATTGTGGGTGGAC	ACACCATAGCCAGGAAAGCC	143 bp
Eomes	CCGGCACCAAACTGAGATGA	GCCAGAACCACTTCCACGAA	123 bp
Epb4.1	ACTGGCTCCAAATCAGACCAAGG	TCCATACATGGACAACTTTTTGGCA	130 bp
Ermard	AGTGCCCCTTTCTCCTAAGA	GCCATGCCACAAGACGTTTC	137 bp
Exph5	CCAGTTGCCAGTGTGTTTGT	GCCTGAAGACTGTTCCTGGG	150 bp
Fam107b	CCGAAATCACCAAGACCTCCA	TGAGCTTCTTCCTCCTTCTGC	141 bp
Fam171b	CCCGCAAAGCCAAGCAAATA	CGTTGCTGATGTGATGGTTGT	140 bp
Fat2	CCAGGTTCTTCCAGCTCAAC	CCCAGTGTTCCCCTCAGTAA	146 bp

Gene name	Forward primer	Reverse primer	product length
Gabra2	CAGAAAACATCCCGTGCCAA	AGGTTTCCCAAAGTGTGACATG	149 bp
Gabra6	CAAAGCCCTCAGTAGAACGC	TCCTGCAAAAGCTACTGGGA	130 bp
Gabrd	TGACATTGGGGACTACGTGG	TCAATGCTGGCCACCTCTAG	150 bp
Gas7	TAAGGACCAGCTGAGCACTC	GTTGACATAGTAACGGCGGC	131 bp
Gdf10	TGGTCGCTATCCACATGCTC	ACACAGGCTTTTGGTCGATC	123 bp
Gm7120	GGATGGCCTCAGAGTCACG	AGCACGGTGGTAAAGCATGA	147 bp
Gm996	CTGCTGGTACCGGGTGTATG	AAAGCTCACAGTCCATGCGA	138 bp
Gprc5c	GCCACGCCACCAAAAGACG	CTGGCCCTGCTCAGATGGAT	135 bp
Grid2	TCCCCTTGCTCTTGTTTCTGT	TGAGGTCACCAACTGCTGTG	144 bp
Grin2c	GAAGTGTGAGGTACCGGCAG	TTTCACTGGGGTCTCATGGC	136 bp
Grm4	CTCCGTCTCGATCATGGTGG	GGCCTGGTATGTGTCCGAG	142 bp
Homer3	CAGGCGAGGAAAAGCTGTTC	CTGAAGCGCGAAGAACTCTG	134 bp
Hspa1b	AAGTAATGTTGGGAGCAGCA	ACTGGGCAGCTAGACTATATGT	142 bp
Icam5	GACATCCGAGAGCCTGAGAC	GTGAAGTTCTCGCCCACTGG	152 bp
Icmt	AGTGGGGTGTATGCTTGGTG	CCTCCTCTTCTGTGCGATCTC	151 bp
Itpr	AAGAGTGTCCGGGAATTGGC	GCTGCCCGGAGATTTCATTG	148 bp
Jchain	TGCATGTGTACCCGAGTTACC	GGGGAGGTGGGATCAGAGAT	131 bp
Kank2	CCCCAGCTCTCCCAGGAAT	GTGAGGGCATTGGGGTTCTC	152 bp
Kit	GATCTGCTCTGCGTCCTGTT	ATCAATGCACGTCAGGCTGA	156 bp
Kitl	TGCATGGAAGAAAACGCACC	CAGTCACTAGTGTCAGATGCCA	149 bp
Lamb1	TTGGTGTCCTAGCCCTATGG	TCGAAGTCACGGAGAGCTTT	138 bp
Lin7a	GGAGAAGTACCAGTGCACAAG	CGGAATTCAGGGCAGCCAT	128 bp
Lnx2	TGAGCTGCCCATCTTTGTGA	GCCTCGCTGTGACTTAGGTT	129 bp
Lrrc17	TCCCCAAGTTCAGGAGCTCT	ATGGCCACTATGCGCATTCT	152 bp
Lrrc17	TCCCCAAGTTCAGGAGCTCT	ATGGCCACTATGCGCATTCT	152 bp
Ltbp2	GGCAGCACATGTGAACCATC	ACCCTTCTCACAGCTGTTGG	142 bp
Mical2	GGTCACAGGAACACGCTAGA	ACCACTGATCTCCTCCACCT	126 bp
Mpp3	CCCCTCTGCCCGATAACATC	CATGATCCTGGCCACCACAA	140 bp
Mpped1	CTCCCAAGCGAGGTGAAGAA	AGTCCTGCTTGATGAGGTCG	130 bp
Mrgprf	CTTCAGCAAGGCCGTGATTG	CAGACACACAGCGTTCGATG	155 bp
Mtcl1	GCAGATGATCGAGGTGGAGG	GCTGACACTTCAAATCCGCA	152 bp
Nab2	GACAAGTAGCCCGAGAGAGC	GAGGAGGCTGCTGGATTTCA	141 bp
Ndst3	CCCCACCTCTTCCACAATGA	TCCAGGCCTCATAAAGCTGAA	152 bp
Neurod1	GCTGCGAGATCCCCATAGAC	TGTACGCACAGTGGATTCGT	147 bp
Neurod2	ACAGCCCACCACGAATCTG	GGGTATGGGTACGGATGCAT	135 bp
Nptx1	TAATGACAAGGTGGCCAAGC	ATGGGCTTGTGTGGGTCATA	138 bp
Nr4a1	AACATCCTGGCCTTCTCACG	ATTCTGCAGCTCTTCCACCC	135 bp
Nr4a3	AGCCCAGTATAGCCCTTCAC	ATGATCCCCGTGCTACCGA	129 bp
Nrep	GAGAGTGAACAGGGAGCGG	CAAACGGTTCTTGGCTGACC	143 bp
Nrk	AGCTCACCTTCATGCACACC	TCCGTCCATTTGTTCTGCTCA	131 bp
Park2	TGAACAGGGCCAGAGGAAAG	GAAGTGGCTCCTGAGGGTTC	135 bp

Gene name	Forward primer	Reverse primer	product length
Park2	TGGACAAAAGAGCCGCTGAG	GGGGCTGAGGACACTTCATG	141 bp
Pde1a	AGCCATGGTCTTTGCAGCT	TAAGTCTGTAGGCTGCGCTG	149 bp
Pde5a	GATCCCCGGTTCAATGCAGA	TTCCTGATTTCTTGTTGATGGCC	130 bp
Phyhip	CTGGCTGGAGTGAGACTGTG	TGGTTGCGGTAGAACACAGA	129 bp
Plch2	GCAAGGTTGAGGAAGACGTG	CGCTGGCCACCTTCTTTATC	126 bp
Prdm8	GACATCCCAGAGAACGCCAT	ATTTGCCGCCGAAGTGTCTA	141 bp
Prkcg	CCTATCTCAGAGTCTGCGGA	AAAACAGGGGTCGGGGTC	151 bp
Ptprr	CAATGCACACAC TATGAGGAGAGCG	GCTTCCAACTCT TCTTTTGACGAATAGCC	131 bp
Rcn1	ACAACCAGAGCTTCCAGTACG	GGCCATCACCATCACTGTCA	138 bp
Reln	GAGGTGCTCATTTCCCTGCA	GACTGGATGCTTGTCGAGGT	140 bp
Rgl3	GCCCAGTTCAATACGGTGAC	AGGATCGCTCGCAATGAAGA	155 bp
Rgs6	GGTGTGCCCATCAGAACAGT	AGGCTTCCCAGGTGTATTGC	134 bp
rgs8	CGCAGGAACAAAGGCATGAG	CGTTGCTTCTTCCGTGGAGA	132 bp
Rtn4rl2	CCTGGCAACATTTTCCGAGGCT	GGAAGAGGTGGCTCAGGTTG	118 bp
Ryr1	GGTTGACGCCTCCTTTATGC	TGTCAGAAGGGGAGATGGTCA	143 bp
Sbk1	GGCAAAGGGACCTACGGGAA	GAAGGGGCTAGACGACAGGC	150 bp
Sel1l3	GCGGAGAAAACACAGGCATC	TGGCCTCGCAATAATGGAGT	138 bp
Sgk1	CAGTAAACCAAGCCGGTGC	GGGCTCTTGATCCATCTTCGT	150 bp
Shisa6	TAGCCCACTTGCCTCCATCA	GTACCACGGGCTGCAAGG	142 bp
Sla	ACATCTCACCAAGGCTCACC	GTGATGGGTGGGATGTTGGA	137 bp
Slc17a7	GCCTCACCTTGTCATGACCA	GAGTATCCGACCACCAGCAG	156 bp
Slc18a2	TCGAAGTCCACCTGCTAAGG	ACGTTAGAGGGGCTCAGTCA	149 bp
Slc1a6	GCCGAATTGAGACTGTCCCA	TTGTCCTTGTCACCACTCGT	132 bp
Slc1a6	GCCGAATTGAGACTGTCCCA	TTGTCCTTGTCACCACTCGT	132 bp
Slc5a1	CCCATTGCAGCTGTCTTCCT	GCAGCTCCCAGTTCCATAGG	138 bp
Slc8a2	CTCCTCTTTTCCTCCAGCGA	GGAACAGGGTAGTTGTGGGT	138 bp
Speg	TGCAGAATATGGTGGTGGCG	CCTTCAGCCCGGATGAGAA	140 bp
Sphkap	CACCACTGATGCATGAAGGT	TCCTCTGGTTCTGCAGCCA	147 bp
Sptbn2	AGATCCAGGGCCAGTACAGT	TTCTTCTGCACGGCTTCTCG	143 bp
Syne1	GCTGCCAAGATCCAGGGAAA	TGGATGACTGAATGAAAGGCCA	137 bp
Tbata	AGACCACAAAGCCCCAAACA	AGTGCTCCAGGTCCTCTCTT	147 bp
Tbr1	CCGAGTCCAGACGTTCACTT	GCCCGTGTAGATCGTGTCAT	146 bp
Tcf7l2	CGCACTTACCAGCTGACGTA	GCTGACCTTGCTGTGGTACT	147 bp
Tcp11l1	GCTCTGGCCCATGAAATTGT	TGGACACTCAAGCAATCCCA	128 bp
Tiam1	AAGAAGGTGGAGTCGGCTAC	ATGCTGTTCTCCACCCAGAC	149 bp
Tmem132a	CTCCTACCCACCCTTTGCC	TAGGGTTCTGCTGGAGTCAC	126 bp
Tmem178	CCACTGTTCGCCACCTACTC	GCGGATTGGCTGAGAAAAGTG	138 bp
Tmem 181b-ps	TCCCATGTACCAGTATCGGG	CGTAAGGCATATGACGGAGCT	140 bp
Trabd2b	TGTGCTGGACCTCTACCTGG	TGGTTCAGGGCAAACAACAC	132 bp
Trim62	TCAAGCTCTTCTGCCTCACG	CTGTCCTGAAGGGCCTGA	151 bp

Gene name	Forward primer	Reverse primer	product length
Tspan11	CGGTGGGTATTGGGGTAGC	GAGATGTGGTCCCTTGGGTG	138 bp
Tspan9	AGAACGGGCTGCTACGAAAA	CGGTGGATGTGCTGGAACA	137 bp
Usp2	AGAGGCTGTACATGCGGGA	TCTGGATCTGGGTCTTGAACT	144 bp
Ust	CTGCGGCAGTATTTGGGAA	TCAGAAGCAAGACCACGGTA	136 bp
Wscd2	CAAGGACACCAGCGAGAGAG	TCCAGGATGCAGCCGATGTA	135 bp
Zbtb18	GATGTCAATGTGCCCACGTG	CTCTCATCACAGGACGCCTC	147 bp
Zfpm2	CTGGACTCGATTCAGCTGCT	CAAATGGGCTTGCAGGTTCC	138 bp
Zic1	GATAAGTCCTACACGCACCCC	GGGTTGTCTGTTGTGGGAGA	149 bp
Zic2	GCCCTTCCCCTGTCCTTTC	TTCTTCCTGTCGCTGCTGTT	153 bp

Table 19: List of all used reference gene primers for qPCR experiments*. Corresponding gene name, sequences, and product length are listed.*

Reference genes	Forward primer	Reverse primer	product length
Aes	GGCGGAAATTGTGAAGAGGC	GGAGCTGTCGGATGATGGAG	146 bp
Acvrl1	CCTAGTGCTATGGGAGATCGC	TGGGTGTCTGCTGGTCAAC	143 bp
Eif4g2	GAGGAGGAAGTAGGGGTGCA	TTGCTGCGGAGTTGTCATCT	138 bp
Gapdh	GCATTGTGGAAGGGCTCATG	TGCAGGGATGATGTTCTGGG	122 bp
Hprt	AGTTCTTTGCTGACCTGCTG	CCACCAATAACTTTTATGTCCCC	139 bp
Mgrn1	GCGTGCTCTACAGTCTGGAA	TGGACGGTCTCAGATTGCAG	142 bp
Oxr1	ACACTGGCCAAAAGAAGACCT	TGGGTGTGGTATCAAATTTCAGG	138 bp
Ube2d2a	GCCACCGTTTCCCACCAT	GCCCCATTATTGTAGCCTGC	134 bp

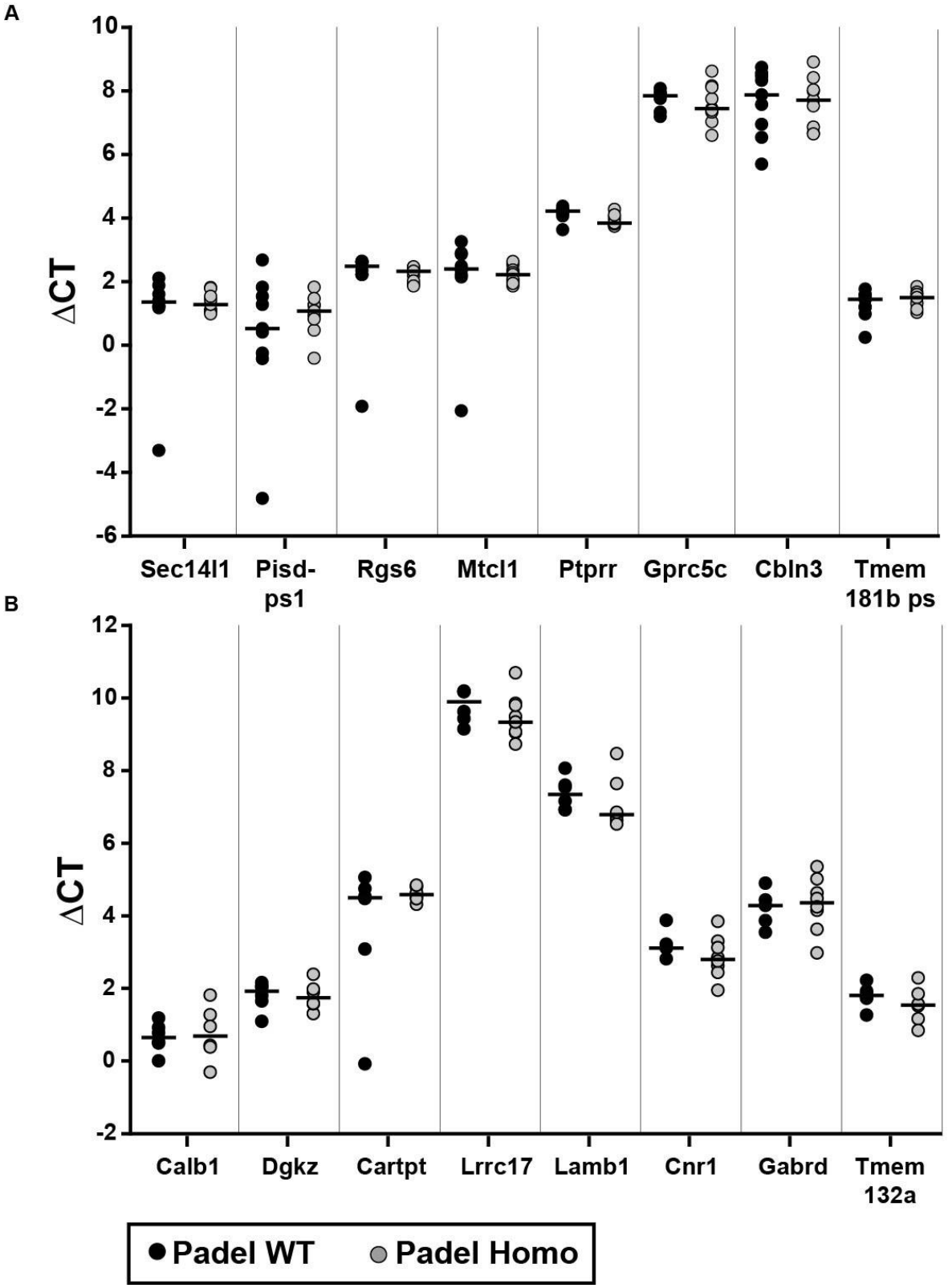

Figure 34: Statistically insignificant gene expression results of substantia nigra tissue *of one-year-old Padel mice with the reference gene Hprt (n=10). Color coding is explained in the legend below. Black bars represent the median of the corresponding groups.*

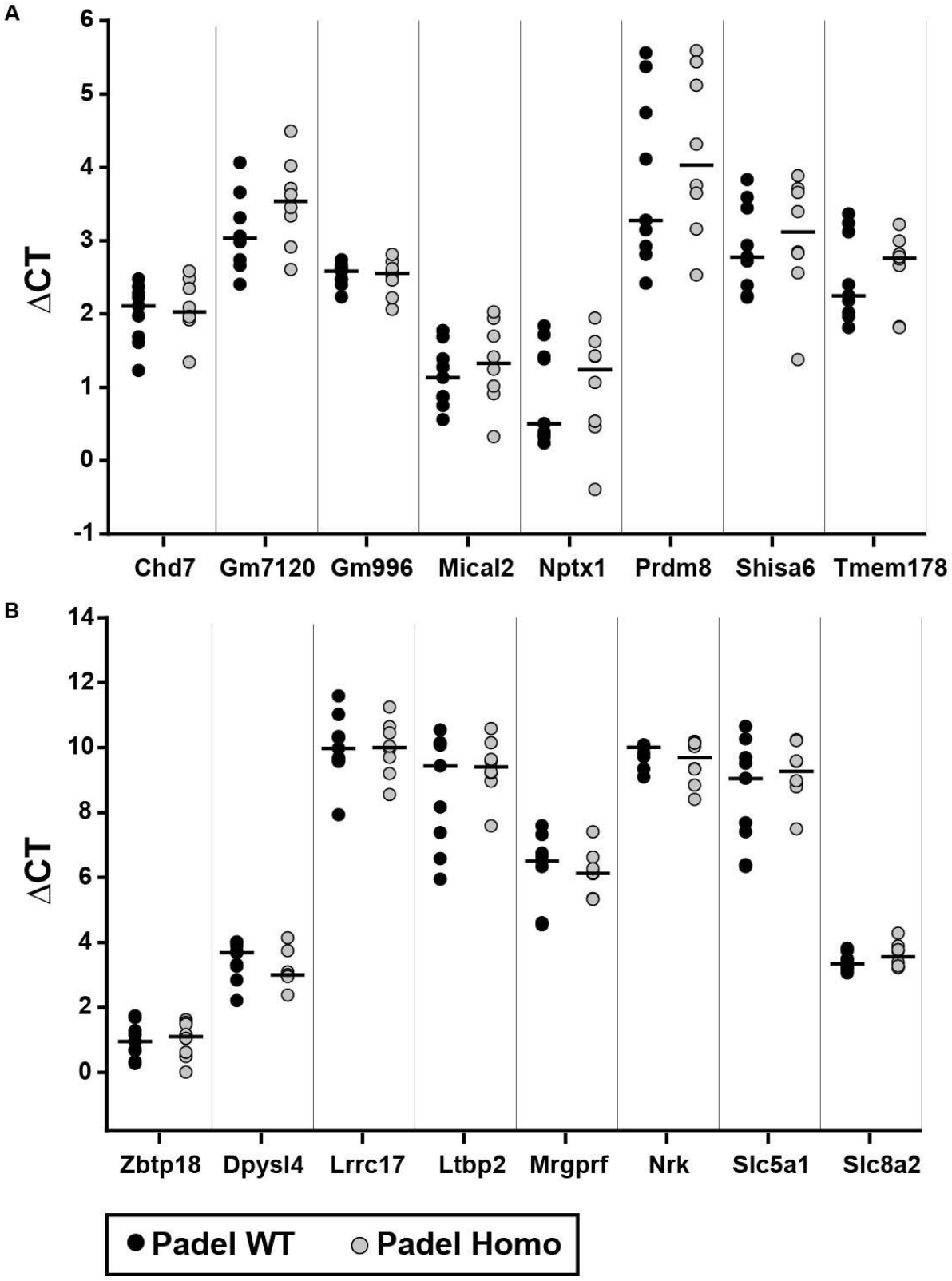

Figure 35: Statistically insignificant gene expression results of substantia nigra tissue *of one-year-old Padel mice with the reference gene Hprt (n=10). Color coding is explained in the legend below. Black bars represent the median of the corresponding groups.*

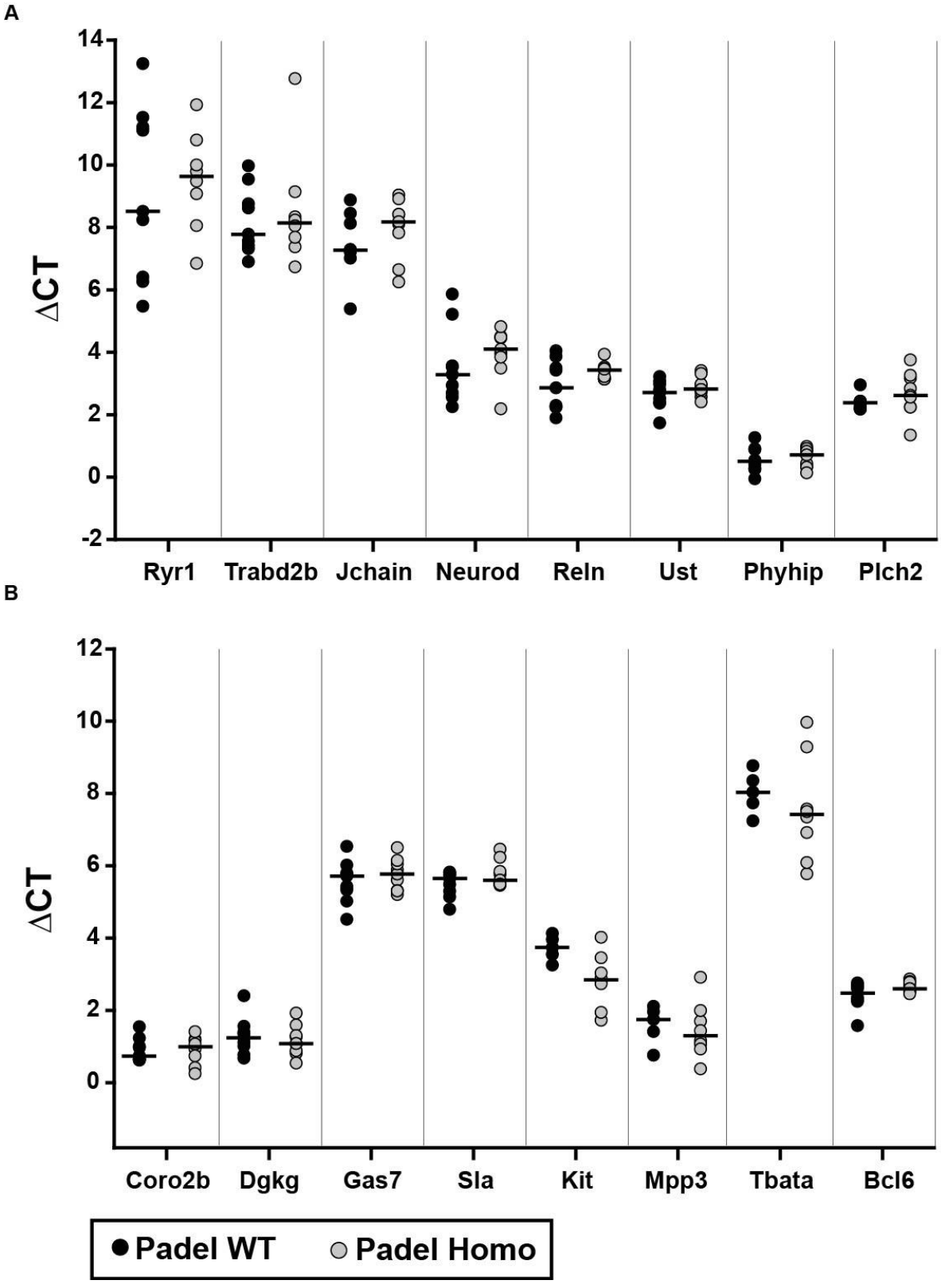

Figure 36: Statistically insignificant gene expression results of substantia nigra tissue *of one-year-old Padel mice with the reference gene Hprt (n=10). Color coding is explained in the legend below. Black bars represent the median of the corresponding groups.*

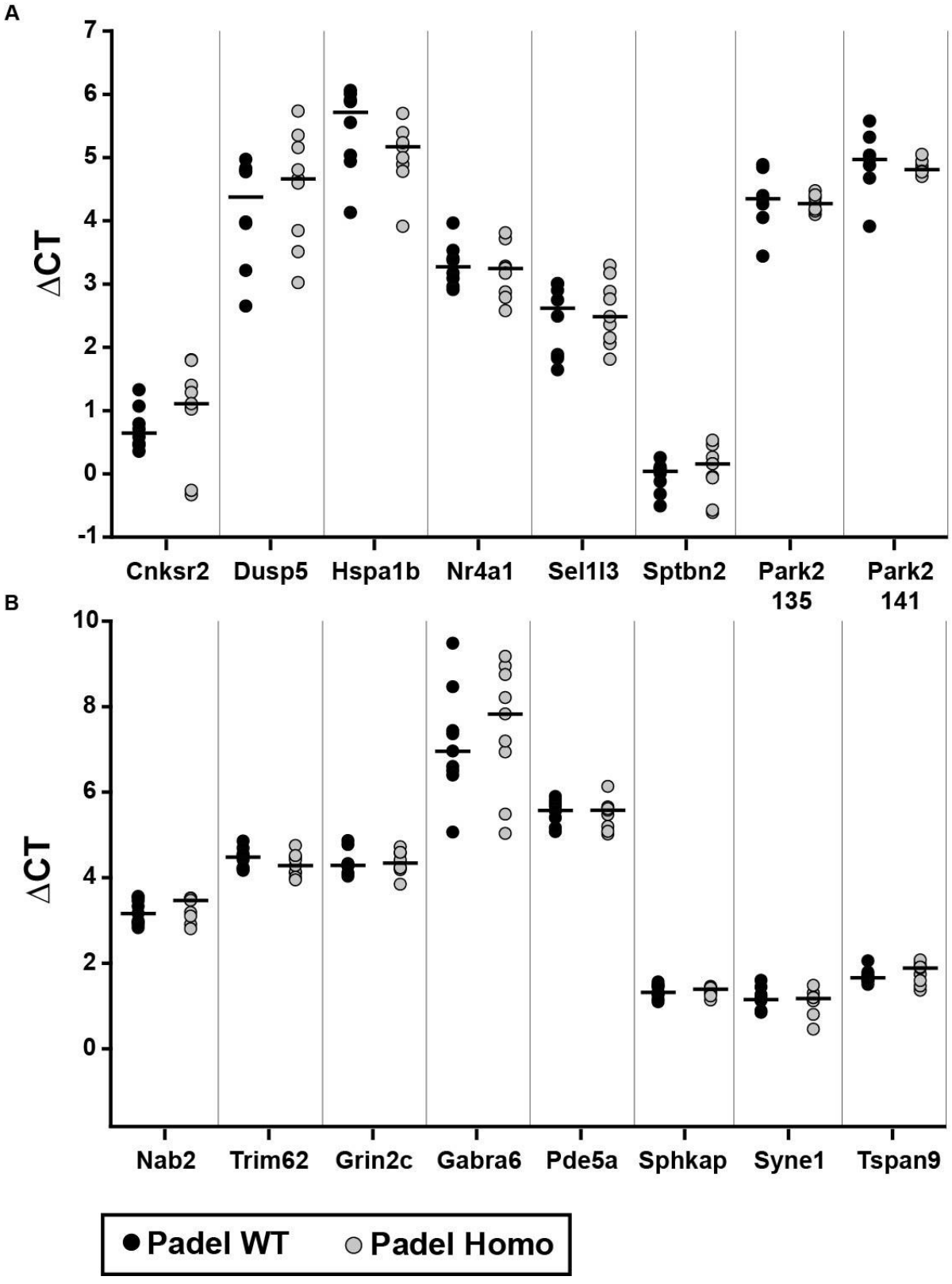

Figure 37: Statistically insignificant gene expression results of substantia nigra tissue *of one-year-old Padel mice with the reference gene Hprt (n=10). Color coding is explained in the legend below. Black bars represent the median of the corresponding groups.*

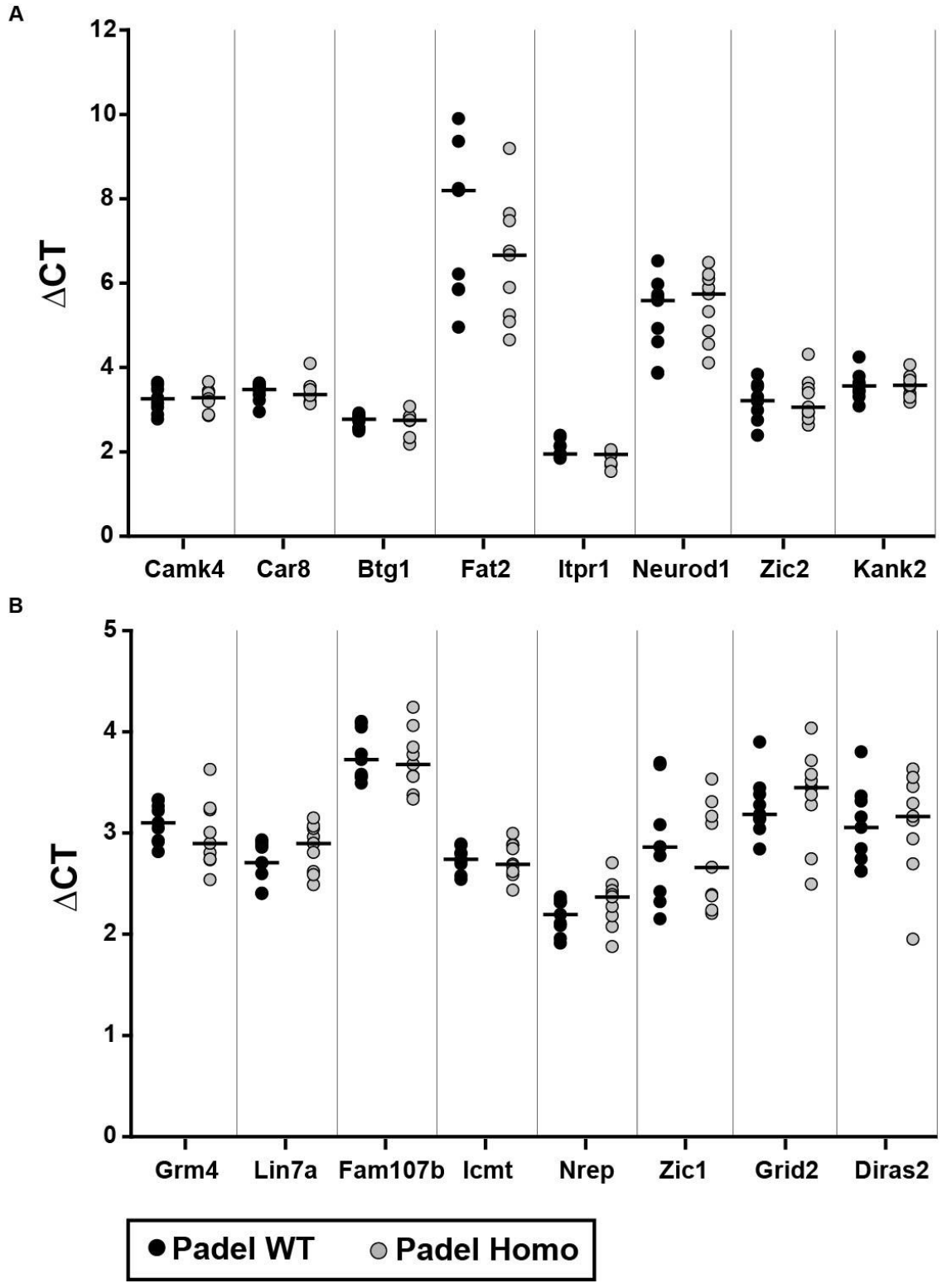

Figure 38: Statistically insignificant gene expression results of substantia nigra tissue *of one-year-old Padel mice with the reference gene Hprt (n=10). Color coding is explained in the legend below. Black bars represent the median of the corresponding groups.*

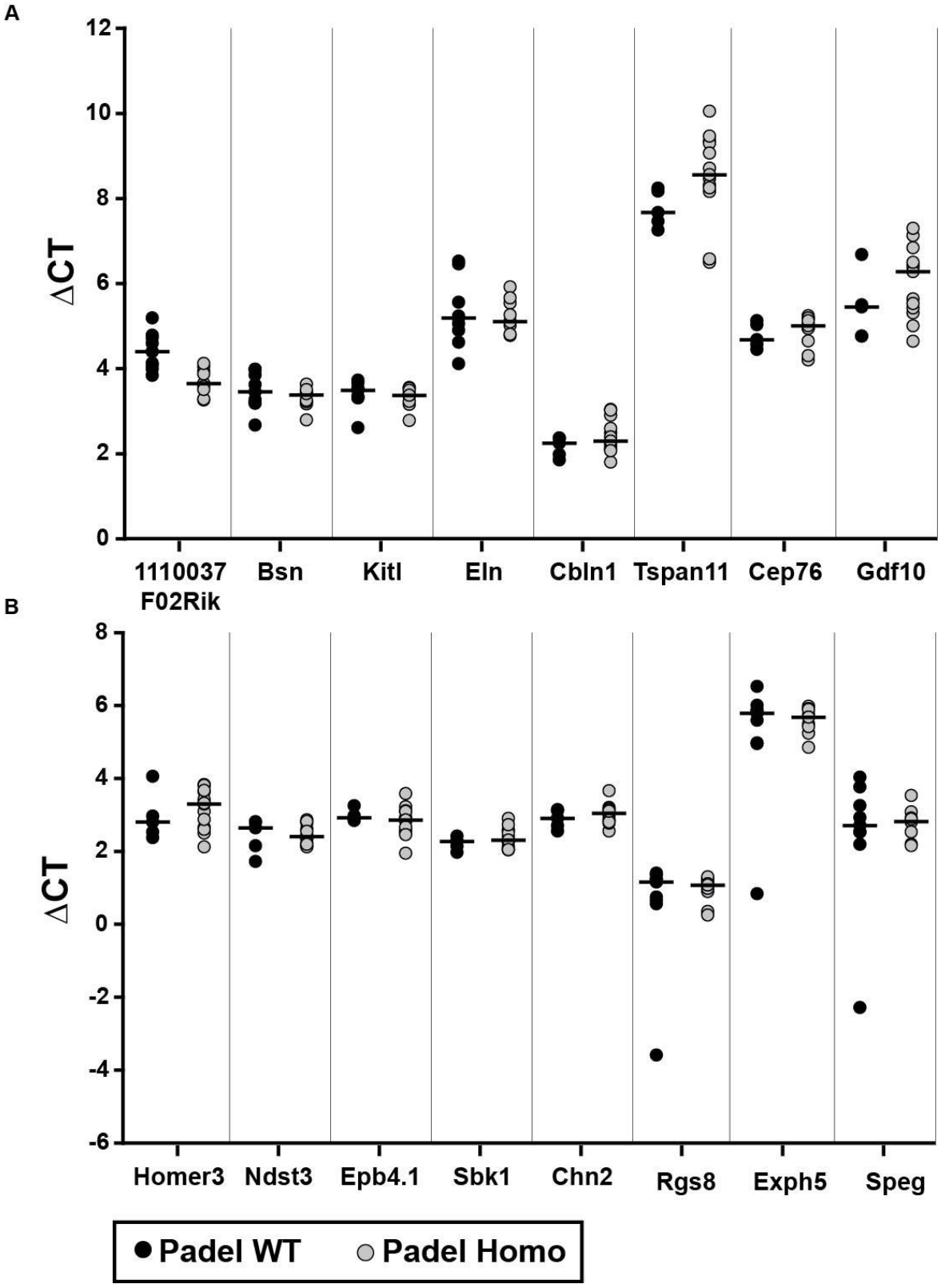

Figure 39: Statistically insignificant gene expression results of substantia nigra tissue *of one-year-old Padel mice with the reference gene Hprt (n=10). Color coding is explained in the legend below. Black bars represent the median of the corresponding groups.*

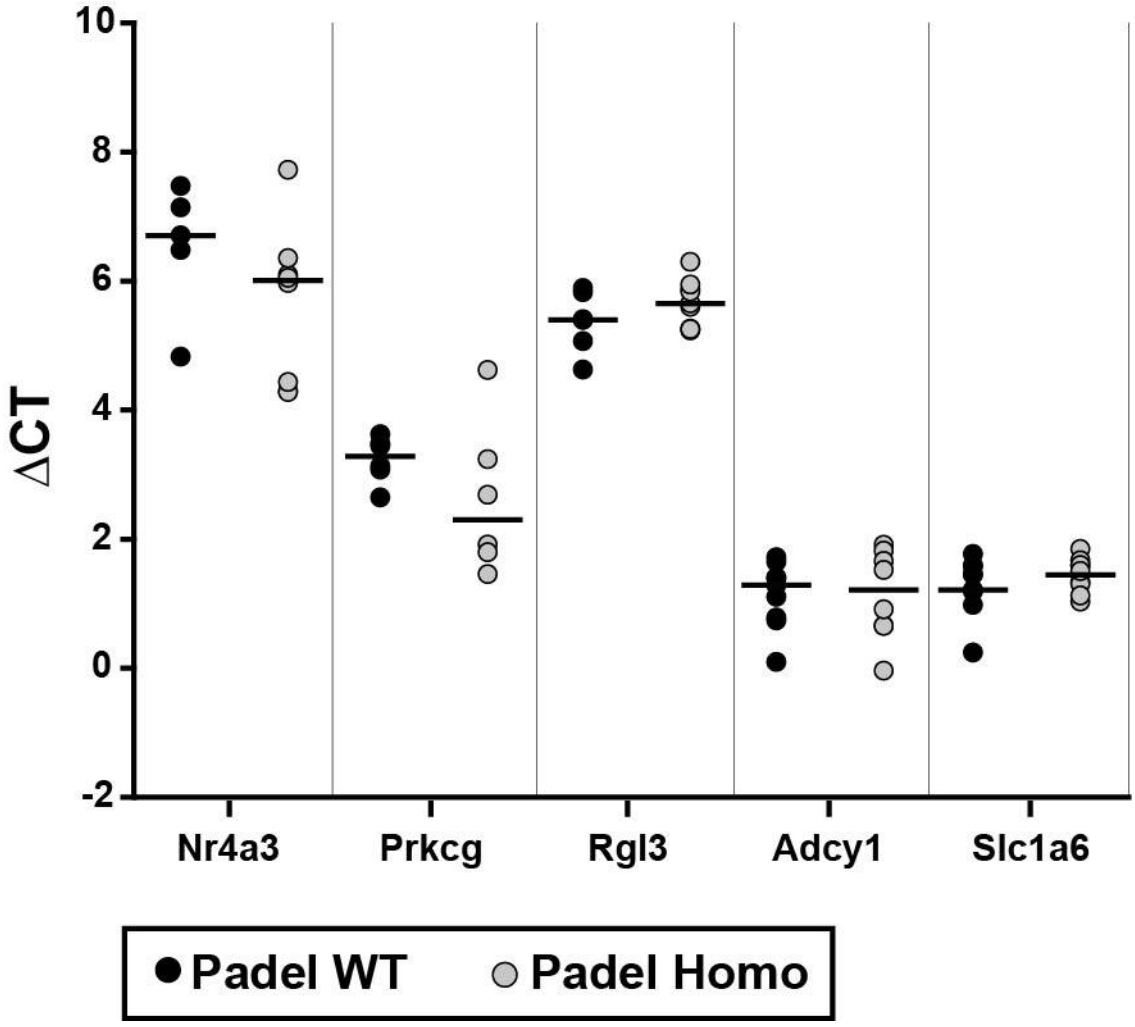

Figure 40: Statistically insignificant gene expression results of substantia nigra tissue *of one-year-old Padel mice with the reference gene Hprt (n=10). Color coding is explained in the legend below. Black bars represent the median of the corresponding groups.*

Table 20:* ∆*CT values of negative results from qPCR experiments with substantia nigra tissue *of one-year-old mice. (n=7-10) WT= wild type.*

ΔCT									
1110037 F02Rik		Adcy1		Atp1a1		Atp2a3		Bcl6	
WT	Padel	WT	Padel	WT	Padel	WT	Padel	WT	Padel
4.58	3.56	-0.23	1.29	-0.77	1.43	6.14	6.14	2.09	2.70
4.59	3.26	0.78	0.65	0.13	2.81	5.94	6.39	2.60	2.86
4.73	3.65	1.40	1.91	0.35	0.95	6.64	5.92	2.24	2.56
4.40	3.94	0.74	0.65	0.74	1.47	6.28	5.60	2.71	2.53
4.13	4.05	0.09	1.82	-0.09	0.99	5.64	5.84	2.30	2.69
3.99	3.87	1.28	1.66	-0.17	1.37	6.40	5.61	2.35	2.51
5.19	3.58	1.39	0.91	0.55	1.56	6.70	5.69	1.58	2.79
4.78	4.12	1.10	-0.04	0.75	0.32	5.07	5.78	2.75	2.77
4.08	3.28	1.64	1.52	0.33	0.05	4.84	8.31	2.65	2.60
3.84	3.51	1.71		0.07		4.25	7.15		2.46
means									
4.41	3.68	0.99	1.15	0.19	1.22	5.79	6.24	2.36	2.65
ΔCT									
Bsn		Btg1		Cadps2		Calb1		Camk4	
WT	Padel	WT	Padel	WT	Padel	WT	Padel	WT	Padel
2.77	3.76	2.97	2.81	1.39	1.63	-0.15	1.37	3.36	3.44
3.98	3.63	2.78	2.18	1.22	1.75	0.49	0.43	3.26	3.43
3.98	3.17	2.56	2.75	1.10	1.70	0.00	-0.31	2.88	3.44
3.18	3.22	2.56	2.75	1.42	1.83	1.18	0.38	3.48	3.66
3.20	3.38	2.92	2.74	1.55	1.18	0.92	1.27	2.78	2.86
3.45	3.25	2.71	2.83	1.06	1.83	0.77	0.95	3.27	3.28
3.85	3.43	2.49	2.84	1.30	1.60	0.52	1.81	3.15	3.39
3.27	3.41	2.87	3.07	1.32	1.42			3.60	3.25
3.62	3.50	2.78	2.75	1.86	1.29			3.06	3.19
2.67	2.79	2.83	2.34		1.65			3.65	2.88
means									
3.40	3.36	2.75	2.71	1.36	1.59	0.53	0.85	3.25	3.28

Table 21:* ∆*CT values of negative results from qPCR experiments with substantia nigra tissue *of one-year-old mice. (n=6-14) WT= wild type.*

ΔCT									
Car8		**Cartpt**		**Cbln1**		**Cbln3**		**Cep76**	
WT	**Padel**	**WT**	**Padel**	**WT**	**Padel**	**WT**	**Padel**	**WT**	**Padel**
3.84	3.62	4.54	4.70	2.30	2.61	8.73	7.95	4.39	4.56
3.46	3.32	3.08	4.32	2.37	1.80	8.56	7.99	4.57	4.20
3.54	3.53	4.53	4.53	1.98	2.16	8.46	6.67	4.68	4.65
3.48	3.36	5.06	4.79	1.85	2.49	6.94	7.71	4.45	4.30
3.63	4.09	4.75	4.64	2.36	2.59	8.74	6.86	5.03	4.95
3.35	3.18	4.47	4.47	2.25	2.39	8.33	8.41	5.13	5.24
3.61	3.14	-0.08	4.84		2.90	7.88	6.64		5.18
3.22	3.33				3.04	7.57	7.52		5.06
3.54	3.54				2.24	6.53	8.03		5.17
2.95	3.47				2.11	5.69	8.90		5.19
					2.28				4.96
					2.29				4.94
					2.07				5.01
					3.02				5.12
means									
3.46	3.46	3.76	4.61	2.18	2.43	7.74	7.67	4.71	4.90
ΔCT									
Chd7		**Chn2**		**Cmya5**		**Cnksr2**		**Cnr1**	
WT	**Padel**	**WT**	**Padel**	**WT**	**Padel**	**WT**	**Padel**	**WT**	**Padel**
1.49	2.58	2.94	3.35	6.82	8.49	0.64	0.31	2.35	2.97
1.61	1.92	3.14	2.55	8.26	8.58	1.33	1.05	3.12	2.63
2.22	2.09	3.11	3.20	8.27	9.23	1.07	-0.33	2.81	1.95
1.23	1.34	2.90	2.77	10.00	9.46	0.35	1.40	3.87	2.44
2.28	1.96	2.70	3.04	8.27	10.38	0.71	1.02	3.11	2.85
2.37	1.96	2.55	3.05	9.39	9.91	0.45	1.28	3.22	3.30
2.11	2.48		3.66	9.14	9.65	0.58	1.80		3.85
1.97	2.34		3.17	8.94	9.48	0.79	1.79		2.75
2.48	2.58		2.96	9.03	9.32	0.48	1.11		3.12
1.69			3.13	8.30			-0.26		
			2.85						
			2.86						
			2.80						
			3.10						
means									
1.94	2.14	2.89	3.04	8.64	9.39	0.71	0.92	3.08	2.87

Table 22:* ∆*CT values of negative results from qPCR experiments with substantia nigra tissue *of one-year-old mice. (n=6-14) WT= wild type.*

ΔCT									
Coro2b		**Crym**		**Ctsc**		**Dgkg**		**Dgkz**	
WT	**Padel**	**WT**	**Padel**	**WT**	**Padel**	**WT**	**Padel**	**WT**	**Padel**
1.49	2.58	2.94	3.35	6.82	8.49	0.64	0.31	2.35	2.97
1.61	1.92	3.14	2.55	8.26	8.58	1.33	1.05	3.12	2.63
2.22	2.09	3.11	3.20	8.27	9.23	1.07	-0.33	2.81	1.95
1.23	1.34	2.90	2.77	10.00	9.46	0.35	1.40	3.87	2.44
2.28	1.96	2.70	3.04	8.27	10.38	0.71	1.02	3.11	2.85
2.37	1.96	2.55	3.05	9.39	9.91	0.45	1.28	3.22	3.30
2.11	2.48		3.66	9.14	9.65	0.58	1.80		3.85
1.97	2.34		3.17	8.94	9.48	0.79	1.79		2.75
2.48	2.58		2.96	9.03	9.2	0.48	1.11		3.12
1.69			3.13	8.30			-0.26		
			2.85						
			2.86						
			2.80						
			3.10						
means									
1.94	2.14	2.89	3.04	8.64	9.39	0.71	0.92	3.08	2.87
ΔCT									
Diras2		**Dpysl4**		**Dusp5**		**Eln**		**Eomes**	
WT	**Padel**	**WT**	**Padel**	**WT**	**Padel**	**WT**	**Padel**	**WT**	**Padel**
2.81	2.83	3.07	4.21	3.18	3.97	5.20	5.31	6.90	11.63
2.84	2.69	3.26	4.14	4.77	4.66	5.19	5.11	8.24	10.85
3.31	3.12	2.84	3.00	2.65	3.51	4.11	5.02	5.00	10.67
2.62	2.94	3.90	3.09	4.97	5.16	5.23	5.92	5.59	10.41
3.05	3.63	3.72	2.98	4.83	4.80	4.62	5.54	5.21	9.67
3.36	3.46	4.02	3.00	3.96	3.84	4.90	5.10	10.07	9.59
3.80	3.55	2.21	2.38	3.98	5.73	6.46	5.66	9.85	12.50
2.74	3.29	3.31	2.95	4.80	5.35	6.53	5.26	10.15	10.62
3.16	3.16	4.00	3.74	3.21	4.59	5.56	4.78	9.56	10.98
2.62	1.95	3.69			3.02	5.06	4.80	12.18	9.74
means									
3.03	3.06	3.40	3.28	4.04	4.46	5.29	5.25	8.28	10.67

Table 23:* ∆*CT values of negative results from qPCR experiments with substantia nigra tissue *of one-year-old mice. (n=7-14) WT= wild type.*

ΔCT									
Epb4.1		**Ermard**		**Exph5**		**Fam107b**		**Fam171b**	
WT	**Padel**	**WT**	**Padel**	**WT**	**Padel**	**WT**	**Padel**	**WT**	**Padel**
3.05	3.20	1.15	2.60	5.05	4.95	3.97	3.73	1.22	1.37
3.25	2.82	0.91	2.29	5.88	5.24	4.10	3.68	1.10	0.94
2.97	3.22	1.58	3.02	6.52	5.48	3.58	3.77	1.59	1.07
2.88	2.52	1.14	3.12	5.85	5.42	3.49	4.24	1.54	1.02
2.92	3.11	2.60	2.85	6.00	4.85	3.72	3.85	0.93	0.80
2.84	2.89	1.06	3.00	4.97	5.74	3.78	3.56	1.25	0.96
	3.58	1.05	2.05	5.79	5.97	4.08	3.37	1.10	1.30
	2.93	1.11	3.22	5.59	5.91	3.55	4.06	1.52	0.72
	3.09		3.31	4.95	5.89	4.04	3.33	0.79	0.75
	2.86		2.72	0.83	5.68	3.56	3.56	1.72	0.70
	1.94								
	2.57								
	2.66								
	2.45								
means									
2.98	2.85	1.33	2.82	5.14	5.51	3.79	3.71	1.28	0.96
ΔCT									
Fat2		**Gabra2**		**Gabra6**		**Gabrd**		**Gas7**	
WT	**Padel**	**WT**	**Padel**	**WT**	**Padel**	**WT**	**Padel**	**WT**	**Padel**
5.47	4.72	1.44	0.63	8.61	5.17	3.26	4.52	5.88	5.64
8.24	6.76	1.60	0.91	7.36	6.94	3.87	4.15	5.33	5.88
9.36	5.24	0.98	0.96	8.46	7.82	3.55	2.98	6.02	5.60
4.95	7.65	0.98	1.10	7.44	8.95	4.90	3.63	5.76	5.20
8.19	5.90	1.11	0.27	6.96	7.19	4.29	4.63	6.53	6.50
9.90	5.08	1.73	1.05	9.48	8.74	4.43	4.47	5.72	5.77
5.84	7.48	1.74	1.41	5.06	5.03		5.35	4.52	6.05
8.20	9.19			6.60	9.17		4.24	5.42	5.31
5.86	4.65			6.50	8.21		5.02	5.79	6.14
6.21	6.66			6.39	5.48			5.02	5.30
means									
7.22	6.33	1.37	0.90	7.29	7.27	4.05	4.33	5.60	5.74

Table 24:* ∆*CT values of negative results from qPCR experiments with substantia nigra *tissue of one-year-old mice. (n=6-14) WT= wild type.*

ΔCT									
Gdf10		**Gm7120**		**Gm996**		**Gprc5c**		**Grid2**	
WT	**Padel**	**WT**	**Padel**	**WT**	**Padel**	**WT**	**Padel**	**WT**	**Padel**
4.88	5.25	3.07	4.15	1.80	2.69	7.22	7.19	2.30	3.10
4.76	5.31	3.66	2.91	2.63	2.52	7.92	7.44	3.15	2.49
6.68	5.00	3.31	3.71	2.58	2.71	7.76	7.03	3.13	3.45
5.45	5.64	3.04	3.33	2.62	2.06	7.33	6.60	3.44	3.28
4.76	7.13	4.06	4.02	2.66	2.59	7.19	8.62	3.38	3.71
5.50	7.30	2.40	3.45	2.40	2.46	7.85	8.16	3.04	3.51
	6.43	2.74	4.49	2.47	2.81	8.07	7.33	3.90	3.38
	5.42	2.98	2.61	2.23	2.22	7.94	7.75	3.28	4.03
	5.53	2.66	3.62	2.74	2.62		8.11	3.18	2.74
	6.84	3.06		2.48			7.39	2.84	3.58
	6.38								
	6.28								
	6.50								
	4.64								
means									
5.34	5.97	3.10	3.59	2.46	2.52	7.66	7.56	3.16	3.33
ΔCT									
Grin2c		**Grm4**		**Homer3**		**Hspa1b**		**Icam5**	
WT	**Padel**	**WT**	**Padel**	**WT**	**Padel**	**WT**	**Padel**	**WT**	**Padel**
4.57	4.00	2.47	3.14	3.17	1.82	4.49	5.17	2.68	6.05
4.77	4.18	3.22	2.73	2.53	3.09	6.06	5.21	2.06	3.46
4.28	4.23	2.81	3.23	4.05	2.50	5.04	3.91	7.04	7.71
4.33	4.57	3.05	2.54	2.96	2.65	5.91	4.89	6.05	3.62
4.03	4.34	3.33	2.80	2.37	3.83	4.13	5.70	2.46	4.40
4.29	4.41	2.91	2.90	2.80	3.63	4.94	5.17	4.92	3.25
4.11	3.84	2.92	2.74		3.30	5.88	5.00	5.63	4.21
4.27	4.72	3.10	3.24		2.60	6.01	5.39	4.74	3.10
4.86	4.59	3.32	3.00		2.87	5.55	5.23	5.89	5.74
4.29	4.23	3.26	3.63		3.81		4.78	5.06	3.58
					3.42				
					3.67				
					3.32				
					2.12				
means									
4.38	4.31	3.04	3.00	2.98	3.04	5.33	5.05	4.65	4.51

Table 25:* ∆*CT values of negative results from qPCR experiments with substantia nigra tissue *of one-year-old mice. (n=6-10) WT= wild type.*

ΔCT									
Icmt		**Itrp1**		**Jchain**		**Kank2**		**Kit**	
WT	**Padel**	**WT**	**Padel**	**WT**	**Padel**	**WT**	**Padel**	**WT**	**Padel**
2.76	2.86	2.21	2.07	7.65	9.13	4.06	3.59	2.64	4.28
2.80	2.43	2.39	1.92	8.88	8.10	3.42	3.38	3.96	2.81
2.73	2.88	1.87	1.95	7.29	8.41	3.08	3.60	3.25	1.72
2.69	2.69	1.84	2.01	7.01	8.42	3.58	4.06	4.13	1.94
2.74	2.99	1.93	1.97	8.45	9.03	3.31	3.78	3.55	2.88
2.58	2.67	2.14	1.69	5.39	8.91	3.46	3.54	3.74	3.45
2.89	2.59	1.95	1.94	7.22	6.25	4.25	3.58		4.02
2.88	2.88	2.13	1.73	7.26	8.18	3.79	3.69		2.73
2.79	2.62	2.35	1.53	8.13	7.83	3.64	3.18		3.03
2.54	2.84	1.94	2.05		6.64	3.56	3.29		
means									
2.74	2.75	2.08	1.89	7.47	8.09	3.62	3.57	3.54	2.99
ΔCT									
Kitl		**Lamb1**		**Lin7a**		**Lnx2**		**Lrrc17**	
WT	**Padel**	**WT**	**Padel**	**WT**	**Padel**	**WT**	**Padel**	**WT**	**Padel**
2.06	3.46	7.22	6.75	2.76	2.94	5.14	6.15	9.95	8.59
3.54	3.42	7.16	6.73	2.91	2.49	5.98	6.27	9.14	9.04
3.51	3.16	7.54	6.63	2.86	2.96	5.54	6.80	9.43	8.73
2.61	3.55	6.92	8.47	2.60	2.90	5.39	6.31	10.17	9.31
3.73	3.36	6.92	6.52	2.70	3.04	5.38	6.34	10.19	9.85
3.49	3.53	8.06	6.85	2.40	3.07	5..5	6.28	10.18	9.07
3.32	3.23	7.60	7.64	2.88	2.62	5.85	6.92	9.62	9.49
3.34	3.49			2.71	3.15	5.72	5.78		9.34
3.66	2.78			2.93	2.59	6.03	5.77		9.80
3.31	3.37			2.40	2.81	5.76	6.06		10.69
means									
3.26	3.34	7.34	7.08	2.72	2.85	5.60	6.27	9.81	9.39

Table 26:* ∆*CT values of negative results from qPCR experiments with substantia nigra tissue *of one-year-old mice. (n=6-14) WT= wild type.*

ΔCT									
Ltbp2		**Mical2**		**Mpp3**		**Mpped1**		**Mrgprf**	
WT	**Padel**	**WT**	**Padel**	**WT**	**Padel**	**WT**	**Padel**	**WT**	**Padel**
6.64	9.56	0.03	1.28	0.99	3.17	2.54	3.27	4.41	6.08
7.38	10.58	0.87	0.91	2.11	2.91	3.14	3.21	4.54	6.62
5.94	7.58	1.77	1.94	1.75	0.38	3.23	3.52	4.60	5.35
10.54	8.96	1.39	1.01	0.76	1.16	3.54	2.92	7.32	6.11
6.58	10.14	1.13	2.03	1.41	1.70	2.93	3.08	4.58	7.40
8.17	9.22	0.56	1.69	1.96	1.44	2.37	3.01	6.51	5.32
9.43	9.24	0.87	1.41		1.99	2.75	3.13	6.33	6.12
10.14	9.56	0.75	0.32		1.06	3.44	2.98	6.66	6.14
10.12	9.63	1.68	1.24		0.93	3.02	3.56	7.59	6.27
10.07		1.27				3.15	2.84	6.75	
means									
8.50	9.39	1.03	1.32	1.50	1.64	3.01	3.15	5.93	6.16
ΔCT									
Mtcl1		**Nab2**		**Ndst3**		**Neurod1**		**Neurod2**	
WT	**Padel**	**WT**	**Padel**	**WT**	**Padel**	**WT**	**Padel**	**WT**	**Padel**
2.61	2.52	3.80	3.02	2.45	2.85	6.62	4.64	1.36	3.69
3.25	2.52	3.46	2.91	2.81	2.78	5.66	5.74	2.56	4.46
2.89	2.63	2.98	3.52	2.64	2.86	4.61	5.88	3.28	3.49
2.86	2.36	3.53	3.47	2.80	2.61	6.53	5.32	5.86	4.50
2.40	2.04	2.95	3.18	2.15	2.36	4.92	4.55	2.69	4.48
2.22	2.28	3.16	3.52	1.72	2.45	5.59	6.49	2.25	3.97
2.15	2.22	2.91	3.10		2.14	3.86	4.86	5.21	4.82
2.36	2.06	3.33	3.51		2.82	5.73	6.09	3.53	4.09
2.49	1.86	2.83	3.47		2.40	3.88	6.20	3.56	3.84
-2.07	1.94	3.56	2.80		2.33	5.97	4.11	2.94	2.18
					2.23				
					2.54				
					2.12				
					2.19				
means									
2.11	2.24	3.25	3.25	2.43	2.48	5.34	5.39	3.32	3.95

Table 27:* ∆*CT values of negative results from qPCR experiments with substantia nigra tissue *of one-year-old mice. (n=6-10) WT= wild type.*

ΔCT									
Nptx1		**Nr4a1**		**Nr4a3**		**Nrep**		**Nrk**	
WT	**Padel**	**WT**	**Padel**	**WT**	**Padel**	**WT**	**Padel**	**WT**	**Padel**
0.53	0.77	2.69	3.12	6.70	7.23	2.56	2.31	9.29	9.22
0.32	0.46	3.37	3.28	7.47	7.72	1.96	1.88	9.83	10.19
1.83	1.62	3.40	2.87	6.70	4.29	1.91	2.70	9.34	8.40
0.50	0.53	3.96	3.25	4.82	4.27	2.33	2.49	10.02	9.35
1.71	1.94	3.17	3.25	7.14	4.43	2.08	2.43	9.09	10.16
0.34	1.42	2.96	2.79	6.48	5.96	2.19	2.07	10.03	8.84
0.39	1.43	3.09	3.71		6.09	2.31	2.18	9.71	10.03
0.24	-0.40	3.53	3.81		6.35	2.31	2.27	10.03	10.13
1.38	1.06	2.91	3.17		6.05	2.11	2.39	10.08	9.33
1.41			2.58			2.37	2.37	10.01	
means									
0.70	1.12	3.32	3.09	6.55	5.65	2.17	2.31	9.60	9.36
ΔCT									
Park2 135bp		**Park2 141 bp**		**Pde1a**		**Pde5a**		**Phyhip**	
WT	**Padel**	**WT**	**Padel**	**WT**	**Padel**	**WT**	**Padel**	**WT**	**Padel**
4.62	4.08	5.21	4.79	0.96	3.03	6.37	5.64	-0.62	0.03
4.40	4.10	4.97	4.81	1.11	1.36	5.81	5.47	-0.06	0.98
4.89	4.27	5.58	4.86	2.92	2.57	5.57	5.65	0.50	0.35
4.35	4.47	5.04	4.94	3.02	1.56	5.07	5.64	0.88	0.85
4.84	4.15	5.32	4.70	1.40	1.41	5.67	5.19	0.28	0.43
4.26	4.36	4.88	4.78	2.04	1.62	5.74	5.58	0.40	0.31
4.05	4.18	4.67	4.77	2.63	0.87	5.16	5.61	0.91	0.91
3.44	4.41	3.91	5.05	2.23	1.59	5.89	6.13	1.26	0.82
				2.87	2.48	5.56	5.02	0.54	0.71
				2.52	0.66	5.40	5.08	0.25	0.13
means									
4.36	4.25	4.95	4.84	2.17	1.71	5.62	5.50	0.43	0.55

Table 28:* ∆*CT values of negative results from qPCR experiments with substantia nigra tissue *of one-year-old mice. (n=7-10) WT= wild type.*

ΔCT									
Park2 135bp		**Park2 141 bp**		**Pde1a**		**Pde5a**		**Phyhip**	
WT	**Padel**	**WT**	**Padel**	**WT**	**Padel**	**WT**	**Padel**	**WT**	**Padel**
4.62	4.08	5.21	4.79	0.96	3.03	6.37	5.64	-0.62	0.03
4.40	4.10	4.97	4.81	1.11	1.36	5.81	5.47	-0.06	0.98
4.89	4.27	5.58	4.86	2.92	2.57	5.57	5.65	0.50	0.35
4.35	4.47	5.04	4.94	3.02	1.56	5.07	5.64	0.88	0.85
4.84	4.15	5.32	4.70	1.40	1.41	5.67	5.19	0.28	0.43
4.26	4.36	4.88	4.78	2.04	1.62	5.74	5.58	0.40	0.31
4.05	4.18	4.67	4.77	2.63	0.87	5.16	5.61	0.91	0.91
3.44	4.41	3.91	5.05	2.23	1.59	5.89	6.13	1.26	0.82
				2.87	2.48	5.56	5.02	0.54	0.71
				2.52	0.66	5.40	5.08	0.25	0.13
means									
4.36	4.25	4.95	4.84	2.17	1.71	5.62	5.50	0.43	0.55
ΔCT									
Pisd-ps1		**Plch2**		**Prdm8**		**Prkcg**		**Ptprr**	
WT	**Padel**	**WT**	**Padel**	**WT**	**Padel**	**WT**	**Padel**	**WT**	**Padel**
1.35	1.15	1.50	2.79	1.88	3.68	2.27	1.56	3.89	3.99
1.28	1.25	2.17	3.17	3.14	3.16	2.64	1.45	4.25	3.75
1.82	1.82	2.39	2.83	5.37	5.12	3.48	2.68	4.25	4.05
2.68	0.47	2.95	3.26	4.11	3.75	3.07	1.91	4.06	3.74
1.53	-0.42	2.32	2.24	4.74	5.59	3.62	1.79	4.37	4.27
0.25	1.27	2.23	2.62	2.42	5.44	3.13	3.23	3.63	3.82
0.41	1.47	2.43	3.75	2.81	4.31	3.44	4.62	4.22	3.95
0.52	0.93	2.43	2.24	2.92	2.53			4.16	3.81
0.43	1.07	2.19	2.56	5.56	3.64				3.84
4.82	0.82	2.38	1.34	3.28					4.10
means									
0.41	0.98	2.30	2.68	3.62	4.14	3.09	2.46	4.10	3.93

Table 29:* ∆*CT values of negative results from qPCR experiments with substantia nigra tissue *of one-year-old mice. (n=6-14) WT= wild type.*

ΔCT									
Rcn1		**Reln**		**Rgl3**		**Rgs6**		**Rgs8**	
WT	**Padel**	**WT**	**Padel**	**WT**	**Padel**	**WT**	**Padel**	**WT**	**Padel**
3.29	3.27	1.71	3.62	4.80	4.62	2.19	2.27	1.15	0.78
3.90	3.40	2.25	3.93	4.62	5.87	2.64	2.19	1.24	0.35
3.97	3.29	2.86	3.17	5.82	5.60	2.61	2.45	1.40	1.21
3.79	3.24	2.29	3.42	5.40	5.65	2.22	2.34	0.74	0.89
3.12	2.84	2.24	3.13	5.06	5.83	2.61	1.93	1.34	0.25
3.43	3.07	1.90	3.14	5.89	5.94	2.22	2.44	0.65	1.21
3.83	3.58	4.05	3.52	5.39	5.23	2.62	2.46	1.15	1.30
3.93	3.18	3.86	3.47		5.26	2.49	2.32	1.24	1.11
3.36	2.87	3.49	3.22		6.29	2.35	2.02	0.56	0.98
3.53	3.32	3.42	3.46		5.25	-1.93	1.86	-3.59	1.07
means									
3.61	3.21	2.81	3.41	5.28	5.55	0.59	0.92	0.59	0.92
ΔCT									
Rtn4rl2		**Ryr1**		**Sbk1**		**Sec14l1**		**Sel1l3**	
WT	**Padel**	**WT**	**Padel**	**WT**	**Padel**	**WT**	**Padel**	**WT**	**Padel**
3.07	6.86	6.24	11.43	1.97	1.98	0.95	0.78	1.99	1.96
2.98	4.30	6.41	11.93	2.14	2.08	1.23	1.10	3.00	2.36
7.11	8.18	5.47	6.84	2.27	2.04	1.88	1.09	1.88	2.06
6.60	4.07	13.24	8.06	1.97	2.13	1.36	1.07	3.01	2.88
3.44	3.94	6.26	9.79	2.27	2.40	2.11	0.98	2.90	2.76
5.13	4.43	8.51	10.80	2.41	2.58	1.17	1.28	2.49	2.15
6.41	3.88	8.24	9.07		2.90	1.60	1.81	1.83	3.29
4.79	4.18	11.11	9.48		2.57	1.40	1.79	2.75	3.17
7.30	5.67	11.52	10.00		2.26	1.23	1.43	1.64	2.48
5.81	3.36	11.21			2.50	-3.32	1.54		1.81
					2.26				
					2.30				
					2.73				
					2.04				
means									
5.26	4.89	8.82	9.71	2.17	2.34	0.96	1.29	2.39	2.49

Table 30:* ∆*CT values of negative results from qPCR experiments with substantia nigra tissue *of one-year-old mice. (n=6-10) WT= wild type.*

ΔCT									
Sgk1		**Shisa6**		**Sla**		**Slc17a7**		**Slc18a2**	
WT	**Padel**	**WT**	**Padel**	**WT**	**Padel**	**WT**	**Padel**	**WT**	**Padel**
3.00	3.03	1.24	2.99	4.30	5.55	-0.61	-0.33	2.40	2.81
2.95	2.75	2.78	2.84	5.82	5.45	0.87	-0.50	2.19	1.23
3.12	3.01	3.59	3.71	5.29	5.48	-0.44	-2.10	1.89	2.56
3.07	2.83	2.94	2.83	5.13	5.76	0.15	-2.02	1.18	0.95
2.88	2.85	2.24	3.88	5.76	6.46	0.42	-1.63	1.67	1.08
3.19	3.14	2.39	3.65	5.80	5.54	0.63	-0.41	1.28	0.66
2.82	2.57	2.72	2.56	4.79	6.23		-0.03	1.37	1.54
3.32	2.99	2.22	1.38	5.48	5.84		-2.26	2.10	1.35
3.13	3.31	3.83	3.39	5.65	5.60		-1.76	1.68	0.96
3.07	2.68	3.44		5.73	5.49			1.55	1.59
means									
3.05	2.92	2.74	3.03	5.38	5.74	0.17	-1.23	1.73	1.47
ΔCT									
Slc1a6		**Slc5a1**		**Slc8a2**		**Speg**		**Sphkap**	
WT	**Padel**	**WT**	**Padel**	**WT**	**Padel**	**WT**	**Padel**	**WT**	**Padel**
4.38	4.40	6.92	9.71	3.07	3.25	2.52	2.30	1.71	1.63
4.39	4.23	7.40	10.24	3.22	3.89	2.92	2.81	1.44	1.39
4.39	4.47	6.33	7.49	3.06	3.24	4.03	2.80	1.28	1.43
4.50	4.20	10.65	8.90	3.75	3.73	3.25	2.19	1.56	1.30
4.53	4.12	6.39	8.78	3.27	3.38	3.76	2.15	1.16	1.33
4.74	3.91	7.68	9.57	3.16	3.22	2.19	2.53	1.48	1.45
4.38	4.22	9.05	9.58	3.34	3.77	2.71	3.53	1.27	1.14
4.17	3.87	9.51	8.97	3.48	3.27	2.53	3.08	1.32	1.43
	3.73	10.26	10.21	3.82	4.28	2.53	2.91	1.09	1.42
	3.93	9.69		3.49		-2.29	2.88	1.48	1.23
means									
4.43	4.11	8.39	9.27	3.36	3.56	2.42	2.72	1.38	1.37

Table 31:* ∆*CT values of negative results from qPCR experiments with substantia nigra tissue *of one-year-old mice. (n=6-10) WT= wild type.*

ΔCT									
Sptbn2		**Syne1**		**Tbata**		**Tbr1**		**Tcf7l2**	
WT	**Padel**	**WT**	**Padel**	**WT**	**Padel**	**WT**	**Padel**	**WT**	**Padel**
0.15	-0.15	1.57	1.24	7.44	10.19	5.17	8.34	-0.09	1.77
0.25	0.16	1.60	0.80	8.35	9.96	4.99	6.29	0.45	0.89
0.08	-0.61	1.44	1.30	8.03	5.77	8.95	10.41	0.32	2.44
0.11	0.26	1.22	1.17	8.76	6.09	9.27	7.25	1.07	0.82
0.07	0.16	0.85	1.48	7.24	7.34	5.74	6.38	0.19	1.14
0.12	-0.05	1.12	1.19	7.73	7.57	4.87	6.51	0.69	1.31
0.51	0.46	1.26	0.45		9.28	6.37	5.92	1.19	-0.06
0.01	0.53	1.15	1.13		6.92	6.65	6.79	0.31	0.10
0.32	-0.07	0.87	1.11		7.50	9.53	8.45	0.34	0.55
	-0.58	0.88	1.19			7.71	5.26	1.02	-0.12
means									
0.07	0.01	1.20	1.11	7.93	7.85	6.93	7.16	0.55	0.88
ΔCT									
Tcp11l1		**Tiam1**		**Tmem132a**		**Tmem178**		**Tmem181b-ps**	
WT	**Padel**	**WT**	**Padel**	**WT**	**Padel**	**WT**	**Padel**	**WT**	**Padel**
1.05	0.89	1.40	3.22	1.20	1.50	1.12	2.51	1.98	1.55
1.09	0.72	2.16	3.45	1.26	1.16	1.96	1.82	1.59	1.84
0.94	0.62	2.52	2.82	2.22	2.29	3.36	2.66	1.45	1.67
1.02	0.21	3.28	3.20	1.92	1.52	1.81	2.75	1.45	1.59
1.12	0.62	2.35	3.48	1.86	0.84	3.24	2.81	0.24	1.59
1.06	0.49	1.96	2.98	1.75	1.56	2.02	3.22	1.21	1.33
0.93	0.82	2.71	3.55	1.72	1.85	2.25	2.99	0.98	1.03
0.92	0.79	2.51	2.83			2.18	1.81	1.19	1.30
1.13	0.90	2.32	2.59			3.12	2.78	1.76	1.50
0.72		2.27	2.91			2.40		1.57	1.12
means									
1.05	0.59	2.28	3.19	1.70	1.53	2.25	2.63	1.32	1.60

Table 32:* ∆*CT values of negative results from qPCR experiments with substantia nigra tissue *of one-year-old mice. (n=6-14) WT= wild type.*

ΔCT									
Trab2d		**Trim62**		**Tspan11**		**Tspan9**		**Usp2**	
WT	**Padel**	**WT**	**Padel**	**WT**	**Padel**	**WT**	**Padel**	**WT**	**Padel**
5.17	6.83	4.73	4.78	8.60	7.91	2.20	2.04	1.23	1.22
7.56	8.34	4.85	4.11	8.17	6.50	2.05	1.36	1.27	1.23
6.90	6.73	4.42	4.48	7.67	8.16	1.50	1.74	1.24	1.21
8.62	7.37	4.52	4.13	7.26	6.58	1.61	1.89	1.25	1.21
9.97	12.76	4.17	4.75	7.46	9.35	1.59	1.97	1.25	1.23
7.42	8.23	4.69	4.01	8.24	10.05	1.66	1.89	1.24	1.24
7.32	8.05	4.55	3.94		9.30	1.66	1.46		1.26
8.75	9.14	4.21	4.28		8.47	1.72	2.07		1.21
9.54	7.68	4.48	4.41		8.71	1.79	1.91		1.21
7.78		4.23	4.51		9.46	1.60	1.59		
					8.32				
					8.25				
					9.07				
					8.56				
means									
7.90	8.35	4.48	4.34	7.90	8.48	1.74	1.79	1.25	1.22
ΔCT									
Ust		**Wscd2**		**Zbtb18**		**Zfpm2**		**Zic1**	
WT	**Padel**	**WT**	**Padel**	**WT**	**Padel**	**WT**	**Padel**	**WT**	**Padel**
1.56	2.88	2.82	3.12	-0.53	1.05	3.66	4.00	1.61	2.61
2.52	3.41	3.46	3.52	0.33	0.49	3.47	4.54	2.86	3.09
3.07	2.93	2.64	2.83	1.68	1.62	3.82	3.80	2.15	3.16
3.22	2.57	3.10	3.43	0.27	0.61	3.97	3.69	2.32	3.53
2.39	2.82	3.16	3.27	1.16	1.54	3.50	4.12	2.77	2.39
1.73	2.97	2.87	3.46	0.67	1.48	3.33	4.19	3.67	2.20
2.97	3.31	2.34	3.75	0.95	1.16	2.95	4.23	2.42	2.24
2.36	2.72	2.97	3.98	0.69	0.00	3.72	3.89	2.86	2.66
2.80	2.80	3.20	3.37	1.73	1.04	4.06	3.45	3.69	2.38
2.71	2.40		2.57	1.28			3.87	3.08	3.31
means									
2.53	2.88	2.95	3.33	0.82	1.00	3.61	3.98	2.74	2.76

Table 33:* ∆*CT values of negative results from qPCR experiments with substantia nigra tissue *of one-year-old mice. (n=10) WT= wild type.*

ΔCT									
Zic2									
WT	Padel	WT	Padel	WT	Padel	WT	Padel	WT	Padel
2.92	2.96								
3.30	3.63								
2.39	3.50								
2.98	4.31								
2.75	2.92								
3.59	2.63								
3.20	2.79								
3.22	3.06								
3.84	3.40								
3.54	2.95								
means									
3.17	3.21								

Table 34: ∆CT values of Hprt confirmed genes (Tcp11l1, Cmya5). *Tested again with an independent sample set and multiple reference genes. Substantia nigra tissue of one-year-old mice. (n=10), WT=wild type. PD=Padel homo.*

Tcp11l1 ΔCT													
Acvrl1		Aes		Eif4g2		Hprt		Mgrn1		Oxr1		Ube2d2a	
WT	PD	WT	PD	WT	PD	WT	PD	WT	PD	WT	PD	WT	PD
-2.57	-3.24	4.25	3.89	2.12	1.66	1.27	1.47	1.9	1.48	1.89	1.45	1.67	1.69
-2.5	-2.69	4.4	4.09	2.26	1.68	1.87	1.59	1.92	1.74	1.89	1.41	2.17	1.81
-2.61	-3.09	4.16	3.91	1.84	1.66	1.39	1.36	1.6	1.57	1.59	1.44	2.26	1.69
-2.33	-2.95	4.52	4.02	2.46	1.65	1.73	1.52	1.94	1.48	2.06	1.28	2.3	1.69
-2.56	-2.78	3.91	4.05	2.16	1.78	1.57	1.45	1.72	1.53	1.94	1.3	1.88	1.92
-2.1	-2.65	4.07	4.02	1.82	2.03	1.45	1.53	1.77	1.69	1.62	1.64	1.89	1.94
-2.06	-3.17	4.29	3.55	2.15	1.3	1.55	0.94	1.78	0.99	1.69	1	2	1.34
-2.33	-3.15	3.46	3.56	1.73	1.36	1.11	0.9	1.04	0.79	1.6	1.17	1.59	1.37
-2.5	-3.09	3.77	3.77	1.95	1.6	1.32	1.05	1.25	0.94	1.5	0.91	1.81	1.16
-2.48	-3.17	3.59	3.64	1.69	1.32	1.17	0.86	1.19	0.75	1.57	1.05	1.64	0.99
means													
-2.4	-3	4.04	3.85	2.02	1.6	1.44	1.27	1.61	1.3	1.74	1.27	1.92	1.56
Cmya5 ΔCT													
Acvrl1		Aes		Eif4g2		Hprt		Mgrn1		Oxr1		Ube2d2a	
WT	PD	WT	PD	WT	PD	WT	PD	WT	PD	WT	PD	WT	PD
5.87	5.58	12.5	12.5	10	10	9.65	9.98	9.73	9.76	9.9	9.69	10	9.95
4.85	6.06	11.3	12.5	9.2	10.1	8.88	10	8.79	9.95	8.95	10.1	9.01	10
4.67	5.23	11.5	12.2	9.08	9.51	8.88	9.36	8.86	9.25	9.1	9.39	8.93	9.59
5.75	5.01	12.1	11.3	9.98	8.94	9.64	8.72	9.32	8.76	9.34	8.96	9.54	8.92
4.85	5.1	11.3	11.7	8.95	9.51	8.55	8.9	8.44	8.98	8.72	9.36	8.71	9.39
5.19	5.62	11.9	12.1	9.84	9.96	9.37	9.36	9.02	9.36	9.59	9.81	9.47	9.29
5.76	5.90	11.9	12.6	10.5	10.3	9.73	9.43	8.91	9.53	10.3	9.94	10	10.6
4.67	6.05	10.9	12.3	9.28	10.2	8.58	9.56	8.51	9.55	8.85	9.95	8.9	10.8
4.937	4.4	11.6	11	9.8	9.13	8.79	10.7	9.12	8.23	9.26	8.75	9.44	8.76
5.287	6.74	11.9	13.6	9.89	11	7.98	11.7	9.59	10.4	9.79	10.6	10	11
means													
5.18	5.57	11.7	12.2	9.65	9.87	9	9.77	9.03	9.38	9.38	9.66	9.41	9.83

Table 35:* ∆*CT values of Hprt confirmed genes (Tiam1, Atp1a1). *Tested again with an independent sample set and multiple reference genes. Substantia nigra tissue of one-year-old mice. (n=10), WT=wild type. PD=Padel homo.*

Tiam1 ΔCT													
Acvrl1		Aes		Eif4g2		Hprt		Mgrn1		Oxr1		Ube2d2a	
WT	PD	WT	PD	WT	PD	WT	PD	WT	PD	WT	PD	WT	PD
3.06	2.14	3.76	5	1.64	2.76	0.78	2.58	1.41	2.59	1.4	2.55	1.19	2.79
2.01	1.57	4.88	5.21	2.74	2.8	2.35	2.71	2.41	2.86	2.38	2.53	2.66	2.93
1.15	1.76	5.62	5.25	3.3	3	2.85	2.69	3.05	2.9	3.04	2.77	3.72	3.03
-1.3	1.64	5.54	5.33	3.48	2.96	2.75	2.83	2.97	2.79	3.09	2.59	3.32	3
1.81	0.87	4.67	5.96	2.92	3.68	2.33	3.36	2.47	3.44	2.69	3.2	2.63	3.83
0.69	2.09	5.47	4.58	3.23	2.59	2.86	2.09	3.18	2.25	3.02	2.2	3.29	2.5
0.56	1.05	5.8	5.66	3.66	3.41	3.06	3.05	3.29	3.11	3.2	3.12	3.51	3.45
-1.2	0.67	4.59	6.03	2.86	3.84	2.24	3.38	2.17	3.27	2.73	3.64	2.72	3.85
1.49	1.05	4.78	5.8	2.96	3.63	2.32	3.09	2.25	2.98	2.5	2.95	2.82	3.2
1.09	1.18	4.99	5.63	3.08	3.3	2.56	2.85	2.58	2.74	2.96	3.04	3.04	2.98
means													
1.44	-1.4	5.01	5.45	2.99	3.2	2.41	2.86	2.58	2.89	2.7	2.86	2.89	3.16
Atp1a1 ΔCT													
Acvrl1		Aes		Eif4g2		Hprt		Mgrn1		Oxr1		Ube2d2a	
WT	PD	WT	PD	WT	PD	WT	PD	WT	PD	WT	PD	WT	PD
4.99	3.52	1.91	3.02	-0.3	0.75	-1	0.45	-0.5	0.38	-0.4	0.47	-0.5	0.63
4.39	3.66	2.3	3	-0.2	0.59	-0.4	0.16	-0.2	0.31	-0.2	0.4	-0.1	0.51
4.17	4.75	2.64	1.92	0.37	-0	-0.1	-0.6	0.24	-0.3	0.01	-0.3	0.36	-0.2
4.09	4.38	2.49	2.28	0.24	-0.1	-0.4	-0.7	0.04	-0.2	0.14	-0.2	0.2	-0.2
4.42	5.31	2.04	2.26	-0.2	-0.3	-0.7	-0.7	-0.4	-0	-0.3	-0.2	-0.5	-0.1
3.77	4.32	2.84	2.31	0.72	-0.1	-0	-0.6	0.43	-0.1	0.35	-0.3	0.42	-0.2
3.85	4.19	2.53	2.45	0.52	0.35	-0.1	-0.2	-0	0.14	0.24	-0.2	0.3	0.37
-3.6	4.79	2.77	1.65	0.7	-0.3	0.14	-1.1	0.41	-0.5	0.35	-0.5	0.47	-0.3
3.55	3.87	3.28	2.84	0.94	0.57	0.23	-0	0.21	0.25	0.73	0.2	0.66	0.26
3.58	3.98	2.17	2.51	0.51	0.39	-0.4	-0.3	-0.2	0.04	0.07	0.09	-0.1	0.21
means													
4.04	4.28	2.49	2.42	0.34	0.18	-0.3	-0.4	0	0	0.1	-0.1	0.13	0.11

Table 36: ∆CT values of Hprt confirmed genes (Eomes, Lnx2). *Tested again with an independent sample set and multiple reference genes. Substantia nigra tissue of one-year-old mice. (n=10), WT=wild type. PD=Padel homo.*

Eomes ΔCT													
Acvrl1		Aes		Eif4g2		Hprt		Mgrn1		Oxr1		Ube2d2a	
WT	PD	WT	PD	WT	PD	WT	PD	WT	PD	WT	PD	WT	PD
6.66	5.89	13.3	12.8	10.8	10.3	10.5	10.3	10.5	10.1	10.7	10	10.8	10.3
7	6.65	13.5	13.1	11.4	10.7	11	10.6	10.9	10.5	11.1	10.7	11.2	10.6
6.43	6.36	13.2	13.2	10.8	10.6	10.6	10.4	10.6	10.3	10.9	10.5	10.7	10.7
5.08	6.27	11.4	12.6	9.32	10.2	8.97	9.99	8.65	10	8.68	10.2	8.88	10.2
5.45	6.37	11.9	13	9.56	10.8	9.16	10.2	9.04	10.3	9.33	10.6	9.32	10.7
6.64	6.41	13.3	12.9	11.3	10.8	10.8	10.2	10.5	10.2	11	10.6	10.9	10.1
6.87	5.66	13.1	12.4	11.6	10.1	10.8	9.19	10	9.3	11.4	9.71	11.1	10.4
7.91	6.83	14.2	13.1	12.5	11	11.8	10.3	11.7	10.3	12.1	10.7	12.1	11.6
4.95	7.04	11.6	13.7	9.81	11.8	8.81	13.4	9.13	10.9	9.27	11.4	9.45	11.4
7.26	7.58	13.9	14.4	11.9	11.9	9.96	12.5	11.6	11.2	11.8	11.5	12	11.8
means													
6.43	6.51	12.9	13.1	10.9	10.8	10.3	10.7	10.3	10.3	10.6	10.6	10.7	10.8
Lnx2 ΔCT													
Acvrl1		Aes		Eif4g2		Hprt		Mgrn1		Oxr1		Ube2d2a	
WT	PD	WT	PD	WT	PD	WT	PD	WT	PD	WT	PD	WT	PD
3.08	2.56	9.7	9.45	7.25	7	6.87	6.97	6.94	6.75	7.12	6.68	7.23	6.94
2.59	2.94	9.09	9.38	6.95	7.02	6.63	6.88	6.54	6.84	6.7	6.97	6.76	6.92
2.59	2.64	9.41	9.5	7	6.86	6.8	6.71	6.79	6.6	7.02	6.73	6.85	6.94
3.01	2.92	9.35	9.2	7.25	6.86	6.9	6.64	6.58	6.68	6.61	6.88	6.81	6.83
2.90	2.8	9.34	9.4	7.01	7.21	6.61	6.6	6.5	6.69	6.78	7.07	6.77	7.09
2.57	2.79	9.23	9.27	7.23	7.13	6.75	6.53	6.41	6.53	6.97	6.98	6.85	6.46
3.47	3.02	9.65	9.74	8.17	7.45	7.44	6.55	6.62	6.65	8.04	7.06	7.73	7.74
2.49	3.18	8.74	9.48	7.1	7.33	6.4	6.69	6.33	6.68	6.67	7.08	6.72	7.96
2.17	2.53	8.79	9.15	7.04	7.27	6.03	8.87	6.36	6.37	6.5	6.89	6.68	6.9
1.97	3.33	8.55	10.2	6.58	7.59	4.67	8.25	6.28	6.99	6.47	7.22	6.73	7.56
means													
2.68	2.87	9.19	9.48	7.16	7.17	6.51	7.07	6.53	6.68	6.89	6.96	6.91	7.13

Table 37: ∆CT values of Hprt confirmed genes (Cadps2, Wscd2). *Tested again with an independent sample set and multiple reference genes. Substantia nigra tissue of one-year-old mice. (n=10), WT=wild type. PD=Padel homo.*

Cadps2 ΔCT													
Acvrl1		Aes		Eif4g2		Hprt		Mgrn1		Oxr1		Ube2d2a	
WT	PD	WT	PD	WT	PD	WT	PD	WT	PD	WT	PD	WT	PD
2.89	2.83	3.93	4.31	1.81	2.07	0.95	1.89	1.58	1.9	1.57	1.86	1.36	2.1
2.41	2.03	4.48	4.75	2.34	2.34	1.95	2.25	2.01	2.4	1.98	2.07	2.26	2.47
1.99	2.53	4.78	4.48	2.46	2.23	2.01	1.92	2.21	2.13	2.2	2	2.88	2.26
2.12	2.07	4.73	4.89	2.67	2.52	1.94	2.4	2.15	2.36	2.27	2.15	2.51	2.57
2.43	1.86	4.04	4.96	2.29	2.69	1.7	2.36	1.85	2.44	2.07	2.21	2.01	2.83
1.96	2.37	4.21	4.3	1.96	2.3	1.59	1.8	1.91	1.97	1.76	1.91	2.03	2.22
1.82	2.41	4.54	4.31	2.4	2.06	1.8	1.69	2.03	1.75	1.94	1.76	2.25	2.1
1.81	2.13	3.98	4.57	2.25	2.38	1.63	1.92	1.56	1.81	2.12	2.18	2.11	2.39
2.04	2.15	4.23	4.7	2.41	2.53	1.78	1.99	1.71	1.88	1.96	1.85	2.27	2.1
1.44	-2.3	4.64	4.51	2.73	2.18	2.22	1.73	2.23	1.62	2.61	1.92	2.69	1.86
means													
2.09	2.27	4.36	4.58	2.33	2.33	1.76	2	1.92	2.03	2.05	1.99	2.24	2.29
Wscd2 ΔCT													
Acvrl1		Aes		Eif4g2		Hprt		Mgrn1		Oxr1		Ube2d2a	
WT	PD	WT	PD	WT	PD	WT	PD	WT	PD	WT	PD	WT	PD
1.51	-1.7	5.3	5.43	3.18	3.2	2.33	3.01	2.95	3.02	2.95	2.99	2.73	3.23
1.39	1.14	5.5	5.64	3.36	3.23	2.97	3.14	3.03	3.29	3	2.96	3.28	3.36
0.73	1.21	6.04	5.8	3.72	3.55	3.27	3.24	3.47	3.45	3.46	3.32	4.14	3.58
0.96	1.05	5.89	5.92	3.83	3.55	3.1	3.42	3.32	3.38	3.43	3.18	3.67	3.59
-0.8	0.78	5.67	6.04	3.92	3.77	3.33	3.44	3.48	3.52	3.7	3.29	3.63	3.91
-0.3	-1.8	5.87	4.87	3.62	2.88	3.25	2.38	3.58	2.55	3.42	2.49	3.69	2.8
0.19	0.96	6.17	5.76	4.02	3.51	3.43	3.14	3.66	3.2	3.57	3.21	3.87	3.55
0.29	0.45	5.5	6.26	3.77	4.06	3.14	3.6	3.08	3.49	3.64	3.87	3.63	4.07
0.69	0.86	5.58	6	3.75	3.83	3.12	3.28	3.05	3.17	3.3	3.14	3.61	3.39
0.37	0.98	5.71	5.83	3.8	3.5	3.29	3.05	3.3	2.94	3.68	3.24	3.76	3.18
means													
0.72	1.09	5.72	5.76	3.7	3.51	3.12	3.17	3.29	3.2	3.42	3.17	3.6	3.47

Table 38: ∆CT values of Hprt confirmed genes (Zfpm2, 11113F02Rik). *Tested again with an independent sample set and multiple reference genes. Substantia nigra tissue of one-year-old mice. (n=10), WT=wild type. PD=Padel homo.*

Zfpm2 ΔCT													
Acvrl1		Aes		Eif4g2		Hprt		Mgrn1		Oxr1		Ube2d2a	
WT	PD	WT	PD	WT	PD	WT	PD	WT	PD	WT	PD	WT	PD
-0.75	0.94	6.06	6.19	3.94	3.96	3.09	3.77	3.71	3.78	3.71	3.75	3.49	3.99
-0.75	0.66	6.14	6.12	4	3.71	3.61	3.62	3.67	3.77	3.64	3.44	3.92	3.84
-0.3	-0.4	6.47	6.61	4.15	4.36	3.7	4.05	3.91	4.26	3.9	4.13	4.57	4.39
-0.16	0.79	6.68	6.17	4.62	3.8	3.89	3.68	4.11	3.64	4.23	3.43	4.46	3.85
-0.2	0.13	6.28	6.7	4.53	4.42	3.94	4.1	4.08	4.18	4.3	3.94	4.24	4.57
-0.05	0.84	6.12	5.83	3.87	3.84	3.5	3.34	3.83	3.5	3.67	3.45	3.94	3.75
-0.08	0.04	6.27	6.68	4.13	4.43	3.53	4.06	3.76	4.12	3.67	4.13	3.98	4.47
0.81	0.49	6.6	7.19	4.87	5	4.25	4.54	4.18	4.43	4.74	4.8	4.73	5.01
0.7	0.15	6.97	7.01	5.15	4.84	4.51	4.29	4.44	4.18	4.69	4.15	5.01	4.4
1.2	0.01	7.27	6.8	5.37	4.47	4.85	4.02	4.87	3.91	5.25	4.21	5.32	4.15
means													
0.042	0.32	6.49	6.53	4.46	4.28	3.89	3.95	4.06	3.98	4.18	3.94	4.37	4.24
11113F02Rik ΔCT													
Acvrl1		Aes		Eif4g2		Hprt		Mgrn1		Oxr1		Ube2d2a	
WT	PD	WT	PD	WT	PD	WT	PD	WT	PD	WT	PD	WT	PD
-0.23	0.47	6.59	6.67	4.47	4.43	3.61	4.25	4.24	4.26	4.23	4.22	4.02	4.46
-0.09	0.19	6.8	6.6	4.66	4.19	4.27	4.09	4.33	4.25	4.3	3.92	4.58	4.32
-0.13	0.45	6.64	6.55	4.31	4.3	3.86	4	4.07	4.21	4.06	4.08	4.73	4.33
-0.4	0.54	6.45	6.42	4.39	4.05	3.66	3.92	3.87	3.89	3.99	3.68	4.23	4.1
-0.43	-0.2	6.05	6.63	4.3	4.35	3.71	4.03	3.85	4.11	4.07	3.87	4.01	4.5
0.28	0.33	6.45	6.34	4.2	4.35	3.83	3.85	4.15	4.01	4	3.96	4.27	4.26
0.13	0.09	6.49	6.63	4.34	4.38	3.75	4.02	3.98	4.07	3.89	4.08	4.19	4.42
0.25	0.04	6.04	6.74	4.31	4.55	3.68	4.09	3.62	3.98	4.17	4.35	4.16	4.56
-0.37	0.02	5.9	6.84	4.07	4.67	3.44	4.12	3.37	4.01	3.62	3.98	3.93	4.23
0.59	0.18	6.66	6.63	4.76	4.3	4.24	3.85	4.26	3.74	4.64	4.04	4.71	3.98
means													
-0.04	0.24	6.41	6.61	4.38	4.36	3.81	4.02	3.97	4.05	4.1	4.02	4.28	4.32

***Table 39:* ∆*CT values of Hprt confirmed genes (Gabra2, Usp2*).** *Tested again with an independent sample set and multiple reference genes. Substantia nigra tissue of one-year-old mice. (n=10), WT=wild type. PD=Padel homo.*

Gabra2 ΔCT													
Acvrl1		Aes		Eif4g2		Hprt		Mgrn1		Oxr1		Ube2d2a	
WT	PD	WT	PD	WT	PD	WT	PD	WT	PD	WT	PD	WT	PD
2.57	3.24	4.25	3.89	2.12	1.66	1.27	1.47	1.9	1.48	1.89	1.45	1.67	1.69
-2.5	2.69	4.4	4.09	2.26	1.68	1.87	1.59	1.92	1.74	1.89	1.41	2.17	1.81
2.61	3.09	4.16	3.91	1.84	1.66	1.39	1.36	1.6	1.57	1.59	1.44	2.26	1.69
2.33	2.95	4.52	4.02	2.46	1.65	1.73	1.52	1.94	1.48	2.06	1.28	2.3	1.69
2.56	2.78	3.91	4.05	2.16	1.78	1.57	1.45	1.72	1.53	1.94	1.3	1.88	1.92
-2.1	2.65	4.07	4.02	1.82	2.03	1.45	1.53	1.77	1.69	1.62	1.64	1.89	1.94
2.06	3.17	4.29	3.55	2.15	1.3	1.55	0.94	1.78	0.99	1.69	1	2	1.34
2.33	3.15	3.46	3.56	1.73	1.36	1.11	0.9	1.04	0.79	1.6	1.17	1.59	1.37
-2.5	3.09	3.77	3.77	1.95	1.6	1.32	1.05	1.25	0.94	1.5	0.91	1.81	1.16
2.48	3.17	3.59	3.64	1.69	1.32	1.17	0.86	1.19	0.75	1.57	1.05	1.64	0.99
means													
2.40	3.00	4.04	3.85	2.02	1.60	1.44	1.27	1.61	1.30	1.74	1.27	1.92	1.56
Usp2 ΔCT													
Acvrl1		Aes		Eif4g2		Hprt		Mgrn1		Oxr1		Ube2d2a	
WT	PD	WT	PD	WT	PD	WT	PD	WT	PD	WT	PD	WT	PD
5.87	5.58	12.49	12.46	10.03	10.01	9.65	9.98	9.73	9.76	9.90	9.69	10.02	9.95
4.85	6.06	11.34	12.50	9.20	10.13	8.88	10.00	8.79	9.95	8.95	10.08	9.01	10.03
4.67	5.30	11.48	12.16	9.08	9.51	8.88	9.36	8.86	9.25	9.10	9.39	8.93	9.59
5.75	5.01	12.09	11.29	9.98	8.94	9.64	8.72	9.32	8.76	9.34	8.96	9.54	8.92
4.85	5.10	11.28	11.70	8.95	9.51	8.55	8.90	8.44	8.98	8.72	9.36	8.71	9.39
5.19	5.62	11.85	12.10	9.84	9.96	9.37	9.36	9.02	9.36	9.59	9.81	9.47	9.29
5.76	5.90	11.94	12.62	10.46	10.34	9.73	9.43	8.91	9.53	10.33	9.94	10.02	10.63
4.67	6.05	10.92	12.35	9.28	10.20	8.58	9.56	8.51	9.55	8.85	9.95	8.90	10.82
4.94	4.40	11.55	11.01	9.80	9.13	8.79	10.73	9.12	8.23	9.26	8.75	9.44	8.76
5.29	6.74	11.87	13.58	9.89	11.00	7.98	11.66	9.59	10.40	9.79	10.62	10.04	10.97
means													
5.18	5.57	11.68	12.18	9.65	9.87	9.00	9.77	9.03	9.38	9.38	9.66	9.41	9.83

Table 40: ∆CT values of Hprt confirmed genes (Slc17a7, Fam171b). *Tested again with an independent sample set and multiple reference genes. Substantia nigra tissue of one-year-old mice. (n=10), WT=wild type. PD=Padel homo.*

Slc17a7 ΔCT													
Acvrl1		Aes		Eif4g2		Hprt		Mgrn1		Oxr1		Ube2d2a	
WT	PD	WT	PD	WT	PD	WT	PD	WT	PD	WT	PD	WT	PD
3.06	2.14	3.76	5	1.64	2.76	0.78	2.58	1.41	2.59	1.4	2.55	1.19	2.79
2.01	1.57	4.88	5.21	2.74	2.8	2.35	2.71	2.41	2.86	2.38	2.53	2.66	2.93
1.15	1.76	5.62	5.25	3.3	3	2.85	2.69	3.05	2.9	3.04	2.77	3.72	3.03
-1.3	1.64	5.54	5.33	3.48	2.96	2.75	2.83	2.97	2.79	3.09	2.59	3.32	3
1.81	0.87	4.67	5.96	2.92	3.68	2.33	3.36	2.47	3.44	2.69	3.2	2.63	3.83
0.69	2.09	5.47	4.58	3.23	2.59	2.86	2.09	3.18	2.25	3.02	2.2	3.29	2.5
0.56	1.05	5.8	5.66	3.66	3.41	3.06	3.05	3.29	3.11	3.2	3.12	3.51	3.45
-1.2	0.67	4.59	6.03	2.86	3.84	2.24	3.38	2.17	3.27	2.73	3.64	2.72	3.85
1.49	1.05	4.78	5.8	2.96	3.63	2.32	3.09	2.25	2.98	2.5	2.95	2.82	3.2
1.09	1.18	4.99	5.63	3.08	3.3	2.56	2.85	2.58	2.74	2.96	3.04	3.04	2.98
means													
1.44	1.40	5.01	5.45	2.99	3.20	2.41	2.86	2.58	2.89	2.70	2.86	2.89	3.16
Fam171b ΔCT													
Acvrl1		Aes		Eif4g2		Hprt		Mgrn1		Oxr1		Ube2d2a	
WT	PD	WT	PD	WT	PD	WT	PD	WT	PD	WT	PD	WT	PD
4.99	3.52	1.91	3.02	0.26	0.75	1.01	0.45	0.51	0.38	0.45	0.47	0.47	0.63
4.39	3.66	2.30	3.00	0.16	0.59	0.38	0.16	0.16	0.31	0.15	0.40	0.10	0.51
4.17	4.75	2.64	1.92	0.37	0.02	0.06	0.60	0.24	0.29	0.01	0.34	0.36	0.15
4.09	4.38	2.49	2.28	0.24	0.06	0.40	0.74	0.04	0.17	0.14	0.23	0.20	0.17
4.42	5.31	2.04	2.26	0.22	0.31	0.75	0.75	0.41	0.01	0.29	0.24	0.46	0.05
3.77	4.32	2.84	2.31	0.72	0.15	0.04	0.62	0.43	0.14	0.35	0.25	0.42	0.22
3.85	4.19	2.53	2.45	0.52	0.35	0.14	0.21	0.04	0.14	0.24	0.22	0.30	0.37
3.60	4.79	2.77	1.65	0.70	0.31	0.14	1.07	0.41	0.49	0.35	0.53	0.47	0.29
3.55	3.87	3.28	2.84	0.94	0.57	0.23	0.04	0.21	0.25	0.73	0.20	0.66	0.26
3.58	3.98	2.17	2.51	0.51	0.39	0.44	0.33	0.19	0.04	0.07	0.09	0.06	0.21
means													
4.04	4.28	2.49	2.42	0.34	0.18	0.29	0.38	0.00	0.00	0.10	0.06	0.13	0.11

Table 41: ∆CT values of Hprt confirmed genes (Atp2a3, Ermard). *Tested again with an independent sample set and multiple reference genes. Substantia nigra tissue of one-year-old mice. (n=10) WT= wild type. PD= Padel homo.*

Atp2a3 ΔCT													
Acvrl1		Aes		Eif4g2		Hprt		Mgrn1		Oxr1		Ube2d2a	
WT	PD	WT	PD	WT	PD	WT	PD	WT	PD	WT	PD	WT	PD
6.7	5.9	13.3	12.8	10.8	10.3	10.5	10.3	10.5	10.1	10.7	10.0	10.8	10.3
7.0	6.7	13.5	13.1	11.4	10.7	11.0	10.6	10.9	10.5	11.1	10.7	11.2	10.6
6.4	6.4	13.2	13.2	10.8	10.6	10.6	10.4	10.6	10.3	10.9	10.5	10.7	10.7
5.1	6.3	11.4	12.6	9.3	10.2	9.0	10.0	8.7	10.0	8.7	10.2	8.9	10.2
5.5	6.4	11.9	13.0	9.6	10.8	9.2	10.2	9.0	10.3	9.3	10.6	9.3	10.7
6.6	6.4	13.3	12.9	11.3	10.8	10.8	10.2	10.5	10.2	11.0	10.6	10.9	10.1
6.9	5.7	13.1	12.4	11.6	10.1	10.8	9.2	10.0	9.3	11.4	9.7	11.1	10.4
7.9	6.8	14.2	13.1	12.5	11.0	11.8	10.3	11.7	10.3	12.1	10.7	12.1	11.6
5.0	7.0	11.6	13.7	9.8	11.8	8.8	13.4	9.1	10.9	9.3	11.4	9.4	11.4
7.3	7.6	13.9	14.4	11.9	11.9	10.0	12.5	11.6	11.2	11.8	11.5	12.0	11.8
means													
6.4	6.5	12.9	13.1	10.9	10.8	10.3	10.7	10.3	10.3	10.6	10.6	10.7	10.8
Ermard ΔCT													
Acvrl1		Aes		Eif4g2		Hprt		Mgrn1		Oxr1		Ube2d2a	
WT	PD	WT	PD	WT	PD	WT	PD	WT	PD	WT	PD	WT	PD
3.08	2.57	9.70	9.45	7.25	7.00	6.87	6.97	6.94	6.75	7.12	6.68	7.23	6.94
2.60	2.94	9.09	9.38	6.95	7.02	6.63	6.88	6.54	6.84	6.70	6.97	6.76	6.92
2.60	2.64	9.41	9.50	7.00	6.86	6.80	6.71	6.79	6.60	7.02	6.73	6.85	6.94
3.01	2.92	9.35	9.20	7.25	6.86	6.90	6.64	6.58	6.68	6.61	6.88	6.81	6.83
2.91	2.80	9.34	9.40	7.01	7.21	6.61	6.60	6.50	6.69	6.78	7.07	6.77	7.09
2.57	2.79	9.23	9.27	7.23	7.13	6.75	6.53	6.41	6.53	6.97	6.98	6.85	6.46
3.47	3.02	9.65	9.74	8.17	7.45	7.44	6.55	6.62	6.65	8.04	7.06	7.73	7.74
2.49	3.18	8.74	9.48	7.10	7.33	6.40	6.69	6.33	6.68	6.67	7.08	6.72	7.96
2.18	2.54	8.79	9.15	7.04	7.27	6.03	8.87	6.36	6.37	6.50	6.89	6.68	6.90
1.97	3.33	8.55	10.18	6.58	7.59	4.67	8.25	6.28	6.99	6.47	7.22	6.73	7.56
means													
2.69	2.87	9.19	9.48	7.16	7.17	6.51	7.07	6.53	6.68	6.89	6.96	6.91	7.13

***Table 42: ∆CT values of Hprt confirmed genes (Slc1a6, Rcn1)**. Tested again with an independent sample set and multiple reference genes. Substantia nigra tissue of one-year-old mice. (n=10) WT= wild type. PD= Padel homo.*

Slc1a6 ΔCT													
Acvrl1		Aes		Eif4g2		Hprt		Mgrn1		Oxr1		Ube2d2a	
WT	PD	WT	PD	WT	PD	WT	PD	WT	PD	WT	PD	WT	PD
-2.89	-2.83	3.93	4.31	1.81	2.07	0.95	1.89	1.58	1.90	1.57	1.86	1.36	2.10
-2.41	-2.03	4.48	4.75	2.34	2.34	1.95	2.25	2.01	2.40	1.98	2.07	2.26	2.47
-1.99	-2.53	4.78	4.48	2.46	2.23	2.01	1.92	2.21	2.13	2.20	2.00	2.88	2.26
-2.12	-2.07	4.73	4.89	2.67	2.52	1.94	2.40	2.15	2.36	2.27	2.15	2.51	2.57
-2.43	-1.86	4.04	4.96	2.29	2.69	1.70	2.36	1.85	2.44	2.07	2.21	2.01	2.83
-1.96	-2.37	4.21	4.30	1.96	2.30	1.59	1.80	1.91	1.97	1.76	1.91	2.03	2.22
-1.82	-2.41	4.54	4.31	2.40	2.06	1.80	1.69	2.03	1.75	1.94	1.76	2.25	2.10
-1.81	-2.13	3.98	4.57	2.25	2.38	1.63	1.92	1.56	1.81	2.12	2.18	2.11	2.39
-2.04	-2.15	4.23	4.70	2.41	2.53	1.78	1.99	1.71	1.88	1.96	1.85	2.27	2.10
-1.44	-2.30	4.64	4.51	2.73	2.18	2.22	1.73	2.23	1.62	2.61	1.92	2.69	1.86
means													
-2.09	-2.27	4.36	4.58	2.33	2.33	1.76	2.00	1.92	2.03	2.05	1.99	2.24	2.29
Rcn1 ΔCT													
Acvrl1		Aes		Eif4g2		Hprt		Mgrn1		Oxr1		Ube2d2a	
WT	PD	WT	PD	WT	PD	WT	PD	WT	PD	WT	PD	WT	PD
-1.51	-1.70	5.30	5.43	3.18	3.20	2.33	3.01	2.95	3.02	2.95	2.99	2.73	3.23
-1.39	-1.14	5.50	5.64	3.36	3.23	2.97	3.14	3.03	3.29	3.00	2.96	3.28	3.36
-0.73	-1.21	6.04	5.80	3.72	3.55	3.27	3.24	3.47	3.45	3.46	3.32	4.14	3.58
-0.96	-1.05	5.89	5.92	3.83	3.55	3.10	3.42	3.32	3.38	3.43	3.18	3.67	3.59
-0.80	-0.78	5.67	6.04	3.92	3.77	3.33	3.44	3.48	3.52	3.70	3.29	3.63	3.91
-0.30	-1.80	5.87	4.87	3.62	2.88	3.25	2.38	3.58	2.55	3.42	2.49	3.69	2.80
-0.19	-0.96	6.17	5.76	4.02	3.51	3.43	3.14	3.66	3.20	3.57	3.21	3.87	3.55
-0.29	-0.45	5.50	6.26	3.77	4.06	3.14	3.60	3.08	3.49	3.64	3.87	3.63	4.07
-0.69	-0.86	5.58	6.00	3.75	3.83	3.12	3.28	3.05	3.17	3.30	3.14	3.61	3.39
-0.37	-0.98	5.71	5.83	3.80	3.50	3.29	3.05	3.30	2.94	3.68	3.24	3.76	3.18
means													
-0.72	-1.09	5.72	5.76	3.70	3.51	3.12	3.17	3.29	3.20	3.42	3.17	3.60	3.47

Table 43: ∆CT values of Rcn1 qPCRs of Padel with C57BL/6 as control group with multiple reference genes. *Substantia nigra tissue of one-year-old mice (upper row). Neonatal mesencephalon tissue (bottom row). (n=10), Bl6= C57BL/6. PD= Padel homo.*

Rcn1 ΔCT													
Acvrl1		Aes		Eif4g2		Hprt		Mgrn1		Oxr1		Ube2d2a	
Bl6	Padel	Bl6	Padel	Bl6	Padel	Bl6	Padel	Bl6	Padel	Bl6	Padel	Bl6	Padel
1.23	-1.06	5.95	6.35	4.70	4.95	3.07	3.43	3.66	3.73	4.08	3.95	3.99	3.96
0.28	-1.08	6.76	6.66	5.52	5.30	4.01	3.93	4.32	4.15	4.72	4.50	4.16	4.18
1.47	-2.19	5.83	5.98	4.52	4.60	3.23	3.09	3.53	3.31	3.68	3.47	4.10	3.83
0.78	-1.00	6.83	6.51	5.69	5.07	4.23	3.69	4.23	4.09	4.65	4.43	4.65	4.17
0.45	-1.70	6.63	6.14	5.39	4.67	4.21	3.28	4.42	3.47	4.82	3.65	4.44	3.80
0.98	-1.83	6.11	6.12	4.97	4.87	3.31	3.10	3.71	3.59	4.15	4.09	4.12	4.10
1.08	-1.95	6.06	6.12	5.00	4.95	3.47	3.33	3.87	3.53	4.03	4.07	4.27	4.09
0.39	-2.28	6.76	5.72	5.71	4.37	4.13	3.09	4.52	3.07	4.93	3.61	4.75	3.80
1.45	-1.65	5.73	5.84	4.42	4.61	3.30	3.27	3.47	3.42	3.65	3.97	3.60	3.50
0.83		6.29		5.03		3.63		3.79		4.10		3.89	
Means													
0.89	-1.64	6.30	6.16	5.09	4.82	3.66	3.36	3.95	3.60	4.28	3.97	4.20	3.94

Rcn1 ΔCT (P1 Mes)	
Bl6	Padel
4.58	3.56
4.59	3.26
4.73	3.65
4.40	3.94
4.13	4.05
3.99	3.87
5.19	3.58
4.78	4.12
4.08	3.28
3.84	3.51
means	
4.41	3.68

Table 44: New transcriptome analysis of the substantia nigra and striatum of one-year-old Padel mice, using Basyn as control group. *Aligning algorithm: Hisat2. Expression analysis: Cuffdiff. Displayed are gene names, fold change (log2 Basyn/Padel) and statistical result (q value).*

Substantia nigra			*Striatum*		
Gene	Foldchange Basyn/Padel	q value	Gene	Foldchange Basyn/Padel	q value
1700086L19Rik	1.1013	0.0045	1500015O10Rik	0.5436	0.0101
2010300C02Rik	0.8982	0.0045	3110035E14Rik	-0.3640	0.0101
3110035E14Rik	0.6257	0.0227	9030025P20Rik	1.7079	0.0101
4933412E12Rik	1.2589	0.0196	A2m	0.8650	0.0101
6330403A02Rik	1.1297	0.0045	Abca4	0.6389	0.0101
Agap2	0.7293	0.0045	Adra2c	-0.4581	0.0101
Akap5	0.8594	0.0045	Alox12b	-0.6091	0.0353
Ankrd33b	0.7803	0.0045	Ankrd33b	-0.3518	0.0353
Ankrd63	3.4616	0.0045	Aqp1	0.4054	0.0254
Ano2	2.2101	0.0045	Arl4d	-0.5239	0.0101
Arhgap33	0.7526	0.0045	Asphd2	-0.5928	0.0101
Arpp21	0.7772	0.0045	Bfsp2	0.7228	0.0101
Avil	-0.8581	0.0196	Cacng8, Gm23450	-0.3308	0.0182
Baiap2	0.5911	0.0045	Cdh3	0.8405	0.0101
Bcl11b	0.8825	0.0045	Cebpb	-0.5212	0.0254
Bhlhe22	0.6337	0.0045	Cldn2	0.5683	0.0101
Bmp3	0.9539	0.0292	Clic6	0.3672	0.0101
C1ql2	0.6232	0.0045	Col4a4	0.8111	0.0101
C1ql3	0.5640	0.0088	Col8a1	0.6743	0.0101
Cacnb3	0.5203	0.0045	Col8a2	0.6001	0.0101
Calca	-0.7193	0.0045	Col9a3	0.3947	0.0101
Calcr	-0.7520	0.0227	Cpxm2	0.8205	0.0101
Camk2a	1.4631	0.0045	Crym	-0.3636	0.0101
Camkv	0.9924	0.0045	Ctgf	-0.4234	0.0310
Car12	1.5009	0.0045	Ctsc	0.8368	0.0101
Cartpt	1.9147	0.0045	Dab2	0.4417	0.0101
Cck	1.1421	0.0045	Dact3	-0.3329	0.0182
Ccnd2	0.6483	0.0045	Dancr, Snora26	1.7505	0.0101
Ccsap	0.6754	0.0045	Dlx5	-0.8415	0.0101
Cd74, Mir5107	0.8715	0.0045	Dlx6os1	-0.7010	0.0101
Cdh9	0.7891	0.0045	Dusp11	0.3403	0.0310
Cdkl4	0.8875	0.0045	Egr4	-0.5997	0.0101
Cecr6	0.7987	0.0045	Elovl7	0.3483	0.0310
Celf3	0.6012	0.0045	Enpp2	0.5225	0.0101

Substantia nigra			*Striatum*		
Gene	Foldchange Basyn/Padel	q value	Gene	Foldchange Basyn/Padel	q value
Celf5	0.5919	0.0045	Entpd4	2.2762	0.0101
Chat	-0.7747	0.0439	Erdr1	1.7804	0.0101
Chodl	-0.9581	0.0045	F5	0.5468	0.0101
Chrm1	1.7999	0.0045	Fam177a	1.0789	0.0182
Cnih3	0.7775	0.0045	Folr1	0.5722	0.0101
Cnksr2	0.4584	0.0196	Glp2r	-1.0298	0.0182
Col23a1	0.6170	0.0126	Gm11549	-0.5158	0.0353
Cort	2.1133	0.0415	Gpr27	-0.5891	0.0101
Cplx3	1.7281	0.0045	Hba-a1, Hba-a2	0.7618	0.0101
Cpne6	0.4441	0.0322	Icam5	-0.3310	0.0101
Cpne7	1.0265	0.0045	Igf2	0.4351	0.0101
Crb1	2.4320	0.0045	Inadl	0.3423	0.0182
Crym	2.3620	0.0045	Itpka	-0.3128	0.0353
Ctsc	0.8170	0.0045	Junb	-0.4915	0.0101
Ctxn1	0.9896	0.0045	Kcna5	-0.5586	0.0310
Cyp4f15	0.7070	0.0260	Kcne2	0.7496	0.0101
D430019H16Rik	0.5134	0.0162	Kcng2	-0.4308	0.0101
Dbh	-1.1503	0.0045	Kcnk2	-0.3720	0.0101
Dbpht2	0.8248	0.0045	Kcnq5	-0.3183	0.0400
Dcn	0.7678	0.0045	Kitl	0.3423	0.0101
Ddn	2.4083	0.0045	Kl	0.5736	0.0101
Ddx3y	0.5133	0.0088	Lamp5	-0.3678	0.0310
Dio3	4.0232	0.0045	Lbp	0.4994	0.0101
Dlx5	1.8374	0.0491	Lingo3	-0.3856	0.0101
Dlx6os1	3.1659	0.0045	Lrrc10b	-0.3484	0.0101
E130012A19Rik	0.6148	0.0045	Mctp2	0.4741	0.0310
Egr3	1.7618	0.0045	Miat	0.3203	0.0458
Emx1	2.1037	0.0045	Mir124a-1, Mir124a-1hg, Mir3078	0.4110	0.0310
Enc1	0.7183	0.0045	Mir5121, Rpl13a, Snord33	-0.8938	0.0101
Erdr1	3.1199	0.0045	Mpped1	-0.3089	0.0400
Fam131a	0.7586	0.0045	Myoc	-0.3524	0.0353
Fam212b	0.6059	0.0045	Neat1	0.3473	0.0254
Fam81a	0.9982	0.0045	Nr4a2	-0.4352	0.0101
Fbxl16	0.4746	0.0162	Ntng1	0.3686	0.0182
Fezf2	3.3833	0.0045	Oprk1	-0.5128	0.0353

Substantia nigra			*Striatum*		
Gene	Foldchange Basyn/Padel	q value	Gene	Foldchange Basyn/Padel	q value
Fibcd1	0.7498	0.0045	Otx2	0.4818	0.0101
Fosl2	0.7857	0.0045	Park2	0.8927	0.0101
Foxg1	2.7527	0.0045	Pde1a	-0.3747	0.0254
Gabra4	0.5140	0.0126	Penk	-0.4646	0.0101
Gda	2.1631	0.0045	Pisd-ps3	-0.3102	0.0400
Gldc	0.6994	0.0045	Plcb4	0.3137	0.0353
Glra1	-0.4614	0.0354	Pon3	0.5705	0.0182
Gm11549	2.7142	0.0045	Prlr	0.7987	0.0101
Gng7	0.5230	0.0045	Rbm47	0.6615	0.0400
Gpc4	0.7471	0.0088	Rgs16	0.3665	0.0101
Gpr88	0.7264	0.0045	Rnf152	0.3355	0.0400
Gprin1	0.4254	0.0439	Rprm	-0.5581	0.0101
Gpx3	-0.4253	0.0465	Rprml	-0.4079	0.0101
Grasp	0.6008	0.0491	Rtn4rl2	-0.3916	0.0182
Grhl1	1.1091	0.0045	Scara5	0.6706	0.0458
Grin2b	0.5626	0.0126	Sema3b	0.4753	0.0101
Grp	0.7969	0.0045	Sez6l	-0.4196	0.0101
H2-Aa	0.9636	0.0045	Sfrp1	0.4416	0.0254
H2-Ab1	0.7948	0.0045	Sgk1	-0.3632	0.0101
H2-Eb1	0.8911	0.0045	Sgms2	0.4712	0.0254
Hba-a1, Hba-a2	-0.5608	0.0088	Sh3d19	0.3332	0.0353
Hpcal4	1.2128	0.0045	Slc13a4	0.3739	0.0310
Hrk	1.0413	0.0045	Slc18a2	0.6275	0.0101
Htr3a	0.8084	0.0322	Slc4a2	0.3372	0.0101
Icam5	2.0159	0.0045	Slc4a5	0.5702	0.0101
Igflr1	1.0605	0.0465	Slc6a3	0.7435	0.0101
Iqgap2	1.0328	0.0045	Snhg11	0.4155	0.0101
Islr2	1.0064	0.0045	Sostdc1	0.5156	0.0101
Itpka	1.1967	0.0045	Srp54b	1.3867	0.0101
Kalrn	0.9625	0.0045	Steap2	0.3385	0.0353
Kcnf1	1.1083	0.0045	Synpo2	0.3651	0.0101
Kcng1	1.3478	0.0045	Tbr1	-0.4243	0.0101
Kcng2	0.7371	0.0227	Tcf7l2	0.4044	0.0101
Kcnip2	1.1391	0.0045	Tmem158	-0.4747	0.0101
Kcnj4	2.4056	0.0045	Tmem72	0.4327	0.0400
Kcnv1	1.3618	0.0045	Trpv4	0.6642	0.0101
Kctd16	0.9173	0.0045	Tuft1	0.6511	0.0101
Kdm5d	0.6821	0.0045	Wdr86	0.6690	0.0101
Krt12	2.4295	0.0196	Wfdc2	0.7032	0.0101

Substantia nigra			*Striatum*		
Gene	Foldchange Basyn/Padel	q value	Gene	Foldchange Basyn/Padel	q value
Krt2	1.8523	0.0045	Xist	0.6589	0.0101
Krt77	1.2769	0.0045	Zic1	0.4254	0.0101
Krt9	1.0649	0.0227			
Lhx2	1.4727	0.0045			
Lhx6	2.3723	0.0045			
Lmo7	0.7956	0.0045			
Lpl	1.2223	0.0045			
Lppr4	0.6243	0.0045			
Lrrc7	0.5758	0.0088			
Mal2	0.4500	0.0415			
Mef2c	1.1060	0.0045			
Mfge8	0.6175	0.0045			
Miat	0.6450	0.0045			
Mical2	0.4276	0.0465			
Mir124a-1, Mir124a-1hg, Mir3078	0.7058	0.0045			
Mmd	0.5217	0.0088			
Moxd1	1.3721	0.0045			
Mpped1	0.7193	0.0045			
Myo5b	0.6075	0.0045			
Neurl1b	1.6196	0.0045			
Neurod6	1.1844	0.0045			
Nov	2.1471	0.0045			
Npas2	0.8605	0.0045			
Npy	0.9080	0.0045			
Npy1r	0.5617	0.0386			
Npy2r	0.8748	0.0045			
Nr2e1	1.9617	0.0045			
Nrgn	1.3846	0.0045			
Nsmf	0.5426	0.0045			
Ntf3	1.2927	0.0126			
Ntn5	1.7417	0.0162			
Ntrk1	-1.2253	0.0227			
Otp	-0.7943	0.0354			
Pak6	0.4790	0.0322			
Park2	0.9436	0.0045			
Pax7	-0.6967	0.0415			
Pcdh20	0.4859	0.0465			
Pde1a	0.7018	0.0045			
Pde2a	0.5677	0.0045			

Substantia nigra					
Gene	Foldchange Basyn/Padel	q value	Gene	Foldchange Basyn/Padel	q value
Pdzrn3	0.6902	0.0196	Snhg11	0.5494	0.0126
Pkd2l1	-0.7588	0.0260	Sowaha	0.9960	0.0045
Plk2	0.5780	0.0045	Sprn	0.7291	0.0045
Plxnd1	0.6367	0.0045	Sstr1	0.5094	0.0227
Prdm8	0.5725	0.0439	Sstr4	1.2402	0.0045
Prkcg	0.4771	0.0045	St6galnac5	1.1091	0.0045
Prph	-0.5923	0.0045	Stk32a	-0.5963	0.0126
Psd	0.5397	0.0045	Stx1a	0.6991	0.0045
Psrc1	1.8158	0.0045	Susd2	-0.4538	0.0260
Ptk2b	1.5323	0.0045	Sv2c	-0.4427	0.0227
Ptpn14	0.5421	0.0491	Syne1	0.5904	0.0045
Pxdn	0.6482	0.0045	Syngap1	0.5803	0.0045
Rab40b	0.8770	0.0045	Synpo	0.8649	0.0045
Rasal1	0.9349	0.0045	Tac2	1.6962	0.0045
Rasgrp1	0.8289	0.0045	Tbr1	2.5581	0.0045
Rfx3	0.5933	0.0126	Tcf7l2	0.5921	0.0162
Rgs14	2.1810	0.0045	Tfap2d	1.0443	0.0439
Rin1	1.9785	0.0045	Tnfaip8l3	0.9065	0.0045
Rln3	-2.0601	0.0045	Trh	1.0901	0.0045
Rnaset2b	0.9373	0.0045	Trpc4	0.7217	0.0045
Rprml	0.9100	0.0045	Trpc6	0.8774	0.0196
Rspo2	1.0572	0.0045	Ttr	-1.0359	0.0045
Rtn4r	0.5479	0.0045	Ucn	1.7620	0.0045
Rtn4rl1	0.6464	0.0045	Uts2	-2.3854	0.0045
Rtn4rl2	2.1491	0.0045	Vip	1.2249	0.0045
Satb2	1.2940	0.0045	Vipr1	1.3688	0.0045
Sgk1	-0.6016	0.0045	Vsx2	-0.9110	0.0045
Shisa7	0.5522	0.0045	Wasf1	0.4554	0.0292
Slc10a4	-0.5501	0.0045	Wipf3	0.5989	0.0045
Slc17a7	0.8721	0.0045	Xist	-0.6712	0.0045
Slc18a2	-0.4881	0.0162	Zfp365	0.4441	0.0260
Slc18a3	-0.9005	0.0045	Zfp831	1.5548	0.0045
Slc24a4	0.6369	0.0292			
Slc26a4	1.5160	0.0045			
Slc5a7	-0.7622	0.0045			
Slc6a2	-1.0727	0.0045			
Slc8a2	0.4678	0.0162			
Slc9a4	1.9568	0.0045			
Slit3	0.4675	0.0322			
Smoc2	0.7971	0.0045			
Snca	0.4568	0.0439			
Sncg	-0.4356	0.0386			

Table 45: ∆CT values of qPCR examined genes from the new transcriptome analysis. *Hprt normalized. Substantia nigra tissue of one-year-old mice. C57BL/6, Padel, Basyn (n=10).*

ΔCT								
Crym			**Icam5**			**Mpped1**		
C57BL/6	**Padel**	**Basyn**	**C57BL/6**	**Padel**	**Basyn**	**C57BL/6**	**Padel**	**Basyn**
1.22	6.39	3.74	2.68	6.05	2.92	2.54	3.27	3.34
1.27	2.12	3.64	2.06	3.46	4.39	3.14	3.21	3.66
7.49	8.25	5.89	7.04	7.71	5.73	3.23	3.52	3.33
6.16	2.26	2.87	6.05	3.62	4.09	3.54	2.92	3.39
1.91	2.34	3.50	2.46	4.40	5.03	2.93	3.08	3.11
4.13	2.64	6.86	4.92	3.25	3.22	2.37	3.01	3.32
7.65	1.85	4.30	5.63	4.21	5.29	2.75	3.13	3.32
3.06	2.25	2.49	4.74	3.10	3.95	3.44	2.98	3.50
7.94	4.61		5.89	5.74	4.50	3.02	3.56	2.78
4.28	1.90		5.06	3.58	0.85	3.15	2.84	1.81
means								
4.51	3.46	4.16	4.65	4.51	4.00	3.01	3.15	3.16
ΔCT								
Pde1a			**Rtn4rl2**			**Sgk1**		
C57BL/6	**Padel**	**Basyn**	**C57BL/6**	**Padel**	**Basyn**	**C57BL/6**	**Padel**	**Basyn**
0.96	3.03	3.23	3.07	6.86	5.30	3.00	3.03	3.40
1.11	1.36	2.70	2.98	4.30	5.62	2.95	2.75	3.69
2.92	2.57	3.05	7.11	8.18	5.91	3.12	3.01	3.25
3.02	1.56	2.16	6.60	4.07	4.56	3.07	2.83	3.32
1.40	1.41	3.13	3.44	3.94	6.96	2.88	2.85	3.36
2.04	1.62	2.48	5.13	4.43	4.19	3.19	3.14	3.23
2.63	0.87	2.81	6.41	3.88	6.63	2.82	2.57	3.24
2.23	1.59	2.68	4.79	4.18	5.39	3.32	2.99	3.44
2.87	2.48	2.27	7.30	5.67	5.00	3.13	3.31	3.23
2.52	0.66	1.01	5.81	3.36	2.48	3.07	2.68	2.76
means								
2.17	1.71	2.55	5.26	4.89	5.20	3.05	2.92	3.29

Table 46: ∆CT values of qPCR examined genes from the new transcriptome analysis. *Hprt normalized. Substantia nigra tissue of one-year-old mice. C57BL/6, Padel, Basyn (n=10).*

ΔCT								
Slc18a2			**Tbr1**			**Tcf7l2**		
C57BL/6	**Padel**	**Basyn**	**C57BL/6**	**Padel**	**Basyn**	**C57BL/6**	**Padel**	**Basyn**
2.40	2.81	3.55	5.17	8.34	11.31	-0.09	1.77	1.85
2.19	1.23	2.92	4.99	6.29	8.87	0.45	0.89	1.21
1.89	2.56	2.34	8.95	10.41	7.29	0.32	2.44	-0.34
1.18	0.95	2.30	9.27	7.25	6.88	1.07	0.82	0.18
1.67	1.08	2.21	5.74	6.38	9.99	0.19	1.14	1.22
1.28	0.66	2.85	4.87	6.51	6.03	0.69	1.31	0.62
1.37	1.54	1.58	6.37	5.92	8.57	1.19	-0.06	1.93
2.10	1.35	1.73	6.65	6.79	6.53	0.31	0.10	3.04
1.68	0.96	2.73	9.53	8.45	4.71	0.34	0.55	0.06
1.55	1.59	3.46	7.71	5.26	2.05	1.02	-0.12	1.78
means								
1.73	1.47	2.57	6.93	7.16	7.22	0.55	0.88	1.15
ΔCT								
Ctsc								
C57BL/6	**Padel**	**Basyn**	**C57BL/6**	**Padel**	**Basyn**	**C57BL/6**	**Padel**	**Basyn**
4.51	3.87	3.69						
4.44	3.78	5.08						
5.05	4.00	5.23						
5.11	3.55	4.23						
4.35	3.84	5.03						
4.61	3.47	5.23						
4.86	3.51	3.95						
5.26	3.52	4.71						
4.95	3.65	5.40						
4.81	3.44	3.67						
means								
4.79	3.66	4.62						

Table 47: ∆CT values of qPCR examined genes from the new transcriptome analysis. *Hprt normalized. Striatum tissue of one-year-old mice. C57BL/6, Padel, Basyn (n=9-10).*

ΔCT								
Crym			**Icam5**			**Mpped1**		
C57BL/6	**Padel**	**Basyn**	**C57BL/6**	**Padel**	**Basyn**	**C57BL/6**	**Padel**	**Basyn**
0.35	0.95	2.17	0.72	0.97	0.98	2.98	2.52	1.83
1.88	0.10	2.28	0.37	0.73	1.52	2.53	3.50	2.84
0.84	1.88	3.02	0.34	0.42	1.60	1.62	2.98	2.96
1.99	-0.15	4.74	0.67	0.33	3.27	2.87	2.77	4.36
1.99	0.66	1.60	0.30	-0.14	0.23	2.31	1.79	1.28
1.01	0.85	1.11	0.74	0.36	0.30	2.92	2.59	1.02
1.15	0.80	1.12	0.50	0.48	0.54	0.98	2.82	2.15
1.66	1.04	2.43	0.56	0.43	1.61	2.83	2.60	3.27
0.87	1.47	2.06	0.20	0.77	0.61	2.07	3.05	1.44
0.45	0.39		0.63	0.38		2.71	2.59	
means								
1.22	0.80	2.28	0.50	0.47	1.19	2.38	2.72	2.35
ΔCT								
Pde1a			**Rtn4rl2**			**Sgk1**		
C57BL/6	**Padel**	**Basyn**	**C57BL/6**	**Padel**	**Basyn**	**C57BL/6**	**Padel**	**Basyn**
2.89	3.18	1.64	7.79	8.16	2.30	1.92	1.84	3.28
2.41	2.72	2.97	5.79	7.37	3.63	1.89	1.89	3.13
1.43	2.42	2.59	2.29	6.18	3.04	2.35	1.82	3.46
2.53	1.47	3.57	7.26	7.35	4.26	2.06	1.85	3.74
2.75	2.16	1.25	5.81	3.74	1.78	2.22	1.50	2.54
1.92	1.36	0.49	6.47	5.62	1.37	2.27	1.58	2.96
2.09	2.24	1.19	1.95	5.17	2.69	2.60	1.91	2.91
2.62	2.13	2.87	6.94	7.85	3.62	2.22	1.58	3.38
0.49	2.18	2.07	4.22	4.55	2.88	1.97	1.56	3.61
1.75	2.55		5.37	7.42		1.88	1.68	
means								
2.09	2.24	2.07	5.39	6.34	2.84	2.14	1.72	3.22

Table 48: ∆CT values of qPCR examined genes from the new transcriptome analysis. *Hprt normalized. Striatum tissue of one-year-old mice. C57BL/6, Padel, Basyn (n=5-10).*

ΔCT								
Slc18a2			**Tbr1**			**Tcf7l2**		
C57BL/6	**Padel**	**Basyn**	**C57BL/6**	**Padel**	**Basyn**	**C57BL/6**	**Padel**	**Basyn**
8.71	8.69	7.63	4.92	7.05	1.96	3.31	4.04	2.30
9.44	8.63	7.89	1.81	7.27	3.53	3.90	4.15	1.81
8.82	8.41	7.59	5.92	4.88	3.72	4.00	1.25	2.14
7.94	8.19	7.36	4.66	5.93	5.54	4.20	2.18	2.24
8.03	8.33	5.08	4.34	6.92	2.24	2.54	3.32	4.61
9.58	8.99		0.84	4.13	1.37	4.18	2.59	2.48
9.13	8.03		6.13	2.97	2.68	2.11	1.96	0.80
8.01	8.41		2.88	4.50	4.63	3.66	2.50	0.32
8.66	8.35		4.29	4.31	3.55	2.88	3.65	0.56
8.11	9.94			5.41		4.05	2.87	
means								
8.64	8.60	7.11	3.98	5.34	3.25	3.48	2.85	1.92
ΔCT								
Ctsc								
C57BL/6	**Padel**	**Basyn**	**C57BL/6**	**Padel**	**Basyn**	**C57BL/6**	**Padel**	**Basyn**
5.29	4.72	4.75						
5.11	4.80	5.02						
5.42	4.60	4.94						
5.39	4.88	5.56						
5.16	4.61	3.97						
4.85	4.44	4.49						
5.62	4.58	4.65						
4.60	5.04	4.48						
5.19	4.81	3.70						
5.41	4.97							
means								
5.20	4.75	4.62						

Table 49: ∆CT values of qPCR examined Rcn1 expression. *Hprt normalized. From left to right: Substantia nigra tissue of one-year-old mice; neonatal mesencephalic tissue; neonatal cortex tissue; primary astrocytes. WT=Padel wild type, Basyn, Padel (n=8-10).*

ΔCT (Hprt normalized)							
Adult SN		Neonatal mes		Neonatal cortex		Primary astrocytes	
WT	Basyn	WT	Padel	WT	Padel	WT	Padel
3.88	3.39	0.33	0.27	1.05	0.85	-0.56	-0.99
3.24	3.48	0.91	0.46	0.89	0.78	0.26	-0.96
4.07	3.23	0.72	0.39	1.12	1.17	0.15	-0.49
4.40	3.44	0.5	0.39	1.24	1.27	-0.81	-1.50
4.01	3.66	0.67	0.32	1.14	0.89	-0.10	-1.48
3.54	3.62	0.76	0.16	1.14	0.73	-0.65	-1.44
4.06	3.62	0.95	0.61	0.86	0.88	-0.35	-1.10
3.52	3.52	0.72	0.53	1.07	0.99		
		0.56	0.29	0.96	0.76		
		0.63	0.07	0.96	1.13		
mean							
3.84	3.49	0.68	0.35	1.04	0.95	-0.29	-1.14

Table 50: Efficiency and toxicity of Rcn1 siRNA knockdown in Padel astrocytes. *From left to right: Vitality measurement via MTS assay after Rcn1 siRNA treatment (normalized against untreated cells, n=9/14). qPCR data of Rcn1 expression after Rcn1 siRNA treatment (Gapdh normalized, n=15/16).*

Vitality (%)		ΔCt	
siRNA	scramble	siRNA	scramble
156.50	50.31	5.647	5.100
156.50	50.31	5.923	5.247
167.01	69.09	4.727	4.123
177.43	18.23	5.233	4.383
92.99	46.59	5.577	4.617
64.54	138.28	6.100	4.307
92.43	223.09	5.543	4.423
74.02	189.52	4.960	4.847
44.82	64.91	5.227	4.343
51.94		4.770	4.713
17.85		5.530	4.720
56.45		4.963	4.223
52.35		4.713	4.317
38.41		4.703	4.483
		5.590	
means			
88.803	94.479	5.280	4.560

Table 51: Calcium response in primary astrocytes after ATP stimulation (100µM). *from left to right: Calcium response peaks ($\Delta F/F_0$). Calcium response integral ($\int F/F_0$). Calcium response duration (t(s)). WT=Padel wild type, Padel (n=9-11).*

Calcium response in primary astrocytes					
Peak		**Integral**		**Duration**	
WT	**Padel**	**WT**	**Padel**	**WT**	**Padel**
0.0948	0.0545	23.4380	22.9490	234.3960	265.7637
0.1380	0.1058	42.9793	38.0342	259.5591	243.3582
0.1027	0.0836	28.9195	36.9276	238.1877	267.4872
0.0793	0.0656	15.1928	25.7536	233.0172	223.7103
0.0666	0.0875	10.6117	21.8030	228.5361	184.4145
0.0830	0.0568	25.7332	14.8207	276.4494	246.8052
0.1231	0.0733	39.9551	25.3131	278.8623	249.5628
0.0937	0.0425	29.4793	15.9917	266.7978	223.7103
0.1126	0.0401	33.5185	13.8558	235.4301	287.1351
0.0909		32.0487		259.2144	
0.0583		14.0854		242.6688	
means					
0.0948	0.0677	26.9056	23.9387	250.2835	243.5497
Replication of experiment					
Peak		**Integral**		**Duration**	
WT	**Padel**	**WT**	**Padel**	**WT**	**Padel**
0.1134	0.1165	29.6605	38.1670	248.5287	224.7444
0.1612	0.0736	41.5273	25.4492	225.0891	246.1158
0.1384	0.1145	51.9721	29.6111	197.5131	254.7333
0.0874	0.1070	33.5753	30.4512	260.5932	236.8089
0.1233	0.1199	42.5757	39.4648	249.5628	246.1158
0.1326	0.0913	38.1973	27.7209	218.8845	233.7066
0.1592	0.1248	51.2390	40.8229	257.8356	293.3397
0.0851	0.1151	31.7486	41.1207	247.8393	266.4531
0.1266	0.0963	38.0184	31.1600	224.3997	242.6688
0.1136	0.1362	33.9748	27.7093	213.7140	218.8845
means					
0.1241	0.1095	39.2489	33.1677	234.3960	246.3571

Table 52: Calcium response in Rcn1 siRNA treated primary astrocytes after ATP stimulation (100µM). *from left to right: Calcium response peaks ($\Delta F/F_0$). Calcium response integral ($\int F/F_0$). Calcium response duration (t(s)). Rcn1 overexpression in SH-SY5Y cells ($\Delta F/F_0$, n=5) WT=Padel wild type, Padel (n=8).*

Peak of calcium response			Integral of calcium response		
Padel	**Padel Rcn1 siRNA**	**WT**	**Padel**	**Padel Rcn1 siRNA**	**WT**
0.0225	0.0357	0.0383	5.417	8.509	11.512
0.0199	0.0374	0.0285	4.591	10.441	9.088
0.0175	0.0235	0.0308	4.191	7.550	8.162
0.0165	0.0280	0.0175	3.895	6.066	6.500
0.0204	0.0189	0.0219	5.056	5.032	7.790
0.0207	0.0336	0.0250	6.014	11.216	8.656
0.0250	0.0251	0.0179	7.146	7.612	4.829
0.0289	0.0277	0.0209	7.115	8.839	5.547
means					
0.0214	0.0287	0.0251	5.4283	8.1584	7.7606

Calcium response duration			SH-SY5Y	
Padel	**Padel Rcn1 siRNA**	**WT**	**pcDNA3.1**	**Rcn1 Plasmid**
239.222	216.127	193.032	-0.0176	-0.0320
243.703	179.244	200.271	-0.0055	-0.0489
209.233	240.256	211.646	-0.0156	-0.0266
246.461	222.676	230.604	-0.0158	-0.0274
241.290	210.267	250.942	-0.0201	-0.0265
258.870	231.983	233.017		
234.741	237.843	222.676		
208.888	214.748	229.915		
means				
235.301	219.143	221.513	-0.015	-0.032

Table 53: Data of the MAM quantification and localization analysis with primary fibroblasts. *From left to right: Western blot analysis of Rcn1 expression (summarized pixel intensity, normalized with β-Actin). Immunocytochemical staining; Rcn1 positive pixels co-localized with ER-marker positive pixels in relation to all Er-marker positive pixels. Rcn1 positive pixels co-localized with ER-marker and mitochondrial-marker positive pixels in relation to all ER-marker and mitochondrial-marker positive pixels. Co-localized Er-marker and mitochondrial-marker positive pixels in relation to all mitochondrial marker positive pixels. WT=Padel wild type (n=9-10). ER=endoplasmic reticulum, MAM=mitochondrial associated membranes*

RCN1 expression		Rcn1 in ER		Rcn1 in MAM		MAM	
WT	Padel	WT	Padel	WT	Padel	WT	Padel
2175452	7128910	0.3230	0.4274	0.4052	0.4944	0.1875	0.2120
964591.2	3056407	0.4689	0.6909	0.5686	0.8009	0.1832	0.4063
1032764	30246782	0.2518	0.6047	0.3118	0.6967	0.4945	0.3760
13462048	40915085	0.2595	0.3508	0.3303	0.5211	0.6129	0.3982
3806113	13258571	0.4402	0.3821	0.5617	0.4809	0.6701	0.6226
8923649	20276491	0.5331	0.7472	0.6452	0.8250	0.2456	0.4537
14459817	20332816	0.6690	0.7120	0.7511	0.7916	0.3698	0.2507
6393800	18098078	0.4477	0.2517	0.5283	0.3148	0.7456	0.3961
7558628	4022512						
means							
6530763	17481739	0,4241	0,5209	0,5128	0,61567	0,4387	0,38944

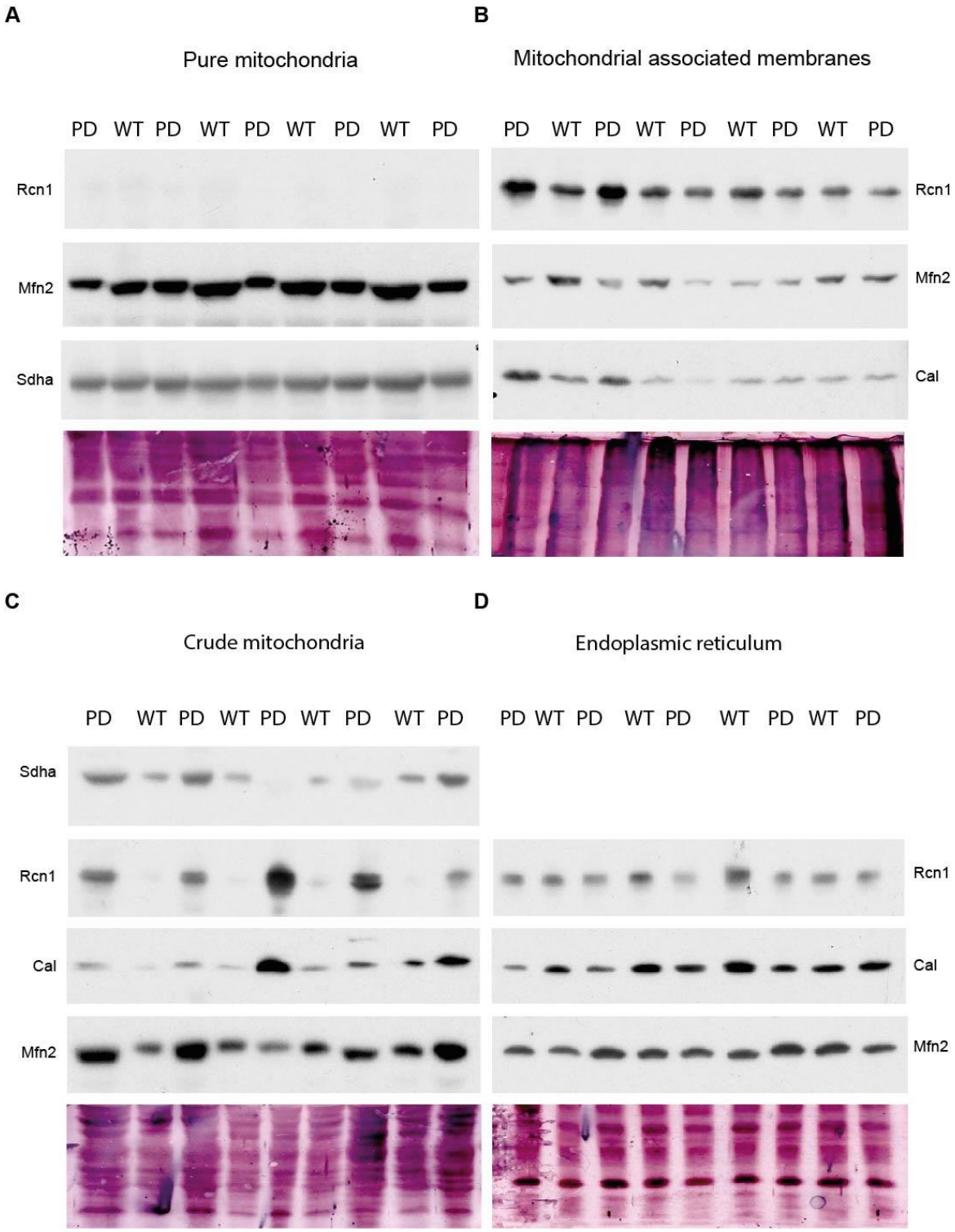

Figure 41: Western blot images of different cell fractions *of 3-month-old Padel and C57Bl/6 brain homogenates. PD=Padel homo, WT=C57BL/6 (n=4-5). Sdha=Succinate dehydrogenase complex subunit A, Cal=Calreticulin, Mfn2=Mitofusin2.*

Table 54: Data of the autophagy/mitophagy analysis of primary Padel fibroblasts. *From left to right: Quantitative western blot analysis ratio of LC3b-II/LC3b-I. Western blot analysis of LC3b-II amount normalized with total protein. Cell profiler analysis of LC3b-GFP transfected primary fibroblasts treated with Mitotracker red: Vesicular LC3b puncta in relation to cell size. Colocalization of LC3b puncta and Mitotracker (pixels in %). Mito density in relation to the cell surface (pixels in %). WT=Padel wild type (n=9-10).*

LC3b-II/I ratio		Lc3b amount	
WT	**Padel**	**WT**	**Padel**
0.73	0.31	22643.49	23296.40
0.39	0.18	5646.16	7951.82
0.10	0.50	3786.84	10205.09
0.64	0.30	20884.44	14224.28
0.23	0.72	9617.47	33991.74
0.65	0.04	26575.67	5554.09
0.49	0.17	59456.47	8723.94
0.67	0.34	34048.37	6353.71
0.72	0.78	36747.07	14004.13
	0.81		14662.05
means			
0.51	0.42	24378.44	13896.72

LC3b-II (%)		Coloc (%)		Mito density (%)	
WT	**Padel**	**WT**	**Padel**	**WT**	**Padel**
0.17	0.11	0.56	0.22	9.99	10.35
0.20	0.18	1.30	0.71	16.17	11.46
0.22	0.51	0.24	0.88	13.51	12.15
0.42	0.27	0.73	0.70	12.09	12.82
0.37	0.14	0.55	0.32	16.06	14.44
0.13	0.40	0.41	0.58	14.15	12.98
0.11	0.33	0.29	0.66	11.26	17.60
0.17	0.23	0.38	0.70	10.41	12.93
0.16	0.21	0.25	0.36	11.93	15.61
	0.37		0.55		16.81
means					
0.22	0.27	0.52	0.57	12.84	13.72

Table 55: Data of neuronal differentiation analysis in astrocyte neuronal co-culture. *From left to right: Surface area (pixels). Soma area (pixels). Longest process (pixels). Sum of processes (pixels). WT=Padel wild type, PD= Padel homo. (n=6-8).*

Surface area				Soma area			
WT/WT	**PD/PD**	**PD/WT**	**WT/PD**	**WT/WT**	**PD/PD**	**PD/WT**	**WT/PD**
2639.15	2497.09	3603.50	1818.99	26.03	18.93	26.06	15.35
1528.32	1496.79	3082.41	3341.37	15.22	15.73	22.42	24.48
1537.01	938.16	3392.08	1513.13	18.50	21.32	29.31	16.63
2205.59	1108.73	1733.88	1425.68	20.20	23.01	23.95	13.58
2482.12	1533.45	2762.61	1279.86	23.14	15.80	28.44	16.35
2446.13	1673.48	2836.14	3187.06	25.98	20.25	19.79	24.15
1955.13	2721.94			20.37	24.08		
1937.66	1185.80			20.86	15.35		
means							
2091.39	1644.43	2901.77	2094.35	21.29	19.31	25.00	18.42
Longest process				**Sum of processes**			
WT/WT	**PD/PD**	**PD/WT**	**WT/PD**	**WT/WT**	**PD/PD**	**PD/WT**	**WT/PD**
177.85	270.99	279.98	205.89	1043.23	828.00	1425.52	916.31
182.90	177.37	235.67	260.17	781.45	669.09	1495.22	1322.75
154.22	130.03	299.56	181.39	637.13	633.61	1717.60	765.08
220.98	155.52	232.66	171.26	955.60	488.66	1294.54	834.65
198.72	154.97	282.80	159.80	858.66	632.06	1507.58	883.63
205.76	186.28	215.09	248.47	1390.75	760.86	1479.62	1631.25
187.22	209.75			1343.06	1151.42		
198.95	157.17			1261.62	609.92		
means							
190.83	180.26	257.63	204.50	1033.94	721.70	1486.68	1058.94